

CHAPTER 4

Conformation and chiroptical properties of dienes and polyenes

PIERO SALVADORI, CARLO ROSINI[†] and LORENZO DI BARI

Centro di Studio del CNR per le Macromolecole Stereordinate ed Otticamente Attive, Dipartimento di Chimica e Chimica Industriale, Via Risorgimento 35, I-56126 Pisa, Italy
Fax: +39(50) 918260; e-mail: psalva@dccci.unipi.it

I. INTRODUCTION	112
II. CONJUGATED DIENES	112
A. Diene Conformations	112
B. Electronic Absorption Features of the Diene Chromophore	112
C. Chiral Dienes and the Origin of Optical Activity	114
1. Static distortion of the chromophore	114
2. Dynamic distortion of the chromophore	114
3. External dissymmetric perturbation	117
D. Intrinsically Chiral Dienes	117
1. The diene chirality rule	117
a. Theoretical models justifying the diene rule	120
2. Allylic axial chirality rule	120
a. Models in support of the allylic axial chirality rule	123
b. Problems in the definition of the allylic axial rule	125
3. Strongly distorted dienes	126
a. Heteroannular <i>s-cis</i> -dienes	126
b. Highly twisted <i>s-cis</i> -dienes	128
4. Transoid dienes	131
5. Conclusions on skewed dienes	131
E. Dienes Owing Their Chirality to a Dynamic Twist	132

[†] Present Address: Dipartimento di Chimica, Università della Basilicata,
Via N. Sauro 85, I-85100 Potenza, Italy

F. External Dissymmetric Perturbation	133
1. Planar <i>s-cis</i> -dienes	133
2. Planar <i>s-trans</i> -dienes	135
III. POLYENES	137
A. Carotenoids	137
1. General aspects	137
2. Origins of the optical activity	138
3. Polymers	141
IV. OLIGOENES	141
V. APPENDIX	141
A. 1,3-Butadiene MOs, Symmetry and Electronic Transitions	141
B. MO Calculation of the Rotational Strength	143
C. Charge-displacement Calculation of <i>R</i>	144
VI. REFERENCES	146

I. INTRODUCTION

Circular dichroism (CD) spectroscopy (and the nowadays less used optical rotatory dispersion, ORD) is a well-recognized and powerful tool for the stereochemical investigation of chiral molecules¹. When dealing with the vast class of dienes and polyenes and their derivatives, it is essential to refer to a specific arrangement of the double bonds. Cumulated systems have been thoroughly reviewed in 1980 by Runge for this same series². Double bonds separated by two or more carbon-carbon single bonds can be successfully described in terms of additive effects arising from the individual olefinic chromophores. In contrast, a conjugated system must be treated as a single chromophore. We shall limit the present discussion to alternating dienes and polyenes only.

A distorted conjugated pair of double bonds is an intrinsically chiral chromophoric system, and its overall chiroptical properties depend on the reduced symmetry of the chromophore itself as well as on the perturbing action of a dissymmetric environment.

The aim of the present chapter is to discuss in some detail the mechanisms giving rise to optical activity in these molecules and to examine the main rules formulated for correlating structure and CD, critically analysing their use and limitations with suitable examples. Further information can be found in the original literature and in two recent review articles, by Gawroński and Walborsky³ and by Buchecker and Noack⁴, covering the diene and polyene (limited to carotenoids) fields, respectively.

II. CONJUGATED DIENES

A. Diene Conformations

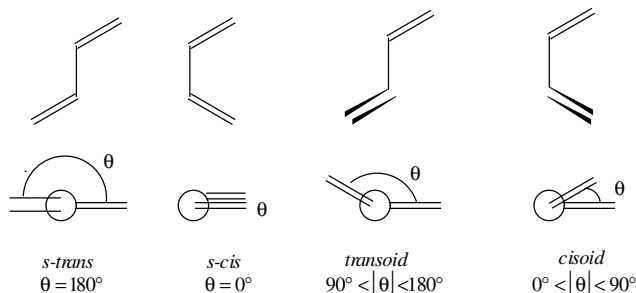
1,3-dienes can exist in two limiting planar conformations defined as *s-trans* and *s-cis* with respect to the single bond C₂-C₃ and in non-planar skewed form, often called *cisoid* or *transoid*, with reference to the nearer planar form. The dihedral angle θ describes this internal degree of freedom, as depicted in Scheme 1.

We shall conventionally define as positive the clockwise rotations from the double bond nearer to the observer to the one farther away.

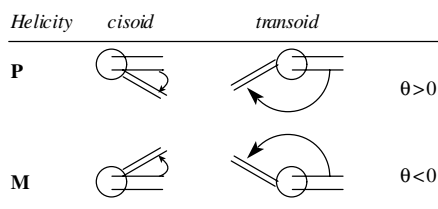
As shown in Scheme 2, positive angles define P-helicity while negative θ values define M-helicity.

B. Electronic Absorption Features of the Diene Chromophore

We give here only a brief summary of the electronic absorption spectrum of the diene chromophore which has been extensively treated by Gross and Schnepf⁵ with reference to α - and β -phellandrene.



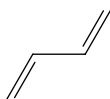
SCHEME 1



SCHEME 2

The possibility of delocalization of the π electrons of the diene system across the formally σ bond between carbon atoms 2 and 3 forces the molecule to be planar, thus we have two limiting conformations⁶:

(1) The planar *s-trans* (e.g. 1,3-butadiene).



This is the most populated form of 1,3-butadiene, which at room temperature is present in about 99% abundance^{5,6}. The characteristic absorption feature of this chromophore is the intense band at about 210 nm showing ϵ_{\max} larger than 20000. It has been unanimously⁶ assigned to the $\pi_- \rightarrow \pi_-^*$ (${}^1A_g \rightarrow {}^1B_u$) transition of the C_{2h} chromophore (see Appendix, Section V).

(2) The *s-cis* conformation (e.g. cyclopentadiene).



In this molecule the diene moiety assumes the C_{2v} symmetry and the prominent feature of its near-UV absorption spectrum is the 240 nm band (ϵ_{\max} 3500), assigned⁶ to the same transition $\pi_- \rightarrow \pi_-^*$, now characterized by ${}^1A_1 \rightarrow {}^1B_2$ symmetry in the C_{2v} point group (see Appendix, Section V).

Actually, as demonstrated by Gross and Schnepf⁵, both the *s-cis* and the *s-trans* chromophores possess many other electronic transitions down to 140 nm. However, the near-UV part of the spectrum has been the most studied and only the lowest energy transition has been used as a structural probe to solve conformational and configurational

problems. The present work will therefore be limited to the discussion of this band alone.

Both theoretical calculations and experimental investigations⁶ on model compounds indicate that the wavelength of the $\pi_- \rightarrow \pi^*$ (also indicated as $N \rightarrow V_1$) transition is longest (around 250 nm) in the *s-cis* conformation, reaches a minimum for skewed forms (190 nm when $\theta \approx 90^\circ$), where conjugation is inhibited, and again increases (to 220 nm) for the *s-trans* structure. The oscillator strength, f , is highest in the *s-trans* and becomes much smaller in the *s-cis* and skewed conformations⁷.

Increasing the number of conjugated double bonds leads to a marked bathochromic shift and to a hyperchromic effect, as predicted by Woodward's and Fieser's rules⁸.

C. Chiral Dienes and the Origin of Optical Activity

The planar C_{2h} and C_{2v} geometries of the 1,3-butadiene moiety are achiral structures and obviously they cannot show optical activity (i.e. ORD and CD). This has, of course, a spectroscopic origin. The optical activity of a transition $\Psi_0 \rightarrow \Psi_i$ is determined by its Rotational Strength (R)¹ defined as the scalar product

$$R = \text{Im}\{\boldsymbol{\mu}_{0i} \cdot \mathbf{m}_{0i}\} = \text{Im}\{\langle \psi_0 | \boldsymbol{\mu} | \psi_i \rangle \cdot \langle \psi_i | \mathbf{m} | \psi_0 \rangle\} \quad (1)$$

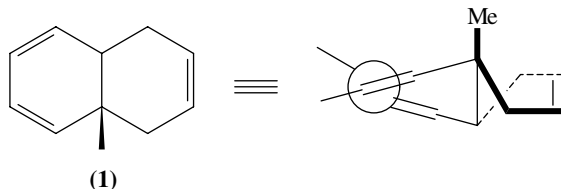
where $\boldsymbol{\mu}$ and \mathbf{m} are the electric and magnetic dipole operators, respectively.

As shown in the Appendix (in Section V), in the C_{2h} point group, the ${}^1A_g \rightarrow {}^1B_u$ (i.e. the mono-electronic $\pi_- \rightarrow \pi^*$ excitation) possesses only an electric dipole moment, while in the C_{2v} structure the electric and magnetic dipole moments, both non-vanishing, are orthogonal. In both cases the product in equation 1 leads to zero rotational strength.

Optical activity can arise only on reducing the molecular symmetry. This can be achieved in the following three ways.

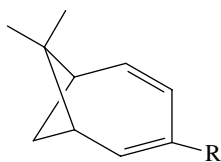
1. Static distortion of the chromophore

In the tetrahydronaphthalene derivative **1**, whose ORD spectrum is shown in Figure 1, the two conjugated double bonds are not coplanar⁹ and define a twist angle of about 17° . The point group is now C_2 and the lowest $\pi \rightarrow \pi^*$ transition is ${}^1A \rightarrow {}^1B$, which is both electrically and magnetically allowed. The two moments are collinear and the transition acquires a non-vanishing rotational strength. This distortion, caused by a chemical constraint (e.g. the cycle in **1**), is present in the molecule in its equilibrium configuration and can therefore be defined as *static*.



2. Dynamic distortion of the chromophore

In molecules like **2**, or **3**, the 1,3-diene chromophore is planar. Formally, the presence of R differentiates the two vertical halves of the molecule, which becomes chiral¹⁰. The physical meaning of this differentiation is that it induces dissymmetric vibrations, which determine, in turn, a *dynamic* twist of the chromophore.



- (2) R = Me
(3) R = D

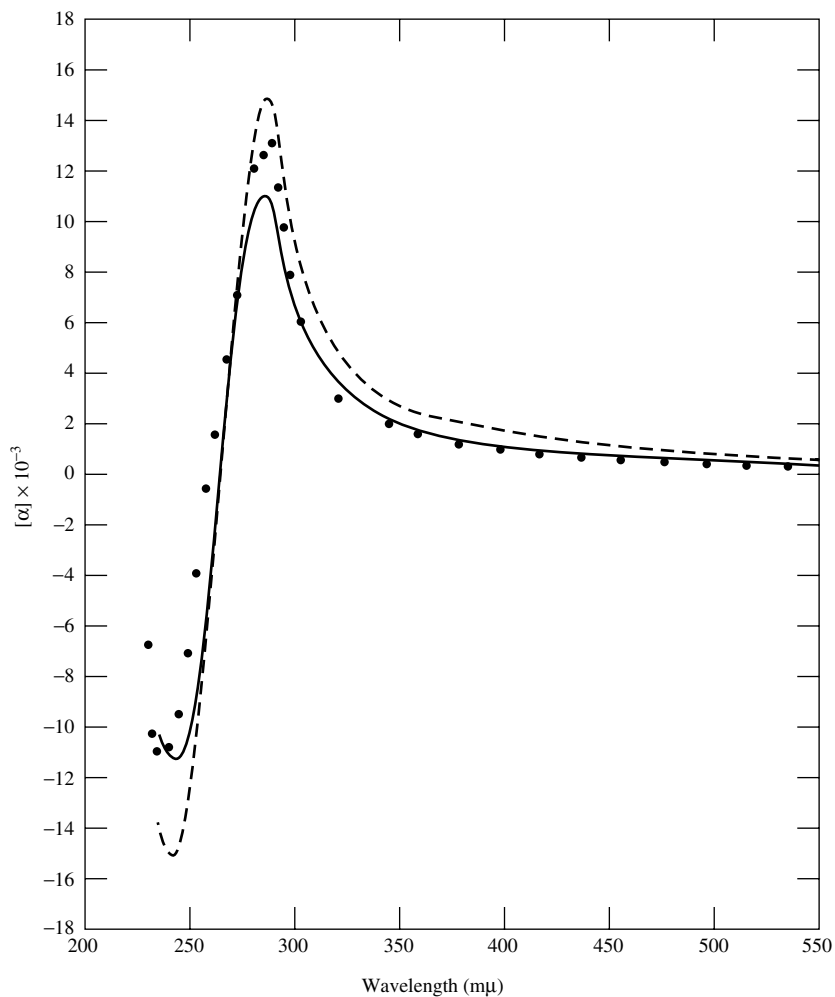


FIGURE 1. ORD spectrum of (+)-*trans*-9-methyl-1,4,9,10-tetrahydronaphthalene, **1** (dots). The two lines are computational results with (dashed) or without (continuous line) correction for the solvent refractive index. Reprinted with permission from Reference 9. Copyright 1961 American Chemical Society

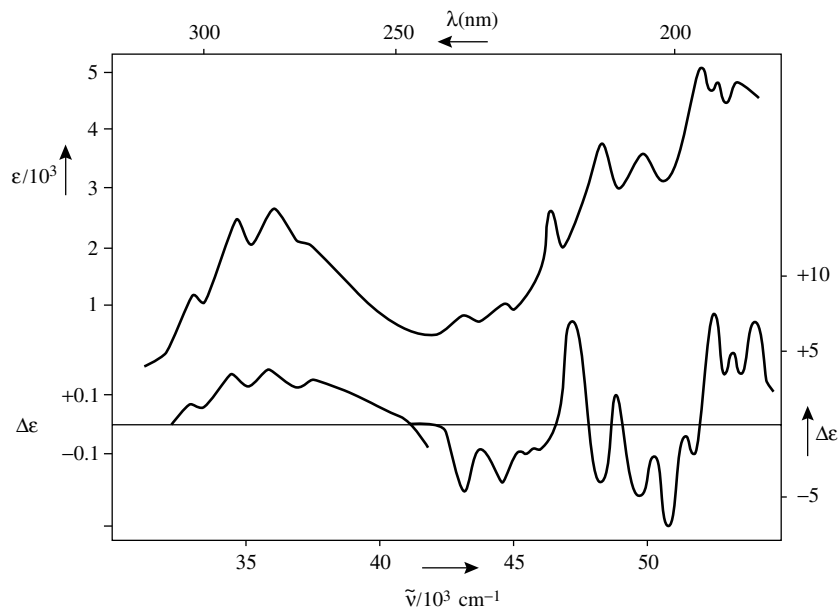


FIGURE 2. UV (upper curve) and CD (lower curve) spectra of **2**. Reprinted with permission from Reference 10. Copyright 1983 American Chemical Society

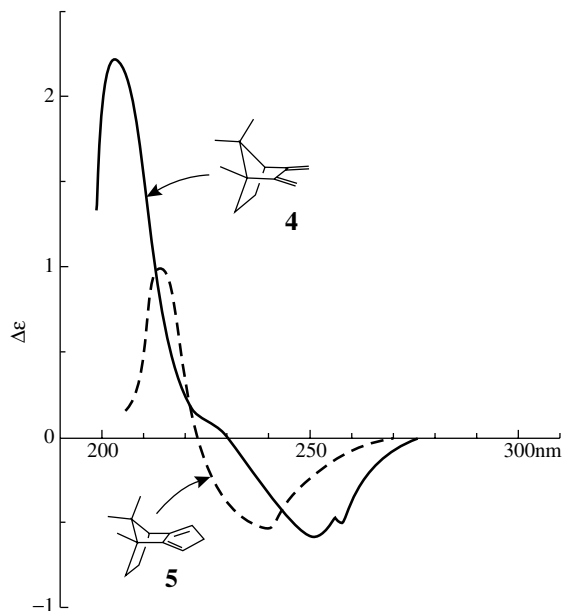
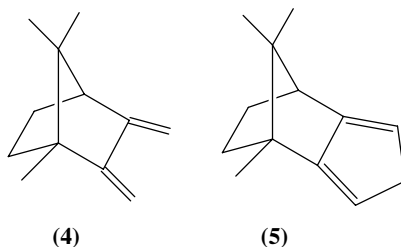


FIGURE 3. CD spectra of compounds **4** and **5**. Reprinted from Reference 11, with kind permission from Elsevier Science Ltd, The Boulevard, Langford Lane, Kidlington OX5 1 GB, UK

The UV and CD spectra of **2** are reported in Figure 2.

3. External dissymmetric perturbation

In **4** and **5** the chromophore is planar and the optical activity arises from the lack of a vertical symmetry plane (i.e. that bisecting the diene moiety), owing to the presence of the C_1-CH_3 bond, which has no counterpart in the other half of the molecule¹¹.



Furthermore, whenever the 1,3-diene group is not embedded in a rigid structure, e.g. in **6**¹² and **7**¹³, it assumes the most stable *s-trans* conformation, just as in the case of 1,3-butadiene. Again dissymmetrically disposed substituents perturb the $\pi \rightarrow \pi^*$ transition, which acquires some magnetic moment parallel to the electric one.

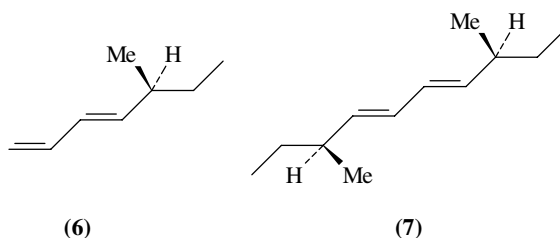


Figure 3 shows the CD spectrum of **4** and **5**, while Figure 4 reports absorption and CD spectra of **7**.

D. Intrinsically Chiral Dienes

As discussed above, the distortion of the 1,3-diene determines the lowering of symmetry of the chromophore from C_{2v} to C_2 . The low-energy $\pi \rightarrow \pi^*$ transition thus acquires non-vanishing rotational strength and becomes optically active^{1,14}. The methods proposed for interpreting the CD of intrinsically chiral dienes tend to attribute the most relevant role either to the distortion of the chromophore or to the perturbation arising from its environment. The two effects add up, sometimes acting in the same sense, sometimes conflicting. This makes it rather difficult to find a definite, general and simple relation between stereochemistry and optical activity for these compounds.

1. The diene chirality rule

The first correlation between the sign of the CD band allied to the $^1A \rightarrow ^1B$ transition and the molecular chirality was formulated just taking into account the lowering of symmetry of distorted dienes only^{9,15}.

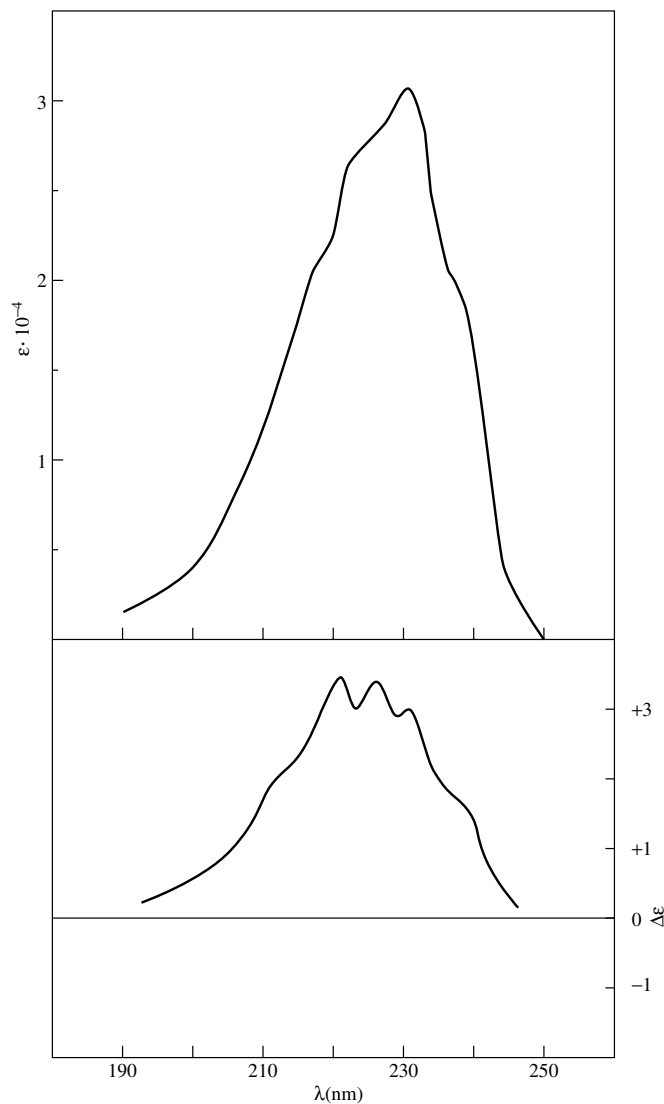
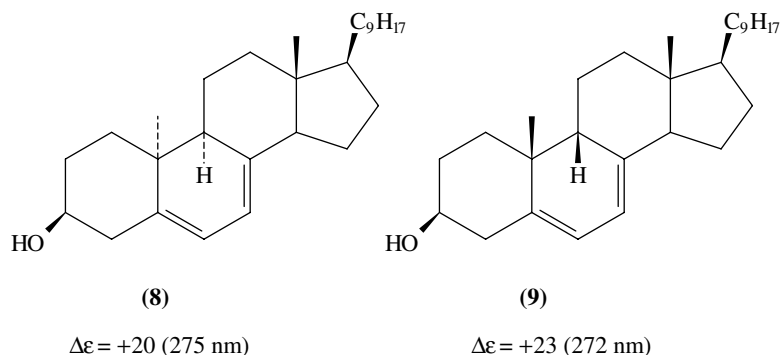


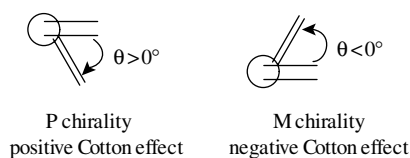
FIGURE 4. UV (upper curve) and CD (lower curve) spectra of **7** (continuous line). Reprinted from Reference 13, with kind permission from Elsevier Science Ltd, The Boulevard, Langford Lane, Kidlington OX5 1 GB, UK

The diene chirality rule (hereafter referred to as DR) constitutes a simple tool for correlating the sign of the lowest energy $\pi \rightarrow \pi^*$ transition (${}^1A \rightarrow {}^1B$ in C_2 symmetry) of the distorted diene to the chirality (left or right-handed) of the chromophore. The validity of this rule is based on the assumption that the CD of the distorted chromophore is determined by its intrinsic helicity alone and that external dissymmetric perturbations have only minor effects on the optical activity.

This point of view finds its justification in the following observations. Compounds **8** (pyrocalciferol) and **9** (isopyrocalciferol), having *opposite* absolute configurations of the stereogenic centres near the dienes, show ${}^1A \rightarrow {}^1B$ Cotton effects at about 275 nm of the *same* sign and intensity. The reason for this is that only the twist of the chromophore determines the optical activity; in fact the diene moieties are distorted in the same sense in **8** and **9**, as found by X-ray diffraction¹⁶.

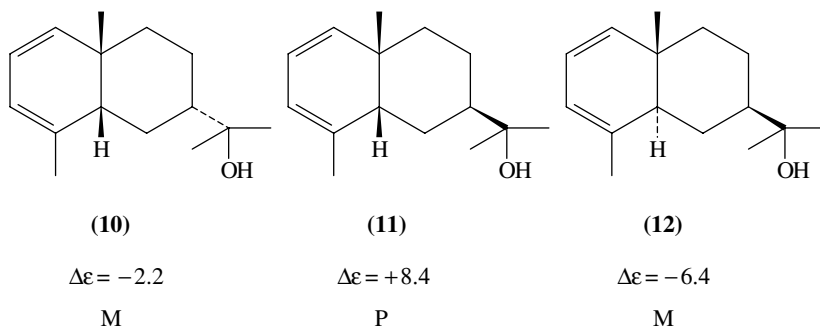


The correlation shown in Scheme 3 has been formulated between the sense of twist and the sign of the ${}^1A \rightarrow {}^1B$ Cotton effect.



SCHEME 3

The diene rule has had much importance in the interpretation of the optical activity of distorted dienes, as in the case of occidantalol, *epi*-occidantalol and *trans*-occidantalol, **10**, **11** and **12**, respectively¹⁷.

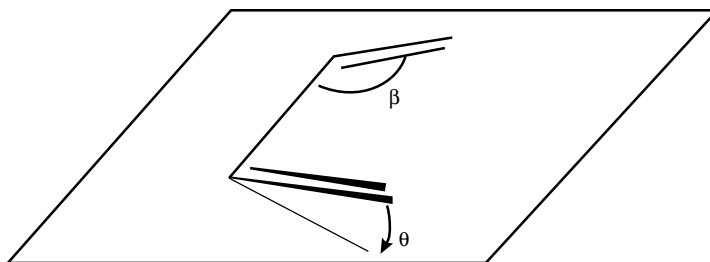


It has been successfully based on various calculations at different degrees of sophistication^{7,18-26}.

a. Theoretical models justifying the diene rule. The rotational strength (R) allied to the longest-wavelength $\pi \rightarrow \pi^*$ transition in twisted butadiene can be calculated according to two simple models: the former uses a molecular orbital approach^{1a,1c,22}, the latter treats the diene as a pair of interacting double bonds, in a coupled-oscillator framework¹⁴. A schematic derivation of the relevant equations is given in the Appendix (Section V). It is interesting to note that these totally independent approaches yield the same result:

$$R_{\pi-\pi^*} \propto \sin^2 \beta \sin \theta \quad (2)$$

according to the definition of the internal angles given in Scheme 4.



SCHEME 4

This means that R is proportional to the sine of the dihedral angle between the two double bonds, with the positive sense defined in Scheme 2. Such a dependence confirms the diene rule because positive angles define positive helicity and imply positive R .

We note that this result is confirmed by the derivation of the rotational strength for a general C_2 chromophore, due to Hug and Wagnière²⁷. They showed, using a pure symmetry token, that the longer-wavelength B transition follows the DR, whereas the higher-energy A transition has opposite sign. This will be shown to have relevant consequences in the case of carotenoids.

The $\sin \theta$ proportionality of $R_{\pi-\pi^*}$ obtained here with two independent, however simplistic, approaches allows us to extend the DR, originally formulated for the cisoid dienes, even to the transoid chromophores, as shown in Scheme 5.

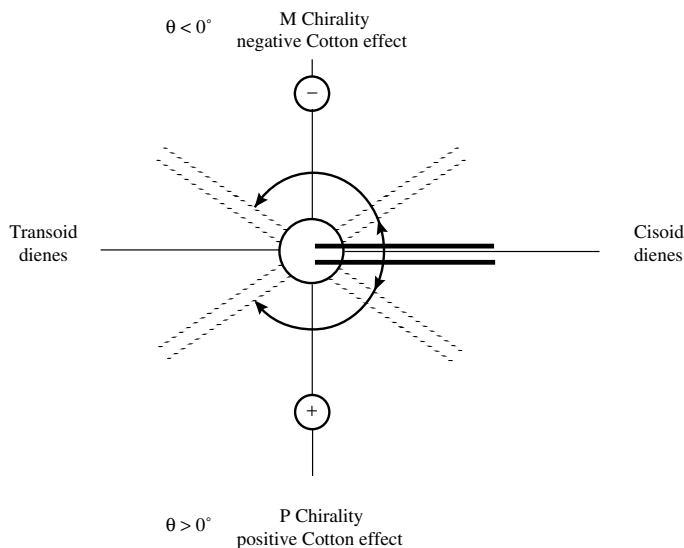
Actually, it is very important to note that this 'general diene rule', covering *s-cis* and *s-trans* systems, has been formulated on the basis of a coupled oscillator model and by means of a simple Hückel MO calculation. More sophisticated MO treatments of the 1,3-butadiene moiety afford contrasting results: while the largest part of the calculations gives positive rotational strengths for all the positive values of θ , in some cases (e.g. CNDO/S²³ and CNDO/2 calculations^{23,28}) anti-DR behaviours (negative R for positive θ) have been reported. The accuracy of the wavefunctions obtained for twist angles around 90° is however questionable, which suggests that reliable results are only for $0^\circ < \theta < 45^\circ$ and $135^\circ < \theta < 180^\circ$ ²⁹.

The problem of interpreting the chiroptical properties of highly distorted dienes remains, however, a different question (see Section II.D.3 below).

2. Allylic axial chirality rule

About 10 years after the first formulation of DR and 5 years after its theoretical justification by Charney, some contradictory results emerged which make its validity questionable.

One of the major problems was the case of the *cisoid* heteroannular dienes^{30,31}, which present a CD band at about 240 nm with a sign opposite to that predicted on the basis of the diene helicity by means of the DR.



SCHEME 5

To account for these cases as well, Burgstahler and Barkhurst developed³⁰ an alternative model for the interpretation of the diene ${}^1A \rightarrow {}^1B$ transition optical activity, focusing their attention on the surroundings of the chromophore. They stated that: '... asymmetric perturbations of the double bond components of the chromophore through excited states interactions with their allylic axial or pseudoaxial bonds (act) as primary factors controlling the sign of the Cotton effect.' This sign should be predictable through analysis of the contributions of the allylic substituents, with the rule (henceforth called AAR) depicted in Figure 5.

With this approach, it is possible to justify the behaviour of a series of compounds, with particular reference to heteroannular *cisoid* dienes, as shown in Figure 6, which exhibit an anti-DR Cotton effect.

Hence, assuming that the axial allylic contribution outweighs that due to the internal twist, the 'anomalous' behaviour of *s-cis* heteroannular dienes is explained.

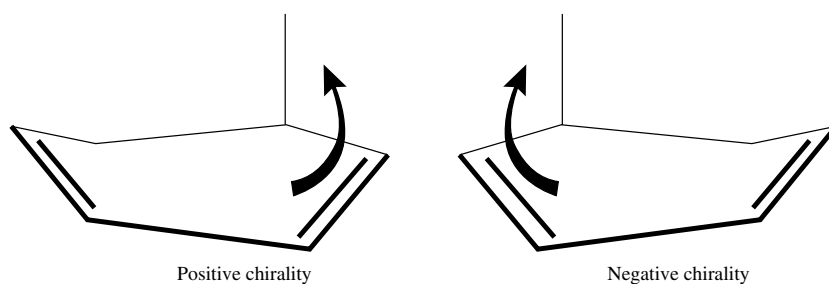


FIGURE 5. On a cyclohexadiene ring, one allylic axial bond has been put in evidence. On the left, it defines a *positive chirality* (right-handed). The reverse holds for the case on the right. This representation is discussed in Section II.D.2.b

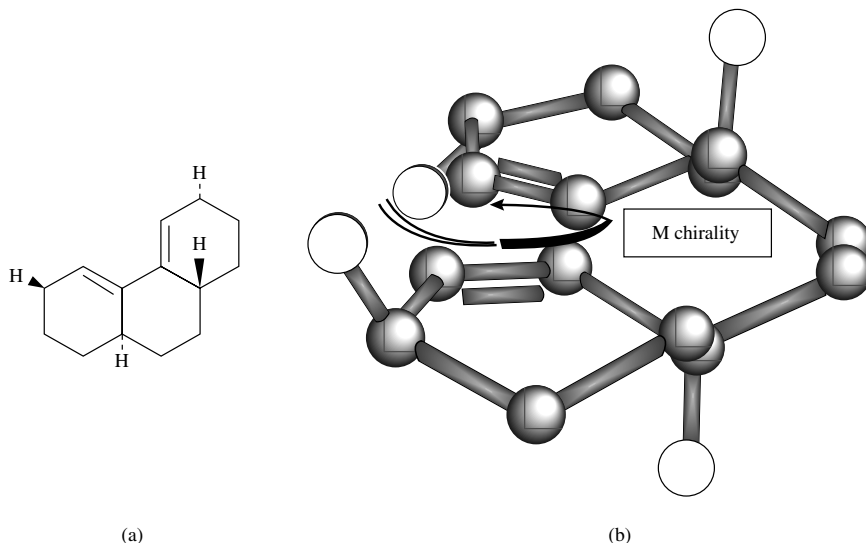
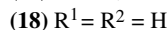
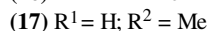
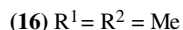
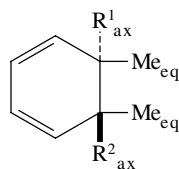
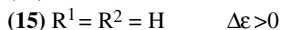
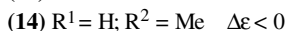
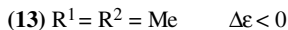
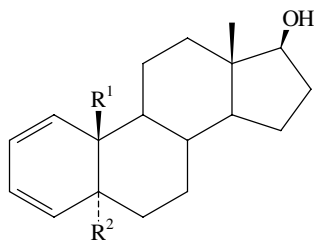


FIGURE 6. A model for heteroannular dienes. In (b) the three-dimensional structure of the molecule shown in (a) is given as an example. The figure indicates that a negative distortion of the conjugated system is allied to a distribution of pseudoaxial substituents (white balls) defining *positive* chiralities according to Figure 5, i.e. positive contributions to the rotational strength of the system

However, an important difficulty is still present: in fact, while for heteroannular *cisoid* dienes the allylic axial contributions are *opposite* in sign to the intrinsic, as depicted in Figure 6, in the case of the homoannular *cisoid* compounds, the two contributions have the same sign, as pointed out already by Burgstahler.

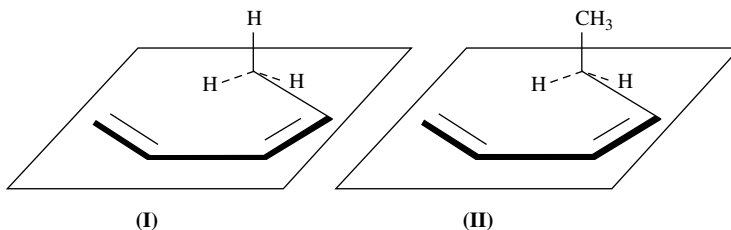
Bearing this in mind, however, it is not possible to interpret the three cases of **13–15**, all characterized by negative diene chirality. If diene chirality and allylic axial contributions act in the same sense, how can we explain a positive $\Delta\epsilon$ for **15**, having M chirality? This question opens the problem of a more thorough evaluation of all the contributions to the diene optical activity.

The relative importance of the intrinsic (twist-related) and external contributions (e.g. stemming from the axial allylic groups) was evaluated for the first time by Rosenfield and Charney²³ who carried out CNDO/S calculations on the model compounds **16–18**.



These molecules are used as models for the steroidal dienes **13**, **14** and **15**. The aim was to clarify the reasons why **15** does not follow the expectations of the DR and the AAR. Geometrical input parameters were taken from X-ray data of a related steroid which represents an exception to the DR. The skew angle for this geometry is 14.4° . The CNDO/S (without CI) calculations successfully predicted the signs and the absolute values of the different rotational strengths. An attempt to rationalize the physical reason of the sign change on passing from **16** and **17** to **18** (and correspondingly from **13** and **14** to **15** for the real compounds) was also made, as summarized below.

In a planar *s-cis*-butadiene the lowest lying $\pi \rightarrow \pi^*$ excited state belongs to a B_2 representation and the related transition from the ground state possesses orthogonal electric and magnetic dipole moments, along y and x directions, respectively. In a chiral *cisoid* diene, R arises from a 'borrowed' magnetic dipole transition moment in the x direction and a 'borrowed' electric moment along y . In these calculations the x and y components of the $\mu \cdot m$ scalar product are of comparable magnitudes and, in the model compounds **16**, **17** and **18**, they have opposite signs. Replacing an allylic axial hydrogen by a methyl, the x component of the dipole velocity operator $\langle \pi | \nabla_x | \pi^* \rangle$ increases and becomes dominant over the y component. This causes the change in sign of R . As this effect arises from an *induced* electric moment, it can be ascribed to the larger polarizability of the C—C compared to the C—H bond. Another important aspect of this investigation is a quantitative evaluation of the allylic axial effect. Calculations were carried out on a *planar* butadiene, bearing either a hydrogen, **I**, or a methyl, **II**, in pseudoaxial position.



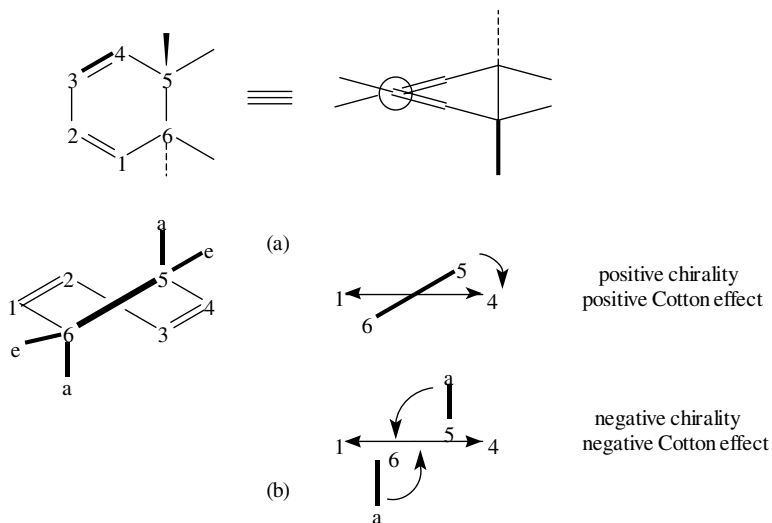
The rotational strength calculated for **I** is as large as that of a butadiene twisted by 20° . In **II**, with an out-of-plane methyl, R increases by a factor of about 2. This shows that the contributions to R of dissymmetric substituents of chiral *cisoid* dienes may be comparable to and even outweigh the contributions arising from the intrinsic dissymmetry of the chromophore.

a. Models in support of the allylic axial chirality rule. Several approaches have been followed to justify the AAR; the most recent, due to Nishio and collaborators, involves CH/ π interactions between the *homoallylic* substituents and the π orbital³². It should be observed that it can be considered in support of the AAR only insofar as in many geometries a substituent in *allylic* relation to a double bond is *homoallylic* to the other. Furthermore, it does not account for non-allylic substituents, whose effect has been demonstrated.

We shall consider here in more detail two models: first a dynamic coupling approach, due to Weigang³³, who considered optical activity deriving from the coupling of electric dipoles (the diene chromophore and the polarizable bonds around it); and second, a localized orbital investigation, which permits one to separate the contributions from the intrinsic diene optical activity and from the axial substituents.

We have tried to express the results of Weigang's treatment in pictorial form (Scheme 6), applying the language of the exciton chirality rules^{1d} to the coupling of the chromophore transition dipole moments with those induced in the nearby bonds. These are regarded

as strongly anisotropic polarizable units, i.e. we assume that the C–C bonds can be described using only a dipole directed along the bond. A substituted cyclohexadiene having M intrinsic chirality has been considered.



SCHEME 6

Inspection of Scheme 6 reveals that:

(a) The dipole of the diene ${}^1A \rightarrow {}^1B$ transition at 260 nm (polarized along C₁–C₄) and the polarizable C₅–C₆ bond define a positive chirality and thus give rise to a positive contribution to CD, as shown in Scheme 6(a). This effect is *opposite* to the intrinsic (dissignate³⁴) contribution.

(b) Two polarizable allylic bonds oriented as shown in Scheme 6(b) define negative chirality with respect to the diene chromophore, so when they couple with the diene transition dipole, they provide a contribution having the same sign as the intrinsic one (consignate³⁴ contribution).

(c) The allylic equatorial bonds give only negligible contributions, since they are almost parallel to the diene transition dipole.

This approach has the merit of providing a reasonably simple explanation of the signs of the different contributions, and also makes it clear that the observed optical activity arises from a balance of several factors. In order to make reliable predictions, it would be necessary to assess quantitatively with the same technique all the contributions, whilst Weigang's approach can only give an evaluation of the external perturbations.

The problem of the quantitative and homogeneous evaluation of the contributions to the CD intensity in a complex diene (i.e. intrinsic chirality, allylic substituents and other perturbers) has been approached by Lightner and coworkers²⁶, from a completely different standpoint: *ab initio* calculations in the localized random-phase approximation (LORPA) for twisted butadiene and several methyl-substituted 1,3-cyclohexadienes — all compounds distorted with P-chirality and a twist angle of 17°. The use of localized orbitals makes it possible to attribute to each group a signed contribution to the total calculated rotational strength for the ${}^1A \rightarrow {}^1B$ transition. The results are summarized in Table 1 and lend themselves to the following observations:

TABLE 1. Bond contributions (estimated by LORPA²⁶) to the Cotton effect of the $\pi_- \rightarrow \pi_-^*$ transition in substituted 1,3-cyclohexadiene^a

Contribution	[R]	
Diene	-13	
Bond (5,6)	-52	
	if R = H	if R = CH ₃
Bond (5,a)	+60	+97
Bond (5,e)	-3.5	-13.5

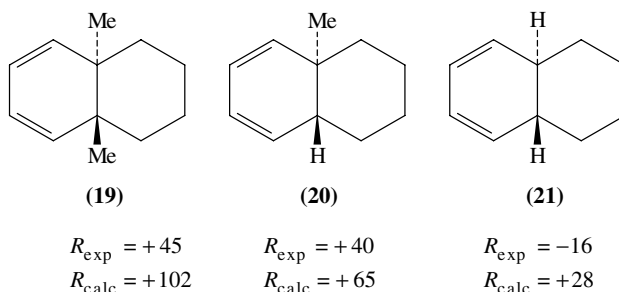
^aThe numbering is that of Scheme 6; R is the substituent occupying the positions a or e.

(a) The intrinsic diene contribution, which is calculated positive (i.e. following the DR) for 1,3-butadiene, becomes negative (anti-DR) in cyclic systems.

(b) The bond *opposite* to the diene gives a large anti-DR contribution.

(c) Allylic axial C–H bonds give smaller contributions than C–C, but both are pro-DR. These conclusions agree with those previously indicated and possibly solve the problem of how to predict the rotational strength, at least for homoannular *cisoid* dienes. In fact, using the values reported in Table 1, Lightner and coworkers calculated *R* for some alkyl substituted 1,3-cyclohexadienes, like **19** and **20**, all with P-chirality, in substantial agreement with the experiments.

In spite of these successes, however, the problem is still open because, using the same group contributions, the wrong sign is calculated for **21**, as already observed by Lightner and coworkers²⁶. Apparently, even such sophisticated calculations cannot give the correct weight to single contributions, over- or underestimating some of them, which makes it impossible to make the right assessment in all cases.

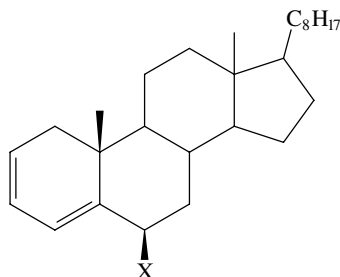


b. Problems in the definition of the allylic axial rule. In the original formulation of the allylic axial rule by Burgstahler and Barkhurst³⁰, the contribution of a substituent to the diene CD is due to the ‘asymmetric perturbations of the double bond components’, i.e. the helicity of the system is defined according to the relative disposition of the perturber and the nearest double bond.

On the other hand, from a spectroscopic point of view it is more correct to consider the diene moiety as a whole. Therefore, it seems that the allylic contribution can be evaluated using two different points of view: the ‘olefin-picture’ (the former) and the ‘diene-picture’ (the latter). This difference has important consequences. In fact, in a vast majority of cases these two pictures lead to the same result, whilst in some instances the two predictions can be opposite. Let us consider the three possible different geometries of

allylic axial substitution, as indicated in Figure 7, where, for each case, the olefin-picture is put above and the diene-picture below. In Figure 7(a) the molecular geometry is such that the two points of view provide the same result: positive allylic helicity and positive CD is predicted. In Figure 7(b) and (c), on the contrary, the olefin-picture should lead to a negative CD, the diene-picture to a positive CD.

Gawroński and Gawrońska³⁵ observed this ambiguity and studied the case represented in Figure 7(b), analysing the following compounds, all characterized by P diene helicity.



X	$\Delta\epsilon$	λ
H	+12.6	(265)
OH	+17.5	(264)
NHAc	+26.3	(264)

It is apparent that on increasing the polarizability of the allylic axial substituent, the Cotton effect becomes stronger. If we refer to the nearest double bond, however, the chirality defined by the C–X bond is *negative*, thus we should expect a *decrease* of $\Delta\epsilon$. Only by considering the diene as a whole (diene-picture), as depicted in the lower part of Figure 7(b), can one justify the reported trend.

Another, very notable, case where the two definitions are in conflict is that of heteroannular *cisoid* dienes. As we have mentioned, this was just the class of molecules that stimulated the introduction of the AAR. Here, in order to have the correct results one should refer the chirality of the axial substituent to the individual double bonds (olefin-picture), as depicted in Figure 6 and in the upper parts of Figure 7(b) and (c). The case of heteroannular dienes is anyway peculiar, because in these compounds the chromophore is unusually distorted. This case is treated in the following section.

3. Strongly distorted dienes

We can collect here two classes of molecules, characterized by very large skew angles, between 40° and 90°. Such a situation is found in the first instance in heteroannular dienes.

a. Heteroannular s-cis-dienes. These compounds (e.g. **22** and **23**) are usually reported to have skew angles around 40–50°.

As anticipated in Section II.D.2, for these molecules anti-DR optical activity is generally found, in agreement with the ‘olefin-picture’ of AAR. Charney and coworkers³⁶ proposed an inverse rule: the inversion of sign was attributed to some change in the electronic properties of the diene when the angle θ becomes large. Indeed, as pointed out at the end of Section II.D.1, there is no general agreement within the computational results, neither on the magnitude nor on the sign of the Cotton effect allied to the longest π – π^* transition of dienes with skew angles larger than 40°. Furthermore, the strong distortion

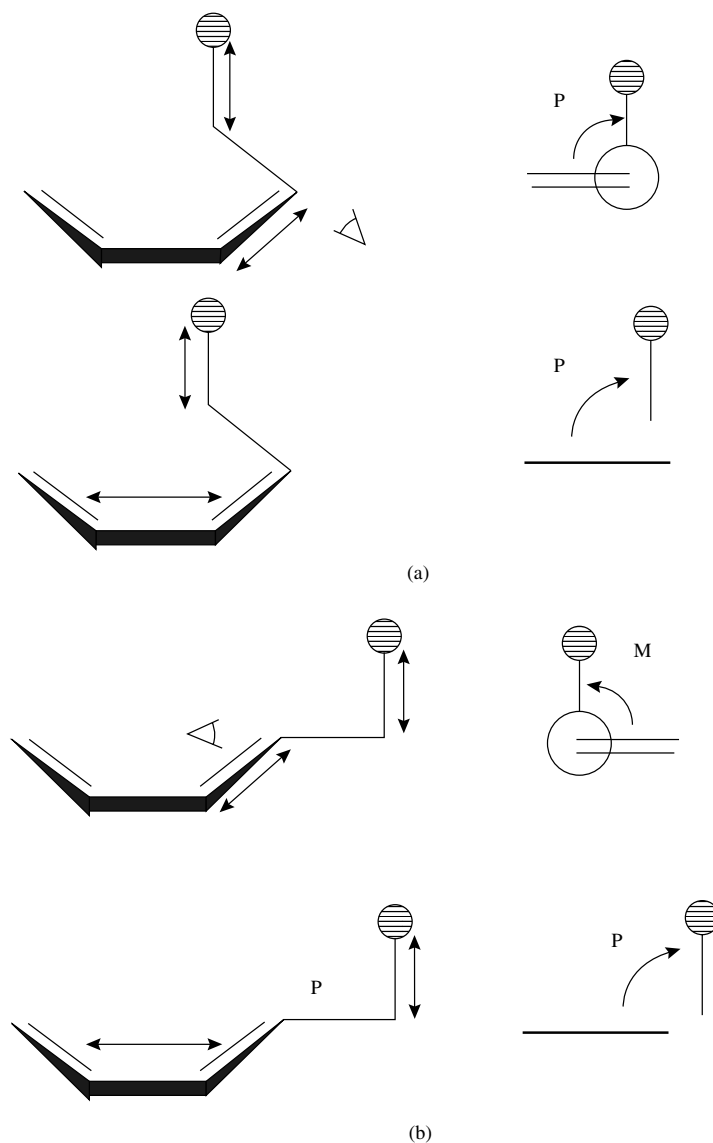


FIGURE 7. The two definitions of the allylic axial chirality rule for the three possible positions of the substituent represented by the shaded circle. For each case the upper part of the Figure represents the original proposal (olefin-picture) and refers to the orientation of the substituent with respect to the nearest double bond; the lower part indicates the 'diene-picture', which takes into account the actual location of the transition dipole. To make the drawings clearer, a planar diene has been considered and, on the right, the projections have been shown. In (a) is shown the case where the two definitions give the same result (P-chirality in this case). This is, for example, the case of a homoannular allylic axial substituent. In (b) and (c), the two definitions lead to different conclusions: M-chirality for the olefin picture, P-chirality, again, for the diene picture. The latter two instances can only be found when the axial substituent is on a different ring from the diene. It should furthermore be noted that knowledge of the exact location of the transition dipole is essential in case (b) for the 'diene-picture'

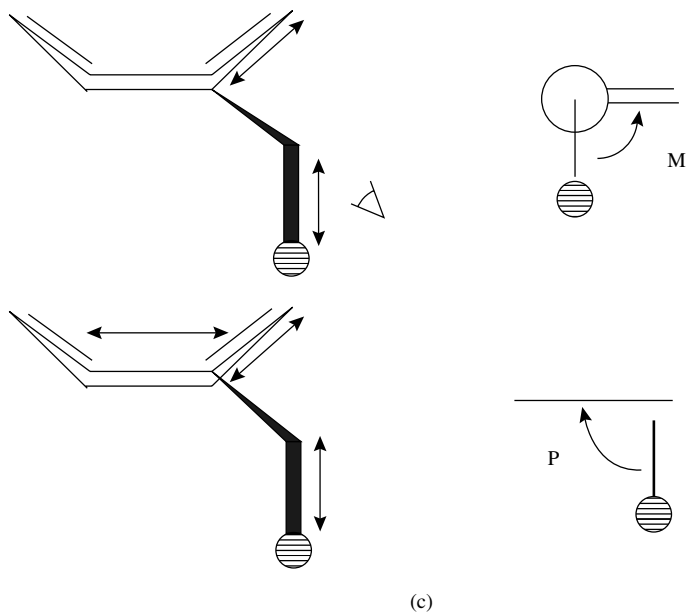
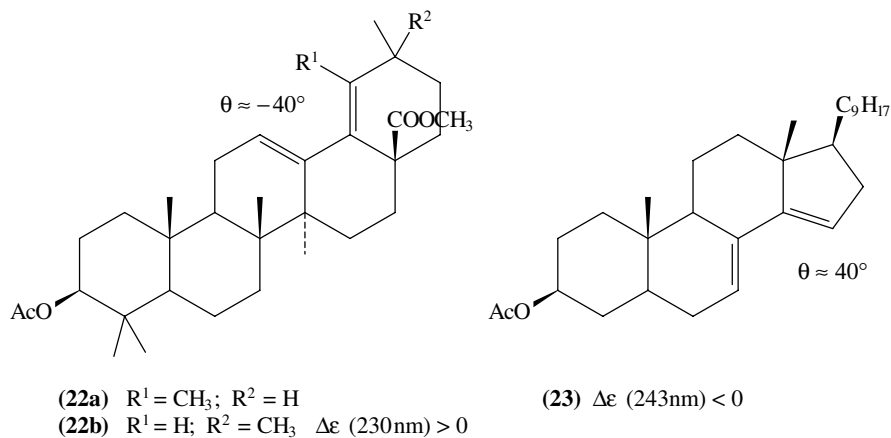
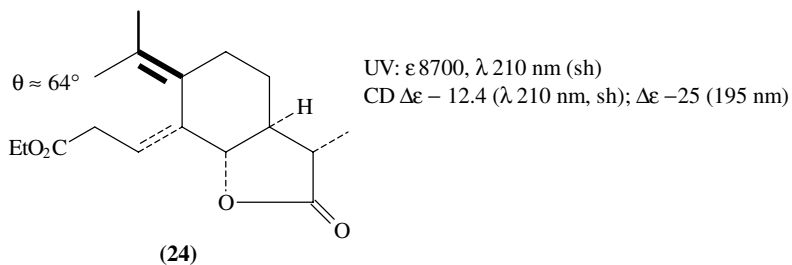


FIGURE 7. (continued)



could imply a substantial reduction of conjugation in the π -system, which might become better represented by the individual olefins than by a whole chromophore. It should be pointed out, however, that the experimental evidence (in terms of absorption wavelength) for such an interpretation is rather weak (see below).

b. Highly twisted s-cis-dienes. A typical example of a very distorted diene is photosantonin³⁷ (**24**), which presents a twist angle of 64° in the solid state as determined by X-ray diffraction.

TABLE 2. Structural (molecular mechanics) and spectral parameters of selected distorted dienes^a

Compound	Chirality	θ (deg)	UV CD	Double bond torsion angle (deg)
 (25)	P	+3.7	ϵ 4300 (sh), 224 nm [R] -3.9, 246 nm	6.8
 (26)	P	+22.7	ϵ 8300 (infl), 220 nm [R] -9.6, 224 nm	18.9 19.0
 (27)	M	-1.5	ϵ 13100, 249 nm [R] 1.98, 250 nm	4.0
 (28)	M	-16.3	ϵ 10100, 249 nm [R] 3.3, 257 nm	-15.4 -14.9

^aThe angle θ is defined according to Scheme 2, the exact definitions of the angles in the last column, describing the double bond torsion, being given in Reference 38. Here we note only that 0° torsion means a planar olefin. The values are reported only for dimethyl-substituted double bonds.

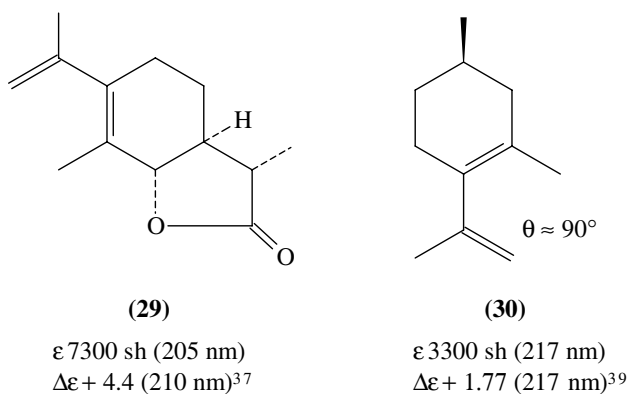
The most striking spectroscopic characteristics of this compound are: (i) there is only a shoulder at about 210 nm in the UV spectrum, which implies a substantial lack of conjugation and brings about further experimental evidence of the large skew angle; (ii) a strongly negative Cotton effect is associated with the P-chirality of the chromophore. The latter observation has been considered an experimental support for an anti-DR behaviour of highly twisted *cisoid* dienes. More recently, Lightner and coworkers³⁸ prepared and studied the CD spectra of a series of distorted dienes, the most relevant of which are reported in Table 2.

The authors pointed out that for M-distorted dienes a positive CD is found, while the P-distorted dienes show a negative CD, supporting the above correlation.

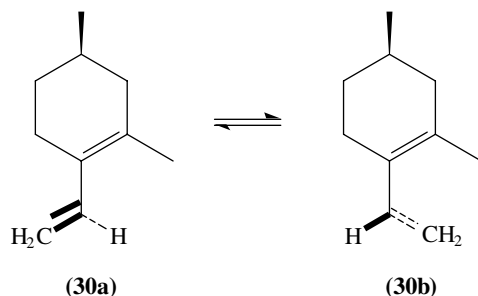
These results deserve comment. First of all, the chemical structure of photosantonin, **24**, is really complex, in particular the lactone chromophore (which, examining the molecular model, appears quite distorted) could contribute strongly to CD, making very difficult the correct assignment of the true CD of the highly distorted diene chromophore. In addition, as far as Lightner's dienes are concerned, it must be observed that in general the molecular mechanics (MM) results reported do not provide high values of the twist angle θ (the maximum is about 23°), nor do the compounds derived from camphor show the spectroscopic behaviour typical of a highly twisted diene. An examination of the conformational analysis carried out by Lightner reveals other interesting aspects. In the case of diene **28**, there are two almost degenerate minimum energy conformations (separated by about 0.4 kcal mol⁻¹) which must both be significantly populated but *show opposite intrinsic chirality*.

Furthermore, for both **28** and for **26**, MM calculations indicate that even the individual double bonds are highly twisted (15–20°). This could be (*vide infra*) a further mechanism giving rise to optical activity of the π - π^* transition of the diene chromophore.

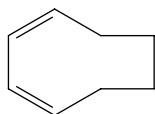
Other interesting examples of highly distorted dienes are **29** and **30**. In these cases there is a further difficulty. For **30**³⁹, for instance, two low-energy conformations in equilibrium are possible: These two conformations are differentiated essentially by the interaction between the methyldiene groups and the equatorial and axial hydrogens on the ring.



It is apparent that the π systems in **30a** and **30b** are distorted in opposite senses. The measured rotational strength is thus the weighted average over these two conformations, which depends on the relative populations as well as on the individual rotational strengths.



A peculiar case of a strongly distorted diene is represented by *cis,trans*-1,3-cyclooctadiene⁴⁰:



The main interest of this molecule resides in the fact that the principal source of rotational strength of the $\pi \rightarrow \pi^*$ lowest energy transition has been attributed⁴⁰ to the twist of one of the two double bonds ($\alpha = -136^\circ$, as in *trans*-cyclooctene) rather than to the twist of the 1,3-butadiene moiety ($\theta = +50.2^\circ$)

4. *Transoid dienes*^{21,35}

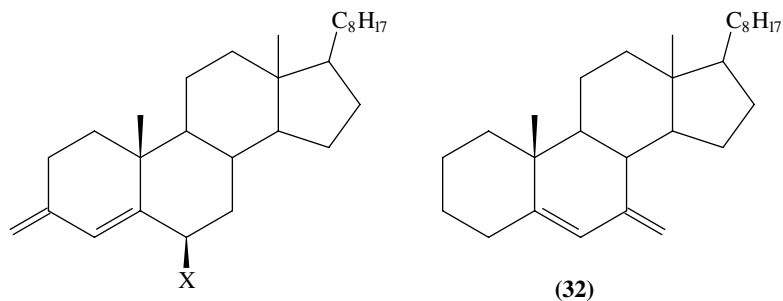
Dienes in quasi-*s-trans* conformation are found only in cyclic structures where perfect planarity is hindered. The DR also holds valid for this kind of conformation, as demonstrated by the considerations of Section II.D.1.a and also confirmed by all the reported calculations. Indeed, contrary to what is sometimes found for *cisoid* systems, the rotational strength evaluated by many types of calculation is invariably found to follow the diene rule for *transoid* systems. However, very small skew angles are usually found in real molecules and this implies that the main contribution to the observed optical activity cannot come from the weak intrinsic distortion, but is more likely to stem from the dissymmetric perturbations, notably of the allylic axial substituents.

A few examples will illustrate the case. The parent *trans*-diene derivatives **31a** and **32**³⁵ have nearly planar chromophores, but the Cotton effects are quite strong and opposite in sign (+15 and -27.9, respectively). This can be attributed mainly to the allylic axial C-CH₃ bonds, which provide a positive contribution for compounds **31** and a negative for **32**. Furthermore, the $\Delta\varepsilon$ values of P-chiral *s-trans*-**31** are strongly dependent on the polarizability of the allylic C-X bond.

5. Conclusions on skewed dienes

The interpretation of the optical activity of these compounds is rather debatable and no single theory seems to effectively accommodate the whole variety of cases.

The intrinsic contribution, accounted for by the diene rule, seems to be easily outweighed by the perturbations arising from the allylic axial substituents, which in turn define the allylic axial chirality rule. This latter can be formulated in two ways: The 'olefin-picture', where chirality is referred to the nearest double bond, and the 'diene-picture',



	X	$\Delta\epsilon$	λ (nm)
31a	H	+15.0	(237)
31b	OH	+7.85	(239)
31c	NHAc	+0.8	(253)

$$\Delta\epsilon = -27.9 \text{ (238 nm)}$$

which considers the electric-dipole transition moment of the diene chromophore as a whole.

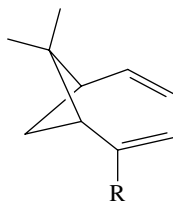
The two representations lead to the same result in the majority of the cases studied so far, where agreement with experiment is rather good and there are only few exceptions. The cases in which the two pictures are in conflict can be divided into two classes: strongly versus 'normally' distorted dienes ($\theta \geq 30^\circ$). The former is typified by the heteroannular dienes, which seem to obey the 'olefin-picture'. The latter, much less well characterized, seems to be better interpreted in terms of the 'diene-picture'.

We consider it rather reasonable to suppose that when the distortion is small the π -electron system is delocalized, justifying the diene-picture; whereas in the presence of large skew angles the contribution of localized double bonds can be much more important, supporting the olefin-picture.

A further mechanism, based on the distortion of the individual olefin plane, has also been proposed⁴⁰, but has received rather little attention. It is possible that its role has been unjustifiedly neglected in many cases.

E. Dienes Owing Their Chirality to a Dynamic Twist¹⁰

Mason and coworkers¹⁰ studied the chiral bicyclic derivatives **2**, **3**, **33** and **34**, having known absolute configuration. These molecules possess a planar *s-cis* diene chromophore and formally their chirality is due to the presence of the D or CH₃ substituents, which rule out all the symmetry planes. However, it is interesting to point out a peculiar structural



(33) R = D

(34) R = CH₃

feature of these compounds with respect to analogous molecules also having a planar *s-cis* diene, like **4** and **5**. While in the latter molecules the C-10 methyl group (i.e. the substituent responsible for the molecular chirality) is displaced from the chromophore at equilibrium, the methyl group bonded to the diene moiety of **2** and **34** lies *in the plane* of the diene, at least in the equilibrium conformation. In this case, therefore, the origin of optical activity of the planar diene chromophore cannot be found in a simple interaction between the chromophore itself and the substituent responsible for the overall molecular chirality. The detailed analysis of the absorption and CD data carried out by Mason and coworkers reveals that there is a chiral distortion of the diene chromophore in **2**, **3**, **33** and **34** of dynamic origin¹⁰, i.e. it arises from a vibrational mode (or modes) with inequivalent turning points, resulting from the mass difference between the groups occupying the 2- and 3-positions in each of these dienes. The out-of-plane bending modes of the groups in the 2-position of **33** and **34** could be the most effective. As far as **2** and **3** are concerned, it has been observed that the rotatory strength of the $\pi \rightarrow \pi^*$ in **2** is some 7 times larger than that of the deuterio derivative **3**, a factor close to the mass ratio of the substituents replacing hydrogen in the parent diene. This relation suggests a common vibronic perturbation of the symmetric diene chromophore in **2** and **3**.

F. External Dissymmetric Perturbation

1. Planar *s-cis*-dienes

When there is no intrinsic chirality, because the internal distortion is completely absent, as for example in **4** and **5**¹¹, optical activity can only arise from the perturbation of the ${}^1A_1 \rightarrow {}^1B_2$ transition, due to the presence around the chromophore of chirally distributed substituents. The origin of optical activity can be found in a dynamic coupling mechanism and in such cases a coupled oscillator treatment (like that of DeVoe^{1,47}) can be used to evaluate $R^{1,41}$. In this approach, a chiral molecule is regarded as a set of suitable subsystems (the chromophore and the perturbers that make it chiral), which are polarized by the external electromagnetic field and are coupled together by their own local fields. The optical properties (absorption, refraction and circular dichroism) can be calculated by taking into account the above interactions among the subsystems. Of course, for this purpose, each subsystem has to be fully characterized in terms of one (or several) oscillators, representing an electric-dipole-allowed transition defined by the polarization direction \mathbf{e}_i and the complex polarizability $\alpha_i(\tilde{\nu}) = R_i(\tilde{\nu}) + iI_i(\tilde{\nu})$. Here, $I_i(\tilde{\nu})$ can be obtained from experiment, i.e. from the absorption spectrum of compounds which can be considered good models of the subsystem; $R_i(\tilde{\nu})$ can be calculated from $I_i(\tilde{\nu})$ by means of a Krong–Kramers transform. A molecule like **4** (or **5**) can be considered as the aggregate of only two subsystems: the chromophore (i.e. the *cis*-diene moiety) and a perturber, which, for symmetry reasons, can be found in the C–C bond linking the methyl group to the bicyclic skeleton. Each of these groups can be represented by a single oscillator: the former is polarized along the line joining the midpoints of the double bonds and the latter along the C–CH₃ axis. As for the values of $I_i(\tilde{\nu})$ and $R_i(\tilde{\nu})$, a Lorentzian polarizability of $25 D^2$ centred at 250 nm gives a satisfactory representation of the absorption band of the *cis*-diene chromophore, while to describe the polarizability of the C–CH₃ bond a Lorentzian polarizability of $2 D^2$ at 134 nm is known to be reasonable^{41b}.

At this point we have the geometrical and spectroscopic parameters necessary to calculate $\Delta\varepsilon(\tilde{\nu})$ from the general DeVoe equations^{41a}. In the present case of two different oscillators we have

$$\Delta\varepsilon(\tilde{\nu}) = 0.014\pi^2 N \mathbf{e}_1 \times \mathbf{e}_2 \cdot \mathbf{R}_{12} G_{12} \tilde{\nu}^2 [I_1(\tilde{\nu})R_2(\tilde{\nu}) + I_2(\tilde{\nu})R_1(\tilde{\nu})] \quad (3a)$$

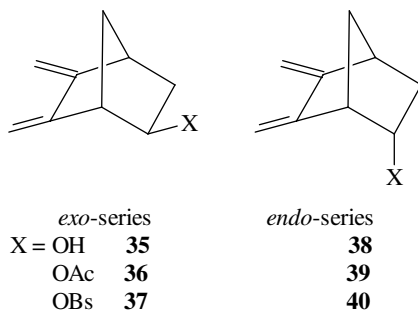
$$G_{12} = \left(\frac{1}{r_{12}} \right)^3 [\mathbf{e}_1 \cdot \mathbf{e}_2 - 3(\mathbf{e}_1 \cdot \mathbf{e}_{12})(\mathbf{e}_2 \cdot \mathbf{e}_{12})] \quad (3b)$$

Here \mathbf{e}_1 and \mathbf{e}_2 are the unit vectors of oscillator 1 (the diene chromophore) and 2 (the C-CH₃ dipole), respectively; \mathbf{R}_{12} is the vector joining their midpoints, G_{12} is the point-dipole interaction term and N is the Avogadro number; all quantities are expressed in c.g.s. units. In the absorption region of the chromophore, where the perturber does not show a significant absorption, the above formula reduces to the simpler equation^{41c}

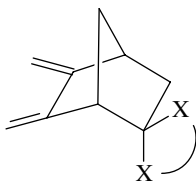
$$\Delta\varepsilon(\tilde{\nu}) = 0.014\pi^2 N \mathbf{e}_1 \times \mathbf{e}_2 \cdot \mathbf{R}_{12} G_{12} \tilde{\nu}^2 I_1(\tilde{\nu}) R_2(\tilde{\nu}) \quad (4)$$

In this way, a $\Delta\varepsilon$ value of -0.57 is calculated at 250 nm, as compared with an experimental value of -0.63 . This excellent agreement between the experimental and calculated values is a strong indication that a dynamic coupling mechanism is the major source of optical activity in these molecules.

Another group of chiral dienes where a planar *s-cis*-1,3-butadiene chromophore is present, is that of the compounds **35–40** prepared by Sonney and Vogel⁴². These compounds have the general structures indicated below.



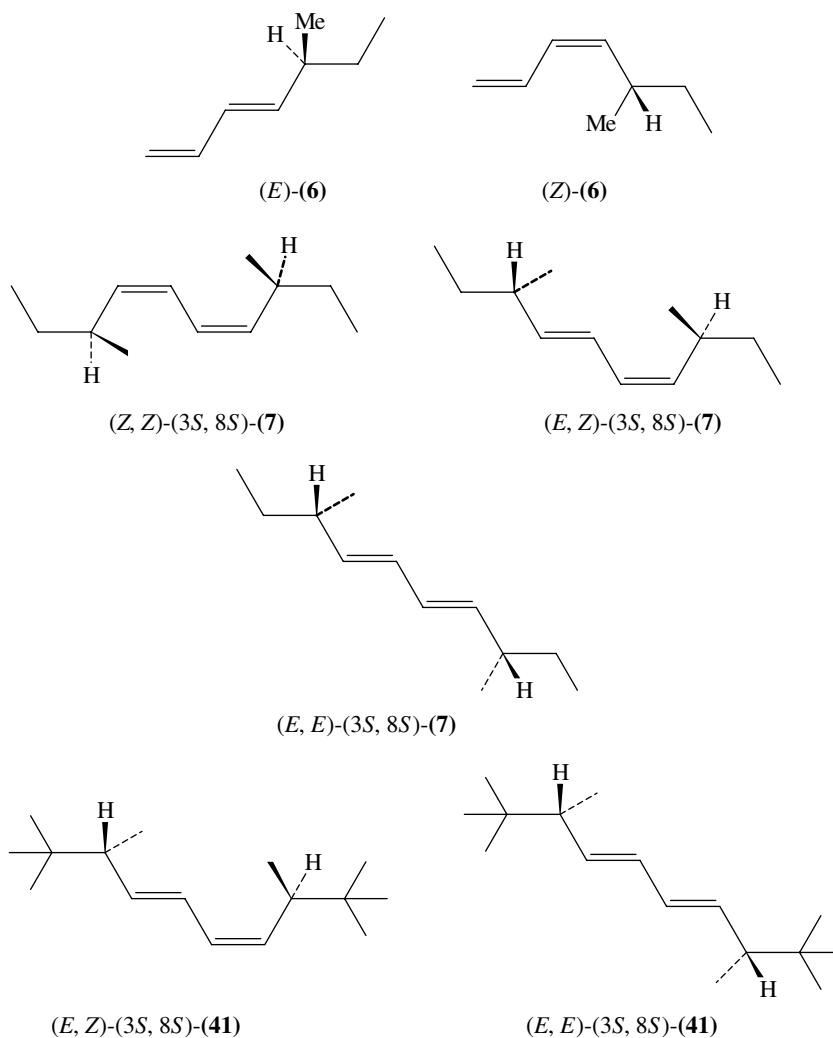
The CD spectra of the dextrorotatory isomers of **35–39** show a weak positive band corresponding to the lowest π - π^* transition (${}^1A_1 \rightarrow {}^1B_2$) of the *s-cis*-butadiene. Their behaviour is strictly analogous to that of **4** and **5**. The sign of the CD band can be predicted by taking into account the interaction of the diene dipole with that on C-X. The spectrum of **40** is complicated by the presence of a couplet-like feature, probably resulting from the coupling of the diene and the brosylate (OBs) chromophore. In a more recent paper, Vogel and coworkers⁴³ describe the CD data of several 5,6-dimethylidenebicyclo[2.2.1]hept-2-yl derivatives, having the general formula



Unfortunately, no general rule can be proposed for interpreting the experimental data. In particular, if the substituent at C(2) is a π -system, different from >C=O , the Cotton effect associated with the ${}^1A_1 \rightarrow {}^1B_2$ transition of the *cis*-diene is opposite in sign to that of the exciton chirality of the two homoconjugated π -chromophores.

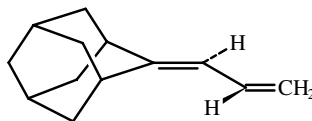
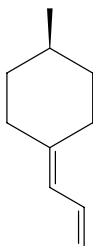
2. Planar *s-trans*-dienes

The first report of the chiroptical properties of a planar *s-trans*-diene chromophore is due to Di Corato¹², who described the CD data of (+)-(*S*)-**6**, which shows a positive weak ($\Delta\epsilon \approx +0.2$) Cotton effect at about 220 nm, in both the *E* and *Z* isomers. Lardicci and coworkers¹³ described in 1978 the absorption and CD spectra of the planar *s-trans*-diene derivatives **7** and **41**.



These compounds show typical *s-trans*-1,3-butadiene absorption bands between 230 and 235 nm, with $\epsilon_{\max} \approx 30000$. In correspondence, the CD spectra show an intense ($\Delta\epsilon \approx 3-5$) Cotton effect, positive for the (*S*) absolute configuration of the chiral centres. It is noteworthy that if one considered (*E*)-(*S*)-**6** as a 'half' of (*E, E*)-(3*S*, 8*S*)-**7** a value of $\Delta\epsilon$ of about 0.4 would be predicted: the actual $\Delta\epsilon$ of +3 is one order of magnitude larger!

An interesting series of *s-trans* planar dienes is that due to Walborsky and co-workers^{44,45}. They prepared and studied the chiroptical properties of several compounds where the diene moiety is linked to a chirally substituted ring, such as **42** and **43**.



(42): (*aR*)-(+)-(4-methylcyclohexylidene)propene $\epsilon_{237.5} = 24300$
 $\Delta\epsilon_{237.5} = + 3.7$

(43): (*aS*)-(-)-(5-methyladamantylidene)propene $\epsilon_{240} = 30600$
 $\Delta\epsilon_{236} = -0.45$

Walborsky and coworkers⁴⁴ proposed a sector rule, the planar diene rule, to correlate the sign of the ${}^1A_g \rightarrow {}^1B_u$ transition Cotton effect of these derivatives with the absolute configuration and, in addition, they provided a qualitative interpretation of the CD data of the molecules by means of the two-group electric-dipole mechanism^{44c}. Later on, in

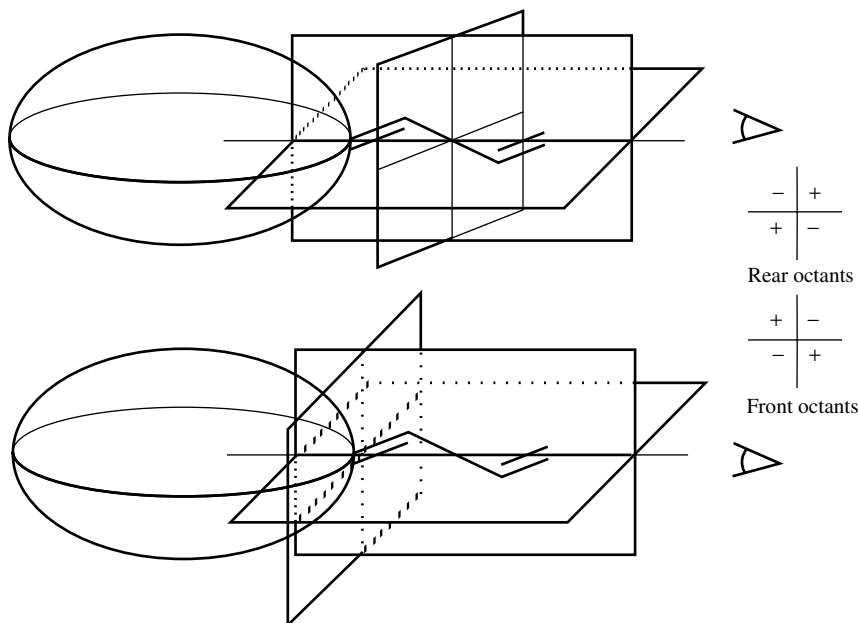


FIGURE 8. Sector rules for exocyclic *s-trans* dienes. Top: 'bond-centred', bottom: 'atom-centred' rule. The ellipsoid represents the rest of the molecule and also defines the direction opposite to the observer. In both cases two planes are defined by the transition dipole and the plane containing the diene; only the third plane is located differently. The 'bond-centred' rule holds for cyclohexylidene compounds, while the 'atom-centred' rule should apply to adamantylidene derivatives

1988, Walborsky, Reddy and Brewster⁴⁵ introduced a more complex empirical rule, which replaced the first one. The space around the chromophore is divided into sectors by the plane of the diene, the plane perpendicular to it and containing the transition moment (usually directed along the line C_1-C_4) and a third plane. The latter has been placed either in the middle of the diene (the so-called bond-centred model) or on the end atom of the chromophore, the one inserted in the ring (atom-centred model). The signs of the contributions to CD of the various substituents are given in Figure 8.

In spite of the practical usefulness of such empirical sector rules, the physical origin of the optical activity in these molecules remains an open question. In fact, polarizability calculations^{41c} (both by means of the Weigang amplified sector rule for allowed transitions and the DeVoe dynamic coupling model), taking full account of the interaction between the $^1A_g \rightarrow ^1B_u$ transition dipole and the polarizable matter around it, give the wrong sign. The correct sign and order of magnitude for this Cotton effect can be reproduced only by assuming the existence of a very small (less than 5°) distortion of the chromophore; this is in conflict with the results of MM and *ab initio* calculations, which clearly indicate the presence of a planar *s-trans* chromophore^{41c}.

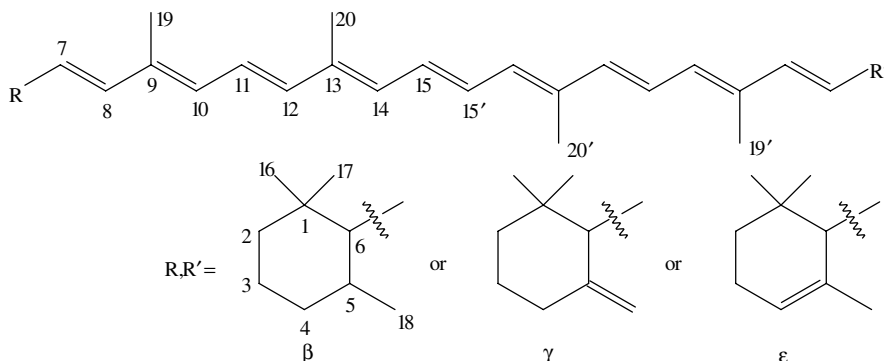
These observations suggest an interesting question: can CD spectroscopy be so sensitive to minute conformational details as to challenge apparently sophisticated computational methods?

III. POLYENES

A. Carotenoids

1. General aspects

Carotenoids are natural compounds characterized by a conjugated polyenic chain connecting two terminal groups, as represented in Scheme 7. Terminal groups can be of different natures; they often contain a cyclic double bond and allow one to classify carotenoids.



The two terminal groups, R and R', are in most cases totally responsible for the chirality of carotenoids, which can thus be further classified into the three categories: *homodichiral*, with two identical end groups, of symmetry C_2 ; *heterodichiral*, with two different end groups; or *monochiral*, with one chiral and one achiral terminal group. Naturally, the chiral terminal groups are responsible for the CD of these molecules, a subject which

has been recently thoroughly reviewed by Buchecker and Noack⁴, Liaaen-Jensen^{46a} and Noack^{46b}. A few general statements have been found true for the CD of carotenoids:

1. Carotenoids with one or two terminal groups containing a double bond formally conjugated with the polyenic chain have conservative CD spectra, i.e. in the region of $\pi-\pi^*$ transitions (220–500 nm) there are 5 or 6 maxima of opposite signs, whose intensities add up to zero.

2. The signs of the bands in conservative spectra of *all-trans* forms are opposite to those of the corresponding derivatives containing one *cis* double bond (the spectra of di-*Z* compounds are analogous to the *all-trans*).

3. Molecules having terminal groups with non-conjugated double bonds feature non-conservative spectra.

4. The effects of terminal groups are additive.

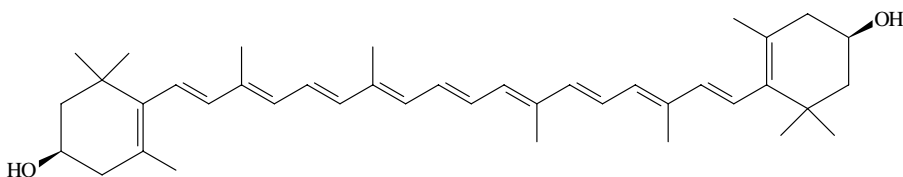
5. The CD spectra are strongly temperature-dependent.

2. Origins of the optical activity⁴⁷

Carotenoid spectra are characterized by several absorptions in the normally accessible range of UV-Vis spectrometers. In fact, the large number of conjugated double bonds creates a manifold of easily accessible excited states. Fortunately, some features of the diene spectroscopy are retained, which allows one to correlate, at least in some cases, the CD to conformation and configuration by simple symmetry tokens. As long as we can recognize a C_2 symmetry of the chromophoric system, the lowest-lying excited state belongs to a *B* representation, just as in 1,3-dienes. The other $\pi-\pi^*$ excitations are often alternately *A* and *B*. The *A*-type transitions are electrically polarized along the C_2 axis, the *B*-type are polarized parallel to the chain. They have opposite rotational strengths and thus give rise to the typical feature of CD of carotenoids with alternating signs.

In order to deal with one transition of a specific symmetry, that of longest wavelength ${}^1A \rightarrow {}^1B$ is usually chosen.

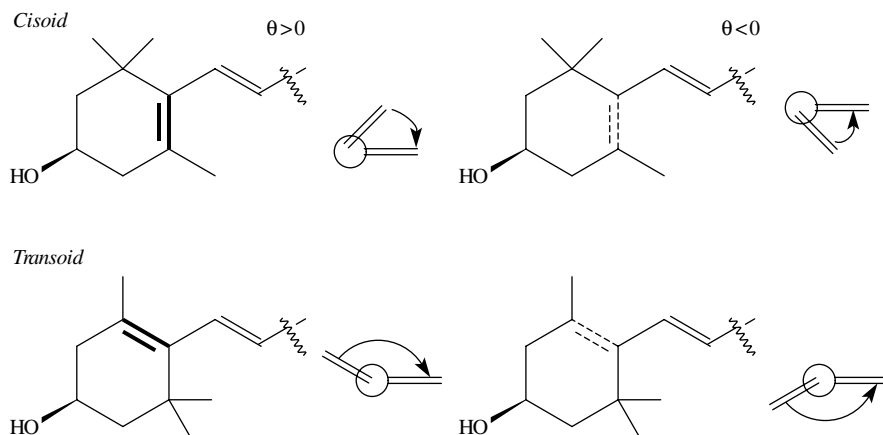
Let us consider a carotenoid system having a β end group, i.e. a molecule with the possibility of conjugation between the terminal double bond of the polyenic chain and the ring double bond, for example zeaxanthin, **44**.



(44)

The planar conformations *s-cis* and *s-trans* cannot be appreciably populated owing to the repulsive steric interaction between the C_8-H and C_5 -methyl (in the *s-cis*) or between the same C_8-H and the methyl group on (C_1 in the *s-trans*). This repulsion is minimized by introducing a twist around the C_6-C_7 bond. Limiting conformations, with skew angles of about $\pm 40^\circ$ and $\pm 140^\circ$, can be assumed, as shown in Scheme 8. In this way, an intrinsically dissymmetric chromophore is created.

Owing to the presence of the substituent in position 3 of the cycle, this assumes the more stable chair conformation with the substituent in the equatorial position: the other one, with the substituent axial, is about 1 kcal mol^{-1} less stable.



SCHEME 8

The two twisted conformations discussed above are thus in a diastereoisomeric relationship, one being more populated than the other. Molecular mechanics calculations show that in the case of zeaxanthin the most stable conformation by about $0.3\text{--}0.4\text{ kcal mol}^{-1}$ is that depicted in Figure 9.

The optical activity of such a molecule has been interpreted using a model that stresses the similarity with a twisted butadiene. The long and planar polyenic chain formally acts as the bond (2,3) in a 1,3-butadiene, as long as it allows conjugation between the two terminal double bonds. The same considerations regarding the distortion of the chromophore and the sign of the rotational strength of the longest-wavelength transition should therefore apply. This means that the optical activity is expected to follow the diene rule, presented in Section II.D, with reference to the helicity defined by the two terminal double bonds.

The CD spectrum of such a structure can be predicted as follows, once we represent this conformation as in Figure 10.

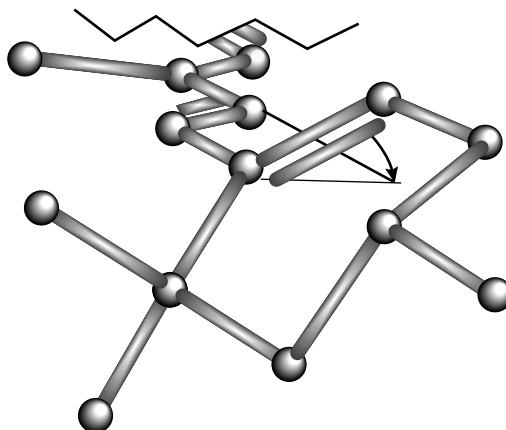


FIGURE 9. Molecular mechanics most stable conformation for zeaxanthin (**44**) showing a positive twist of about 40° between the first two double bonds

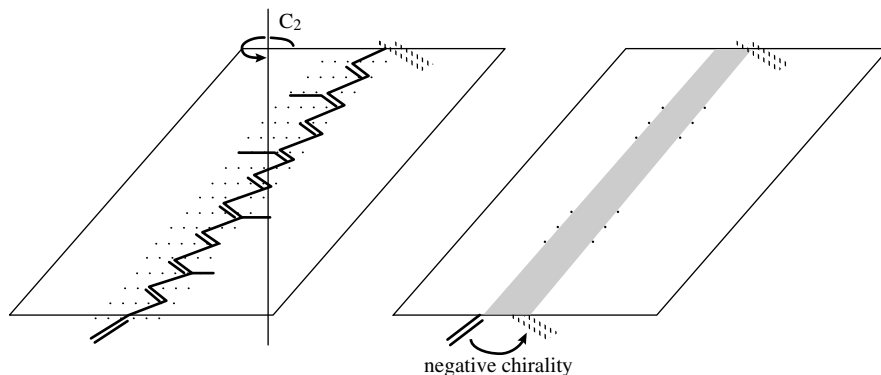


FIGURE 10. On the left is shown the conjugated system of *all-trans* zeaxanthin (**44**) in its most stable conformation. On the right, the planar part of the system is represented as a grey band to make clearer the similarity with a 1,3-butadiene

The terminal double bonds define a *trans*-butadiene with negative helicity, for which the ${}^1A \rightarrow {}^1B$ transition (the lowest-energy $\pi \rightarrow \pi^*$ excitation) is predicted to have a negative rotational strength on the basis of the twisted diene rule. This is indeed what is found experimentally. The same considerations explain the change in sign of the CD bands on passing from the *all-trans* to the mono-*cis* systems. The case of 15-*cis*-zeaxanthin is revealing. In Figure 11 we show the relative positions of the double bonds in the most stable conformation of the molecule.

In this situation the two end-ring double bonds define a positive chirality. Application of the twisted diene rule gives a positive sign for the lowest-energy ${}^1A \rightarrow {}^1B$ transition, and in the case of 15-*cis*-(3*R*,3'*R*)-zeaxanthin this is confirmed by experiment.

The behaviour of the CD of (3*R*,3'*R*)-zeaxanthin at low temperature can also be explained on the basis of simple conformational considerations. On lowering the temperature, the most stable form becomes more populated and gives a predominant contribution to the spectrum. Obviously there may be instances where the CD as a function of temperature is much more complicated than that just discussed, one example being (3*S*,3'*S*)-astaxanthin. However, the low-temperature spectra can be interpreted even here by

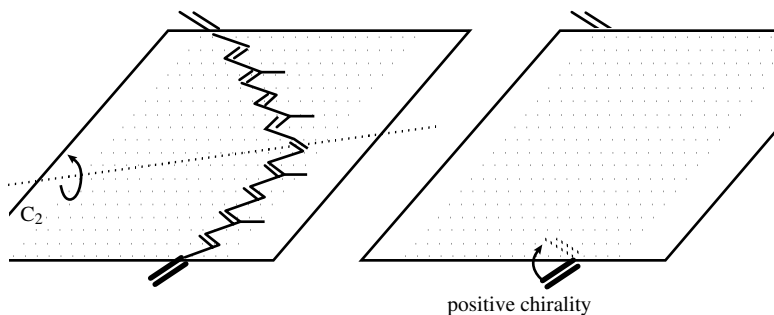


FIGURE 11. In analogy with Figure 10, the conjugated system in the most stable conformation of 15-*cis*-zeaxanthin is depicted, demonstrating the helicity defined by the terminal double bonds of the conjugated chain

means of MM calculations, which show that the most stable conformer again obeys the diene helicity rule. The CD spectra of compounds featuring non-conservative behaviour, i.e. of molecules where a twist of the conjugated system is not present, have not been studied so much and a theoretical interpretation of the spectroscopic data has not been provided so far⁴.

3. Polymers⁴⁸

Polyacetylenes are the most important class of synthetic polymers containing conjugated carbon-carbon double bonds. Some optically active monomers have been used with the following conclusions. Polymers of 1-alkynes having a branched side-chain assume in solution a helical conformation. A chiral side-chain induces a predominant screw sense in these helices. In particular, for alkyl branching, it has been shown that (*S*) monomers lead to a left-handed screw sense.

The CD spectra of polymers of a series of homologue chiral terminal acetylenes⁴⁸ shows a marked dependence on the distance of the asymmetric centre from the triple bond. The relation between the two facts is however unclear, even because the UV spectrum results from the superposition of several bands, owing to the extended conjugation.

IV. OLIGOENES

We have considered so far two extreme cases: the simplest diene chromophore and a long chain of conjugated double bonds, trying to find out a few keys to interpret the relation between structure and chiroptical properties. Intermediate systems, i.e. molecules with a limited number ($2 < n < 10$) of double bonds, have received much less attention in this respect. In fact, they do not constitute a homogeneous class of compounds and any extrapolation would have limited scope. Nevertheless, considerable attention has been devoted to some oligoenes of biological importance, such as the members of the vitamin D and vitamin A families. These molecules often undergo important photochemical reactions and CD spectroscopy has been used to reveal labile intermediates. An example is provided by an unstable rotamer of tachisterol₃, which occurs during the irradiation of previtamin D₃ at 92 K⁴⁹.

The analysis of CD and absorption data has been used since 1974, mainly by Nakanishi and his coworkers, to study the structure of the rhodopsins, pigments involved in the mechanism of vision, and of their chromophores⁵⁰.

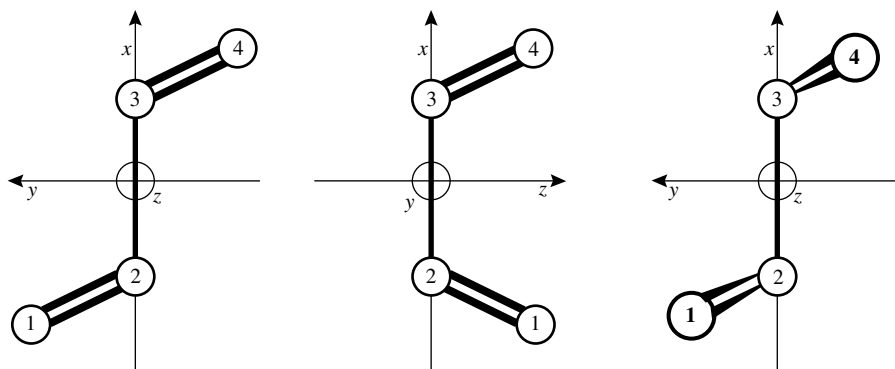
A special field of application of CD to oligoenes is that of some antibiotics, like filipin⁵¹ and amphotericin B⁵². These molecules are characterized by a strong tendency to autoaggregation, which causes the CD spectra to be strongly solvent, temperature and concentration dependent. In fact, in the presence of dimers, the CD is dominated by the appearance of a strong exciton couplet between the polyenic chains of neighbouring molecules.

V. APPENDIX

A. 1,3-Butadiene MOs, Symmetry and Electronic Transitions

Butadiene can exist in two planar conformations, *s-trans* and *s-cis*. They belong to the C_{2h} and C_{2v} symmetry point group, respectively. Obviously, both forms have symmetry planes. A skewed conformation, instead, has only a C_2 axis. We can choose the reference frames depicted in Figure 12, characterized by z as the symmetry axis and x directed along the single bond.

Treating the π -system butadiene molecule with a HMO (Hückel molecular orbital) approach, we get four MOs, which are linear combinations of the four atomic p orbitals

FIGURE 12. Reference axes and numbering of *s-trans*, *s-cis* and skewed butadiene

and are given by the equations

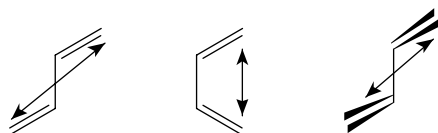
$$\pi_{\pm} = c_1 p_1 \pm c_2 p_2 + c_2 p_3 \pm c_1 p_4 \quad (5a)$$

and

$$\pi_{\pm}^* = c_2 p_1 \pm c_1 p_2 - c_1 p_3 \mp c_2 p_4 \quad (5b)$$

where c_1 and c_2 represent the two distinct coefficients in the linear combinations of AOs and depend on Hückel's parameters α and β .

Inspecting the character tables of Figure 13, we notice that the first (lowest-energy) excited state, corresponding to the electronic transition $\pi_- \rightarrow \pi_-^*$, is, for the *s-trans* isomer, B_u , for the *s-cis*, B_2 and finally for the skewed form, B . This transition is therefore electrically allowed in all three cases, being in-plane polarized for the former two cases as shown in Scheme 9.



SCHEME 9

The long-wavelength, $\pi_- \rightarrow \pi_-^*$, transition is also magnetically allowed for the skewed and for the *s-cis* conformations, as seen by inspection of the character tables. It is therefore apparent that for the planar isomers, *s-trans* and *s-cis*, there is no optical activity allied to the $\pi_- \rightarrow \pi_-^*$ transition (as obviously expected). In fact, for the *s-trans* form $\mathbf{m}_{B_u} = 0$, while for the *s-cis* μ and \mathbf{m} are orthogonal. In both cases the scalar product in equation 1 vanishes.

In the skewed form, instead, the transition is allowed both electrically and magnetically, with parallel transition moments. The product in equation 1 is hence non-vanishing, implying that this transition has finite rotational strength. This observation leads to the conclusion that skewed 1,3-butadiene is an *intrinsically dissymmetric* chromophore.

C_{2v}	E	C_2	σ_1	σ_2		
A_1	1	1	1	1	μ_z	
A_2	1	1	-1	-1	m_z	π_+, π_-^*
B_1	1	-1	1	-1	μ_x, m_y	π_-, π_-^*
B_2	1	-1	-1	1	μ_y, m_x	

C_{2h}	E	C_2	i	σ		
A_g	1	1	1	1	m_z	
A_u	1	1	-1	-1	μ_z	π_+, π_-^*
B_g	1	-1	1	-1	m_x, m_y	π_-, π_-^*
B_u	1	-1	-1	1	μ_x, μ_y	

C_2	E	C_2		
A	1	1	μ_z, m_z	π_+, π_-^*
B	1	-1	m_x, m_y	π_-, π_+^*

FIGURE 13. Character tables for symmetry point groups C_{2h} , C_2 and C_{2v}

B. MO Calculation of the Rotational Strength

In order to calculate R from equation 3, we have to evaluate the integrals $\mu_{\pi_+^* \pi_-}$ and $\mathbf{m}_{\pi_+^* \pi_-}$, with the MO π_- and π_-^* given in equations 5a and 5b. We assume only nearest-neighbour interactions and equal β -integrals in all the integrals for the pairs (1,2) and (3,4), as justified by symmetry. The electric dipole will be described by the velocity operator ∇ , in order to ensure origin-independent results, and equation 6 follows:

$$\begin{aligned}
 \langle \pi_-^* | \boldsymbol{\mu} | \pi_- \rangle &= \langle \pi_-^* | \nabla | \pi_- \rangle \\
 &= c_1 c_2 [-\nabla_{12} + \nabla_{21} - \nabla_{34} + \nabla_{43}] - c_1^2 [\nabla_{23} - \nabla_{32}] \\
 &= -2c_1 c_2 [\nabla_{12} + \nabla_{34}] - 2c_1^2 \nabla_{23}
 \end{aligned} \tag{6}$$

where $\nabla_{ij} = \langle p_i | \nabla | p_j \rangle$.

We can simplify this expression by decomposing the vectors along the three axes, with unit vectors $\hat{\mathbf{i}}$, $\hat{\mathbf{j}}$ and $\hat{\mathbf{k}}$ and introducing the direction cosines of the bond (1,2), namely $\cos x_{12}$, $\cos y_{12}$ and $\cos z_{12}$. The z -components of ∇_{12} and ∇_{34} , cancel, while ∇_{23} is directed along x . This yields the equation

$$\langle \pi_-^* | \boldsymbol{\mu} | \pi_- \rangle = -4c_1 c_2 \nabla_{12} (\hat{\mathbf{i}} \cos x_{12} + \hat{\mathbf{j}} \cos y_{12}) - 2c_1^2 \nabla_{23} \hat{\mathbf{i}} \tag{7}$$

The calculation of the magnetic moment

$$\langle \pi_-^* | \mathbf{m} | \pi_- \rangle = \langle \pi_-^* | \mathbf{r} \times \nabla | \pi_- \rangle \tag{8}$$

seems more involved, owing to the presence of the vector product. However, following Charney²², the expression can be decomposed into the product of the individual integrals:

$$\langle P_i | \mathbf{m} | p_j \rangle = \rho_{ij} \times \nabla_{ij} \quad (9)$$

where ρ_{ij} is the polar vector from the origin to the midpoint of the bond (i, j). We observe that ρ_{23} is trivially vanishing, in our coordinate system, thus $\mathbf{m}_{23} = 0$. This reduces the preceding expression to

$$\langle \pi_-^* | \mathbf{m} | \pi_- \rangle = -2c_1 c_2 (\mathbf{m}_{12} + \mathbf{m}_{34}) = -2c_1 c_2 (\rho_{12} \times \nabla_{12} + \rho_{34} \times \nabla_{34}) \quad (10)$$

Again, using the direction cosines and the coordinates of the midpoint of the bond, \bar{x}_{ij} , \bar{y}_{ij} and \bar{z}_{ij} , and observing that $(\bar{y}_{12} \cos z_{12} - \bar{z}_{12} \cos y_{12}) = 0$, we obtain the equation

$$\langle \pi_-^* | \mathbf{m} | \pi_- \rangle = -4c_1 c_2 \nabla_{12} \hat{\mathbf{j}} (\bar{z}_{12} \cos x_{12} - \bar{x}_{12} \cos z_{12}) \quad (11)$$

We are now able to calculate the rotational strength according to equation 3:

$$R_{\pi_-^* \pi_-} = 16c_1^2 c_2^2 \nabla_{12}^2 (\bar{z}_{12} \cos x_{12} \cos y_{12} - \bar{x}_{12} \cos z_{12} \cos y_{12}) \quad (12)$$

On using $\bar{x}_{12} = (x_1 + x_2)/2$ and $\cos x_{12} = (x_2 - x_1)/r_{12}$, with r_{12} the internuclear distance between 1 and 2, and similar expressions for the other components, we obtain

$$R_{\pi_-^* \pi_-} = 16c_1^2 c_2^2 \nabla_{12}^2 \left(\frac{x_2 y_1 z_1}{r_{12}^2} \right) \quad (13)$$

We note that y_1 and z_1 are functions of the skew angle θ and of the bend angle β (see Scheme 4):

$$y_1 = a \sin \beta \sin \frac{\theta}{2} \quad \text{and} \quad z_1 = a \sin \beta \cos \frac{\theta}{2} \quad (14)$$

a being the length of bond (1,2). This leads to the final result

$$R_{\pi_-^* \pi_-} \propto \sin^2 \beta \sin \theta \quad (15)$$

C. Charge-displacement Calculation of R

We shall now assume a classical picture to describe the transition $\pi_- \rightarrow \pi_-^*$.

On the basis of the analysis of Figure 14 we deduce that the $\pi_- \rightarrow \pi_-^*$ transition can be seen as the sum of two electric dipoles, $\mathbf{e}_1 + \mathbf{e}_2$. We notice that this transition has B character and is therefore antisymmetric. Hence, even from the classical point of view, we may conclude that this will be the lowest-energy transition.

The sum of the two vectors is given by

$$\boldsymbol{\mu} = \mathbf{e}_1 + \mathbf{e}_2 \quad (16)$$

and the same vectors serve to describe a rotation of charge, yielding a magnetic moment \mathbf{m} given by

$$\mathbf{m} = (\mathbf{r}_1 \times \mathbf{e}_1) + (\mathbf{r}_2 \times \mathbf{e}_2) \quad (17)$$

where \mathbf{r}_1 and \mathbf{r}_2 are the vectors joining the origin to the midpoints of \mathbf{e}_1 and \mathbf{e}_2 , respectively.

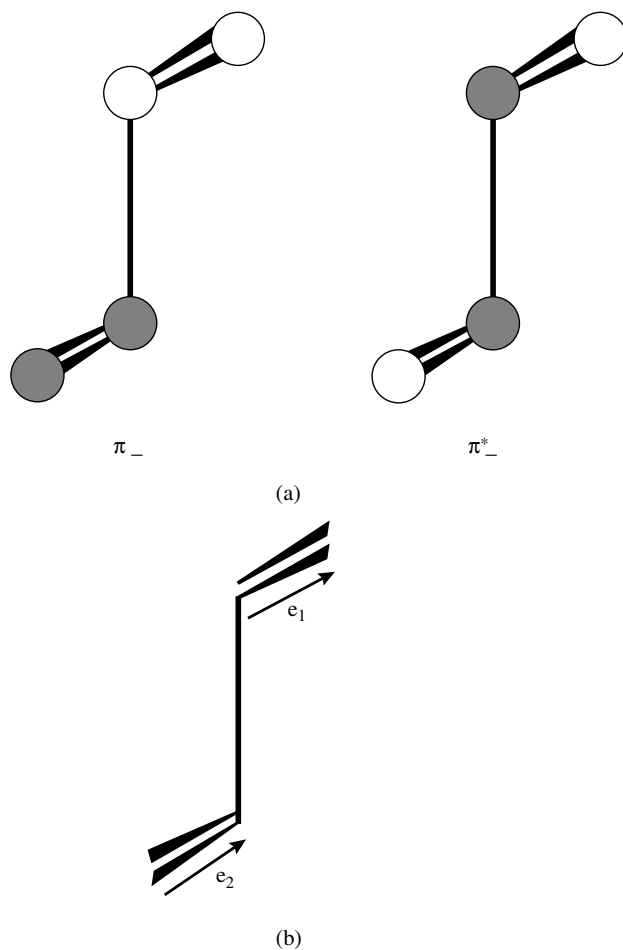


FIGURE 14. (a) Representation of charge excess, ●, and defect, ○, on the four carbon atoms for the two orbitals π_- (left) and π^*_- (right) for 1,3-butadiene. (b) Electric transition moments arising from the $\pi_- \rightarrow \pi^*_-$ transition

The rotational strength is then easily calculated by the equation

$$\begin{aligned}
 R &= \boldsymbol{\mu} \cdot \mathbf{m} \\
 &= (\mathbf{e}_1 + \mathbf{e}_2) \cdot [(\mathbf{r}_1 \times \mathbf{e}_1) + (\mathbf{r}_2 \times \mathbf{e}_2)] \\
 &= \mathbf{e}_1 \cdot [(\mathbf{r}_1 \times \mathbf{e}_1) + (\mathbf{r}_2 \times \mathbf{e}_2)] + \mathbf{e}_2 \cdot [(\mathbf{r}_1 \times \mathbf{e}_1) + (\mathbf{r}_2 \times \mathbf{e}_2)] \\
 &= \mathbf{e}_1 \cdot (\mathbf{r}_2 \times \mathbf{e}_2) + \mathbf{e}_2 \cdot (\mathbf{r}_1 \times \mathbf{e}_1)
 \end{aligned} \tag{18}$$

Remembering that for any three vectors $\mathbf{a} \cdot \mathbf{b} \times \mathbf{c} = \mathbf{a} \times \mathbf{b} \cdot \mathbf{c}$, and defining $\mathbf{r} = \mathbf{r}_1 - \mathbf{r}_2$, we obtain

$$R = \mathbf{r} \cdot (\mathbf{e}_1 \times \mathbf{e}_2) \tag{19}$$

where

$$\mathbf{r} \equiv (x_1 + x_2, y_1, 0) \quad (20)$$

The x - and y -components of the vector product in equation 19 are given by

$$(\mathbf{e}_1 \times \mathbf{e}_2)_x = 2y_1z_1 \quad (\mathbf{e}_1 \times \mathbf{e}_2)_y = 2z_1(x_2 - x_1) \quad (21)$$

On combining the latter two equations in equation 19, we obtain

$$R = 4x_2y_1z_1 \quad (22)$$

which, just like equation 16, contains the product (y_1z_1) . Therefore we obtain again

$$R_{\pi^*_\pi} \propto \sin^2 \beta \sin \theta \quad (23)$$

This result is in agreement with that reported by Norden⁵³ in a context only formally different.

VI. REFERENCES

- (a) E. Charney, *The Molecular Basis of Optical Activity*, Wiley, New York, 1979.
(b) S.F. Mason, *Molecular Optical Activity and the Chiral Discriminations*, Cambridge University Press, Cambridge, 1982.
(c) D. J. Caldwell and H. Eyring, *The Theory of Optical Activity*, Wiley, New York, 1971.
(d) N. Harada and K. Nakanishi, *Circular Dichroic Spectroscopy*, University Science Books, Oxford, 1983.
(e) K. Nakanishi, N. Berova and R. W. Woody, *Circular Dichroism*, VCH Publ. Inc., New York, 1994.
- W. Runge, in *The Chemistry of Ketenes, Allenes and related Compounds* (Ed. S. Patai), Wiley, New York, 1980, Chap. 3, pp 94–154.
- J. K. Gawroński and H. M. Walborsky, in Reference 1e, pp. 301–334.
- R. Buchecker and K. Noack, in *Carotenoids*, Vol. 1B, Birkhäuser Verlag, Basel, 1995, pp. 63–116.
- K. P. Gross and O. Schnepp, *J. Chem. Phys.*, **68**, 2647 (1978).
- (a) H. Suzuki, *Electronic Absorption Spectra and Geometry of Organic Molecules*, Academic Press, Oxford, 1967.
(b) H. H. Jaffé and M. Orchin, *Theory and Applications of UV Spectroscopy*, Wiley, New York, 1962.
(c) J. N. Murrell, *The Theory of the Electronic Spectra of Organic Molecules*, Methuen, London, 1963.
- A. Rauk and H. A. Peoples, *J. Comput. Chem.*, **1**, 240 (1980).
- A. I. Scott, *Interpretation of the Ultraviolet Spectra of Natural Products*, Pergamon Press, New York, 1964.
- A. Moscovitz, E. Charney, U. Weiss and H. Ziffer, *J. Am. Chem. Soc.*, **83**, 4661 (1961).
- A. R. Browne, A. F. Drake, F. R. Kearney, S. F. Mason and L. A. Paquette, *J. Am. Chem. Soc.*, **105**, 6123 (1983).
- A. W. Burgstahler, D. L. Boger and N. C. Naik, *Tetrahedron*, **32**, 309 (1976).
- A. Di Corato, *Gazz. Chim. Ital.*, **98**, 810 (1968).
- G. Giacomelli, L. Lardicci, C. Bertucci and A. M. Caporusso, *Tetrahedron*, **34**, 2015 (1978).
- G. Wagnière and W. Hug, *Tetrahedron Lett.*, 4765 (1970).
- A. W. Burgstahler, H. Ziffer and U. Weiss, *J. Am. Chem. Soc.*, **83**, 4660 (1961).
- (a) A. J. De Kok, C. Romers and J. H. Hoogendorp, *Acta Crystallogr., Sect. B*, **31**, 2818 (1975).
(b) A. J. De Kok and C. Romers, *Acta Crystallogr. Sect. B*, **31**, 1535 (1975).
- A. G. Hortmann, D. S. Daniel and J. E. Martinelli, *J. Org. Chem.*, **38**, 728 (1973).
- K. K. Cheong, A. Oshita, D. J. Caldwell and H. Eyring, *Proc. Natl. Acad. Sci. U.S.A.*, **67**, 1727 (1970).
- (a) M. C.A. Donkersloot and H. M. Buck, *J. Mol. Struct.*, **137**, 347 (1986).
(b) A. Julg, *J. Mol. Struct.*, **152**, 357 (1987).
(c) M. C.A. Donkersloot and H. M. Buck, *J. Mol. Struct.*, **180**, 389 (1988).

20. U. Weiss, H. Ziffer and E. Charney, *Tetrahedron*, **21**, 3105 (1965).
21. E. Charney, H. Ziffer and U. Weiss, *Tetrahedron*, **21**, 3121 (1965).
22. E. Charney, *Tetrahedron*, **21**, 3127 (1965).
23. J. S. Rosenfield and E. Charney, *J. Am. Chem. Soc.*, **99**, 3209 (1977).
24. E. Charney, C. H. Lee and J. S. Rosenfield, *J. Am. Chem. Soc.*, **101**, 6802 (1979).
25. P. Palmieri, G. Poggi and J. Vrbancich, *J. Comput. Chem.*, **4**, 260 (1983).
26. D. A. Lightner, T. D. Bouman, J. K. Gawroński, K. Gawrońska, J. L. Chappuis, B. V. Crist and A. E. Hansen, *J. Am. Chem. Soc.*, **103**, 5314 (1981).
27. W. Hug and G. Wagnière, *Tetrahedron*, **28**, 1241 (1972).
28. A. Rauk, J. O. Jarvie, H. Ichimura and J. M. Barriol, *J. Am. Chem. Soc.*, **97**, 5656 (1975).
29. W. Hug and G. Wagnière, *Helv. Chim. Acta*, **54**, 633 (1971).
30. A. W. Burgstahler and R. C. Barkhurst, *J. Am. Chem. Soc.*, **92**, 7601 (1970).
31. A. W. Burgstahler, L. O. Weigel and J. K. Gawroński, *J. Am. Chem. Soc.*, **98**, 3015 (1976).
32. S. Araki, T. Seki, K. Sakakibara, M. Hirota, Y. Kodama, and M. Nishio, *Tetrahedron: Asymmetry*, **4**, 555 (1993).
33. O. E. Weigang, Jr., *J. Am. Chem. Soc.*, **101**, 1965 (1979).
34. Following Reference 26, *dissignate* and *consignate* mean having sign opposite or equal to that predicted by the DR respectively.
35. J. Gawroński and K. Gawrońska, *J. Chem. Soc. Chem. Commun.*, 346 (1980).
36. E. Charney, J. M. Edwards, U. Weiss and H. Ziffer, *Tetrahedron*, **28**, 973 (1972).
37. A. W. Burgstahler, *J. Org. Chem.*, **46**, 1741 (1981).
38. B. V. Crist, S. L. Rodgers, J. K. Gawronski and D. A. Lightner, *Spectrosc. Int. J.*, **4**, 19 (1985).
39. D. A. Lightner and B. V. Crist, *Tetrahedron*, **37**, 685 (1981).
40. R. Isaksson, J. Roschester, J. Sandström and L. G. Wistrand, *J. Am. Chem. Soc.*, **107**, 4074 (1985).
41. (a) H. DeVoe, *J. Chem. Phys.*, **43**, 3199 (1965).
(b) C. Rosini, M. Zandomenighi and P. Salvadori, *Tetrahedron: Asymmetry*, **4**, 545 (1993).
(c) M. Clericuzio, C. Rosini, M. Persico and P. Salvadori, *J. Org. Chem.*, **56**, 4343 (1991).
42. J. M. Sonney and P. Vogel, *Helv. Chim. Acta*, **63**, 1034 (1980).
43. Z. Zhichen, L. Schwager, P. A. Carrupt and P. Vogel, *Helv. Chim. Acta*, **71**, 419 (1988).
44. (a) M. Duraisamy and H. M. Walborsky, *J. Am. Chem. Soc.*, **105**, 3264 (1983).
(b) M. Duraisamy and H. M. Walborsky, *J. Am. Chem. Soc.*, **105**, 3252 (1983).
(c) J. Gawroński and H. M. Walborsky, *J. Org. Chem.*, **51**, 2863 (1986).
45. (a) H. M. Walborsky, S. M. Reddy and J. H. Brewster, *J. Org. Chem.*, **53**, 4832 (1988).
(b) H. M. Walborsky and S. M. Reddy, *J. Org. Chem.*, **53**, 4846 (1988).
46. (a) S. Liaaen-Jensen, in *Acta of the IV International Conference on CD*, Bochum (1991).
(b) K. Noack, in *Carotenoid Chemistry and Biochemistry* (Eds. G. Britton and T. W. Goodwin), Pergamon Press, Oxford, 1981 pp. 135-153.
47. (a) K. Noack and A. J. Thomson, *Helv. Chim. Acta*, **62**, 1902 (1979);
(b) V. Sturzenegger, R. Buchecker and G. Wagniere, *Helv. Chim. Acta*, **63**, 1074 (1980).
48. F. Ciardelli, S. Lanzillo and O. Pieroni, *Macromolecules*, **7**, 174 (1974).
49. P. A. Maessen, H. J. C. Jacobs, J. Cornelisse and E. Havinga, *Angew. Chem., Int. Ed. Engl.*, **22**, 718 (1983).
50. (a) W. K. Chan, K. Nakanishi, T. G. Ebrey and B. Honig, *J. Am. Chem. Soc.*, **96**, 3642 (1974).
(b) F. Derguini, K. Nakanishi, U. Hämmerling and J. Buck, *Biochemistry*, **33**, 623 (1994).
(c) Y. Katsuta, K. Yoshihara, K. Nakanishi and M. Ito, *Tetrahedron Lett.*, **35**, 905 (1994).
(d) T. Kinumi, K. Tsujimoto, M. Ohashi, R. Hara, T. Hara, K. Ozaki, M. Sakai, Y. Katsuta, A. Wada and M. Ito, *Photochem. Photobiol.*, **58**, 409 (1993).
(e) S. Steinmüller, V. Buss and W. Gärtner, *J. Photochem. Photobiol.*, **B**, **31**, 139 (1995).
51. (a) A. R. Balakrishnan and K. R.K. Easwaran, *J. Biomol. Struct. Dynam.*, **11**, 417 (1993).
(b) S. D. Rychnovsky and T. I. Richardson, *Angew. Chem., Int. Ed. Engl.*, **34**, 1227 (1995).
(c) About the interactions of Filipin with steroids, see: J. Milhaud, J. Bolard, P. Benevise and M. A. Hartmann, *Biochem. Biophys. Acta*, **943**, 315 (1988).
52. (a) H. Rinnert, G. Thirion, G. Dupont and J. Lematre, *Biopolymers*, **16**, 2419 (1977).
(b) H. G. Brittain, *Chirality*, **6**, 665 (1994).
(c) About the interactions of Filipin with steroids, see: J. Mazerski, J. Bolard and E. Borowski, *Biochim. Biophys. Acta*, **1236**, 170 (1995).
53. B. Nordén, *Chem. Scr.*, **7**, 226 (1975).

CHAPTER 5

Ultraviolet/visible, infrared and Raman spectra

YUKIO FURUKAWA

Department of Chemistry, School of Science, The University of Tokyo, Bunkyo-ku,
Tokyo 113, Japan
Fax: +81-3-3814-2627; e-mail: furukawa@chem.s.u-tokyo.ac.jp

I. INTRODUCTION	149
II. ELECTRONIC AND VIBRATIONAL SPECTROSCOPIES	151
A. Infrared and Raman Spectroscopies	151
B. Absorption and Fluorescence Spectroscopies	151
C. Normal Coordinate Calculations	151
D. Vibronic Theory of Resonance Raman Scattering	152
III. ELECTRONIC SPECTRA	154
A. Electronic Structure	154
B. Ultraviolet/Visible Absorption Spectra	155
IV. VIBRATIONAL SPECTRA	158
A. Butadiene	158
1. <i>s-Trans</i> conformer	158
2. <i>Gauche</i> conformer	161
B. Hexatriene	161
1. <i>Trans</i> conformer	162
2. <i>Cis</i> conformer	163
3. Other conformers	166
C. Long Chain Polyenes	166
1. All- <i>trans</i> conformers	166
2. <i>Cis</i> conformers	169
V. REFERENCES	169

I. INTRODUCTION

Ultraviolet/visible absorption, fluorescence, infrared and Raman spectroscopies are useful for studying structures (configuration, conformation, symmetry etc.) of electronically ground and excited states of linear polyenes, which have attracted much attention of

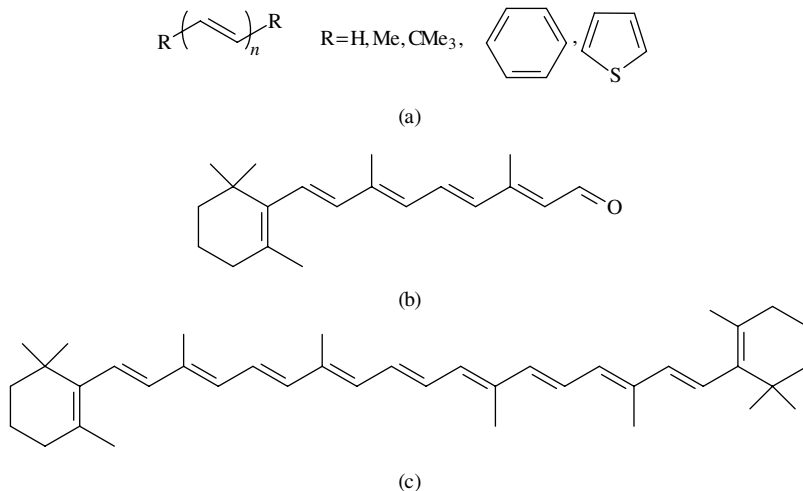


FIGURE 1. Chemical structures of various polyenes: (a) unsubstituted and α,ω -disubstituted polyenes; (b) retinal; (c) β -carotene

researchers in quantum chemistry, solid-state physics, biophysics etc. Linear polyenes exhibit interesting chemical and physical properties originating from π -electrons. Firstly, these compounds show novel spectroscopic properties due to electron correlation¹⁻³. Hudson and coworkers¹ and Kohler² have reviewed the electronic states of unsubstituted polyenes and α,ω -diphenylpolyenes (Figure 1a), emphasizing the ordering of the electronically excited states, 1^1B_u and 2^1A_g . Orlandi and coworkers³ have reviewed vibrational analyses based on quantum chemical calculations for the electronically ground and excited states of unsubstituted polyenes, and have explained the frequency increase of the in-phase C=C stretch upon excitation to the 2^1A_g state. Secondly, polyenes are model compounds of polyacetylene $[(\text{CH}=\text{CH})_n]$ which is the prototype of conducting polymers. Polyacetylene shows new electrical, magnetic and optical properties; for example, it shows high electrical conductivities when doped with electron acceptors (iodine, AsF₅ etc.) or electron donors (Na, K etc.)⁴. The application of vibrational spectroscopy to polyacetylene is described in previous reviews⁵⁻⁷. Lastly, retinal (Figure 1b) and its Schiff base play important roles in retinal proteins⁸, and so do carotenoids in photosynthetic bacteria⁹. The chemical structure of β -carotene, which is one of the carotenoids, is shown in Figure 1c. Several reviews¹⁰⁻¹⁴ have described the application of vibrational spectroscopy to polyenes in biological systems. There exist geometrical isomers around C=C double bonds and rotamers around C-C single bonds for polyenes. Vibrational studies on the conformers of polyenes may lead us to a better understanding of the functions of polyacetylene and biological systems. In this chapter, we mainly present the spectroscopic properties of various conformers of unsubstituted polyenes. We focus our attention on the structures (configuration, conformation etc.) of the ground states of polyenes and the relation between the number of conjugated C=C bonds and spectroscopic properties. In Section II, we mention experimental techniques and outlines of normal coordinate calculations and resonance Raman spectroscopy. In Section III, we describe the electronic absorption spectra of polyenes. In Section IV, we describe vibrational spectra of polyenes from 1,3-butadiene to polyacetylene.

II. ELECTRONIC AND VIBRATIONAL SPECTROSCOPIES

A. Infrared and Raman Spectroscopies

Vibrational spectra of polyenes can be obtained by infrared and Raman spectroscopies. Infrared and Raman spectra are measured by means of dispersive-type or Fourier transform spectrophotometers. The combination of matrix-isolation infrared spectroscopy and a high-temperature nozzle technique (or photoexcitation) is useful for studying the ground states of unstable conformers of polyenes¹⁵. A sample is diluted with an inert gas, such as argon, xenon and nitrogen. This mixture is passed through a pipe (or a cell) at a high temperature and immediately sprayed onto a cold CsI plate maintained at a low temperature (e.g. 10 K). Then, unstable conformers can be trapped in the matrices. Biological systems have been studied by resonance Raman spectroscopy^{10,12,13} and Fourier transform infrared spectroscopy¹⁴. These systems consist of various components, such as proteins, membranes and pigments; resonance Raman spectroscopy can give us information about a pigment, when the excitation wavelength for Raman scattering is within the electronic absorption of the pigment. On the other hand, very small absorbance changes associated with external stimuli such as light irradiation can be detected by Fourier transform infrared spectroscopy. Thus, short-lived polyene conformers which are reaction intermediates in biological systems have been studied by the use of steady-state and time-resolved resonance Raman spectroscopy^{10,12} and Fourier transform infrared spectroscopy¹⁴. Strong fluorescence often prevents us from observing Raman spectra. This is the major obstacle in Raman measurements. Coherent anti-Stokes Raman spectroscopy (CARS)¹⁶ can partly solve this fluorescence problem. Since fluorescence appears in the Stokes region, anti-Stokes Raman spectra are not disturbed by fluorescence in principle. It is difficult to measure spontaneous anti-Stokes Raman scattering with high signal-to-noise ratios, because their intensities are very weak. However, coherent anti-Stokes scatterings are strong enough to be measured with high signal-to-noise ratios.

B. Absorption and Fluorescence Spectroscopies

Absorption and fluorescence spectra of polyenes in the region from ultraviolet to visible in the condensed phases (liquid, solid, solutions etc.) are very broad in most cases. Thus, bands arising from distinct vibronic transitions are not resolved. However, the spectra of polyenes in hydrocarbon environments at very low temperatures or in supersonic expansions show fine structures originating from vibrational transitions^{1,2}. Absorption and fluorescence excitation spectra provide us with the vibrational frequencies of electronically excited states, whereas fluorescence spectra provide us with those of ground states. Two-photon absorption spectroscopy is complementary to one-photon absorption spectroscopy. Let us consider a molecule with a centre of inversion. The transitions between the ground state and electronically excited states with ungerade symmetry are allowed for one-photon processes, but forbidden for two-photon processes. On the other hand, the selection rules are just reversed for the transitions between the ground state and excited states with gerade symmetry. The electronically excited states labelled with 1^1B_u and 2^1A_g of polyenes have been studied by means of one- and two-photon absorption (fluorescence excitation) experiments^{1,2}.

C. Normal Coordinate Calculations

The frequencies of some vibrational bands are sensitive to molecular conformation. Normal coordinate calculations are useful for assigning observed vibrational spectra and deducing from them precise structural information. Normal coordinate calculations were

previously performed by means of empirical methods^{17,18}. It has recently been demonstrated that *ab initio* molecular orbital (MO) methods are useful for evaluating vibrational spectra¹⁹. The frequencies calculated at the Hartree–Fock (HF) level are usually higher than those obtained from experiments. Then, the calculated force constants are fitted by the use of parameters, which are called scale factors, to the observed frequencies. In most cases, the scale factor for an off-diagonal force constant is the geometric mean of the scale factors for the corresponding diagonal force constants. The force field thus obtained is called a scaled quantum mechanical (SQM) force field¹⁹. It is noted that electron correlation is not taken into account explicitly under the HF approximation. Electron correlation is usually introduced by adding the Moller–Plesset (MP) perturbation correction to the HF result. The second-order MP perturbation method is abbreviated to MP2.

D. Vibronic Theory of Resonance Raman Scattering

Resonance Raman spectroscopy has been applied to studies of polyenes for the following reasons. The Raman spectrum of a sample can be obtained even at a dilute concentration by the enhancement of scattering intensity, when the excitation laser wavelength is within an electronic absorption band of the sample. Raman spectra can give information about the location of dipole forbidden transitions, vibronic activity and structures of electronically excited states. A brief summary of vibronic theory of resonance Raman scattering is described here.

The intensity of a Raman transition from the initial vibrational level i of the ground electronic state g to the final vibrational level j of the g state is given by equation 1:

$$I_{gi,gj} = CI_0\nu_0\nu_S^3 \sum_{\rho\sigma} |(\alpha_{\rho\sigma})_{gi,gj}|^2 \quad (1)$$

where C is a constant, I_0 and ν_0 are the intensity and the frequency of the incident laser light, ν_S is the frequency of the scattered light and $(\alpha_{\rho\sigma})_{gi,gj}$ is the Raman polarizability tensor element, with ρ and σ being labels for the Cartesian coordinates in the molecular frame. Second-order perturbation theory gives equation 2 for the Raman polarizability tensor^{20,21}.

$$(\alpha_{\rho\sigma})_{gi,gj} = \sum_{ev} \left[\frac{\langle ig|M_\sigma|ev\rangle\langle ve|M_\rho|gj\rangle}{E_{ev} - E_{gi} - E_0 - i\Gamma_{ev}} + \frac{\langle ig|M_\rho|ev\rangle\langle ve|M_\sigma|gj\rangle}{E_{ev} - E_{gj} + E_0 - i\Gamma_{ev}} \right] \quad (2)$$

Here $|gi\rangle$, $|gj\rangle$ and $|ev\rangle$ are the vibronic wavefunctions of the initial, final and intermediate states, respectively; M_σ and M_ρ are the electronic dipole operators of σ and ρ polarizations, respectively; E_0 is the energy of the incident laser photon; E_{gi} , E_{gj} and E_{ev} are the energies of the initial, final and intermediate vibronic levels, respectively; and Γ_{ev} is a damping factor which defines the linewidth of the $|ev\rangle$ vibronic state. When the wavelength of the incident laser light coincides with the electronic absorption band (i.e. $E_{ev} - E_{gi} \approx E_0$), the first term is dominant, and the second term can be neglected because it is much smaller than the first term. In the following discussion the second non-resonant term is neglected.

If Born–Oppenheimer wavefunctions are used to describe the vibronic wavefunctions, the electronic and vibrational portions of the wavefunctions can be separable:

$$\langle ig|M_\sigma|ev\rangle = \langle i|(g|M_\sigma|e)|v\rangle = \langle i|M_{ge}^\sigma|v\rangle \quad (3)$$

This integral of the electronic dipole moment operator is a function of a nuclear coordinate Q . The integral may be expanded in a Taylor series with respect to Q (equation 4) and

evaluated at the equilibrium position of the potential surface.

$$M_{ge}^\sigma = (M_{ge}^\sigma)^0 + \sum_a \frac{\partial M_{ge}^\sigma}{\partial Q_a} Q_a + \dots \equiv (M_{ge}^\sigma)^0 + \sum_a (M_{ge}^\sigma)'_a Q_a + \dots \quad (4)$$

Substitution of the first two terms into the Raman polarizability tensor gives the following three terms²²⁻²⁴:

$$(\alpha_{\rho\sigma})_{gi,gf} = \alpha^I + \alpha^{II} + \alpha^{III} \quad (5)$$

where

$$\alpha^I = \sum_e \sum_v \frac{(M_{ge}^\sigma)^0 (M_{eg}^\rho)^0}{E_{ev} - E_{gi} - E_0 - i\Gamma_{ev}} \langle i|v\rangle \langle v|j\rangle \quad (6)$$

$$\begin{aligned} \alpha^{II} = & \sum_e \sum_v \sum_a \frac{(M_{ge}^\sigma)'_a (M_{eg}^\rho)^0 \langle i|Q_a|v\rangle \langle v|j\rangle}{E_{ev} - E_{gi} - E_0 - i\Gamma_{ev}} \\ & + \sum_e \sum_v \sum_b \frac{(M_{ge}^\sigma)^0 (M_{eg}^\rho)'_b \langle i|v\rangle \langle v|Q_b|j\rangle}{E_{ev} - E_{gi} - E_0 - i\Gamma_{ev}} \end{aligned} \quad (7)$$

$$\alpha^{III} = \sum_e \sum_v \sum_{ab} \frac{(M_{ge}^\sigma)'_a (M_{eg}^\rho)'_b \langle i|Q_a|v\rangle \langle v|Q_b|j\rangle}{E_{ev} - E_{gi} - E_0 - i\Gamma_{ev}} \quad (8)$$

In these terms, the electronic integrals such as $(M_{ge}^\sigma)^0$ and $(M_{ge}^\sigma)'_a$ are constrained by the symmetry of the electronic states. While term I involves Frank-Condon overlap integrals, terms II and III involve integrals of the form $\langle i|Q_a|v\rangle$; in the harmonic approximation, the integrals of this type obey the selection rule $v = i + 1$. Keeping these considerations in mind, we will next discuss how terms I, II and III contribute to distinct vibrational transitions.

(1) The term I scattering (equation 6) is dominant when the excitation laser wavelength is resonant with an allowed electronic transition ($M^0 \neq 0$, $|M^0| \gg |M^I|$). The term I scattering becomes significant if the Frank-Condon overlap integrals $\langle i|v\rangle$ and $\langle v|j\rangle$ have non-zero values simultaneously; it usually provides the enhancement of a series of fundamental, overtone and combination transitions of totally symmetric modes. When the displacement between the adiabatic potential minima of the g and e states is large, the intensities of overtone and combination transitions are greatly enhanced. This term corresponds to the A term of the Albrecht theory²⁵.

(2) The term II scattering (equation 7) from vibronic activity in allowed electronic transitions mainly results in fundamental transitions of non-totally symmetric vibrations. This term corresponds to the B and C terms of the Albrecht theory²⁵.

(3) The term III scattering (equation 8) is the weakest in the three scattering mechanisms, as shown by two derivative terms (M^I) in the electronic transition integrals. Clearly, for a dipole forbidden transition ($M^0 = 0$) the only non-zero term is term III. The term III scattering results in binary overtone and combination transitions of vibronically active modes. It is noted that no fundamental transition survives.

In the case of polyenes, the term I scattering is dominant in the Raman spectra resonant with the 1^1B_u excited states^{22,26}; the contribution of the term III scattering is important in the Raman spectra resonant with the 2^1A_g excited states²⁷. In addition, an interference effect between the 1^1B_u and 2^1A_g states in a Raman-intensity vs excitation-photon-energy plot (which is called an excitation profile) of the in-phase C=C stretch has been suggested²⁸.

III. ELECTRONIC SPECTRA

A. Electronic Structure

Let us consider an unsubstituted linear polyene with N C=C double bonds, i.e. $2N\pi$ -electrons. The number of molecular orbitals equals the number of π -electrons. These molecular orbitals can be classified into two types: N bonding orbitals and N antibonding orbitals. It has been shown^{1,2} that three low-lying singlet states of linear polyenes are described in terms of the configurations shown in Figure 2. The ground state S_0 is well described by the single configuration in which the N bonding orbitals are doubly occupied (Figure 2a). For a normal π -system, the first excited state S_1 is described by the single configuration which is derived from the ground state by promoting one electron from the highest occupied molecular orbital (HOMO) to the lowest unoccupied molecular orbital (LUMO), as shown in Figure 2b. However, in linear polyenes this state is the second excited state S_2 . The S_1 state is a correlated state that cannot be written in terms of a single configuration because of electron correlation, but is approximately described by a linear combination of the doubly excited configuration in which two electrons are promoted from the HOMO to the LUMO (Figure 2c) and the double jump configuration in which one electron is promoted from the HOMO to the LUMO + 1 (Figure 2d). Electron correlation is essential for a correct description of the electronic state ordering for linear polyenes^{1,2}. In the all-*trans* planar structure (C_{2h} symmetry), S_0 and S_1 have A_g symmetry and are called 1^1A_g and 2^1A_g , respectively; S_2 has B_u symmetry and is called 1^1B_u . As a result, the transition between S_0 and S_1 is dipole forbidden, whereas the transition between S_0 and S_2 is dipole allowed.

The ultraviolet/visible absorption spectrum of a polyene shows an intense absorption band and an extremely weak absorption band which is located below the strong absorption band, as described in the following section. This spectral pattern is a general property of linear polyenes of all chain lengths independent of local symmetry and/or the presence of *cis* bonds. This is the reason why in the literature on polyenes the labels 1^1A_g for S_0 , 2^1A_g for S_1 and 1^1B_u for S_2 are used even in cases where C_{2h} symmetry is not realized. The ordering that the 2^1A_g excited state is located below the 1^1B_u excited state is peculiar to linear polyenes.

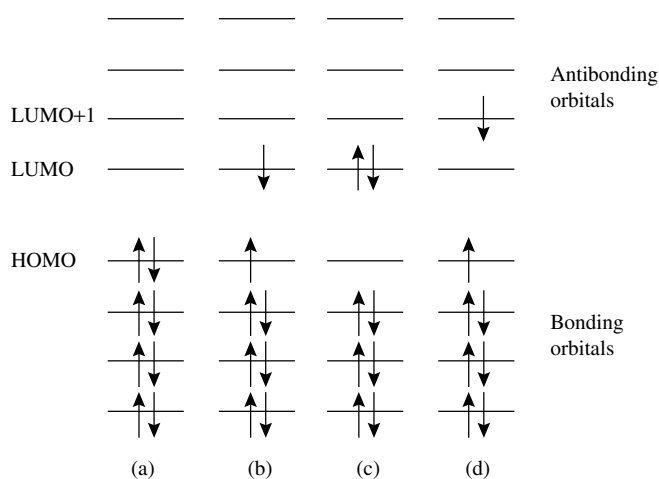


FIGURE 2. Some configurations describing the low-energy singlet states of linear polyenes

TABLE 1. Observed absorption maxima (λ_{\max}) and molar absorption coefficients (ϵ) of unsubstituted all-*trans*-polyenes

$N_{C=C}$	λ_{\max}/nm ($\epsilon/10^3$ l mol ⁻¹ cm ⁻¹)	Solvent	Reference
2	218.5 (23.0)	cyclohexane	30
3	268 (34.6), 257 (42.7), 248 (30.5)	iso-octane	29
4	303 (53), 289 (54.3), 276 (37), 264 (19.9)	95% ethanol	31
5	334 (121), 317 (115), 303 (71.2), 290 (37.1)	iso-octane	29
6	364 (138), 344 (127), 328 (73.2), 313 (37.3)	iso-octane	29
8	410 (108), 386 (112), 367 (72.8), 349 (35.8)	iso-octane	29
10	447, 420, 397, 376	iso-octane	29

TABLE 2. Observed absorption maxima (λ_{\max}) and molar absorption coefficients (ϵ) of all-*trans*- α,ω -dimethylpolyenes

$N_{C=C}$	λ_{\max}/nm ($\epsilon/10^3$ l mol ⁻¹ cm ⁻¹)	Solvent	Reference
2	226.5 (24.0)	cyclohexane	30
3	274.5 (30.2)	hexane	32
4	310 (76.5)	hexane	32
5	341 (122)	hexane	32
6	380 (146.5)	chloroform	32
7	398 (52.5), 375 (56.2), 355 (33.9)	dichloromethane	33
8	420 (53.7), 395 (56.2), 375 (36.3)	dichloromethane	33
9	443 (58.9), 416 (63.1), 393 (43.7)	dichloromethane	33
10	460 (39.8), 431 (60.3), 406 (36.3)	dichloromethane	33

TABLE 3. Observed absorption maxima (λ_{\max}) and molar absorption coefficients (ϵ) of all-*trans*- α,ω -dibutylpolyenes³⁴

$N_{C=C}$	λ_{\max}/nm ($\epsilon/10^3$ l mol ⁻¹ cm ⁻¹)	Solvent
2	237.2, 227.8, 219.8	<i>n</i> -pentane
3	275.6, 264.8, 255.6	<i>n</i> -pentane
4	311.4, 297.4, 284.8, 274.6	<i>n</i> -pentane
5	343.0, 325.8, 311.0, 297.8	<i>n</i> -pentane
6	371.2, 351.0, 334.2, 319.0	<i>n</i> -pentane
7	396.2, 373.6, 355.6, 338.0	<i>n</i> -pentane
8	418.8, 394.0, 374.0, 354.2	<i>n</i> -pentane
	432 (111), 406 (103), 384 (643)	dichloromethane
9	438.8, 411.2, 390.2, 371.8	<i>n</i> -pentane
	452 (114), 424 (101), 402 (65)	dichloromethane
10	456.4, 427.8, 405.2, 382.6	<i>n</i> -pentane
11	468.8, 439.4, 414.4, 393.4	<i>n</i> -pentane
13	494, 462, 438, 412	<i>n</i> -pentane

B. Ultraviolet/Visible Absorption Spectra

The absorption bands or peaks reported for the all-*trans* conformers of unsubstituted polyenes^{29–31}, α,ω -dimethylpolyenes^{30,32,33}, α,ω -di-*tert*-butylpolyenes³⁴, α,ω -diphenylpolyenes^{35,36} and α,ω -dithienylpolyenes³⁷ are compiled in Tables 1–5, respectively. The data for carotenoids are described in a previous review³⁸. These absorptions are attributed to the $1^1B_u \leftarrow 1^1A_g$ transitions ($\pi-\pi^*$ transitions).

TABLE 4. Observed absorption maxima (λ_{\max}) and molar absorption coefficients (ϵ) of all-*trans*- α,ω -diphenylpolyenes in benzene³⁶

$N_{C=C}$	λ_{\max}/nm ($\epsilon/10^3$ l mol ⁻¹ cm ⁻¹)
1	319 (21.7), 306 (24.3), 294 (23.5)
2	352 (26.1), 334 (40.0), 316 (30.4)
3	377 (52.1), 358 (74.7), 343 (54.3)
4	404 (76.9), 384 (86.0), 363 (58.2)
5	424 (88.6), 403 (93.8), 387 (60.8)
6	445 (109), 420 (113), 400 (76.4)
7	465 (122), 435 (135), 413 (86.9)

TABLE 5. Observed absorption maxima (λ_{\max}) of all-*trans*- α,ω -dithienylpolyenes in dichloromethane³⁷

$N_{C=C}$	$\lambda_{\max}(nm)$
3	404, 382, 364
4	426, 402, 380
5	443, 416, 395
6	461, 432, 409

As a typical example of polyene spectroscopy, absorption and fluorescence spectra³⁹ of *trans,trans*-1,3,5,7-octatetraene in hexane at 23 °C are shown in Figure 3. An absorption band with several peaks is observed in Figure 3a. It should be noted that the positions of electronic absorption bands strongly depend on solvents^{1,2}. This absorption band is dipole allowed, because the molar absorption coefficient of this band is very large (Table 1). This band is attributed to the transition from the $1A_g$ ground state to the $1B_u$ excited state ($\pi-\pi^*$ transition). Although the absorption peaks are due to vibrational transitions, a precise vibrational analysis cannot be made because of the broad band widths. The position of the observed emission spectrum (Figure 3b) shows a considerable red shift in

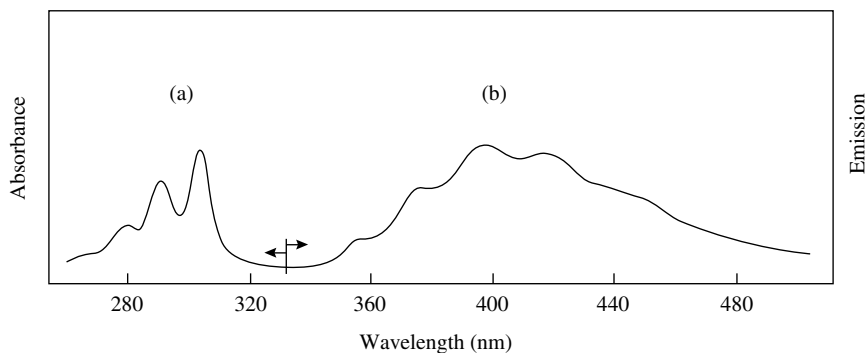


FIGURE 3. (a) Absorption and (b) fluorescence spectra of *trans,trans*-1,3,5,7-octatetraene in hexane at 23 °C. Reproduced by permission of American Institute of Physics from Reference 39

comparison with the position of the absorption spectrum. In other words, a large Stokes shift is observed. This emission band is due to the transition from the 2^1A_g excited state to the 1^1A_g ground state. The absorption band associated with the $2^1A_g \leftarrow 1^1A_g$ transition is not observed, because this absorption is expected to be extremely weak. These assignments of the absorption and emission spectra have been confirmed by the following experiments. In one- and two-photon excitation spectra of *trans,trans*-1,3,5,7-octatetraene in *n*-octane at 4.2 K (not shown), fine structures are observed, and these vibronic bands have been analysed⁴⁰. As a result, it has been shown that the 0-0 transition between the 2^1A_g and 1^1A_g states is observed at 28561 cm^{-1} (350 nm) and the 0-0 transition between the 1^1B_u and 1^1A_g states is observed at 32100 cm^{-1} (312 nm).

The reported^{2,41,42} 0-0 transition energies associated with the 2^1A_g and 1^1B_u excited states are plotted against $N_{C=C}$ in Figure 4. The transition energy for the 2^1A_g excited state is always lower than that for the 1^1B_u state for each polyene. The transition energy for a series of excited states decreases with increasing number of C=C bonds ($N_{C=C}$). The observed $1^1B_u \leftarrow 1^1A_g$ (0-0) transition energy, E_n , has been fitted by equation 9^{34,43}:

$$E_n(\text{eV}) = E_\infty + \frac{k}{N_{C=C}} \quad (9)$$

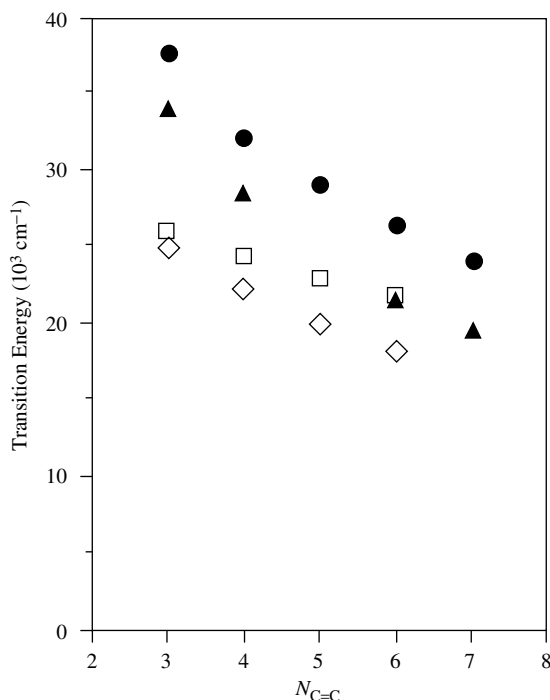


FIGURE 4. Observed 0-0 electronic transition energies (cm^{-1}) of linear polyenes^{2,41,42}: ●, $1^1B_u \leftarrow 1^1A_g$ and ▲, $2^1A_g \leftarrow 1^1A_g$ for unsubstituted polyenes; □, $1^1B_u \leftarrow 1^1A_g$ and ◇, $2^1A_g \leftarrow 1^1A_g$ for α,ω -diphenylpolyenes

where E_∞ and k are constants. From observed transition energies of α,ω -dibutylpolyenes (Table 3), E_∞ and k are determined to be about 1.56 and 9.5 eV in carbon disulfide, respectively, and about 1.79 and 9.4 eV in pentane, respectively³⁴. The differences between these estimated values come from the fact that the observed transition energies are sensitive to solvents. Equation 9 suggests that the 1^1B_u transition energy approaches a finite limit (E_∞) at infinite chain length. A *trans*-polyacetylene film prepared from the polymerization of acetylene shows a very broad absorption band in the visible region; the peak of the absorption is 1.95 eV and the edge of the absorption is 1.4 eV⁴⁴. The E_∞ values, 1.56 and 1.79 eV, estimated from the data of α,ω -dibutylpolyenes are not in good agreement with the absorption edge, 1.4 eV, of *trans*-polyacetylene.

IV. VIBRATIONAL SPECTRA

A. Butadiene

1. *s-Trans* conformer

1,3-Butadiene ($\text{CH}_2=\text{CH}-\text{CH}=\text{CH}_2$) has two C=C bonds and one C-C bond. It has been shown experimentally that the most stable rotamer has the planar *s-trans* structure⁴⁵⁻⁴⁷. The lengths of the C=C and C-C bonds are 1.341 and 1.463 Å, respectively⁴⁷. The infrared and Raman spectra of 1,3-butadiene in the vapour, liquid and solid phases have been studied⁴⁸⁻⁵¹. The spectra of deuterated⁵¹⁻⁵⁵ and ¹³C-substituted⁵⁶ analogs have been studied for the purpose of the assignments of vibrational spectra. On the basis of these vibrational spectra, normal coordinate calculations have been performed by the use of empirical force fields⁵⁴⁻⁶⁰. The structure and vibrational frequencies of the *s-trans* conformer have been calculated by *ab initio* MO methods⁶¹⁻⁶⁵. The assignments of all the fundamental bands have been established.

The *s-trans* conformer of 1,3-butadiene belongs to C_{2h} symmetry. There are 24 normal modes: $9a_g + 4a_u + 3b_g + 8b_u$. The a_g and b_u modes are the in-plane vibrations, while the a_u and b_g modes are the out-of-plane vibrations; the vibrations of a_g and b_g are Raman active and the vibrations of a_u and b_u are infrared active. The observed and calculated vibrational frequencies of *s-trans*-1,3-butadiene are listed in Table 6. Most of the frequencies calculated even at the MP2/6-311G* level⁶⁴ (column 6) are higher than those observed (column 3); most of the frequencies calculated at the MP2/6-31G* level⁶⁴ (not shown) are also higher than those observed. However, the frequencies obtained by a scaled MP2/6-31G* calculation⁶⁵ (column 7) are in good agreement with those observed. Vibrational modes of some strong Raman and infrared bands are as follows. The 1644- cm^{-1} Raman band (ν_4) is assigned to the vibrational mode in which two C=C bonds stretch in phase. The 1279- cm^{-1} Raman band (ν_6) is assigned to the CH in-plane bending, and the 1206- cm^{-1} Raman band (ν_7) to the C-C stretch. The infrared bands observed at 1022 and 905 cm^{-1} (ν_{10} and ν_{11} , respectively) are assigned to the CH out-of-plane bending and CH_2 wagging, respectively.

The group-coordinate force constants (not shown) obtained by an empirical method⁶⁰ are in good agreement with those obtained by a scaled *ab initio* MO calculation at MP2/6-31G* level⁶⁵. Guo and Karplus⁶⁴ have calculated group-coordinate force constants at the HF and MP2 levels with various basis sets (6-31G, 6-31G*, 6-311G and 6-311G*). In most cases in-plane diagonal force constants decrease by 5%–15% from the corresponding HF values when electron correlation is included via the MP2 method; the C=C stretch force constant shows an especially larger decrease (20%) with all the basis sets, whereas the C-C stretch force constant shows a smaller decrease (3%) with the 6-31G* and 6-311G* basis sets. It is noted that the C=C/C-C off-diagonal force constant increases by 15%–20% with all the basis sets in going from the HF to the MP2 method.

TABLE 6. Observed and calculated vibrational frequencies (cm^{-1}) of *s-trans*-1,3-butadiene

Sym	No.	Obsd ^d		Calcd			Description
				Empirical ^c	MP2/6-311G ^{*d}	Scaled MP2/6-31G ^{*e}	
a_g	ν_1	3105	R, w	3102	3284	3107.0	CH ₂ a-stretch
	ν_2	3025	R, m	3039	3178	3020.4	CH stretch
	ν_3	3014	R, m	2997	3189	3005.9	CH ₂ s-stretch
	ν_4	1644	R, vs	1645	1719	1643.5	C=C stretch
	ν_5	1441	R, s	1446	1495	1444.8	CH ₂ scis
	ν_6	1279	R, s	1296	1325	1285.8	CH ip-bend
	ν_7	1206	R, s	1203	1248	1209.7	C-C stretch
	ν_8	887	R, w	901	914	892.0	CH ₂ rock
	ν_9	513	R, m	510	521	511.3	CCC deform
a_u	ν_{10}	1022	IR, vs	1019	1038	1016.4	CH op-bend
	ν_{11}	905	IR, vs	908	891	909.6	CH ₂ wag
	ν_{12}	535	IR, m	527	525	526.6	CH ₂ twist
b_g	ν_{13}	163 ^b	IR, vw	162	156	163.3	C-C torsion
	ν_{14}	974	R, vw	969	980	969.8	CH op-bend
	ν_{15}	908	R, m	910	891	910.6	CH ₂ wag
	ν_{16}	754	R, w	751	764	751.4	CH ₂ twist
b_u	ν_{17}	3103	IR, m	3101	3284	3115.7	CH ₂ a-stretch
	ν_{18}	3062	IR, m	3029	3192	3042.6	CH stretch
	ν_{19}	2986	IR, m	2997	3182	3026.0	CH ₂ s-stretch
	ν_{20}	1597	IR, vs	1601	1651	1601.3	C=C stretch
	ν_{21}	1381	IR, s	1387	1429	1387.7	CH ₂ scis
	ν_{22}	1297	IR, w	1293	1335	1293.9	CH ip-bend
	ν_{23}	988	IR, w	995	1016	987.2	CH ₂ rock
	ν_{24}	301 ^b	IR, vw	300	298	299.8	CCC deform

^aReference 60. In an Ar matrix. R, Raman; IR, infrared; vs, very strong; s, strong; m, medium; w, weak; vw, very weak.

^bReference 51.

^cReference 60.

^dReference 64.

^eReference 65.

Resonance Raman spectra of 1,3-butadiene vapour have been observed with several laser lines between 239.5 and 165.7 nm^{27,66,67}. A broad absorption spectrum due to the $1^1B_u \leftarrow 1^1A_g$ transition is observed in the region from 230 to 190 nm; the peak which is attributed to the 0-0 transition is observed at 215.2 nm²⁷. Figure 5 shows the Raman spectra taken with excitation wavelengths between 239.5 and 199.8 nm. The intensities of fundamental, combination and overtone transitions of totally symmetric modes are prominent in the spectra taken with the 212.8- and 199.8-nm laser lines (Figures 5e and 5f); these features appear because of the resonance enhancement with the allowed 1^1B_u state through the term I (Frank-Condon) scattering mechanism. The ν_4 (the C=C stretch) and ν_7 (the C-C stretch) transitions and their overtone and combination transitions are especially enhanced, because the ν_4 and ν_7 modes suffer the largest displacement in equilibrium position in going from the ground electronic state to the 1^1B_u excited state. Since the 1^1B_u state results from a $\pi-\pi^*$ excitation, one would expect the C=C double bond distances to become longer and the C-C single bond distance to become shorter. On the other hand, a Raman spectrum resonant with the 1^1B_u excited state has been calculated from the quantum chemical force field (QCFF/PI) method²²; the results

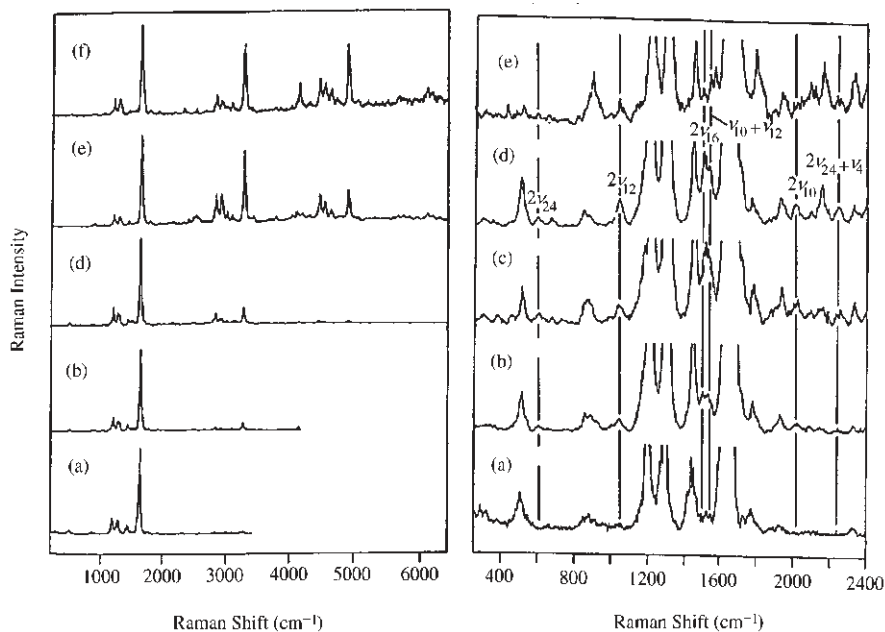


FIGURE 5. Raman spectra of *s-trans*-1,3-butadiene vapour. Excitation wavelengths: (a) 239.5 nm; (b) 228.7 nm; (c) 223.1 nm; (d) 217.9 nm; (e) 212.8 nm; (f) 199.8 nm. The spectra shown on the right are expansions. Reproduced by permission of American Institute of Physics from Reference 27

obtained have shown that the term I contributions to the a_g modes are much larger than the corresponding term II contributions.

In the case of the forbidden $2^1A_g \leftarrow 1^1A_g$ transition, the contribution of the term III scattering to Raman intensities is important, as described in Section II.D. In the Raman spectra taken with the 228.7-, 223.1- and 217.9-nm laser lines (Figures 5b–5d), the intensity of the 600-cm^{-1} band due to the binary overtone of $\nu_{24}(b_u)$ is enhanced; the ν_{24} band is assigned to the in-plane CCC deform (Table 6). It has been shown^{27,66} that $2\nu_{24}$ is enhanced by resonance with the 2^1A_g state through the $\langle 0_{24}|Q_{24}|1_{24}\rangle\langle 1_{24}|Q_{24}|2_{24}\rangle$ term. It should be noted that the ν_{24} fundamental band is not enhanced through the term III scattering mechanism. The vibronic coupling matrix elements between the 2^1A_g and 1^1B_u excited states are non-zero for promoting modes with b_u symmetry; calculations of these matrix elements for the eight b_u modes have shown that ν_{24} is expected to be the most active mode²⁷. In the case of *trans,trans*-1,3,5,7-octatetraene, a similar b_u CCC deform is a promoting mode which is active in vibronic coupling between the 1^1B_u and 2^1A_g excited states¹. From the Raman results of 1,3-butadiene, the 2^1A_g electronic state has been estimated to be about 2000 cm^{-1} below the 1^1B_u state.

The Raman spectra of 1,3-butadiene have also been taken with the excitation wavelengths in the range between 425 and 270 nm (pre-resonance conditions)⁶⁸. The pre-resonance Raman excitation profiles have been analysed by the term I scattering mechanism associated with the 1^1B_u state, and the bond lengths and bond angles of this state have been estimated; for example, the estimated lengths of the C_1C_2 and C_2C_3 bonds are 1.418 and 1.403 Å, respectively. The term II contributions to the b_g

(non-totally symmetric) modes in a non-resonant condition are clearly shown in the spectrum calculated at the QCFF/PI method²².

2. *Gauche conformer*

The potential energy function around the C–C bond of 1,3-butadiene has been studied by measuring the fundamental and overtones of the C–C torsional vibration⁶⁹. The structure of the second stable conformer (planar *s-cis* or *gauche*), however, was not determined, because few bands due to the second stable conformer were observed. The second stable conformer has been detected by means of the combination of matrix-isolation infrared spectroscopy and a high-temperature nozzle technique^{56,60,70}. The structure of the second stable conformer has been proposed to be planar *s-cis*, on the basis of the following reasons⁷¹. The position of the observed electronic absorption maximum of the second stable conformer is lower in energy than that of the *s-trans* conformer; this red shift has been attributed to the *s-cis* conformer on the basis of the results of molecular orbital calculations⁷¹. On the other hand, a *gauche* structure is proposed from a vibrational study⁶⁰. A polarized infrared study has supported the *s-cis* conformation (maximum dihedral angle, 10–15°)⁷². However, Bock and Panchenko⁷³ have argued that there is no direct correlation between the shift of the electronic absorption maximum and the conformation of 1,3-butadiene, and the polarization measurements can be interpreted in terms of a *gauche* structure. *Ab initio* MO calculations at high levels^{63,64,74–76} have been performed, and all the results have indicated that the second stable conformer has *gauche* structures. High-level *ab initio* MO calculations^{63,64,74–76} indicate that CCCC dihedral angles are in the range between 35° and 40° and barriers to the *s-cis* transition state are in the range between 0.5 and 1.0 kcal mol⁻¹.

Vibrational spectroscopy has given us evidence that the second stable conformer has a *gauche* structure. A *gauche* structure has C_2 symmetry. There are 24 normal modes: $13a + 11b$. The *a* and *b* modes are both Raman and infrared active. On the other hand, the *s-cis* conformer has C_{2v} symmetry. There are 24 normal modes: $9a_1 + 4a_2 + 8b_1 + 3b_2$. The a_1 and b_1 modes are the in-plane vibrations whilst the a_2 and b_2 modes are the out-of-plane vibrations. The vibrations of a_1 , b_1 and b_2 species are infrared active, whereas all the vibrations are Raman active. It is noted that the infrared inactive a_2 vibrations of the *s-cis* conformer are correlated with the infrared active *a* vibrations of a *gauche* conformer. The observed infrared bands have been reasonably assigned to a *gauche* conformer, on the basis of the results of empirical normal coordinate calculations⁶⁰ and high-level *ab initio* MO calculations^{63,64,75,76}. The observed and calculated vibrational frequencies of *gauche*-1,3-butadiene are listed in Table 7. What is important is that the 727-cm⁻¹ band is reasonably assigned to $\nu_{11}(a)$. The corresponding bands are observed at 594, 587 and 731 cm⁻¹ for 1,3-butadiene-1,1,4,4-d₄-d₆ and -1,4-¹³C₂, respectively^{56,60}. These observations support the assignment of $\nu_{11}(a)$. The 1087-cm⁻¹ band has been attributed to ν_{20} in Reference 56 and 64, but to ν_7 in Reference 60. A scaled MP2/6-31G* calculation⁶³ indicates that the infrared intensity of ν_{20} is much larger than that of ν_7 . The 1087-cm⁻¹ band is thus assigned to ν_{20} .

The second stable conformer of isoprene ($H_2C=C(CH_3)CH=CH_2$) has also been studied experimentally^{77,78} and theoretically^{79–81}. It has been concluded that the second stable conformer has a *gauche* structure^{78–81}.

B. Hexatriene

1,3,5-Hexatriene ($CH_2=CH-CH=CH-CH=CH_2$) has three C=C bonds and two C–C bonds. There exist geometrical isomers around the central C=C bond and rotamers around

TABLE 7. Observed and calculated vibrational frequencies (cm^{-1}) of *gauche*-1,3-butadiene

Sym	Sym ^a	No.	Obsd ^b	Calcd			Description	
				Empirical ^f	MP2/6-311G ^{*g}	Scaled MP2/6-31G ^{*h}		
<i>a</i>	<i>a</i> ₁	ν_1	3103 ^c	IR, m	3098	3286	3110	CH ₂ a-stretch
	<i>a</i> ₁	ν_2	3014 ^c	IR, w	3032	3197	3035	CH stretch
	<i>a</i> ₁	ν_3	2986 ^c	IR, m	3000	3183	3024	CH ₂ s-stretch
	<i>a</i> ₁	ν_4	1633	IR, w	1629	1687	1641	C=C stretch
	<i>a</i> ₁	ν_5	1425	IR, m	1432	1487	1464	CH ₂ scis
	<i>a</i> ₁	ν_6	—	—	1328	1350	1313	CH ip-bend
	<i>a</i> ₁	ν_7	—	—	1081	1086	1057	CH ₂ rock
	<i>a</i> ₂	ν_8	983	IR, vw	982	1001	1004	CH op-bend
	<i>a</i> ₂	ν_9	915 ^d	IR, vs	915	914	943	CH ₂ wag
	<i>a</i> ₁	ν_{10}	—	—	872	905	859	C—C stretch
	<i>a</i> ₂	ν_{11}	727	IR, w	731	754	733	CH ₂ twist
	<i>a</i> ₁	ν_{12}	—	—	256	277	281	CCC deform
	<i>b</i>	<i>a</i> ₂	ν_{13}	136 ^e	—	137	190	151
<i>b</i> ₁		ν_{14}	3103 ^c	IR, m	3098	3284	3108	CH ₂ a-stretch
<i>b</i> ₁		ν_{15}	3014 ^c	IR, w	3032	3179	3028	CH stretch
<i>b</i> ₁		ν_{16}	2986 ^c	IR, m	3001	3188	3014	CH ₂ s-stretch
<i>b</i> ₁		ν_{17}	1612	IR, vw	1619	1688	1645	C=C stretch
<i>b</i> ₁		ν_{18}	1403	IR, w	1413	1453	1431	CH ₂ scis
<i>b</i> ₁		ν_{19}	—	—	1278	1317	1284	CH ip-bend
<i>b</i> ₁		ν_{20}	1087	IR, w	1040	1112	1101	CH ₂ rock
<i>b</i> ₂		ν_{21}	996	IR, vs	996	1024	1017	CH op-bend
<i>b</i> ₂		ν_{22}	914	IR, vs	907	910	946	CH ₂ wag
<i>b</i> ₁		ν_{23}	596	IR, w	597	632	619	CCC deform
<i>b</i> ₂		ν_{24}	470	IR, m	465	462	455	CH ₂ twist

^aCorresponding symmetry species of the *s-cis* conformer with C_{2v} symmetry.

^bReference 60. In an Ar matrix. R, Raman; IR, infrared; vs, very strong; s, strong; m, medium; w, weak; vw, very weak.

^cDouble assignments.

^dEstimated from the observed 1829 cm^{-1} band ($\nu_9 + \nu_{22}$).

^eReference 69.

^fReference 60.

^gReference 64.

^hReference 63.

the C—C bonds (Figure 6). The *trans* and *cis* structures around the central C=C bond are denoted as T and C, respectively, and the *trans*, *gauche* and *cis* structures around the C—C bonds as t, g and c, respectively. The two stable conformers, tTt (Figure 6a) and tCt (Figure 6d), exist at room temperature; the tTt and tCt conformers are called *trans*- and *cis*-1,3,5-hexatriene, respectively.

1. *Trans* conformer

A gas-phase electron diffraction study⁸² has shown that *trans*-hexatriene has a planar structure and the lengths of the terminal C=C, central C=C and C—C bonds are 1.337, 1.368 and 1.458 Å, respectively. The infrared and Raman spectra of *trans*-hexatriene^{83–86} and its deuterated analogs^{87–89} have been reported. Normal coordinate calculations have been performed by the extended Pariser–Parr–Pople CI method⁹⁰, the QCFF/PI method⁸⁸ and *ab initio* MO methods^{62,91–94}. There are 36 normal modes: $13a_g + 6a_u + 12b_u + 5b_g$.

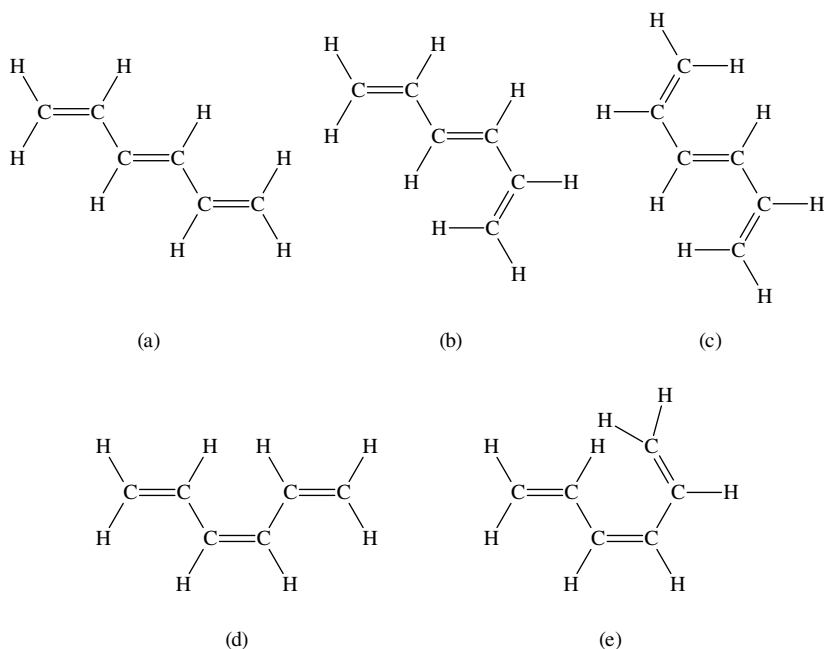


FIGURE 6. Conformers of 1,3,5-hexatriene: (a) tTt (*trans*); (b) gTt; (c) gTg; (d) tCt (*cis*); (e) gCt

The a_g and b_u modes are the in-plane vibrations whilst the a_u and b_g modes are the out-of-plane vibrations. The observed vibrational spectra and calculated frequencies are shown in Table 8. The assignments of the fundamental bands except ν_2 , ν_8 and ν_{23} have been established. The 3017-cm^{-1} Raman band reported in Reference 89 is tentatively assigned to ν_2 , although this band is not observed in References 85, 86 and 93. The medium-intensity Raman band observed at 1288 cm^{-1} in Reference 85 probably corresponds to the 1283-cm^{-1} band in Reference 86; this band is assigned to ν_9 . The very weak Raman band at 1320 cm^{-1} has been assigned to ν_9 in Reference 85, whereas the Raman band observed at 1288 cm^{-1} as a shoulder in a carbon disulphide solution has been assigned to ν_9 in Reference 86. According to the assignments in Reference 93, the Raman band observed at 651 cm^{-1} in the solid state has been tentatively assigned to ν_{23} . Vibrational modes of some strong Raman and infrared bands are as follows. The 1626-cm^{-1} Raman band (ν_5) is assigned to the vibrational mode in which three C=C bonds stretch in-phase. The 1288-cm^{-1} band (ν_9) is assigned to the CH in-plane bend. The 1191-cm^{-1} Raman band (ν_{10}) is assigned to the in-phase C—C stretch. The 1009-cm^{-1} infrared band (ν_{14}) is assigned to the in-phase CH out-of-plane bending of *trans* —CH=CH—. The 900-cm^{-1} infrared band (ν_{16}) is assigned to the CH₂ wagging.

2. *Cis* conformer

A gas-phase electron diffraction study⁹⁵ has shown that *cis*-hexatriene has a slightly twisted structure (torsional angle of 10° around the central C=C bond) and the lengths of the terminal C=C, central C=C and C—C bonds are 1.336, 1.362 and

TABLE 8. Observed and calculated vibrational frequencies (cm^{-1}) of *trans*-1,3,5-hexatriene

Sym	No.	Obsd ^a	Calcd		Description	
			Scaled HF/6-31G ^g	Scaled MP2/ 6-31G ^{*h}		
a_g	ν_1	3089	R, m	3097	3106	CH ₂ a-stretch
	ν_2	3017 ^b	R, w	3022	3019	CH ₂ s-stretch
	ν_3	3000	R, m	3012	3005	CH stretch
	ν_4	2992	R, m	3008	2992	CH stretch
	ν_5	1626	R, vs	1649	1637	C=C stretch
	ν_6	1576	R, w	1558	1571	C=C stretch
	ν_7	1399	R, m	1405	1397	CH ₂ scis
	ν_8	1288 ^c ; 1320 ^d	R, w, sh; R, vw	1298	1296	CH ip-bend
	ν_9	1288 ^d	R, m	1275	1288	CH ip-bend
	ν_{10}	1191	R, s	1197	1195	C-C stretch
	ν_{11}	932	R, w	930	938	CH ₂ rock
	ν_{12}	443	R, w	429	436	CCC deform
	ν_{13}	353	R, w	344	349	CCC deform
a_u	ν_{14}	1009	IR, vs	1018	1020	CH op-bend
	ν_{15}	941	IR, m	939	942	CH op-bend
	ν_{16}	900	IR, vs	903	901	CH ₂ wag
	ν_{17}	682	IR, m	672	680	CH ₂ twist
	ν_{18}	248 ^e	IR, vw	246	245	C=C torsion
	ν_{19}	94 ^e	IR, vw	98	98	C-C torsion
b_g	ν_{20}	986	R, vw	991	988	CH op-bend
	ν_{21}	903	R, w	913	901	CH ₂ wag
	ν_{22}	868	R, vw	858	866	CH op-bend
	ν_{23}	615 ^f	R, vw	589	600	C=C torsion
	ν_{24}	215 ^e	R, vw	221	215	C-C torsion
b_u	ν_{25}	3091	IR, m	3097	3106	CH ₂ a-stretch
	ν_{26}	3039	IR, m	3022	3018	CH stretch
	ν_{27}	3008	IR, m	3017	3006	CH ₂ s-stretch
	ν_{28}	2969	IR, w	3006	2994	CH stretch
	ν_{29}	1624	IR, s	1618	1624	C=C stretch
	ν_{30}	1429	IR, m	1444	1431	CH ₂ scis
	ν_{31}	1294	IR, w	1293	1287	CH ip-bend
	ν_{32}	1255	IR, w	1251	1254	CH ip-bend
	ν_{33}	1128	IR, w	1125	1123	C-C stretch
	ν_{34}	964	IR, vw	955	960	CH ₂ rock
	ν_{35}	541	IR, w	533	544	CCC deform
	ν_{36}	152 ^e	IR, w	145	148	CCC deform

^aReference 93. Observed in liquid.^bReference 89.^cReference 86. Observed in CS₂ solution.^dReference 85. Observed in liquid.^eReference 86. Observed in vapour.^fObserved in solid at low temperature.^gReference 93.^hReference 94.

1.462 Å, respectively. The infrared and Raman spectra of *cis*-hexatriene^{84–86,96} and its deuterated analogs^{87,88} have been reported. The structures and vibrational frequencies have been calculated by means of MO methods^{87,88,91,93,94}. According to *ab initio* MO calculations^{91,93,94} (HF/6-31G, HF/6-31G* and MP2/6-31G* levels), *cis*-hexatriene has a planar structure. The observed vibrational spectra have been reasonably explained by the

TABLE 9. Observed and calculated vibrational frequencies (cm^{-1}) of *cis*-1,3,5-hexatriene

Sym	No.	Obsd ^a	Calcd		Description	
			Scaled HF/631G ^c	Scaled MP2/ 6-31G ^{sd}		
<i>a</i> ₁	ν_1	3090	R, w	3097	3105	CH ₂ a-stretch
	ν_2	—	—	3051	3038	CH stretch
	ν_3	3011	R, m	3032	3016	CH stretch
	ν_4	2995	R, m	3014	3012	CH ₂ s-stretch
	ν_5	1626	R, vs	1649	1637	C=C stretch
	ν_6	1580	R, vw	1548	1558	C=C stretch
	ν_7	1397	R, m; IR, vw	1405	1397	CH ₂ scis
	ν_8	1318	R, m; IR, w	1317	1314	CH ip-bend
	ν_9	1247	R, s	1254	1249	CH ip-bend
	ν_{10}	1084	R, w; IR, vw	1080	1085	C—C stretch
	ν_{11}	883	R, w	862	875	CH ₂ rock
	ν_{12}	392	R, m	383	390	CCC deform
	ν_{13}	166	R, w	164	173	CCC deform
<i>a</i> ₂	ν_{14}	990; 1032 ^b	R, vw; R, vw	1007	985	CH op-bend
	ν_{15}	953	R, w	962	918	CH op-bend
	ν_{16}	905	R, w	908	901	CH ₂ wag
	ν_{17}	705	R, w	701	689	CH ₂ twist
	ν_{18}	331	R, w	324	312	C=C torsion
	<i>b</i> ₁	ν_{19}	155 ^b	R, vw	148	140
ν_{20}		3089	IR, s	3096	3105	CH ₂ a-stretch
ν_{21}		3045	IR, m	3033	3025	CH stretch
ν_{22}		3014	IR, m	3015	3013	CH ₂ s-stretch
ν_{23}		2979	IR, w	3007	2994	CH stretch
ν_{24}		1616	IR, s	1611	1617	C=C stretch
ν_{25}		1449	IR, s; R, vw	1456	1448	CH ₂ scis
ν_{26}		1355	IR, vw	1347	1350	CH ip-bend
ν_{27}		1279	IR, w	1284	1274	CH ip-bend
ν_{28}		1185	IR, w; R, w	1189	1192	C—C stretch
ν_{29}		950	IR, m; R, w	944	950	CH ₂ rock
ν_{30}		675	IR, vw	675	679	CCC deform
ν_{31}		356	IR, w; R, vw	346	352	CCC deform
<i>b</i> ₂		ν_{32}	989	IR, s	994	988
	ν_{33}	906	IR, vs	915	904	CH ₂ wag
	ν_{34}	815	IR, m	789	838	CH op-bend
	ν_{35}	590	IR, s	576	587	CH ₂ twist
	ν_{36}	100 ^b	IR	101	101	C—C torsion

^aReference 93. Observed in liquid.^bReference 86.^cReference 93.^dReference 94.

planar structure (C_{2v} symmetry). There are 36 normal modes: $13a_1 + 6a_2 + 12b_1 + 5b_2$. The a_1 and b_1 modes are the in-plane vibrations and the a_2 and b_2 modes are the out-of-plane vibrations. The a_1 , b_1 and b_2 vibrations are infrared active and all the vibrations are Raman active. The observed and calculated vibrational frequencies are shown in Table 9. The assignments of the fundamental bands except ν_2 , ν_{14} and ν_{26} have been established. Vibrational modes of some strong Raman and infrared bands are as follows. The 1626-cm^{-1} Raman band (ν_5) is assigned to the in-phase C=C stretch. The frequency of this mode is almost equal to that of *trans*-1,3,5-hexatriene. The 1247-cm^{-1} Raman band (ν_9) is assigned to the CH in-plane bending. The 883-cm^{-1} Raman band (ν_{11}) is

assigned to the C–C stretch. The 906-cm^{-1} infrared band (ν_{33}) is assigned to the CH_2 wagging. The 815-cm^{-1} infrared band (ν_{34}) is assigned to the CH out-of-plane bending of *cis* –CH=CH–.

3. Other conformers

Unstable conformers of *trans*- and *cis*-hexatriene have been detected by means of the combination of matrix-isolation infrared spectroscopy and photoexcitation (or the high-temperature nozzle technique)⁸⁴. *Ab initio* MO calculations at the HF/6-31G level have been performed for several conformers of 1,3,5-hexatriene⁹³. The observed infrared bands of unstable conformers have been attributed to the gTt (major species) and gTg (minor species) conformers of *trans*-hexatriene and the gCt conformer of *cis*-hexatriene⁹³. It is noted that, in the previous paper⁹³, the notation c is used for twisted structures for the sake of simplicity. The calculated torsional angles around C–C bonds for the gTt, gTg and gCt conformers are in the range between 32° and 45° . The observed and calculated vibrational frequencies of gTt and gCt are reported in Reference 93.

C. Long Chain Polyenes

1. All-*trans* conformers

The Raman spectra of all-*trans*- α,ω -dibutylpolyenes have been studied⁹⁷ systematically as a function of $N_{\text{C}=\text{C}}$ from 3 to 12. The observed Raman spectra of α,ω -dibutylpolyenes are shown in Figure 7. Four branches which are called ν_1 , ν_2 , ν_3 and ν_4 are observed. Figure 8 shows the plots of observed Raman frequencies against $N_{\text{C}=\text{C}}$ for unsubstituted polyenes^{60,93,98,99}, α,ω -dibutylpolyenes⁹⁷ and carotenoids [β -carotene¹⁰⁰ (Figure 1c), rhodovibrin¹⁰¹, spirilloxanthin¹⁰¹, decapreno- β -carotene¹⁰² ($\text{C}_{50}\text{H}_{68}$) and dodecapreno- β -carotene¹⁰² ($\text{C}_{60}\text{H}_{80}$)]. *Trans*-polyacetylene gives rise to the Raman bands similar to those of polyenes^{103–107}. A *trans*-polyacetylene film consists of all-*trans* conjugated segments with various conjugation lengths^{5–7}. The all-*trans* structure is schematically shown in Figure 9a. Figure 4 and Tables 1–5 show that with increasing $N_{\text{C}=\text{C}}$, the electronic absorption maximum of the $1^1\text{B}_u \leftarrow 1^1\text{A}_g$ transition shifts to longer wavelengths. Thus, a Raman spectrum taken with a red laser line provides Raman bands arising from a long segment, whose conjugation length is not accurately determined. In the Raman spectrum taken with the 632.8-nm laser line¹⁰⁷, the 1457-, 1294-, 1174- and 1066-cm^{-1} Raman bands are observed. These frequencies are shown as dotted lines in Figure 8, in comparison with those of the polyenes. The 1457-, 1294- and 1066-cm^{-1} bands are assigned to optically active a_g modes under the infinite all-*trans* structure (C_{2h} symmetry), whereas the 1174-cm^{-1} band is assigned to an optically inactive mode¹⁰⁷. Normal coordinate calculations have been performed for the all-*trans* conformers of unsubstituted polyenes ($N_{\text{C}=\text{C}} = 4\text{--}6$)^{59,62,98,99,108–112} and the infinite all-*trans* structure^{107,111,113–121}.

The frequency of the ν_1 band, which is assigned to the in-phase C=C stretch, is not affected by the substitution of hydrogen atoms with alkyl groups. The ν_1 frequency is sensitive to $N_{\text{C}=\text{C}}$ ^{102,103}. As $N_{\text{C}=\text{C}}$ increases, the ν_1 frequency decreases drastically; the ν_1 frequency shows a downshift of about 190 cm^{-1} in going from 1,3-butadiene to *trans*-polyacetylene. *Ab initio* MO calculations^{99,111,112} at the HF and MP levels have shown that electron correlation has a profound effect on the frequency of the in-phase C=C stretches (ν_1). While these unusually low frequencies of the ν_1 bands for the ground state (1^1A_g) are observed, unusually high frequencies of corresponding modes are observed for the 2^1A_g electronically excited state; these results have been explained³ by the vibronic

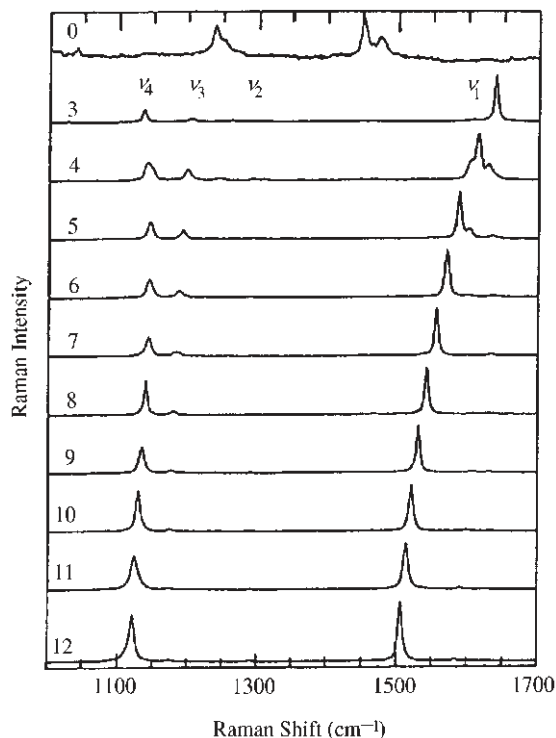


FIGURE 7. Raman spectra of α,ω -dibutylpolyenes in solid ($N_{C=C} = 3-12$). Reproduced by permission of American Institute of Physics from Reference 97

coupling between the $1A_g$ ground state and the $2A_g$ excited state. The observed ν_1 frequencies have been fitted by equation 10¹²² and equation 11⁹⁷:

$$\nu_1(\text{cm}^{-1}) = \nu_\infty + \frac{K}{N_{C=C} + 1} \quad (10)$$

where $\nu_\infty = 1454 \text{ cm}^{-1}$ (the observed ν_1 frequency of *trans*-polyacetylene) and $K = 727 \text{ cm}^{-1}$, and

$$\nu_1(\text{cm}^{-1}) = \nu'_\infty + \frac{K'}{N_{C=C}} \quad (11)$$

where $\nu'_\infty = 1438 \text{ cm}^{-1}$ and $K' = 830 \text{ cm}^{-1}$; these values have been obtained from the observed ν_1 frequencies of α,ω -dibutylpolyenes ($N_{C=C} = 7-12$). By using equation 10 or 11, it is possible to estimate $N_{C=C}$ of the all-*trans* structure from the observed ν_1 frequency. It should be noted that equation 10 or 11 gives a rough estimation of $N_{C=C}$ in the region of large $N_{C=C}$ values.

The ν_2 band is assigned to a mixture of the C–C and C=C stretches. The frequencies of the ν_2 bands are insensitive to $N_{C=C}$.

The ν_3 and ν_4 bands are assigned to mixtures of CH in-plane bend and C=C and C–C stretches. The frequencies of these bands are affected significantly by the substitution of

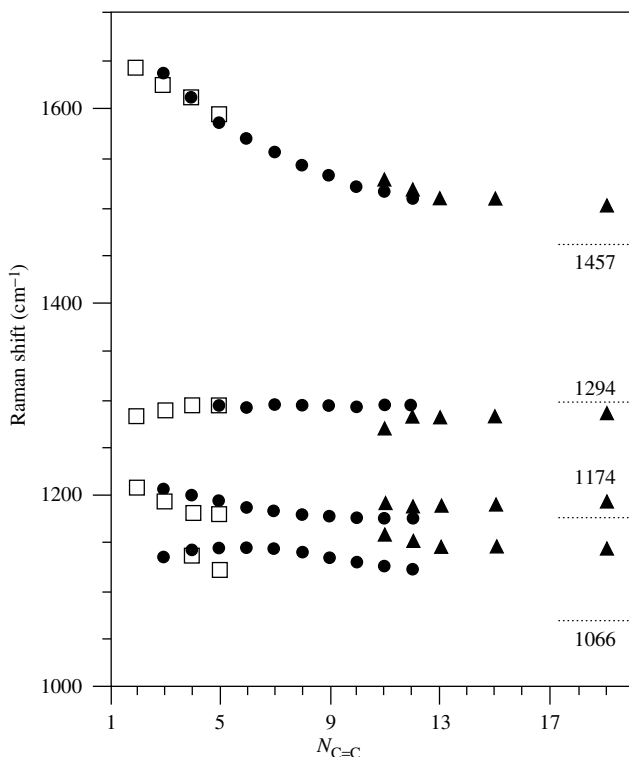


FIGURE 8. Relationship between $N_{C=C}$ and observed Raman frequencies: \square , unsubstituted polyenes^{60,93,98,99}; \bullet , α,ω -dibutylpolyenes⁹⁷; \blacktriangle , carotenoids (β -carotene¹⁰⁰ [$N_{C=C} = 11$], rhodovibrin¹⁰¹ [$N_{C=C} = 12$], spirilloxanthin¹⁰¹ [$N_{C=C} = 13$], decapreno- β -carotene¹⁰² [$N_{C=C} = 15$] and dodecapreno- β -carotene¹⁰² [$N_{C=C} = 19$]). Dotted lines and figures refer to the observed Raman frequencies of *trans*-polyacetylene¹⁰⁷

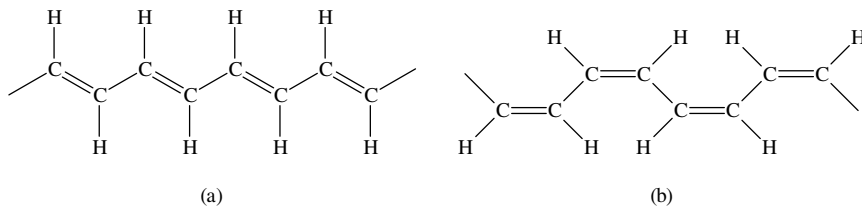


FIGURE 9. Chemical structures of polyacetylene: (a) *trans-transoid* (*trans*); (b) *cis-transoid* (*cis*)

hydrogen atoms with alkyl groups. In a series of unsubstituted polyenes, the intensity of the ν_3 band is much larger than that of the ν_4 band. On the other hand, for a series of α,ω -dibutylpolyenes, the intensity of the ν_4 band is much larger than that of the ν_3 band. These observations indicate that the mode mixing between ν_3 and ν_4 for α,ω -dibutylpolyenes is different from that for unsubstituted polyenes. The spectral features of α,ω -dibutylpolyenes are similar to that of *trans*-polyacetylene.

It has been reported¹²³ that infrared frequencies of the CH out-of-plane bending vibrations of olefins are sensitive to the number and position of hydrogen atoms attached to the C=C bond. The in-phase CH out-of-plane bending vibrations are observed in the range between 1009 and 1015 cm⁻¹: 1009, 1011, 1010 and 1015 cm⁻¹, for *trans*-hexatriene⁹⁰, *trans,trans*-1,3,5,7-octatetraene⁹⁸, all-*trans*-1,3,5,7,9-decapentaene⁹⁹ and *trans*-polyacetylene¹²⁴, respectively.

2. *Cis* conformers

In addition to the vibrational spectra of *cis*-hexatriene, only the frequencies 1604 and 1260 cm⁻¹ of *cis,cis*-octatetraene¹²⁵ have been reported for unsubstituted polyenes. Raman studies^{13,126} of the β -carotene conformers with one or two *cis* C=C bonds have shown that frequencies and intensities of several Raman bands in the region between 1300 and 1100 cm⁻¹ are sensitive to the conformation of β -carotene. The Raman and infrared spectra of all-*trans* retinal and its geometrical isomers with one or two *cis* bonds are described in a previous review¹¹. A *cis*-polyacetylene film contains mainly all-*cis* conjugated segments^{7,124}. The all-*cis* structure is shown schematically in Figure 9b. In the Raman spectrum¹²⁷ of a *cis*-polyacetylene film, strong bands are observed at 1540, 1250 and 910 cm⁻¹; these bands have been assigned to the a_g modes of the infinite all-*cis* structure (D_{2h} symmetry). Normal coordinate calculations have been performed for the infinite all-*cis* structure^{118,128}. The 1540-, 1250- and 910-cm⁻¹ bands of *cis*-polyacetylene correspond to the 1626-, 1247- and 883-cm⁻¹ bands of *cis*-1,3,5-hexatriene, respectively. Since the number of the C=C bonds of all-*cis* conjugated segments in *cis*-polyacetylene is believed to be large, it is likely that the frequency dispersion of the C=C stretches for all-*cis* polyenes is smaller than that for all-*trans* polyenes. It has been reported¹²³ that the CH out-of-plane bending vibrations of *cis* -CH=CH- are observed between 675 and 730 cm⁻¹ for olefins. The corresponding vibration is observed at 815 cm⁻¹ for *cis*-hexatriene. The strong infrared band observed at 740 cm⁻¹ for *cis*-polyacetylene is assigned to the CH out-of-plane bending¹²⁴; the corresponding bands are observed at 810, 800, 760 and 748 cm⁻¹ for *cis*-copoly(acetylene + acetylene-d₂), and these bands have been attributed to the *cis* CH out-of-plane bending vibrations of (-CH=CH-)₁, (-CH=CH-)₂, (-CH=CH-)₃₋₅ and (-CH=CH-)_n ($n \geq 6$), respectively¹²⁴. The CH out-of-plane bending is thus a marker for *cis* -CH=CH-.

Since there are few studies on the vibrational spectra of polyenes with *cis* C=C bonds, experimental studies of *cis* polyenes are required.

V. REFERENCES

1. B. S. Hudson, B. E. Kohler and K. Schulten, *Excited States*, **6**, 1 (1982).
2. B. Kohler, in *Conjugated Polymers* (Eds. J. L. Brédas and R. Silbey), Klumer Academic Publisher, Dordrecht, 1991, pp. 405-434.
3. G. Orlandi, F. Zerbetto and M. Z. Zgierski, *Chem. Rev.*, **91**, 867 (1991).
4. H. Kiess (Ed.), *Conjugated Conducting Polymers*, Springer-Verlag, Berlin, 1992.
5. H. Kuzmany, *Makromol. Chem., Macromol. Symp.*, **37**, 81 (1990).
6. M. Gussoni, C. Castiglioni and G. Zerbi, in *Spectroscopy of Advanced Materials* (Eds. R. J. H. Clark and R. E. Hester), Wiley, Chichester, 1991, pp. 251-353.
7. I. Harada and Y. Furukawa, in *Vibrational Spectra and Structure*, Vol. 19 (Ed. J. R. Durig), Elsevier, Amsterdam, 1991, pp. 369-469.
8. R. R. Birge, *Annu. Rev. Phys. Chem.*, **41**, 683 (1990).
9. G. Britton and T. W. Goodwin (Eds.), *Carotenoid Chemistry and Biochemistry*, Pergamon Press, Oxford, 1982.

10. J. Terner and M. A. El-Sayed, *Acc. Chem. Res.*, **18**, 331 (1985).
11. B. Curry, I. Palings, A. D. Broek, J. A. Pardo, J. Lugtenburg and R. Mathies, in *Advances in Infrared and Raman Spectroscopy*, Vol. 12 (Eds. R. J. H. Clark and R. E. Hester), Wiley, Chichester, 1985, pp. 115–178.
12. M. Stockburger, T. Alshuth, D. Oesterhelt and W. Gärtner, in *Spectroscopy of Biological Systems* (Eds. R. J. H. Clark and R. E. Hester), Wiley, Chichester, 1986, pp. 483–535.
13. Y. Koyama, in *Carotenoids: Chemistry and Biology* (Ed. N. I. Krinsky), Plenum Press, New York, 1990, pp. 207–222.
14. F. Siebert, in *Biomolecular Spectroscopy, Part A* (Eds. R. J. H. Clark and R. E. Hester), Wiley, Chichester, 1993, pp. 1–54.
15. M. Tasumi and M. Nakata, *J. Mol. Struct.*, **126**, 111 (1985).
16. R. J. H. Clark and R. E. Hester (Eds.), *Advances in Non-Linear Spectroscopy*, Wiley, Chichester, 1987.
17. T. Shimanouchi, in *Physical Chemistry*, Vol. 4 (Eds. H. Eyring, D. Henderson and W. Jost), Academic Press, New York, 1970, pp. 233–306.
18. H. Matsuura and M. Tasumi, in *Vibrational Spectra and Structure*, Vol. 12 (Ed. J. R. Durig), Elsevier, Amsterdam, 1983, pp. 69–143.
19. G. Fogarasi and P. Pulay, in *Vibrational Spectra and Structure*, Vol. 14 (Ed. J. R. Durig), Elsevier, Amsterdam, 1985, pp. 125–219.
20. H. A. Kramers and W. Heisenberg, *Z. Phys.*, **31**, 681 (1925).
21. P. A. M. Dirac, *Proc. Roy. Soc. (London)*, **114**, 710 (1927).
22. A. Warshel and P. Dauber, *J. Chem. Phys.*, **66**, 5477 (1977).
23. L. D. Ziegler and B. Hudson, *J. Chem. Phys.*, **74**, 982 (1981).
24. S. Li and B. Hudson, *Chem. Phys. Lett.*, **148**, 581 (1988).
25. A. C. Albrecht, *J. Chem. Phys.*, **34**, 1476 (1961).
26. F. Inagaki, M. Tasumi and T. Miyazawa, *J. Mol. Spectrosc.*, **50**, 286 (1974).
27. R. R. Chadwick, M. Z. Zgierski and B. S. Hudson, *J. Chem. Phys.*, **95**, 7204 (1991).
28. I. W. Sztainbuch and G. E. Leroi, *J. Chem. Phys.*, **93**, 4642 (1990).
29. F. Sondheimer, D. A. Ben-Efraim and R. Wolovsky, *J. Am. Chem. Soc.*, **83**, 1675 (1961).
30. W. F. Forbes, R. Shilton and A. Balasubramanian, *J. Org. Chem.*, **29**, 3527 (1964).
31. C. W. Spangler and D. A. Little, *J. Chem. Soc., Perkin Trans. 1*, 2379 (1982).
32. P. Nayler and M. C. Whiting, *J. Chem. Soc.*, 3037 (1955).
33. C. W. Spangler and R. A. Rathunde, *J. Chem. Soc., Chem. Commun.*, 26 (1989).
34. K. Knoll and R. R. Schrock, *J. Am. Chem. Soc.*, **111**, 7989 (1989).
35. K. W. Hausser, R. Kuhn, A. Smakula and K. H. Kreuchen, *Z. Phys. Chem.*, **B29**, 363 (1935).
36. K. W. Hausser, R. Kuhn and A. Smakula, *Z. Phys. Chem.*, **B29**, 384 (1935).
37. C. W. Spangler, P.-K. Liu, A. A. Dembek and K. O. Havelka, *J. Chem. Soc., Perkin Trans. 1*, 799 (1991).
38. L. Zechmeister, *Cis-Trans Isomeric Carotenoids, Vitamins A, and Arylpolynes*, Academic Press, New York, 1962.
39. R. M. Gavin, Jr., C. Weisman, J. K. McVey and S. A. Rice, *J. Chem. Phys.*, **68**, 522 (1978).
40. M. F. Granville, G. R. Holtom and B. E. Kohler, *J. Chem. Phys.*, **72**, 4671 (1980).
41. H. L. -B. Fang, R. J. Thrash and G. E. Leroi, *Chem. Phys. Lett.*, **57**, 59 (1978).
42. W. J. Buma, B. E. Kohler and K. Song, *J. Chem. Phys.*, **92**, 4622 (1990).
43. J. L. Brédas, R. Silbey, D. S. Boudreaux and R. R. Chance, *J. Am. Chem. Soc.*, **105**, 6555 (1983).
44. S. Etamad, A. J. Heeger, L. Lauchlan, T.-C. Chung and A. G. MacDiarmid, *Mol. Cryst. Liq. Cryst.*, **77**, 43 (1981).
45. A. Almenningsen, O. Bastiansen and M. Traetteberg, *Acta Chem. Scand.*, **12**, 1221 (1958).
46. D. J. Marais, N. Sheppard and B. P. Stoicheff, *Tetrahedron*, **17**, 163 (1962).
47. K. Kuchitsu, T. Fukuyama and Y. Morino, *J. Mol. Struct.*, **1**, 463 (1967).
48. R. S. Rasmussen and R. R. Brattain, *J. Chem. Phys.*, **15**, 131 (1947).
49. C. M. Richards and J. R. Nielsen, *J. Opt. Soc. Am.*, **40**, 438 (1950).
50. R. K. Harris, *Spectrochim. Acta*, **20**, 1129 (1964).
51. A. R. H. Cole, A. A. Green and G. A. Osborne, *J. Mol. Spectrosc.*, **48**, 212 (1973).
52. Yu. N. Panchenko, Yu. A. Pentin, V. I. Tyulin and V. M. Tatevskii, *Opt. Spectrosc.*, **16**, 536 (1964).
53. I. S. Borshagovskaya, Yu. N. Panchenko and Yu. A. Pentin, *Opt. Spectrosc.*, **22**, 194 (1967).
54. Yu. N. Panchenko, *Spectrochim. Acta*, **31A**, 1201 (1975).

55. E. Benedetti, M. Aglietto, S. Pucci, Yu. N. Panchenko, Yu. A. Pentin and O. T. Nikitin, *J. Mol. Struct.*, **49**, 293 (1978).
56. P. Huber-Wälchli and H. H. Günthard, *Spectrochim. Acta*, **37A**, 285 (1981).
57. L. M. Sverdlov and N. V. Tarasova, *Opt. Spectrosc.*, **9**, 159 (1960).
58. E. M. Popov and G. A. Kogan, *Opt. Spectrosc.*, **17**, 362 (1964).
59. R. M. Gavin and S. A. Rice, *J. Chem. Phys.*, **55**, 2675 (1971).
60. Y. Furukawa, H. Takeuchi, I. Harada and M. Tasumi, *Bull. Chem. Soc. Jpn.*, **56**, 392 (1983).
61. C. W. Bock, M. Trachtman and P. George, *J. Mol. Spectrosc.*, **84**, 243 (1980).
62. P. G. Szalay, A. Karpfen and H. Lischka, *J. Chem. Phys.*, **87**, 3530 (1987).
63. K. B. Wiberg and R. E. Rosenberg, *J. Am. Chem. Soc.*, **112**, 1509 (1990).
64. H. Guo and M. Karplus, *J. Chem. Phys.*, **94**, 3679 (1991).
65. W. Tang and T. Bally, *J. Phys. Chem.*, **97**, 4365 (1993).
66. R. R. Chadwick, D. P. Gerrity and B. S. Hudson, *Chem. Phys. Lett.*, **115**, 24 (1985).
67. G. D. Strahan and B. S. Hudson, *J. Chem. Phys.*, **99**, 5780 (1993).
68. R. J. Hemley, J. I. Dawson and V. Vaida, *J. Chem. Phys.*, **78**, 2915 (1983).
69. L. A. Carreira, *J. Chem. Phys.*, **62**, 3851 (1975).
70. P. Huber-Wälchli, *Ber. Bunsenges Phys. Chem.*, **82**, 10 (1978).
71. M. E. Squillacote, T. C. Semple and P. W. Mui, *J. Am. Chem. Soc.*, **107**, 6842 (1985).
72. J. J. Fisher and J. Michl, *J. Am. Chem. Soc.*, **109**, 1056 (1987).
73. C. W. Bock and Yu. N. Panchenko, *J. Mol. Struct. (Theochem)*, **187**, 69 (1989).
74. P. G. Szalay, H. Lischka and A. Karpfen, *J. Phys. Chem.*, **93**, 6629 (1989).
75. J. E. Rice, B. Liu, T. J. Lee and C. M. Rohlffing, *Chem. Phys. Lett.*, **161**, 277 (1989).
76. I. L. Albers and H. F. Schaffer III, *Chem. Phys. Lett.*, **161**, 375 (1989).
77. D. A. C. Compton, W. O. George and W. F. Maddams, *J. Chem. Soc., Perkin Trans. 2*, 1666 (1976).
78. T. Ishibashi, Y. Furukawa and M. Tasumi, *J. Chem. Soc. Jpn., Chem. Industrial Chem.*, 1418 (1989).
79. K. Kavana-Saebø, S. Saebø and J. Boggs, *J. Mol. Struct. (Theochem)*, **106**, 259 (1984).
80. M. Traetteberg, G. Paulen, S. J. Cyvin, Yu. N. Panchenko and V. I. Mochalov, *J. Mol. Struct.*, **116**, 141 (1984).
81. C. W. Bock, Yu. N. Panchenko, S. V. Krasnoshchiokov and R. Aroca, *J. Mol. Struct.*, **160**, 337 (1987).
82. M. Traetteberg, *Acta Chem. Scand.*, **22**, 628 (1968).
83. E. R. Lippincott, C. E. White and J. P. Sibia, *J. Am. Chem. Soc.*, **80**, 2926 (1958).
84. Y. Furukawa, H. Takeuchi, I. Harada and M. Tasumi, *J. Mol. Struct.*, **100**, 341 (1983).
85. R. McDiarmid and A. Sabljic, *J. Phys. Chem.*, **91**, 276 (1987).
86. F. W. Langkilde, R. Wilbrandt, O. F. Nielsen, D. H. Christensen and F. M. Nicolaisen, *Spectrochim. Acta*, **43A**, 1209 (1987).
87. Yu. N. Panchenko, P. Császár and F. Török, *Acta Chim. Hung.*, **113**, 149 (1983).
88. F. Negri, G. Orlandi, A. M. Brouwer, F. W. Langkilde and R. Wilbrandt, *J. Chem. Phys.*, **90**, 5944 (1989).
89. F. W. Langkilde, R. Wilbrandt and A. M. Brouwer, *J. Phys. Chem.*, **94**, 4809 (1990).
90. R. J. Hemley, B. R. Brooks and M. Karplus, *J. Chem. Phys.*, **85**, 6550 (1986).
91. C. W. Bock, Yu. N. Panchenko, S. V. Krasnoshchiokov and V. I. Pupyshev, *J. Mol. Struct. (Theochem)*, **148**, 131 (1986).
92. G. Fogarasi, P. G. Szalay, P. P. Liescheski, J. E. Boggs and P. Pulay, *J. Mol. Struct. (Theochem)*, **151**, 341 (1987).
93. H. Yoshida, Y. Furukawa and M. Tasumi, *J. Mol. Struct.*, **194**, 279 (1989).
94. H. Torii and M. Tasumi, *Vib. Spectrosc.*, **8**, 205 (1995).
95. M. Traetteberg, *Acta Chem. Scand.*, **22**, 2294 (1968).
96. E. R. Lippincott and T. E. Kenny, *J. Am. Chem. Soc.*, **84**, 3641 (1962).
97. H. E. Schaffer, R. R. Chance, R. J. Silbey, K. Knoll and R. R. Schrock, *J. Chem. Phys.*, **94**, 4161 (1991).
98. H. Yoshida and M. Tasumi, *J. Chem. Phys.*, **89**, 2803 (1988).
99. S. Hirata, H. Yoshida, H. Torii and M. Tasumi, *J. Chem. Phys.*, **103**, 8955 (1995).
100. H. Hashimoto, Y. Koyama, Y. Hirata and N. Mataga, *J. Phys. Chem.*, **95**, 3072 (1991).
101. M. Naruse, H. Hashimoto, M. Kuki and Y. Koyama, *J. Mol. Struct.*, **242**, 15 (1991).
102. L. Rimai, M. E. Heyde and D. Gill, *J. Am. Chem. Soc.*, **95**, 4493 (1973).

103. I. Harada, M. Tasumi, H. Shirakawa and S. Ikeda, *Chem. Lett.*, 1411 (1978).
104. L. S. Lichtmann and D. B. Fitchen, *Synth. Met.*, **1**, 139 (1979/1980).
105. H. Kuzmany, *Phys. Stat. Sol. (b)*, **97**, 521 (1980).
106. S. Lefrant, *J. Phys. Colloq.*, **44**, C3-247 (1983).
107. H. Takeuchi, T. Arakawa, Y. Furukawa, I. Harada and H. Shirakawa, *J. Mol. Struct.*, **158**, 179 (1987).
108. R. M. Gavin, Jr. and S. A. Rice, *J. Chem. Phys.*, **55**, 2675 (1971).
109. H. O. Villar, M. Dupuis, J. D. Watts, G. J. B. Hurst and E. Clementi, *J. Chem. Phys.*, **88**, 1003 (1988).
110. F. Negri, G. Orlandi, F. Zerbetto and M. Z. Zgierski, *J. Chem. Phys.*, **91**, 6215 (1989).
111. M. Kofranek, H. Lischka and A. Karpfen, *J. Chem. Phys.*, **96**, 982 (1992).
112. J. Y. Lee, O. Hahn, S. J. Lee, B. J. Mhin, M. S. Lee and K. S. Kim, *J. Phys. Chem.*, **99**, 2262 (1995).
113. I. Inagaki, M. Tasumi and T. Miyazawa, *J. Raman Spectrosc.*, **3**, 335 (1975).
114. F. B. Schügerl and H. Kuzmany, *J. Chem. Phys.*, **74**, 953 (1981).
115. L. Piseri, R. Tubino, L. Paltrinieri and G. Dellepiane, *Solid State Commun.*, **46**, 183 (1983).
116. D. Jumeau, S. Lefrant, E. Faulques and J. P. Buisson, *J. Phys.*, **44**, 819 (1983).
117. G. Zannoni and G. Zerbi, *J. Mol. Struct.*, **100**, 485 (1983).
118. H. Teramae, T. Yamabe and A. Imamura, *J. Chem. Phys.*, **81**, 3564 (1984).
119. H. Takeuchi, Y. Furukawa, I. Harada and H. Shirakawa, *J. Chem. Phys.*, **84**, 2882 (1986).
120. C. X. Cui and M. Kertesz, *J. Chem. Phys.*, **93**, 5257 (1990).
121. S. Hirata, H. Torii and M. Tasumi, *J. Chem. Phys.*, **103**, 8964 (1995).
122. Y. Furukawa, T. Arakawa, H. Takeuchi, I. Harada and H. Shirakawa, *J. Chem. Phys.*, **81**, 2907 (1984).
123. W. J. Potts and R. A. Nyquist, *Spectrochim. Acta*, 679 (1959).
124. H. Shirakawa and S. Ikeda, *Polym. J.*, **2**, 231 (1971).
125. M. Hossain, B. E. Kohler and P. West, *J. Phys. Chem.*, **86**, 4918 (1982).
126. S. Saito, I. Harada, M. Tasumi and C. H. Eugster, *Chem. Lett.*, 1045 (1980).
127. L. S. Lichtmann, E. A. Imhoff, A. Sarhangi and D. B. Fitchen, *J. Chem. Phys.*, **81**, 168 (1984).
128. E. Faulques, J. -P. Buisson and S. Lefrant, *Phys. Rev. B*, **52**, 15039 (1995).

CHAPTER 6

Electronic structure of diene and polyene radical cations

THOMAS BALLY

*Institut de Chimie Physique, Université de Fribourg, Pérolles, CH-1700 Fribourg,
Switzerland
e-mail: Thomas.Bally@unifr.ch*

and

EDGAR HEILBRONNER

Grütstrasse 10, CH-8704 Herrliberg, Switzerland

I. INTRODUCTION	174
II. PHOTOELECTRON (PE) SPECTROSCOPY	175
A. PE Spectrum and Ionization Energies	175
B. PE Spectra of Dienes and Polyenes	178
C. Interpretation of PE Spectra	197
D. Planar Conjugated Polyenes	199
1. Introductory remarks	199
2. Linear combination of two-centre π -orbitals	200
3. The standard Hückel treatment	203
4. Alkyl-substituted planar dienes and polyenes	204
5. Special cases	209
a. Deviations from planarity	209
b. Cumulenes	211
c. π -Systems exhibiting second-order bond fixation	211
6. Some cautionary remarks	213
E. Interaction Between Non-conjugated π -Orbitals	215
1. A naive, independent electron model	215
2. A more detailed analysis of through-space and through-bond interactions	220
3. Some special cases of interaction between non-conjugated π -orbitals	221

a. The interplay of through-bond and through-space interactions in norbornadiene homologues	221
b. Brief comment on symmetry assignments using a correlation technique	223
c. Homoconjugation	224
d. Spiroconjugation	225
III. EXCITED STATES OF POLYENE RADICAL CATIONS	
BY OTHER METHODS	228
A. Introduction	228
B. Experimental Methods	229
1. Gas-phase experiments	229
a. Photodissociation spectroscopy	229
b. Ion emission spectroscopy	229
2. Condensed-phase experiments	232
a. Solution studies	232
b. Frozen glasses	232
c. Matrix isolation experiments	233
C. Theoretical Methods	240
1. Koopmans and non-Koopmans states	240
2. Limitations and extension of single-determinant models	241
3. Semiempirical CI methods	242
4. Many-body perturbation methods	242
D. Linear Conjugated Polyenes	243
1. The minimal CI model	243
2. Long polyenes: Towards the polaron	245
3. Geometry dependence of excited-state energies	246
4. Conformational isomerism in linear conjugated polyene radical cations	248
5. Alkylated and cyclic conjugated dienes and trienes	249
6. Cross-conjugated polyenes	250
E. Interaction Between Non-conjugated π -Orbitals	250
IV. ACKNOWLEDGEMENTS	254
V. REFERENCES	254

I. INTRODUCTION

The present review is intended as a convenient starting point for chemists interested in the electronic structure of diene and polyene radical cations, by providing leading references to publications dealing with particular molecules, and by presenting the essential ground rules governing their electronic structure. With regard to the latter we have tried to avoid—as much as possible—sophisticated treatments dear to the specialists of theoretical chemistry, by using only such concepts of molecular orbital theory that can be found in elementary introductions¹ (in particular, the Hückel HMO model²), or even in modern textbooks such as Atkins's *Physical Chemistry*³. In other words, we shall try to discuss our topic by translating the results of more complex theoretical treatments into the type of HMO formalism to which chemists have become accustomed in the wake of the Woodward–Hoffmann rules^{4,5}. Whenever we need to refer to more advanced theoretical methods, we shall do so on an elementary, qualitative level.

We are aware that our review is by no means complete, the topic of diene and polyene radical cations having ramifications into such diverse fields as biology or interstellar chemistry. In the following we shall first discuss the photoelectron spectra of dienes

and polyenes, not only because of their relative simplicity, but also because the results derived from them form the basis for the detailed investigations using more sophisticated methods. In a second section we turn to other, often complementary methods which have been used for probing the electronic structure of polyene radical cations. In particular we shall discuss the relationship between the photoelectron spectra of polyenes and the electronic absorption spectra of the corresponding radical cations, as well as the necessary implementation of the simple HMO formalism needed for an adequate correlation of such data.

It should be mentioned that the present review does not cover in detail the ground-state electronic and/or molecular structure of diene and polyene radical cations as revealed, for example, by electron spin resonance (ESR) spectroscopy or variants thereof.

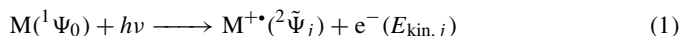
II. PHOTOELECTRON (PE) SPECTROSCOPY

Classical UV photoelectron (PE) spectroscopy as pioneered by D. W. Turner⁶ is nowadays—like futurology—a thing of the past. Much more precise and efficient methods are available for studying the electronic states of radical cations $M^{+\bullet}$, making use of lasers, molecular beams and low-temperature matrices (see Section III). However, because of its inherent simplicity, Turner-type PE spectroscopy can still be a convenient tool for exploratory investigations of the lower electronic states of radical cations $M^{+\bullet}$, yielding the corresponding ionization energies with an accuracy of 0.1 to 0.05 eV.

A. PE Spectrum and Ionization Energies

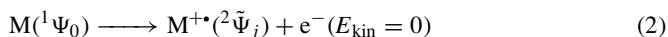
The theoretical and experimental principles of PE spectroscopy have been reviewed extensively^{7–10}. In particular, the reader is referred to the chapter *The Photoelectron Spectra of Saturated Hydrocarbons* in the volume *The Chemistry of Alkanes and Cycloalkanes* of the present series¹¹. Consequently we shall limit ourselves to the essentials needed for following the arguments presented in this chapter.

The primary process taking place in a PE spectrometer is best viewed as a ‘reaction’ in which a closed-shell diene or polyene M in its electronic (singlet) ground state ${}^1\Psi_0$ reacts with a photon of energy $h\nu$ to yield a radical cation $M^{+\bullet}$ in one of its electronic doublet states ${}^2\tilde{\Psi}_j$, and an electron e^- which carries off the excess energy $E_{\text{kin},j}$:



It has become customary to characterize state functions (and also other wave functions) of the radical cation by a tilde, e.g. ${}^2\tilde{\Psi}_j$.

The ionization energy I_j of a closed-shell ground-state molecule M is defined as the energy needed to yield $M^{+\bullet}$ in its electronic state ${}^2\tilde{\Psi}_j$ according to



or, if $E({}^1\Psi_0)$ and $E({}^2\tilde{\Psi}_j)$ are the energies of $M({}^1\Psi_0)$ and of $M^{+\bullet}({}^2\tilde{\Psi}_j)$ respectively, I_j is given by

$$I_j = E({}^2\tilde{\Psi}_j) - E({}^1\Psi_0) \quad (3)$$

If the radical cation $M^{+\bullet}({}^2\tilde{\Psi}_j)$ is created according to equation 2 in its minimum-energy geometry when in the electronic state ${}^2\tilde{\Psi}_j$, and if both $M({}^1\Psi_0)$ and $M^{+\bullet}({}^2\tilde{\Psi}_j)$ are in their

respective vibrational and rotational ground states, then the ionization energy defined by equation 3 is called the *adiabatic* ionization energy, denoted by I_j^a . If the structure of $M(^1\Psi_0)$ is conserved during the process (equation 2), i.e. if $M^{+\bullet}(^2\tilde{\Psi}_j)$ has exactly the same internal structure parameters as the closed-shell molecule $M(^1\Psi_0)$, then the ionization energy defined by equation 3 is called the *vertical* ionization energy I_j^v , which satisfies the condition $I_j^v \geq I_j^a$.

From equations 1–3 it follows that

$$I_j = h\nu - E_{\text{kin},j} \quad (4)$$

which requires that the photon energy $h\nu$ must be larger than the ionization energies I_j in which we are interested, i.e. $h\nu > I_j$. For the spectra discussed below the photon sources used are excited helium atoms, He(I), or helium ions, He(II), yielding photons of $h\nu = 21.2$ eV and $h\nu = 40.8$ eV, respectively.

The photoelectron spectrometer is an instrument which scans the range $0 < E_{\text{kin}} < h\nu$ of the kinetic energies E_{kin} of the ejected photoelectrons and thus—according to equation 4—the range $0 < I < h\nu$ of ionization energies, recording for each value of I the count rate cps (cps = counts per second), i.e. the number of electrons ejected per second from a stream of molecules M in the gas phase. The plot of cps vs I is known as the photoelectron (PE) spectrum of M . Figure 1 shows the PE spectrum of a hypothetical molecule M .

Contrary to naive expectation, the PE spectrum does not consist of sharp lines, but of rather broad, sometimes fine-structured bands. Apart from some minor effects with which we shall not be concerned, this is mainly due to two facts. To begin with, not all neutral molecules $M(^1\Psi_0)$ of the gas sample are present in their vibrational and rotational ground state, but most of them in vibrationally and rotationally excited states. More importantly, the radical cations $M^{+\bullet}(^2\tilde{\Psi}_j)$ are obtained according to equation 1 in various degrees of vibrational and rotational excitation. The corresponding changes in ionization energy lead to the observed band contours, known as ‘Franck–Condon envelopes’. If one vibrational mode dominates, it will lead to a resolvable vibrational fine structure of the band. With reference to Figure 1, we briefly mention how the shape of the Franck–Condon envelope can yield information about the structural changes accompanying the transition from M to $M^{+\bullet}$. Band ①, in which the first vibrational component is the most prominent, is

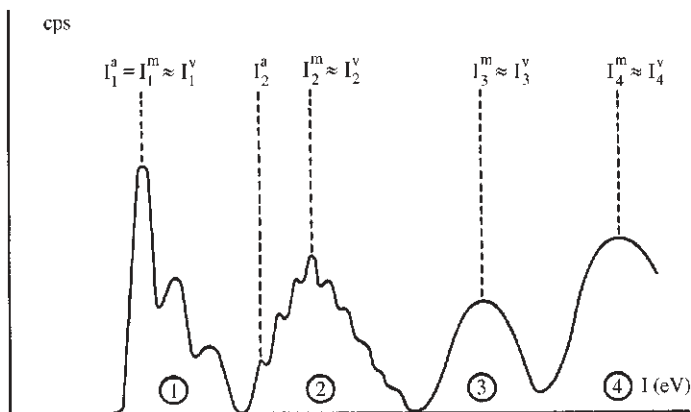


FIGURE 1. Photoelectron spectrum of a hypothetical molecule

traditionally thought to indicate that the transition $M \rightarrow M^{+\bullet}({}^2\tilde{\Psi}_1)$ is accompanied by small changes in geometry, whereas the envelope of band (2) is assumed to be the consequence of a significant change in the equilibrium structure accompanying the transition $M \rightarrow M^{+\bullet}({}^2\tilde{\Psi}_2)$. However, these are only rules-of-thumb which suffer notable exceptions. During the transitions $M \rightarrow M^{+\bullet}({}^2\tilde{\Psi}_3)$ and $M \rightarrow M^{+\bullet}({}^2\tilde{\Psi}_4)$ so many vibrational (and rotational) degrees of freedom are excited that the fine structure of bands (3) and (4) remains unresolved. For this reason, it is usual to characterize the positions of the individual bands in the PE spectrum by quoting the ionization energy I_j^m corresponding to the band maximum. The assumption $I_j^m \approx I_j^v$, i.e. that the band maximum position I_j^m can be roughly identified with the vertical ionization energy I_j^v , is a sufficiently good approximation for most practical applications.

As a real example we show in Figure 2 the PE spectrum of 1,1-divinylcyclopropane (46 in Table 1)¹², taken from the considerable number of diene and polyene PE spectra published by R. Gleiter and his coworkers. In the second column of the insert (5) are listed the I_j^m values in eV corresponding to the first bands of 46.

j	Cation state	I_j^m (eV)	Vacated orbital φ_j
①	\tilde{X}	9.0	$3b_1$
②	\tilde{A}	9.8	$2a_2$
③	\tilde{B}	10.9	$8a_1$
④	\tilde{C}	11.7	$6b_2$
⑤	\tilde{D}	11.9	$2b_1$

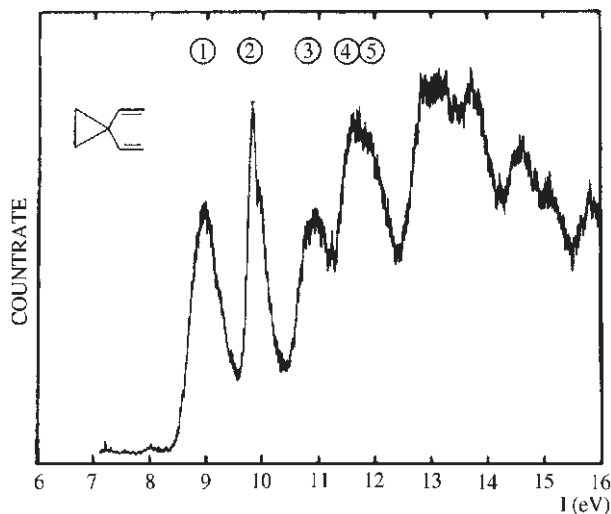
(5)


FIGURE 2. Photoelectron spectrum of 1,1-divinylcyclopropane 46¹²

The symbols in the second column of (5) stand for the electronic doublet states of the radical cation $M^{+\bullet}$, i.e. \tilde{X} for its electronic ground state ${}^2\tilde{\Psi}_1$, and $\tilde{A}, \tilde{B}, \tilde{C} \dots$ for its electronically excited states ${}^2\tilde{\Psi}_2, {}^2\tilde{\Psi}_3, {}^2\tilde{\Psi}_4 \dots$. The conventional labels presented in the fourth column of (5) (which assume that 1,1-divinylcyclopropane **46** has C_{2v} symmetry) are those of the molecular orbitals φ_j having lost the photoelectron according to the theoretical models to be discussed in Section II.C. [The lower-case orbital labels, such as a_1, b_1 etc., refer to the irreducible representations A_1, B_1 etc. of the group to which they belong. In contrast, the state labels \tilde{A}, \tilde{B} , etc. shown in the second column of (5) have no group theoretical meaning.] Such a list of labels is called the ‘assignment’ of the spectrum. With rare exceptions such an assignment cannot be deduced from the PE spectrum alone, but is either derived from a quantum-chemical calculation, or inferred by correlation with the assigned PE spectra of closely related molecules. With reference to the primary process (equation 2), the symmetry implied by the labels of the molecular orbitals φ_j is also that of the corresponding radical cation states ${}^2\tilde{\Psi}_j$, e.g. for 1,1-divinylcyclopropane: $\varphi_1 \equiv 3b_1 \rightarrow \tilde{X} \equiv {}^2\tilde{\Psi}_1(B_1)$; $\varphi_2 \equiv 2a_2 \rightarrow \tilde{A} \equiv {}^2\tilde{\Psi}_2(A_2)$; $\varphi_3 \equiv 8a_1 \rightarrow \tilde{B} \equiv {}^2\tilde{\Psi}_3(A_1)$; etc.

B. PE Spectra of Dienes and Polyenes

Table 1 lists publications containing PE spectra or PE-spectroscopic ionization energies of dienes and polyenes defined by

$$C_nH_m, \quad m = 2(n - d - r + 1) \quad (6)$$

where d is the number of double bonds and r the number of rings. For the smaller molecules the entries have been limited to leading references only. The table is largely based on a computer search, performed in March 1995, using the STN International Beilstein file. For references to work prior to 1970 the reader is referred to the fundamental treatise *Molecular Photoelectron Spectroscopy* by D. W. Turner, C. Baker, A. D. Baker and C. R. Brundle⁷. Another useful source of additional references for the period 1971 to 1981 is the compilation *Ionization Potential and Appearance Potential Measurements* edited by Rhoda D. Levin and Sharon G. Lias¹³.

Concerning the contents of Table 1 the following points should be noted:

(1) Hydrocarbons containing one or more triple bonds in addition to double bonds have been excluded from the file, as have been radicals (e.g. the allyl radical $C_3H_5^\bullet$) and aromatic molecules, i.e. molecules for which more than one ‘unexcited’ resonance structure (Kekule structure) can be written. Consequently, hydrocarbons such as phenyl-substituted polyenes, or annulenes—bridged or unbridged—have not been included.

(2) A rather special case are unsaturated, cyclic hydrocarbons undergoing second-order double-bond localization¹⁴, e.g. cyclobutadiene or pentalene. Although equivalent pairs of Kekule structures can be written for these molecules, they assume a structure with alternant single and double bonds, corresponding to only one of these structures. These molecules will be dealt with later, in a separate section.

(3) Linear and branched molecules, as well as some of the monocyclic ones, are identified only by their IUPAC names if their structure is immediately obvious. In the absence of accepted trivial or easy-to-read systematic names, larger polycyclic dienes and polyenes with rather unwieldy IUPAC names have been given numbers (4th column of the Table), which refer to the formula scheme following Table 1.

(4) Reference numbers followed by ‘He(II)’ refer to PE spectra recorded with He(II) radiation, which therefore show also bands in the ionization energy region above 24 eV.

TABLE 1. PE spectra of dienes and polyenes C_nH_m
 $[m = 2(n - d - r + 1)]$ where $d =$ number of double bonds and $r =$ number of rings]

C_nH_m				Name ^a	References		
r	n	m	No.				
Dienes: $d = 2$							
0	3	4	1	Allene	15, 16 He(II), 17		
			2	1,3-Butadiene	15, 16 He(II), 18–26, 27 He(II)		
	5	8	3	1,2-Butadiene (Methylallene)	16 He(II), 17		
			4	(3 <i>E</i>)-1,3-Pentadiene (1-Methylbutadiene)	16 He(II), 20, 21, 25, 28		
			5	2-Methylbutadiene (Isoprene)	16 He(II), 20, 25, 28		
			6	3-Methylbuta-1,2-diene (1,1-Dimethylallene)	16 He(II), 17		
			7	2,3-Pentadiene (1,3-Dimethylallene)	16 He(II), 17		
	6	10	8	1,4-Pentadiene	29, 30		
			9	4-Methyl-1,3-pentadiene (1,1-Dimethylbuta-1,3-diene)	2		
			10	(2 <i>E</i> , 4 <i>E</i>)-Hexa-2,4-diene	16 He(II), 20		
			11	2,3-Dimethylbuta-1,3-diene	16 He(II), 20, 25, 28		
			12	(3 <i>E</i>)-3-Methylpenta-1,3-diene	25		
			13	(3 <i>E</i>)-2-Methylpenta-1,3-diene	25, 31, 32		
			14	(3 <i>Z</i>)-2-Methylpenta-1,3-diene	31, 32		
			15	2-Methylpenta-2,3-diene (1,1,3-Trimethylallene)	16 He(II), 17		
			16	(3 <i>E</i>)-Hexa-1,3-diene	21, 25, 31, 33		
			17	Hexa-1,5-diene	29, 34		
			7	12	18	2,4-Dimethylpenta-2,3-diene (Tetramethylallene)	16 He(II), 17
					19	2,4-Dimethylpenta-1,3-diene	25
					20	1,1-Dimethylpenta-1,4-diene	30
					21	3,3-Dimethylpenta-1,4-diene	35
					22	1,6-Heptadiene	29
	8	14			23	(4 <i>E</i>)-2,3-Dimethylhexa-2,4-diene	36
					24	(3 <i>E</i>)-Octa-1,3-diene	21
			25	2,5-Dimethylhexa-2,4-diene	16 He(II), 20, 25		
			26	(2 <i>Z</i> , 4 <i>Z</i>)-3,4-Dimethylhexa-2,4-diene	37		
			27	(2 <i>Z</i> , 4 <i>E</i>)-3,4-Dimethylhexa-2,4-diene	37		
			28	(2 <i>E</i> , 4 <i>E</i>)-3,4-Dimethylhexa-2,4-diene	37		
	9	16	29	(4 <i>E</i>)-2,3-Dimethylhexa-2,4-diene	36		
			30	(4 <i>E</i>)-2,4-Dimethylhexa-2,4-diene	36		
			31	(4 <i>Z</i>)-2,4-Dimethylhexa-2,4-diene	36		
			32	Octa-1,7-diene	29		
			33	Nona-1,8-diene	29		
			11	20	34	2,2,6,6-Hepta-3,4-diene (1,1-Di- <i>t</i> -butylallene)	17
					35	2,3-Di- <i>t</i> -butylbuta-1,3-diene	37
36					Methylidenecyclopropene	38	
1			4	37	Cyclopentadiene	39	
				38	3-Vinyl-3-methylcyclopropene	40, 41	
	39	1,2-Dimethylidenecyclobutane		42			
	40	1,3-Dimethylidenecyclobutane		42			
	41	1-Methylcyclopentadiene		43			
	42	5-Methylcyclopentadiene		43			
	43	3-Methylidenecyclopentene		44			
	44	Cyclohexa-1,3-diene		15, 39			
	45	Cyclohexa-1,4-diene		15, 45–47			

(continued overleaf)

TABLE 1. (continued)

C_nH_m				Name ^a	References		
<i>r</i>	<i>n</i>	<i>m</i>	No.				
Dienes: <i>d</i> = 2							
1	7	10	46	1,1-Divinylcyclopropane	12		
			47	3-(2-Propenyl)-3-methylcyclopropene	40		
			48	4-Methylidenecyclohexene	48		
			49	Cyclohepta-1,3-diene	39, 49		
			50	Cyclohepta-1,4-diene	50		
			8	12	51	3-(1-Isobutenyl)-3-methylcyclopropene	40
					52	<i>cis</i> -1,2-Divinylcyclobutane	51
					53	<i>trans</i> -1,2-Divinylcyclobutane	51
					54	<i>cis</i> -1,3-Divinylcyclobutane	51
	55	<i>trans</i> -1,3-Divinylcyclobutane			51		
	56	1,2-Dimethylidenecyclohexane			48		
	57	Cycloocta-1,3-diene			39, 50		
	58	Cycloocta-1,4-diene			50		
	9	14	59	Cycloocta-1,5-diene	50		
			60	(1 <i>E</i> , 1 <i>E</i>)-Di-(1-propenyl)cyclopropane	52		
			61	(1 <i>E</i> , 1 <i>Z</i>)-Di-(1-propenyl)cyclopropane	12		
			62	(1 <i>Z</i> , 1 <i>Z</i>)-Di-(1-propenyl)cyclopropane	16, 52		
			63	Cyclonona-1,2-diene	17		
			10	16	64	1,2,3,4,5-Pentamethylcyclopentadiene	53
					65	3,3,6,6-Tetramethylcyclohexa-1,4-diene	54
	66	(1 <i>Z</i> , 5 <i>E</i>)-Cyclodeca-1,5-diene			39		
	67	(1 <i>Z</i> , 6 <i>Z</i>)-Cyclodeca-1,6-diene			39		
	11	18	68	(1 <i>E</i> , 6 <i>E</i>)-Cyclodeca-1,6-diene	39		
			69	Hexamethylcyclopentadiene	53		
	2	6	6	70	(Bicyclo[2.2.0]hexa-2,5-diene)	55	
				71	(Dewar benzene)		
					Bicyclopropyl-2,2'-diene	56-59	
		7	8	72	6-Methylidenespiro[2.3]hex-4-ene	60	
				73	5-Methylidenebicyclo[2.2.0]hex-2-ene	61	
74				Spiro[2.4]hepta-4,6-diene (Homofulvene)	16, 62, 63		
75				(Bicyclo[2.2.0]hexa-2,5-diene)			
				Norbornadiene	26, 28, 45, 59, 64		
8		10	76	1,1'-Dimethylbicyclopropyl-2,2'-diene	65		
			77	Spiro[3.4]octa-5,7-diene	63, 66		
			78	2,3-Dimethylidenebicyclo[2.1.1]hexane	67, 68		
			79	Bicyclo[4.2.0]octa-2,4-diene	69, 70		
			80	Bicyclo[4.1.1]octa-2,4-diene	68, 71		
			81	Bicyclo[2.2.2]octadiene	16, 45, 56		
			82	5-Methylidenebicyclo[2.2.1]hept-2-ene	48		
			83	Spiro[2.5]octa-4,6-diene	72		
9		12	84	Spiro[4.4]nona-1,3-diene	63, 66		
			85	5-Vinylbicyclo[2.2.1]hept-2-ene	73		
			86	5-Ethylidenebicyclo[2.2.1]hept-2-ene	73		
			87	2,3-Dimethylidenebicyclo[2.2.1]heptane	48		
			88	5-Methylidenebicyclo[2.2.2]oct-2-ene	48		
	89		<i>exo</i> -Bicyclo[4.3.0]nona-3,7-diene	74			
	90		<i>endo</i> -Bicyclo[4.3.0]nona-3,7-diene	74			
	91		Bicyclo[3.2.2]nona-2,6-diene	75			
	92		Bicyclo[3.2.2]nona-6,8-diene	75			
	93		Bicyclo[4.2.1]nona-2,4-diene	76			

TABLE 1. (continued)

C_nH_m				Name	References
r	n	m	No.		
Dienes: $d = 2$					
	10	14	94	7-Isopropylidenebicyclo[2.2.1]hept-2-ene	77
			95	2,3-Dimethylbicyclo[2.2.2]octa-2,5-diene	78
			96	2,3-Dimethylidenebicyclo[2.2.2]octane	48
			97	Bicyclo[6.2.0]deca-2,6-diene	51
	11	16	98	6,7-Dimethylbicyclo[3.2.2]nona-6,8-diene	78
	12	18	99	Hexamethyl-Dewar benzene	58, 79
			100	1,5-Dimethyl-3,7-dimethylidene-bicyclo[3.3.0]octane	80
			101	1,4,5,6-Tetramethyl-2,3-dimethylidene-bicyclo[2.1.1]hexane	67
3	8	8	102	<i>exo</i> -Tricyclo[4.2.0.0 ^{2,5}]octa-3,7-diene	81, 82
			103	<i>endo</i> -Tricyclo[4.2.0.0 ^{2,5}]octa-3,7-diene	81, 82
			104	Tricyclo[5.1.0.0 ^{4,8}]octa-2,5-diene (Semibullvalene)	83
			105	Tricyclo[3.3.0.0 ^{2,6}]octa-3,7-diene	81
			106	3,4-Dimethylidene-tricyclo[3.1.0.0 ^{2,6}]hexane	67, 68
			107	Tricyclo[4.1.1.0 ^{7,8}]octa-2,4-diene	58
	9	10	108	Nortriquinacene	84
			109	7-Cyclopropylidenenorbornadiene	85
			110	7,8-Methanobicyclo[2.2.2]octa-2,5-diene	86
			111	<i>exo</i> -Tricyclo[4.2.1.0 ^{2,5}]nona-3,7-diene	82
			112	<i>endo</i> -Tricyclo[4.2.1.0 ^{2,5}]nona-3,7-diene	82, 87
			113	Tricyclo[5.1.0.1 ^{4,8}]nona-2,5-diene	83
	10	12	114	Dispiro[2.2.2.2]deca-4,9-diene	54, 88
			115	Dispiro[2.0.2.4]deca-7,9-diene	72
			116	<i>endo</i> -Dicyclopentadiene	89, 90
			117	Dihydrobullvalene	91
			118	Tricyclo[5.3.0.0 ^{2,8}]deca-3,5-diene	92
			119	Twistadiene	93
			120	Dimethylidene-bisnortwistane	93
			121	<i>syn</i> -Tricyclo[4.2.1.1 ^{2,5}]deca-3,7-diene	94
	11	14	122	Dispiro[2.0.2.5]undeca-1,5-diene	65
			123	8-Isopropylidene-tricyclo[3.2.1.0 ^{2,4}]octene	77
			124	5,9-Dimethylidene-nortwistane	93
	12	16	125	1,5-Dimethyl-3,7-dimethylidene-tricyclo[3.3.0.0 ^{2,8}]octane	80
			126	1,2,5,6-Tetramethyl-3,4-dimethylidene-tricyclo[3.1.0.0 ^{2,6}]hexane	67
			127	[4.4.2]Propella-3,11-diene	81, 95
			128	2,5-Dimethylidene[4.2.2]propellane	96
			129	Tricyclo[4.2.2.2 ^{2,5}]dodeca-1,5-diene	96
			130	Tricyclo[5.5.0.0 ^{2,8}]dodeca-3,5-diene	92
	13	18	131	2,8-Dimethylidene[3.3.3]propellane	97
	14	20	132	[4.4.4]propella-2,4-diene	98
	16	24	133	3,4,5,6,7,8,12,15-octahydro[2.2]paracyclophane	99
4	10	10	134	Hypostrophene	100, 101

(continued overleaf)

TABLE 1. (continued)

C_nH_m				Name	References	
r	n	m	No.			
Dienes: $d = 2$						
4	12	14	135	Tetracyclo[6.4.0.0 ^{4,12} .0 ^{5,9}]dodeca-2,6-diene	102	
			136	4',5',6',7'-Tetrahydrospiro[cyclopropane-1,2'-[4,7]-methano-2 <i>H</i> -indene]	103	
			137	<i>exo,exo</i> -1,4,4 <i>a</i> ,5,8,8 <i>a</i> -Hexahydro-1,4:5,8-dimethanonaphthalene	104	
			138	<i>exo,endo</i> -1,4,4 <i>a</i> ,5,8,8 <i>a</i> -Hexahydro-1,4:5,8-dimethanonaphthalene	105	
			139	<i>endo,endo</i> -1,4,4 <i>a</i> ,5,8,8 <i>a</i> -Hexahydro-1,4:5,8-dimethanonaphthalene	105	
			140	2,5-Ethano[4.2.2]propella-7,9-diene	56	
			141	2,5-Etheno[4.2.2]propell-3-ene	56	
			142	<i>syn</i> -Sesquinorbornadiene	106	
			143	<i>anti</i> -Sesquinorbornadiene	106	
			144	1,5-Dimethyl-3,7-dimethylene-tetracyclo[3.3.0.0 ^{2,8} .0 ^{4,6}]octane	80	
		14	145	4',5',6',7'-Tetrahydrospiro[cyclopentane-1,2'-[4,7]-methano-2 <i>H</i> -indene]	103	
5	12	12	146	Pentacyclo-[6.4.0.0 ^{2,5} .0 ^{3,10} .0 ^{4,9}]dodeca-6,11-diene	107	
			147	[2.2.1]Triblattadiene	108	
		13	14	148	4,7-Dimethylidene-pentacyclo[6.3.0.0 ^{2,6} .0 ^{3,10} .0 ^{5,9}] undecane	108
		16	20	149	<i>endo,endo</i> -Pentacyclo[10.2.1.1 ^{5,8} .0 ^{2,4} .0 ^{4,9}]hexadeca-6,13-diene	109
6	17	20	150	<i>exo,exo</i> -1,4,4 <i>a</i> ,5,8,8 <i>a</i> ,9,9 <i>a</i> ,10,10 <i>a</i> -Decahydro-1,4:5,8:9,10-trimethanoanthracene	109	
			151	<i>endo,endo</i> -1,4,4 <i>a</i> ,5,8,8 <i>a</i> ,9,9 <i>a</i> ,10,10 <i>a</i> -Decahydro-1,4:5,8:9,10-trimethanoanthracene	109	
7	20	24	152	7,12-Dimethylideneheptacyclo[6.6.0.0 ^{2,6} .0 ^{3,13} .0 ^{4,11} .0 ^{5,9} .0 ^{10,14}]tetradecane	110	
			153	Heptacyclo-[10.8.0.0 ^{2,6} .0 ^{2,11} .0 ^{6,17} .0 ^{7,11} .0 ^{7,16}]icosa-1(12), 16-diene	111	
8	15	12	154	Bis(7-quadricyclylidene)methane	112	
			155	<i>endo,endo</i> -1,4,4 <i>a</i> ,5,5 <i>a</i> ,6,6 <i>a</i> ,7,10,10 <i>a</i> ,11,11 <i>a</i> ,12,12 <i>a</i> -Tetradecahydro-1,4:5, 12:6, 11:7, 10-tetramethylnonaphthacene	109	
9	20	20	156	Bissecododecahedradiene	113	
10	27	32	157	<i>endo,endo</i> -1,4,4 <i>a</i> ,5,5 <i>a</i> ,6,6 <i>a</i> ,7,7 <i>a</i> ,8,11,11 <i>a</i> ,12,12 <i>a</i> ,13,13 <i>a</i> ,14,14 <i>a</i> -octadecahydro-1,4:5,14:6, 13:7, 12:8, 11-pentamethanopentacene	109	

TABLE 1. (continued)

	C_nH_m			Name	References	
	r	n	m			No.
Trienes: $d = 3$						
0	4	4	158	Butatriene	16 He(II), 114, 115	
			159	Tetradeuteriobutatriene	114, 115	
	5	6	160	Penta-1,2,4-triene (Vinylallene)	116	
			161	(3 <i>E</i>)-Hexa-1,3,5-triene	20, 23, 117–119	
	6	8	162	(3 <i>Z</i>)-Hexa-1,3,5-triene	20, 23, 117–119	
			163	(3 <i>E</i> , 5 <i>E</i>)-Hepta-1,3,5-triene	118	
	7	10	164	(3 <i>E</i> , 5 <i>Z</i>)-Hepta-1,3,5-triene	118	
			165	(3 <i>E</i>)-2-Methylhexa-1,3,5-triene	118	
	8	12	166	(3 <i>E</i>)-3-Methylhexa-1,3,5-triene	118	
			167	Trivinylmethane	120	
	8	12	168	Tetramethylbutatriene	114, 115	
			169	(3 <i>E</i>)-6-Methylhepta-1,3,5-triene	118	
	20	36	170	(3 <i>E</i> ,5 <i>E</i>)-5-Methylhepta-1,3,5-triene	118	
			171	(2 <i>E</i> , 4 <i>E</i> , 6 <i>E</i>)-Octa-2,4,6-triene	118	
	1	6	6	172	Tetra- <i>t</i> -butylbutatriene	114, 115
				173	[3]Radialene	121–123
	7	8	8	174	3,4-Dimethylidenecyclobutene	124
175				Fulvene	62, 124–126	
7	8	8	176	1-Methyl-3,4-dimethylidenecyclobutene	127	
			177	6-Methylfulvene	125	
8	10	10	178	5-Methylidenecyclohexa-1,3-diene	61	
			179	Cyclohepta-1,3,5-triene	50	
8	10	10	180	1,2-Dimethyl-3,4-dimethylidenecyclobutene	127	
			181	6-Ethylfulvene	125	
9	12	12	182	6,6-Dimethylfulvene	125	
			183	4,5-Dimethylenecyclohexene	48	
9	12	12	184	Cycloocta-1,3,5-triene	50, 70	
			185	Cycloocta-1,3,6-triene	50, 70	
9	12	12	186	6-Propylfulvene	125	
			187	6-Isopropylfulvene	125	
10	14	14	188	1,6-Dimethylcyclohepta-1,3,5-triene	128	
			189	Cyclonona-1,4,7-triene	26, 49	
10	14	14	190	6-Isobutylfulvene	125	
			191	6- <i>t</i> -Butylfulvene	125	
12	18	18	192	6,6-Diethylfulvene	125	
			193	6,6-Dipropylfulvene	125	
2	7	6	194	Hexamethyl-[3]-radialene	129	
			195	Bicyclo[3.2.0]hepta-1,4,6-triene	130	
8	8	8	196	7-Methylidenenorbornadiene	131	
			197	Barrelene	26, 86, 122, 132	
9	10	10	198	1,2-Dihydropentalene	133	
			199	1,4-Dihydropentalene	133	
9	10	10	200	1,5-Dihydropentalene	133	
			201	5,6-Dimethylidenenorborn-2-ene	48	
9	10	10	202	Spiro[4.4]nona-1,3,5-triene	63	
			203	Spiro[4.4]nona-1,3,6-triene	63	
10	12	12	204	Bicyclo[3.2.2]nona-2,6,8-triene	75	
			205	Bicyclo[4.2.1]nona-2,4,6-triene	49, 76	
10	12	12	206	7-Isopropylidenenorbornadiene	26, 77	
			207	4,5-Dimethylidenebicyclo[2.2.2]octene	48	
10	12	12	208	Bicyclo[4.2.2]deca-3,7,10-triene	134	
			209	1,4,5,8-Tetrahydronaphthalene	26, 47, 135	
10	12	12	210	6,6-Tetramethylenefulvene	125	

(continued overleaf)

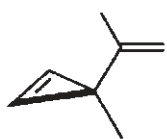
TABLE 1. (continued)

	C_nH_m			Name	References	
	r	n	m			No.
Trienes: $d = 3$						
		11	14	211	Bicyclo[4.4.1]undeca-1,3,5-triene	128
		14	20	212	11,12-Dimethylbicyclo[5.3.2]dodeca-1,6,11-triene	117
3	10	10		213	Triquinacene	136
				214	Bullvalene	91
				215	7-Cyclopropylidenenorbornadiene	137
				216	Tricyclo[5.3.0.0 ^{2,8}]deca-3,5,9-triene	92
	11	12		217	Tricyclo[5.3.1.0 ^{1,7}]undeca-2,4,9-triene	138
				218	Tricyclo[6.2.1.0 ^{2,6}]undeca-2,5,9-triene	139
				219	Tricyclo[6.2.1.0 ^{2,6}]undeca-2,6,9-triene	139
	12	14		220	Tricyclo[4.4.1.1 ^{2,5}]dodeca-3,7,9-triene	89
				221	9-Isopropylidene- <i>endo</i> -tricyclo[4.2.1.0 ^{2,5}]nona-3,7-diene	82
				222	[4.4.2]Propella-2,4,11-triene	95
				223	[4.4.2]Propella-3,8,11-triene	95
	14	18		224	2,8,9-Trimethylidene[3.3.3]propellane	97, 120
4	12	12		225	3,7,9-Trimethylidene-tetracyclo[3.3.1.0 ^{2,8} .0 ^{4,6}]dodecane	140
				226	<i>syn</i> -Sesquinorbornatriene	106
				227	<i>anti</i> -Sesquinorbornatriene	106
	18	24		228	Tetracyclo[8.2.2.2 ^{2,5} .2 ^{6,9}]octadeca-1,5,9-triene	141, 142
5	14	14		229	[2.2.2]Blattatriene	108
				230	4,7,11-Trimethylidenepentacyclo[5.3.9.0 ^{2,6} .0 ^{3,10} .0 ^{5,9}]undecane	108
6	18	20		231	Distella-2,2',6,6'-triene	143
Tetraenes: $d = 4$						
0	5	4		232	Pentatetraene	144
	6	6		233	Hexa-1,2,4,5-tetraene (Bisallenyl)	116
	8	10		234	(3 <i>E</i> , 5 <i>E</i>)-Octa-1,3,5,7-tetraene	23, 145
	9	12		235	Tetravinylmethane	35, 120
1	7	6		236	6-Methylidenefulvene	146
	8	8		237	[4]Radialene	147
				238	<i>p</i> -Quinodimethane	148
				239	Cyclooctatetraene	18, 50, 149
	10	12		240	2,3-Dimethyl- <i>p</i> -quinodimethane	150
				241	2,5-Dimethyl- <i>p</i> -quinodimethane	150
				242	Cyclodeca-1,2,6,7-tetraene	151
	12	16		243	<i>trans, trans, trans</i> -1,2,3,4-Tetravinylcyclobutane	120, 152
				244	<i>syn, trans, syn</i> -1,2,3,4-Tetravinylcyclobutane	152
				245	4,9-Dimethylidencyclodeca-1,6-diene	153
	16	24		246	Octamethyl-[4]radialene	154
2	9	8		247	[4.4]Spiroonattetraene	63, 155
	10	10		248	9-Methylidenebicyclo[4.2.1]deca-2,4,7-triene	156
				249	Bicyclo[4.2.2]deca-2,4,7,9-tetraene	157
	11	12		250	2,2-Dimethyl(2 <i>H</i>)indene	26, 121
				251	2,3,5,6-Tetramethylidenenorbornane	158
	12	14		252	2,3,5,6-Tetramethylidenebicyclo[2.2.2]octane	158
	13	16		253	Bicyclo[5.4.2]trideca-7,9,11,12-tetraene	50

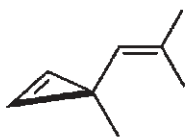
TABLE 1. (continued)

C_nH_m				Name	References
r	n	m	No.		
Tetraenes: $d = 4$					
3	10	8	254	[4.2.2]Propellatetraene	56
	12	12	255	[4.4.2]Propella-3,7,9,11-tetraene	69
			256	Tricyclo[[6.4.0.0 ^{1,7}]dodeca-3,5,9,11-tetraene	95
			257	9,19-Dimethylidene-tricyclo[5.3.0.0 ^{2,8}]deca-3,5-diene	92
			258	Tricyclo[5.5.0.0 ^{2,8}]dodeca-3,5,9,11-tetraene	92
	14	16	259	1,4,5,6,9,11-Hexahydroanthracene	47
			260	[4.4.4]Propella-2,4,7,9-tetraene	98
	16	20	261	<i>anti</i> -1,2,5,6-Tetramethyl-3,4,7,8-tetramethylenetricyclo[4.2.0.0 ^{2,5}]octane	159
			262	1,2,5,6-Tetramethyl-3,4,7,8-tetramethylenetricyclo[3.3.0.0 ^{2,6}]octane	159
			263	2,3',5,6'-Tetrahydro[2.2]paracyclophane	99
4	12	10	264	2,5-Etheno-[4.2.2]propella-3,7,9-triene	56
5	15	14	265	Dispiro-(bicyclo[2.2.1]hepta-2,5-diene-7,1'-cyclopropane-2',7''-bicyclo[2.2.1]hepta-2'',5''-diene	112
		20	24	266	2,2',5,5'-Tetrahydro[2.2.2](1,3,4,6)(1',3',4',6')cyclophane
8	29	18	267	Octacyclo-[12.5.1.0 ^{2,7} .0 ^{2,13} .0 ^{7,18} .0 ^{8,13} .0 ^{8,16} .0 ^{17,20}]eicoso-3,5,9,11-tetraene	160
Polyenes: $d \geq 5$					
$d = 5$					
2	10	8	268	2-Methylidene-(2H)indene	161
	12	12	269	5,6,7,8-Tetramethylidenebicyclo[2.2.2]oct-7-ene	158
3	12	10	270	2a,8b-Dihydrocyclopenta[<i>c,d</i>]azulene	128
			271	[4.4.2]Propellapentaene	95
4	18	20	272	1,4,5,6,7,10,12-Octahydronaphthacene	47
$d = 6$					
2	12	10	273	2,6-Azulylene	162
	14	14	274	2,3,5,6,7,8-Hexamethylidene-bicyclo[2.2.2]octane	163
3	14	12	275	[4.4.4]Propellahexaene	98
4	15	12	276	Bis(7-norbornadienylidene)methane	112
$d = 7$					
4	20	20	277	2,7-Dihydro-2,2,7,7-tetramethylpyrene	164
$d = 8$					
3	22	24	278	7,14-Diisopropylidene-7,14-dihydro- <i>syn</i> -1,6:8,13-bismethano[14]annulene	165
$d = 11$					
2	40	56	279	β -Carotene	166, 167
			280	(15Z)- β -Carotene	168

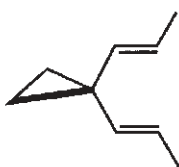
^aIUPAC name is given first, followed by trivial name in parentheses.



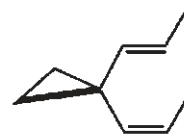
(47)



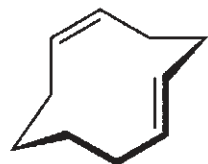
(51)



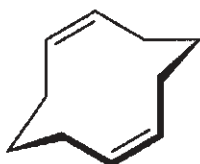
(60)



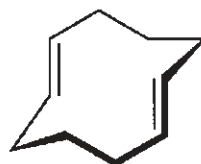
(61)



(66)



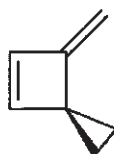
(67)



(68)



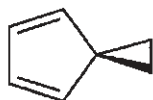
(70)



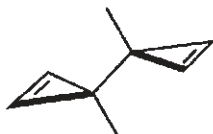
(72)



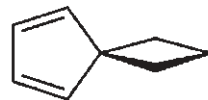
(73)



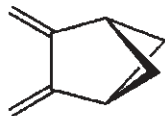
(74)



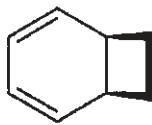
(76)



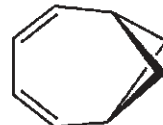
(77)



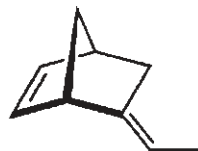
(78)



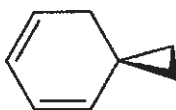
(79)



(80)



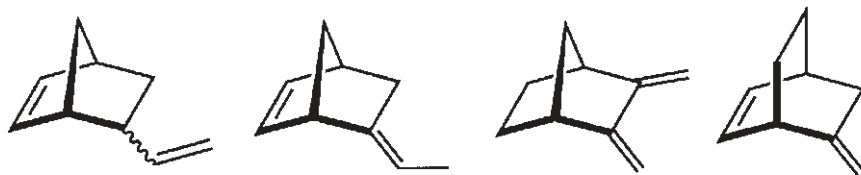
(82)



(83)



(84)



(85)

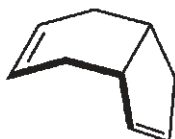
(86)

(87)

(88)



(89)



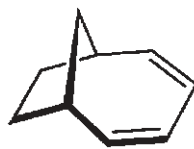
(90)



(91)



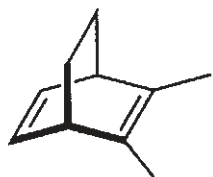
(92)



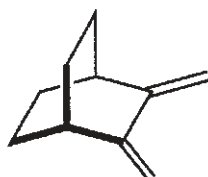
(93)



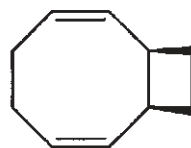
(94)



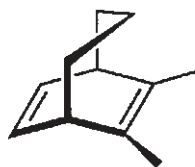
(95)



(96)



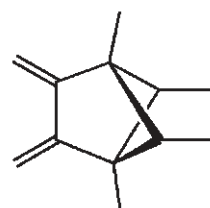
(97)



(98)



(100)



(101)



(102)



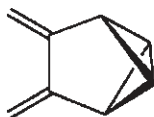
(103)



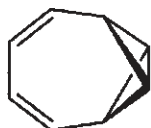
(104)



(105)



(106)



(107)



(108)



(109)



(110)



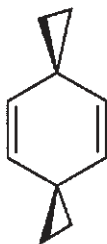
(111)



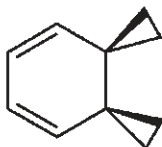
(112)



(113)



(114)



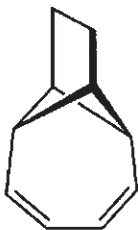
(115)



(116)



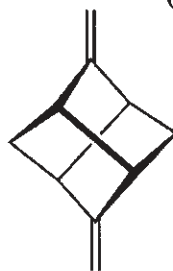
(117)



(118)



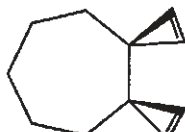
(119)



(120)



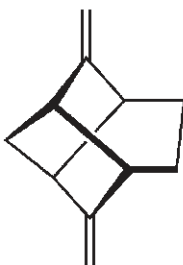
(121)



(122)



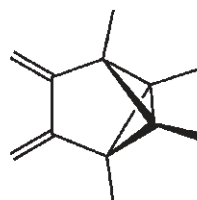
(123)



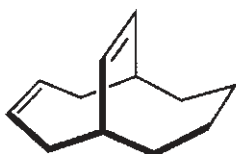
(124)



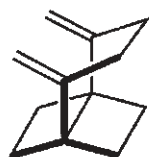
(125)



(126)



(127)



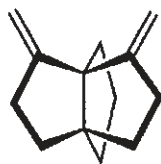
(128)



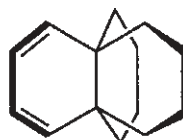
(129)



(130)



(131)



(132)



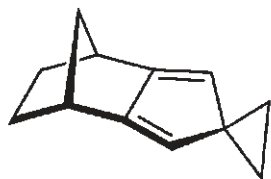
(133)



(134)



(135)



(136)



(137)



(138)



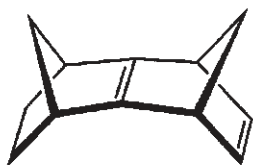
(139)



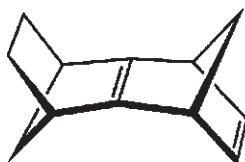
(140)



(141)



(142)



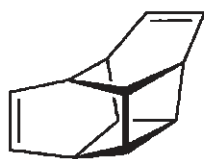
(143)



(144)



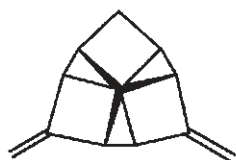
(145)



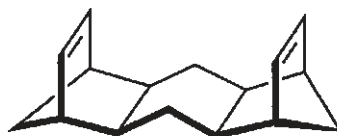
(146)



(147)



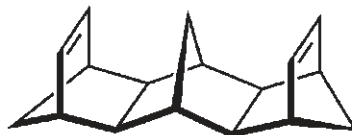
(148)



(149)



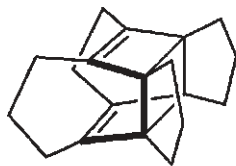
(150)



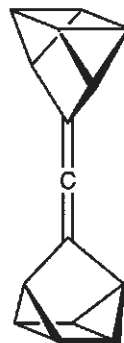
(151)



(152)



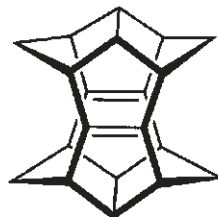
(153)



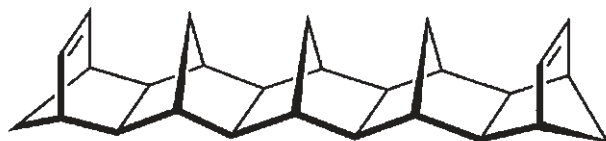
(154)



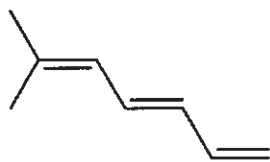
(155)



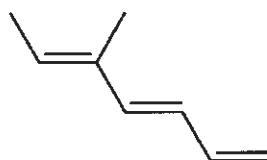
(156)



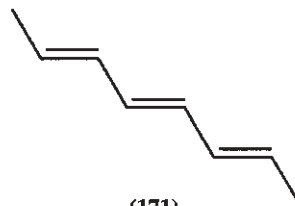
(157)



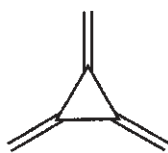
(169)



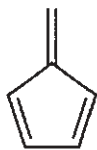
(170)



(171)



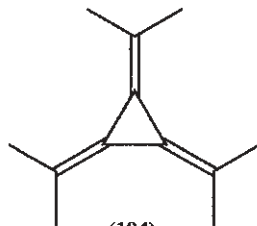
(173)



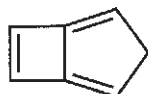
(175)



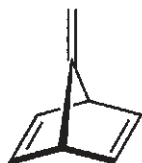
(189)



(194)



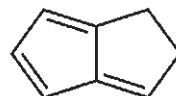
(195)



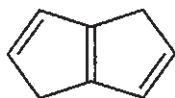
(196)



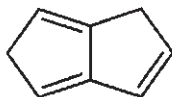
(197)



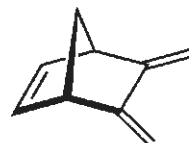
(198)



(199)



(200)



(201)



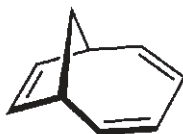
(202)



(203)



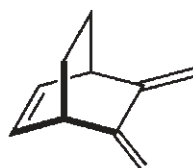
(204)



(205)



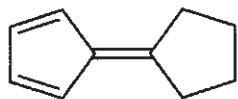
(206)



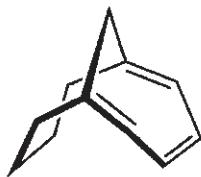
(207)



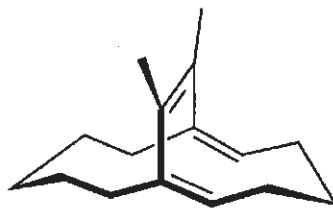
(208)



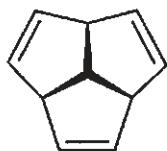
(210)



(211)



(212)



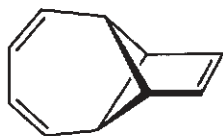
(213)



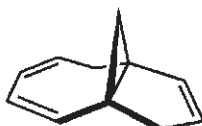
(214)



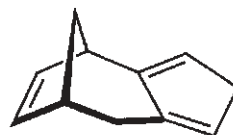
(215)



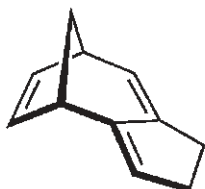
(216)



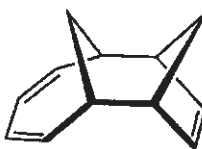
(217)



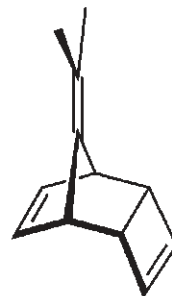
(218)



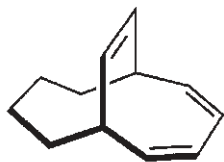
(219)



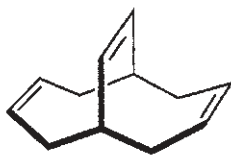
(220)



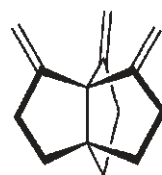
(221)



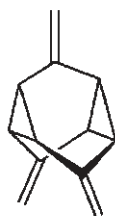
(222)



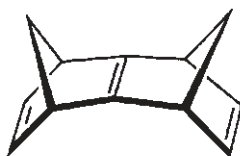
(223)



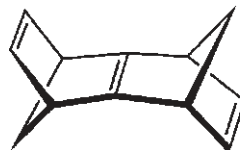
(224)



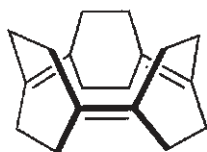
(225)



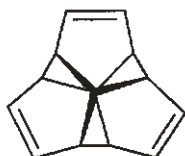
(226)



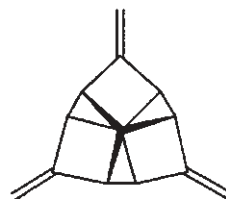
(227)



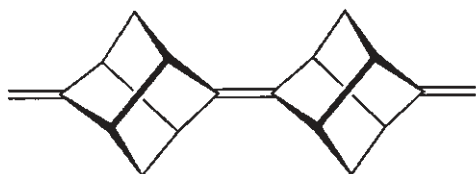
(228)



(229)



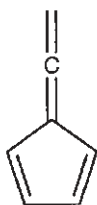
(230)



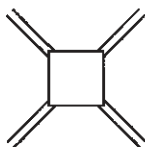
(231)



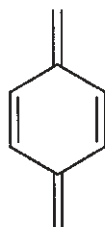
(233)



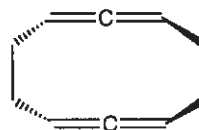
(236)



(237)



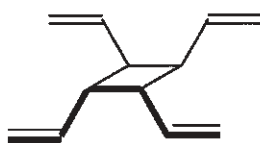
(238)



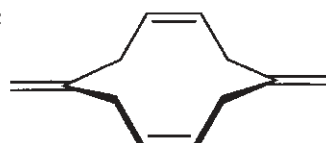
(242)



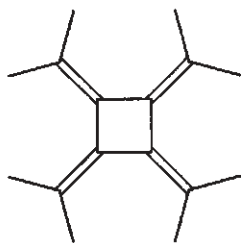
(243)



(244)



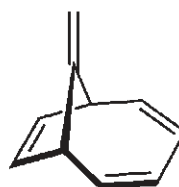
(245)



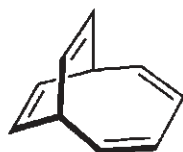
(246)



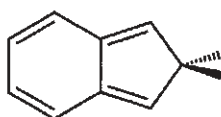
(247)



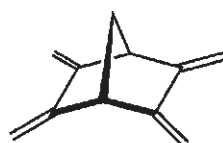
(248)



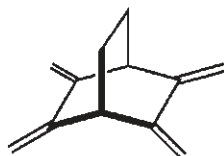
(249)



(250)



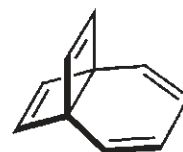
(251)



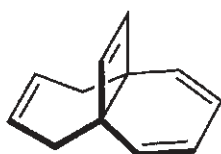
(252)



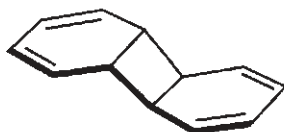
(253)



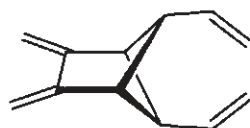
(254)



(255)



(256)



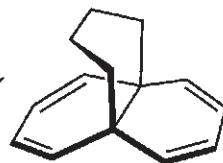
(257)



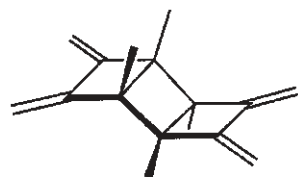
(258)



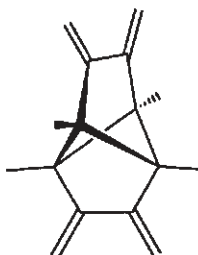
(259)



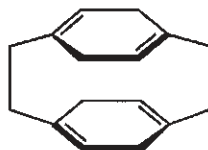
(260)



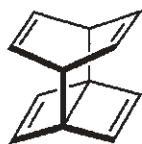
(261)



(262)



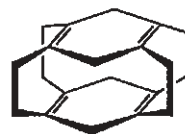
(263)



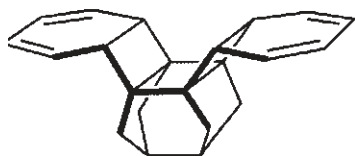
(264)



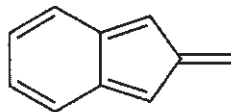
(265)



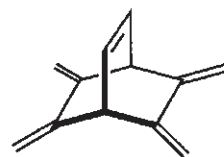
(266)



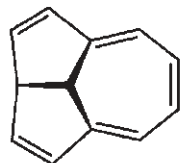
(267)



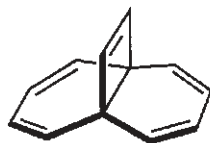
(268)



(269)



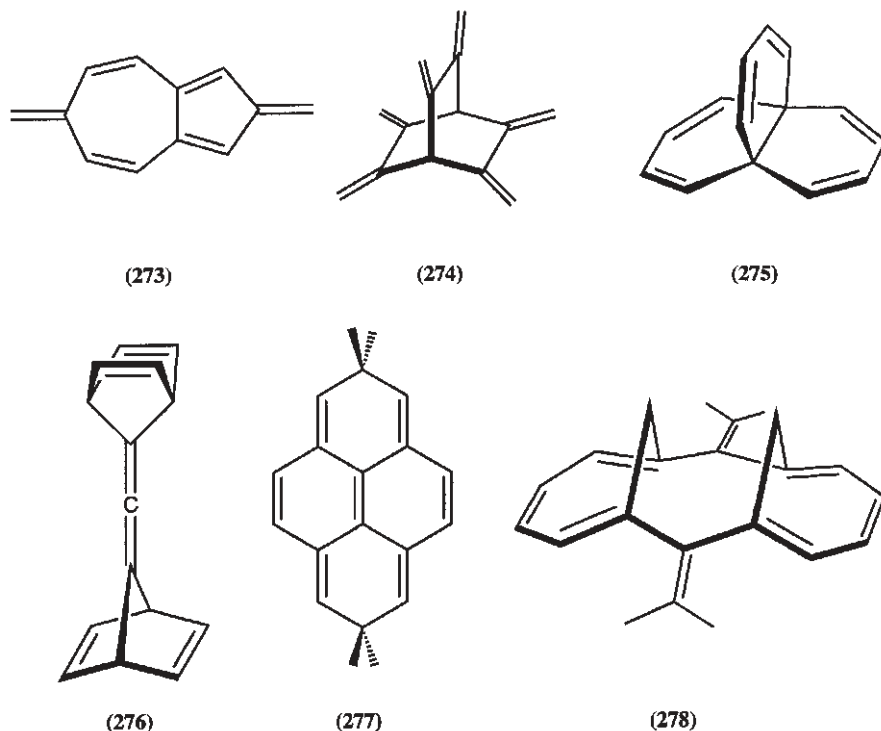
(270)



(271)



(272)



C. Interpretation of PE Spectra

In principle, refined and relatively reliable quantum-theoretical methods are available for the calculation of the energy change associated with the process of equation 2. They take into account the changes in geometry, in electron distribution and in electron correlation which accompany the transition $M(^1\Psi_0) \rightarrow M^{+\cdot}(^2\tilde{\Psi}_j)$, and also vibronic interactions between the radical cation states. Such sophisticated treatments yield not only reliable predictions for the different ionization energies I_j^a, I_j^v or I_j^m , but also rather precise Franck–Condon envelopes for the individual bands in the PE spectrum. However, the computational expenditure of these methods still limits their application to smaller molecules. We shall mention them later in connection with examples where such treatments are required.

For most practical purposes — and certainly for the discussions in this chapter — much simpler models are entirely adequate for a qualitative or semiquantitative rationalization of the features of PE spectra of dienes and polyenes. Before using such models, we first situate them within the genealogy of quantum-mechanical treatments.

A convenient starting point is an *ab initio*¹⁶⁹ or semiempirical¹⁷⁰ SCF calculation yielding the singlet ground configuration $^1\Phi_0$ for a closed-shell molecule M with $2n$ electrons, which is assumed to be a sufficiently good approximation for the ground-state $^1\Psi_0$ of M. This configuration $^1\Phi_0$ is written as a Slater determinant in terms of the n doubly occupied canonical molecular orbitals (CMO) φ_k (equation 7). By convention φ_k

represents a CMO occupied by an electron with spin α , and $\bar{\varphi}_k$ with spin β :

$${}^1\Phi_0 = \left\| \varphi_1 \bar{\varphi}_1 \varphi_2 \bar{\varphi}_2 \cdots \varphi_j \bar{\varphi}_j \cdots \varphi_n \bar{\varphi}_n \right\| \quad (7)$$

The next approximation is to assume that exactly the same CMOs φ_k can be used for writing the electronic doublet configurations ${}^2\tilde{\Phi}_j$ of the radical cation M^+ , by simply removing one of the two electrons occupying the CMO φ_j in the closed-shell molecule M . This yields

$${}^2\tilde{\Phi}_j = \begin{cases} \left\| \varphi_1 \bar{\varphi}_1 \varphi_2 \bar{\varphi}_2 \cdots \varphi_j \cdots \varphi_n \bar{\varphi}_n \right\| \\ \left\| \varphi_1 \bar{\varphi}_1 \varphi_2 \bar{\varphi}_2 \cdots \bar{\varphi}_j \cdots \varphi_n \bar{\varphi}_n \right\| \end{cases} \quad (8)$$

In agreement with the convention for the states ${}^2\tilde{\Psi}_j$ of radical cations, their configurations ${}^2\tilde{\Phi}_j$ are again characterized by a 'tilde'. The top line of equation 8 corresponds to the component of ${}^2\tilde{\Phi}_j$ with spin $S_z = \hbar/2$, and the bottom one to $S_z = -\hbar/2$. Figure 3 shows on the left the energy-level diagram of the lowest three states ${}^2\tilde{\Psi}_j$ of a radical cation $M^{+\bullet}$ relative to the level of the electronic ground-state ${}^1\Psi_0$ of the neutral parent molecule M , and on the right side the symbolic representations of the corresponding configurations (equations 7 and 8), i.e. of ${}^1\Phi_0$ and ${}^2\tilde{\Phi}_j$.

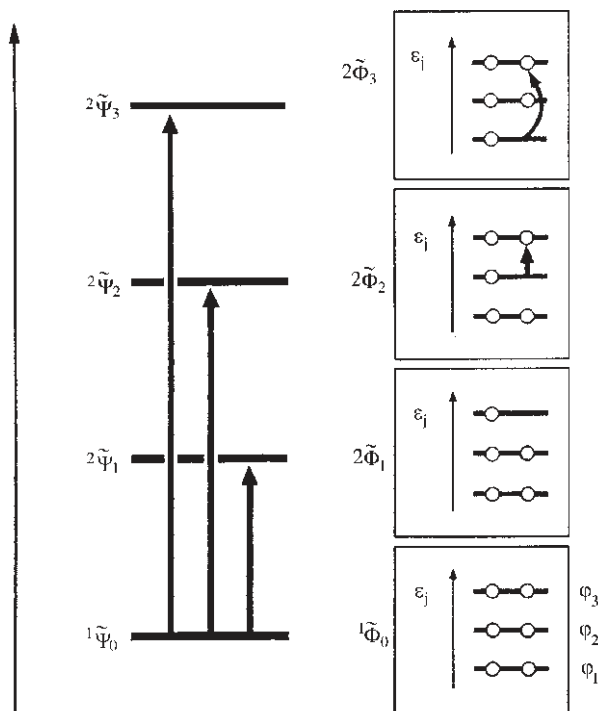


FIGURE 3. Graphical representation of the electron configuration ${}^1\Phi_0$ of a closed-shell molecule M and of the configurations ${}^2\tilde{\Phi}_j$ of its radical cation $M^{+\bullet}$ as approximations to the states ${}^1\Psi_0$ and ${}^2\tilde{\Psi}_j$ ($j = 1, 2, 3$). The arrows in the representations of ${}^2\tilde{\Phi}_2$ and ${}^2\tilde{\Phi}_3$ indicate that these configurations correspond to electronic excitations of M^+ , relative to its ground-state configuration ${}^2\tilde{\Phi}_1$.

The approximation underlying the expression in equation 8 and Figure 3, i.e. using frozen CMOs φ_j , not only implies that M and $M^{+\bullet}$ have the same geometry, but also that we disregard electron rearrangement, i.e. changes in the CMOs φ_k when an electron is removed from φ_j , and changes in electron correlation. Notwithstanding these restrictions, the energy change $E(^2\tilde{\Phi}_j) - E(^1\Phi_0)$ is then a useful approximation for the vertical ionization energy I_j^v :

$$E(^2\tilde{\Phi}_j) - E(^1\Phi_0) = I_j^v \quad (9)$$

It has been shown by Koopmans¹⁷¹ that under the above simplifications (same rigid geometry of M and $M^{+\bullet}$, frozen CMOs φ_k) the energy difference $E(^2\tilde{\Phi}_j) - E(^1\Phi_0)$ is equal, up to sign, to the orbital energy \mathcal{E}_j of the CMO φ_j of the neutral molecule M from which the electron has been ejected:

$$E(^2\tilde{\Phi}_j) - E(^1\Phi_0) = -\mathcal{E}_j \quad (10)$$

The resulting relationship

$$I_j^v = -\mathcal{E}_j \quad (11)$$

known as the Koopmans theorem¹⁷¹, is the basis of almost all qualitative and many semiquantitative discussions of PE spectra.

Under the above assumption that removal of an electron from a CMO φ_j of M will leave the geometry of the system unchanged, both the closed-shell molecule M and the radical cation $M^{+\bullet}$ belong to the same symmetry group \mathcal{G} . Because the closed-shell ground configuration $^1\Phi_0$ is totally symmetric, the radical cation configurations $^2\tilde{\Phi}_j$ must necessarily belong to the same irreducible representation of the group \mathcal{G} as the vacated CMO φ_j . It follows that a discussion of ionization energies based on the Koopmans theorem can be carried out, without loss of generality, on the level of the CMOs φ_k . All that is needed in this approximation are the orbital energies \mathcal{E}_j of the CMOs φ_j of M, their nodal properties, the irreducible representations of \mathcal{G} to which they belong and—in some cases—additional characteristic values that can be derived from the set of the occupied CMOs φ_j , such as bond orders (bond populations) or charge distributions.

All this suggests a further simplification, which has proved to be eminently successful in many cases. It is known that independent electron treatments, such as the Hückel (HMO) treatment² or the extended Hückel treatment (EHT)¹⁷², which do not take the electron–electron interaction explicitly into account, yield—by and large—orbitals φ_j which are close approximations to those derived from sophisticated SCF calculations. In particular, the HMO and ETH molecular orbitals reflect faithfully the symmetry and nodal properties of their counterparts obtained from SCF treatments.

In the following we shall discuss the different models in context with their application to particular problems arising in the discussion of diene and polyene PE spectra.

D. Planar Conjugated Polyenes

1. Introductory remarks

This section concerns unsubstituted planar polyenes C_nH_m , n even and $m = n + 2(1 - r)$, r being the number of rings, i.e. π -systems with all atoms, C and H, in a common plane. Low man on the totem pole of quantum-chemical models adequate for such polyenes (and, of course, for aromatic π -systems) is the Hückel (HMO) treatment² which assumes strict orthogonality between the molecular σ - and π -orbitals. Under the assumption of this so-called ' σ/π -separation' the π -orbitals can be dealt with independently of the σ manifold

by forming linear combinations of appropriate basis orbitals η_μ which are antisymmetric with respect to reflection through the molecular plane:

$$\varphi = \sum_{\mu} \eta_{\mu} c_{\mu} \quad (12)$$

With respect to an otherwise unspecified operator \mathbf{H} one defines the energy a_{μ} of a basis function η_{μ} and the interaction term $b_{\mu\nu}$ between two basis functions η_{μ} and η_{ν} as

$$a_{\mu} = \langle \eta_{\mu} | \mathbf{H} | \eta_{\mu} \rangle \quad (13)$$

and

$$b_{\mu\nu} = \langle \eta_{\mu} | \mathbf{H} | \eta_{\nu} \rangle. \quad (14)$$

To obtain the π -orbitals φ_j of the polyene model system and their orbital energies \mathcal{E}_j one first diagonalizes the $N \times N$ matrix defined by equation 15, N being the number of basis functions η_{μ} :

$$\mathbb{H} = \begin{pmatrix} a_1 & b_{12} & b_{13} & \cdots & b_{1N} \\ b_{21} & a_2 & b_{23} & \cdots & b_{2N} \\ b_{31} & b_{32} & a_3 & \cdots & b_{3N} \\ \vdots & \vdots & \vdots & \ddots & \vdots \\ b_{N1} & b_{N2} & b_{N3} & \cdots & a_N \end{pmatrix} \quad (15)$$

This yields the N orbital energies (eigenvalues)

$$\mathcal{E}_j = \mathcal{E}_j(\cdots a_{\mu} \cdots b_{\mu\nu} \cdots) \quad (16)$$

and the corresponding N eigenvectors $\mathbb{C}_j = (c_{\mu j})^T$, the components $c_{\mu j}$ of which define the molecular orbitals

$$\varphi_j = \sum_{\mu} \eta_{\mu} c_{\mu j} \quad (17)$$

The orbital energies \mathcal{E}_j so obtained depend, as shown in equation 16, on the parameters a_{μ} and $b_{\mu\nu}$, which are thus available for calibration by comparison with experimental data, i.e. by matching the \mathcal{E}_j to observed band positions I_j^{m} for a series of polyenes. To this end we postulate that $I_j^{\text{v}} = -\mathcal{E}_j$. Although this looks suspiciously like the Koopmans theorem (equation 11) it should be realized that $I_j^{\text{v}} = -\mathcal{E}_j$ is now simply the consequence of assuming independent electrons. Whereas \mathcal{E}_j in equation 11 contains the explicit interactions of an electron in φ_j with all the other $2n - 1$ electrons of the molecule M, this is no longer the case if \mathcal{E}_j is calculated by an independent electron procedure. (Notwithstanding this important difference, it has become customary to refer to $I_j^{\text{v}} = -\mathcal{E}_j$ as the Koopmans theorem even if it is applied to an independent electron model.) Once the parameters a_{μ} and $b_{\mu\nu}$ have been calibrated using a limited set of polyenes, it is found that they allow the computation of reasonably reliable predictions of ionization energies for other polyenes.

2. Linear combination of two-centre π -orbitals

The simplest model of this kind—and admittedly a rather naive one—is to choose two-centre π -orbitals π_{μ} as basis functions. The prototype for the π_{μ} is the π -orbital of ethene. Because ejection of an electron from this orbital yields the low-energy band, at $I_1^{\text{v}} = 10.5$ eV, in the ethene PE spectrum shown in Figure 4, $A = -I_1^{\text{v}} = -10.5$ eV is

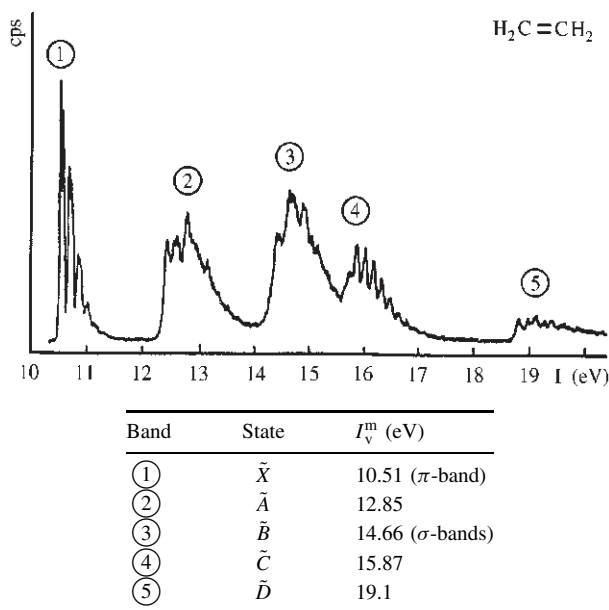


FIGURE 4. Photoelectron spectrum of ethene:

a first, rough estimate of the basis energy of the two-centre π -orbitals π_μ . We introduce the following simplifications:

(1) The basis energies (equation 13) are assumed to be the same for all basis functions π_μ , i.e. $a_\mu = A$:

$$\langle \pi_\mu | \mathbf{H} | \pi_\mu \rangle = A \text{ for all } \mu \quad (18)$$

(2) The cross terms (equation 14) differ from zero only if π_μ and π_ν are conjugated, in which case they are assigned the same value B :

$$\begin{aligned} \langle \pi_\mu | \mathbf{H} | \pi_\nu \rangle &= B \quad \text{if } \mu, \nu \text{ conjugated} \\ &= 0 \quad \text{otherwise} \end{aligned} \quad (19)$$

Under these conditions the π -system of a given polyene with N double bonds can be characterized by a graph \mathcal{G} in which each of the N basis π -orbitals π_μ is represented by a node and each cross term B by an edge, as shown in Figure 5. Such a graph translates into an adjacency matrix $\mathbb{A} = (A_{\mu\nu})$ with $A_{\mu\nu} = 1$ if μ and ν are connected by an edge, and zero otherwise. (Do not confuse A with $A_{\mu\nu}$!) To give an example, the adjacency matrix \mathbb{A} of (3*E*)-hexa-1,3,5-triene **161** (cf Figure 5) is

$$\begin{pmatrix} 0 & 1 & 0 \\ 1 & 0 & 1 \\ 0 & 1 & 0 \end{pmatrix} \quad (20)$$

Diagonalization of \mathbb{A} yields the eigenvalues X_j and the corresponding eigenvectors $\mathbb{C}_j = (C_{\mu j})$. From these one obtains the N orbital energies

$$\mathcal{E}_j = A + X_j B \quad (21)$$

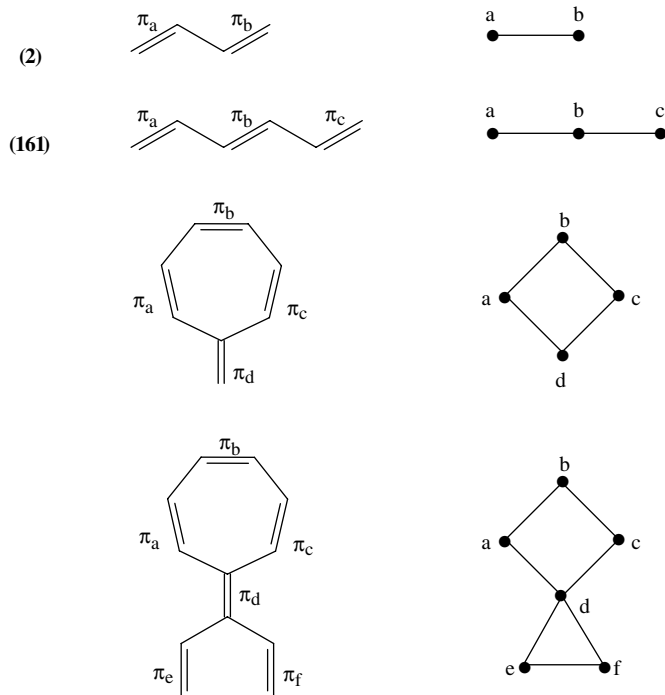


FIGURE 5. Representative graphs \mathcal{G} for an independent electron model based on linear combinations of two-centre π_μ . Examples: 1,3-butadiene **2**, (3E)-hexa-1,3,5-triene **161**, heptafulvene and sesquifulvalene

and the N molecular orbitals

$$\varphi_j = \sum_{\mu} \pi_{\mu} C_{\mu j} \quad (22)$$

Thus the diagonalization of the matrix 20 yields $X_1 = -\sqrt{2}$, $X_2 = 0$, $X_3 = \sqrt{2}$ and, according to equation 21, $\mathcal{E}_1 = A - \sqrt{2}B$, $\mathcal{E}_2 = A$ and $\mathcal{E}_3 = A + \sqrt{2}B$. Using the Koopmans theorem (equation 11) the π -bands in the PE spectrum of (3E)-hexa-1,3,5-triene **161** are therefore expected at positions $I_1^v = -A + \sqrt{2}B$, $I_2^v = -A$ and $I_3^v = -A - \sqrt{2}B$. If this procedure is applied to a series of planar π -systems, e.g. ethene, 1,3-butadiene **2**, (3E)-hexa-1,3,5-triene **161**, fulvene **175** and other unsubstituted polyenes, and if the computed ionization energies $I_{j,\text{calc}}^v = -\mathcal{E}_j$ are compared to the corresponding experimental values I_j^v or I_j^m by means of linear regression techniques, one obtains roughly $A \approx -10.2$ eV and $B \approx -1.2$ eV. Using these values for e.g. (3E,5E)-octa-1,3,5,7-tetraene **234**, one finds, according to the above procedure, $I_{1,\text{calc}}^v = 8.3$ eV, $I_{2,\text{calc}}^v = 9.5$ eV, $I_{3,\text{calc}}^v = 10.9$ eV and $I_{4,\text{calc}}^v = 12.1$ eV, which compare favourably with the experimental findings for **234** shown in Figure 6 and in Table 2.

The limitations of this naive approach are immediately obvious, if one considers that the molecules [3]radialene **173**, 3,4-dimethylenecyclobutene **174** and fulvene **175** give rise to the same graph \mathcal{G} (see display 23) and thus to identical predictions for their three π ionization energies. Using the above parameters one finds $I_{1,\text{calc}}^v = I_{2,\text{calc}}^v = 9.0$ eV,

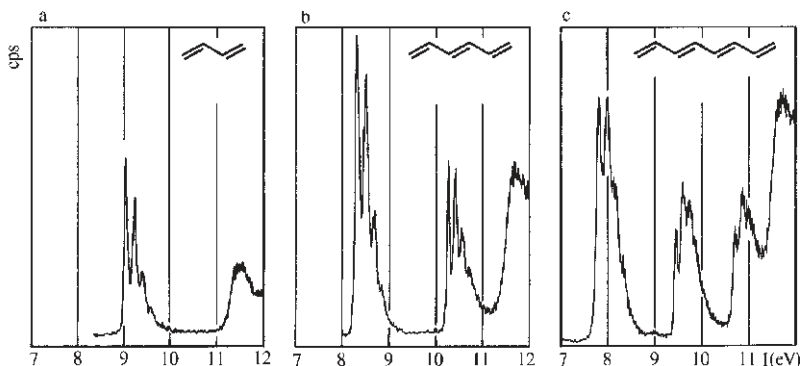
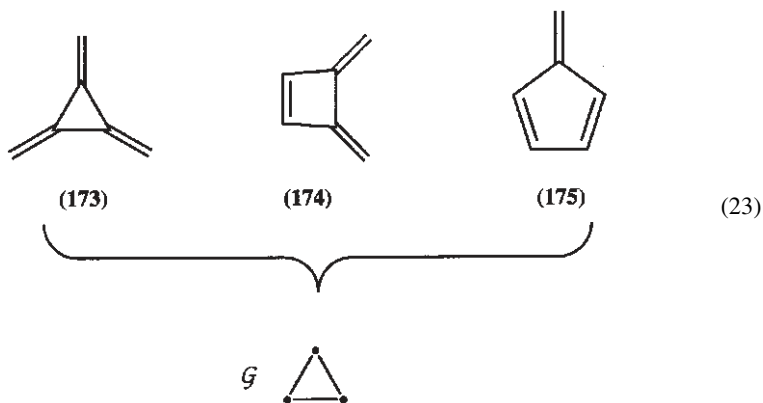


FIGURE 6. Photoelectron spectra of (a) 1,3-butadiene **2**, (b) (*E*)-hexa-1,3,5-triene **161** and (c) (3*E*, 5*E*)-octa-1,3,5,7-tetraene **234**

and $I_{3,\text{calc}}^{\text{v}} = 12.6$ eV, the first two values being degenerate because of the D_{3h} symmetry of the graph \mathcal{G} . Whereas this result is compatible with the experimental results for **173** of the same symmetry as \mathcal{G} (see Table 2), it is at odds with those for **174** and **175**, which lack the symmetry of \mathcal{G} .



This shortcoming could be avoided and the treatment improved by assigning different basis energies A_{exo} and A_{endo} to exocyclic and endocyclic basis orbitals π_{μ} and by adjusting the cross terms, but this is not really worthwhile. (For a more detailed discussion of the model see elsewhere¹⁷³.)

3. The standard Hückel treatment

In the familiar standard Hückel treatment^{2,174} of planar π -systems, the basis functions are atomic orbitals (AO) $2p_{z,\mu} \equiv \phi_{\mu}$, z being the coordinate perpendicular to the molecular plane. In analogy to the previous model, the basis energies of the atomic orbitals ϕ_{μ} and the cross terms between neighbouring pairs of AOs, ϕ_{μ} and ϕ_{ν} , are defined by

$$\langle \phi_{\mu} | \mathbf{H} | \phi_{\mu} \rangle = \alpha \text{ for all } \mu \quad (24)$$

and

$$\begin{aligned} \langle \phi_\mu | \mathbf{H} | \phi_\nu \rangle &= \beta \text{ if } \mu, \nu \text{ conjugated} \\ &= 0 \text{ otherwise} \end{aligned} \quad (25)$$

Under these conditions a π -system extending over N carbon centres is represented by a graph \mathcal{G}^{175} in which the nodes correspond to the basis orbitals ϕ_μ and the edges to those cross terms (equation 25) which are equal to β . Diagonalization of the corresponding adjacency matrix \mathbb{A} — sometimes called the Hückel matrix — yields N eigenvalues x_j and the corresponding eigenvectors $\mathbb{C}_j = (c_{\mu j})$. These quantities define the orbital energies \mathcal{E}_j and the Hückel molecular orbitals φ_j (HMO) according to

$$\mathcal{E}_j = \alpha + x_j \beta \quad (26)$$

and

$$\varphi_j = \sum_{\mu} \phi_{\mu} c_{\mu j} \quad (27)$$

To demonstrate the quality of this simple approach we show in Figures 6 and 7 the PE spectra of 1,3-butadiene **2**, (3*E*)-hexa-1,3,5-triene **161**, (3*E*, 5*E*)-octa-1,3,5,7-tetraene **234**, [3]radialene **173**, 3,4-dimethylenecyclobutene **174** and fulvene **175**. The observed positions I_j^m of the π -bands are collected in the third column of Table 2, and the eigenvalues x_j obtained from standard HMO models in the fourth. A least-squares calculation yields the linear regression

$$I_j^m \text{ (eV)} = 7.15 + 2.60 x_j \quad (28)$$

shown in Figure 8. As can be seen, the agreement is rather satisfactory in view of the simplicity of the treatment. The values $I_{j,\text{calc}}^v$ calculated according to equation 23 are listed in the last column of Table 2. Using the Koopmans theorem (equation 11) in conjunction with equations 26 and 28, the following calibration of the basic parameters is obtained:

$$\alpha = -7.15 \text{ eV}, \quad \beta = -2.60 \text{ eV} \quad (29)$$

4. Alkyl-substituted planar dienes and polyenes

Restricting ourselves, as before, to molecules $C_n H_m$ we shall discuss only the consequences due to the replacement of hydrogen atoms by alkyl groups R . The influence of the substituents R on the orbital energies \mathcal{E}_j of the π -orbital φ_j of the parent molecule — and thus, according to the Koopmans theorem, on the ionization energy $I_{j,\text{calc}}^v$ — is assigned, within an HMO treatment, to two causes: (a) to an inductive effect and (b) to hyperconjugation.

(a) *Inductive effect.* If a hydrogen atom in position ρ of a planar π -system is replaced by an alkyl group R_ρ , the inductive effect of R_ρ is assumed to change the basis energy of the atomic orbital ϕ_ρ from α to

$$\alpha_\rho(R_\rho) = \alpha + \delta\alpha_\rho(R_\rho) \quad (30)$$

The perturbation $\delta\alpha_\rho(R_\rho)$ is positive for all alkyl groups, increasing with increasing size of the group R_ρ . The change $\delta\mathcal{E}_{j,\text{ind}} = \mathcal{E}_j' - \mathcal{E}_j$ of the orbital energy \mathcal{E}_j due to the inductive influence of alkyl substituents R_ρ in positions ρ of the parent molecule can be

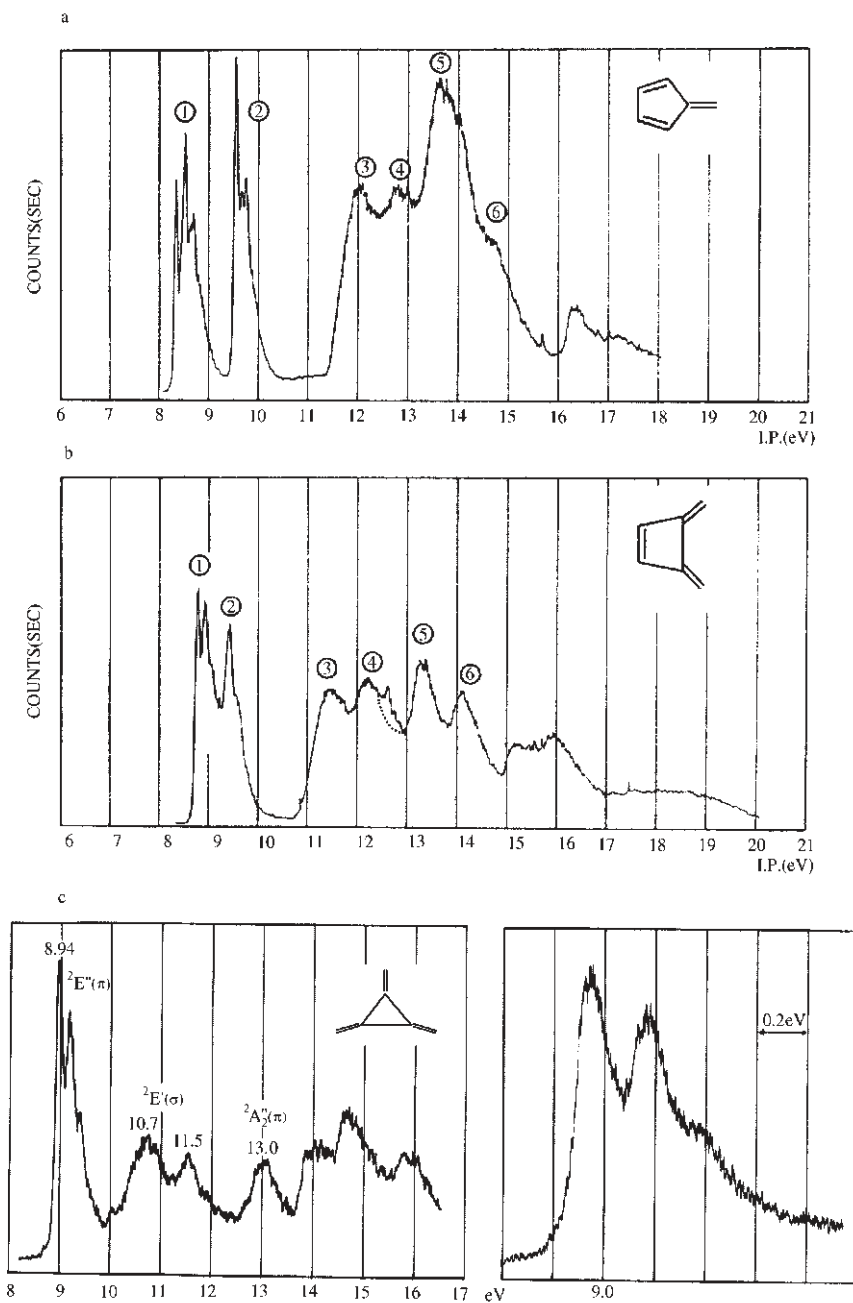


FIGURE 7. Photoelectron spectra of (a) fulvene **175**, (b) dimethylenecyclobutene **174** and (c) [3]radialene **173**

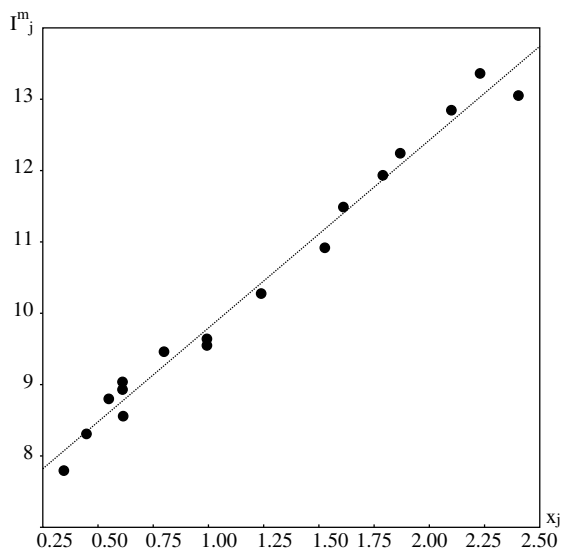


FIGURE 8. Regression of observed vertical ionization energies I_j^m on the corresponding HMO x_j values for the set of planar polyenes listed in Table 2

TABLE 2. Observed band positions I_j^m and calculated HMO ionization energies $I_{j,\text{calc}}^v$ for some polyenes

	Polyene	I_j^m (eV)	x_j	$I_{j,\text{calc}}^v$ (eV)
2	Butadiene	9.03	0.618	8.73
		11.46	1.618	11.33
161	(3 <i>E</i>)-Hexa-1,3,5-triene	8.29	0.445	8.28
		10.26	1.247	10.37
		11.90	1.802	11.81
234	(3 <i>E</i> , 5 <i>E</i>)-Octa-1,3,5,7-tetraene	7.79	0.347	8.03
		9.61	1.000	9.37
		10.89	1.532	11.11
		12.20	1.879	12.01
173	[3]Radialene	8.94	0.618	8.94
		13.00	2.414	13.40
174	3,4-Dimethylenecyclobutene	8.80	0.555	8.57
		9.44	0.802	9.44
		13.30	2.247	13.30
175	Fulvene	8.55	0.618	8.73
		9.54	1.000	9.72
		12.80	2.115	12.62

estimated by a first-order perturbation calculation according to

$$\delta\mathcal{E}_{j,\text{ind}} = \sum_{\rho} \delta\alpha_{\rho}(R_{\rho})c_{\rho j}^2 \quad (31)$$

where the summation carries only over the substituted positions ρ . According to the Koopmans theorem (equation 11) the corresponding change $\delta I_{j,\text{ind}}^v$ of the ionization energy

$I_{j,\text{calc}}^{\text{v}}$ is then given by

$$\delta I_{j,\text{ind}}^{\text{v}} = -\delta \mathcal{E}_{j,\text{ind}} = -\sum_{\rho} \delta \alpha_{\rho}(\text{R}_{\rho}) c_{\rho j}^2 \quad (32)$$

Note that the shift $\delta I_{j,\text{ind}}^{\text{v}}$ is always negative, meaning that the inductive influence of alkyl substituents leads to a reduction of the ionization energies $I_{j,\text{calc}}^{\text{v}}$ relative to the values calculated for the parent molecule.

If one assumes that the substituents R exert only an inductive effect, a crude calibration of $\delta \alpha_{\rho}(\text{R}_{\rho})$ is obtained from π -ionization energy shifts δI_1^{v} observed for alkyl-substituted ethenes¹⁷⁶, as shown in Figure 9. It is seen that the size of $|\delta I_1^{\text{v}}|$ increases with increasing number of C-atoms of the alkyl group. Because both atomic orbital coefficients of the ethene π -orbital $\pi = (\phi_1 + \phi_2)/\sqrt{2}$ are equal to $1/\sqrt{2}$, one obtains from equation 32 the following (upper) estimates for $\delta \alpha_{\rho}(\text{R}_{\rho})$: $\delta \alpha(\text{Me}) = 1.6$ eV; $\delta \alpha(\text{Et}) = 1.8$ eV; $\delta \alpha(i\text{-Pr}) = 2.0$ eV; $\delta \alpha(t\text{-Bu}) = 2.2$ eV. [Note that these $\delta \alpha(\text{R}_{\rho})$ values correlate linearly with the differences $\Delta \sigma^*(\text{R}) = \sigma^*(\text{R}) - \sigma^*(\text{H})$ of Taft's inductive parameters $\sigma^*(\text{R})$ ¹⁷⁷: $\Delta \sigma^*(\text{Me}) = 0.49$, $\Delta \sigma^*(\text{Et}) = 0.59$, $\Delta \sigma^*(i\text{-Pr}) = 0.68$, $\Delta \sigma^*(t\text{-Bu}) = 0.79$.] Such a parametrization has to be taken with a grain of salt, as it implies that alkyl groups exert only an inductive effect. In addition, it refers only to single substitution at a double bond. If a double bond is multiply substituted, the observed shift δI_1^{v} is smaller than the sum of the individual $\delta I_{j,\text{ind}}^{\text{v}}$ values calculated according to equation 32 for each of the substituting alkyl groups.

(b) *Hyperconjugation*. Hyperconjugation between a π -orbital ϕ_j and a pseudo π -orbital ϕ_{R} of a substituting alkyl group R can be taken care of by a model first proposed by Mulliken¹⁷⁸. To this end one assigns a basis energy α_{R} to ϕ_{R} and a cross term

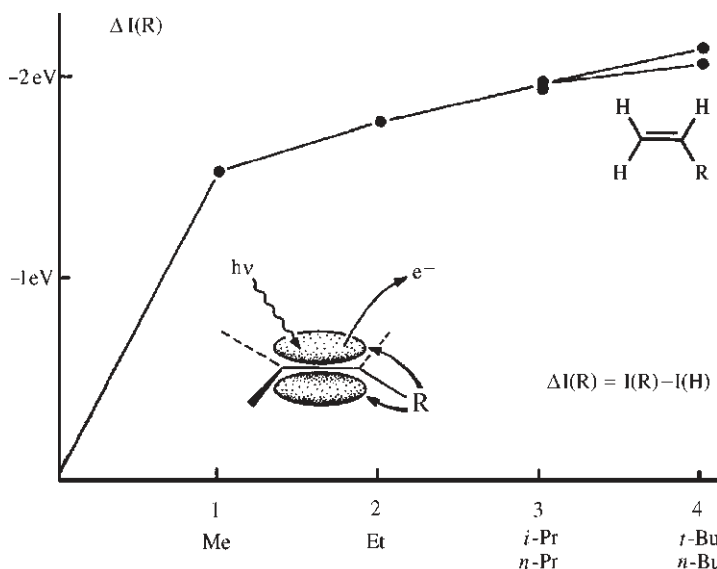


FIGURE 9. Shifts $\Delta I(\text{R})$ of the π -ionization energy of ethene induced by a single alkyl group R = Me, Et, *n*-Pr, *i*-Pr, *n*-Bu and *t*-Bu

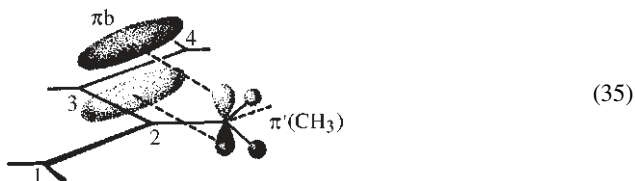
$\beta_{\rho R} = \langle \phi_\rho | \mathbf{H} | \phi_R \rangle$ to the interaction of ϕ_R with the atomic orbital ϕ_ρ at the point of substitution. The shift $\delta\mathcal{E}_{j,\text{hyp}}$ caused by a single substitution can be estimated by second-order perturbation theory according to

$$\delta\mathcal{E}_{j,\text{hyp}} = (c_{\rho j} \beta_{\rho R})^2 / (\mathcal{E}_j - \alpha_R) \quad (33)$$

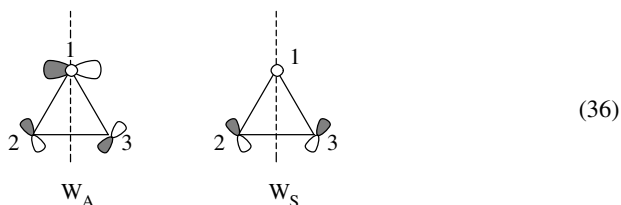
If this is rewritten in the form $\delta\mathcal{E}_{j,\text{hyp}} = [\beta_{\rho R}^2 / (\mathcal{E}_j - \alpha_R)] c_{\rho j}^2$, one sees that for a given alkyl group R this hyperconjugative shift is again proportional to $c_{\rho j}^2$ in analogy to the inductive shift (equation 32). The expression in square brackets increases with decreasing difference $\mathcal{E}_j - \alpha_R$, which is in general positive for the top π -orbitals. This means that π -orbitals φ_j lying closer in energy to the pseudo π -orbital ϕ_R are more strongly affected by hyperconjugation than the upper ones. As long as the π -orbital φ_j lies above ϕ_R , the hyperconjugative shift $\delta I_{j,\text{hyp}}^V = -\delta\mathcal{E}_{j,\text{hyp}}$ calculated according to equation 33 is again towards lower ionization energies, adding to the one due to the inductive effect (see equation 32), with the result that the total shift $\delta I_{j,\text{calc}}^V = \delta I_{j,\text{ind}}^V + \delta I_{j,\text{hyp}}^V$ is given—within our simple model—for a multiply substituted π -system by

$$\delta I_{j,\text{calc}}^V = - \sum_{\rho} \left(\delta\alpha_{\rho}(\mathbf{R}_{\rho}) + \beta_{\rho R}^2 / (\mathcal{E}_j - \alpha_R) \right) c_{\rho j}^2 \quad (34)$$

Hoffmann has pointed out¹⁷⁹ that one should also expect significant through-space interaction (i.e. hyperconjugation) between alkyl groups R and two-centre π -orbitals which are not directly bonded, as shown schematically in diagram 35 for R = Me. (In this example we have used the model described in Section II.D.2, i.e. using as basis a two-centre orbital π and a pseudo π -orbital $\pi'(\text{CH}_3)$ for the methyl group.) The effect of this type of interaction can be shown by comparison of the two π -ionization energies I_1^V and I_2^V of (2E,4E)-hexa-2,4-diene **10** and of 2,3-dimethylbuta-1,3-diene **11**²⁰. Whereas the mean π -ionization energy $(I_1^V + I_2^V) / 2$ is the same for both molecules, i.e. 11.33 eV and 11.31 eV respectively, the split $I_2^V - I_1^V$ is quite different, namely 3.07 eV and 2.28 eV. These observations are nicely explained by Hoffmann's theory, as shown in Figure 10 which is self-explanatory.



A special case is met when the substituent is the cyclopropyl group, because of the presence of high-lying almost π -type σ -orbitals. These orbitals, W_A and W_S , shown schematically in diagram 36, have been introduced by Walsh¹⁸⁰ to explain the properties of molecules containing the cyclopropane moiety.



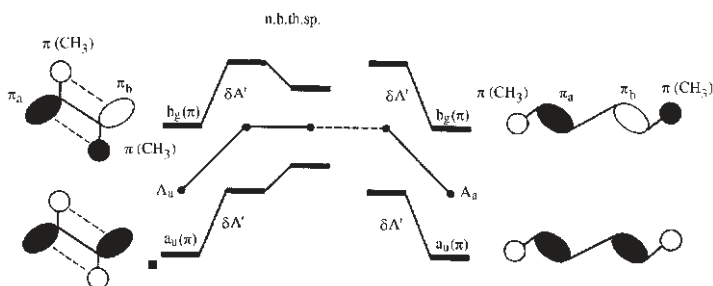
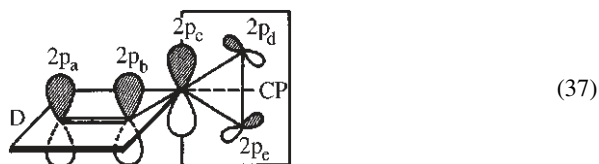
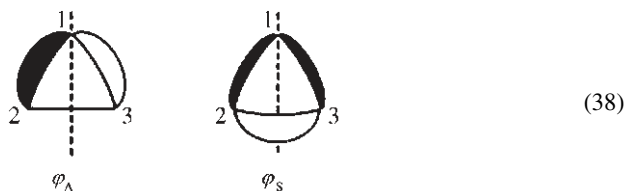


FIGURE 10. Correlation diagram showing the influence of non-bonded through-space (n.b.th.sp) interaction between the pseudo π -orbitals $\pi(\text{CH}_3)$ (circles) and the double-bond π -orbitals π_a and π_b (ovals) on the π -orbital energies of the butadiene π -system. A_a is the basis energy of π_a and π_b and δA the inductive and hyperconjugative destabilization (see equation 34)

Because these orbitals—which are degenerate in cyclopropane because of its D_{3h} symmetry—are close in energy to two-centre π -orbitals, and because the antisymmetric Walsh orbital W_A consists essentially of a 2p-orbital in position 1, a cyclopropyl substituent acts almost as another two-centre π -orbital in direct conjugation with that of the substituted double bond, as sketched in diagram 37. It follows that the PE spectra of molecules in which the cyclopropyl group is ideally aligned for optimal conjugation with a planar π -system, will be very similar to that of the corresponding polyene. For example, the PE spectrum of spiro[2.4]hepta-4,6-diene (homofulvene) **74** resembles that of fulvene **175**, as shown in Figure 11.



However, for a more detailed and reliable rationalization of the PE spectroscopic consequences due to conjugation with a cyclopropyl moiety, it is of advantage to use a model originally proposed by Förster¹⁸¹ and later by Coulson and Moffitt¹⁸². The advantages of this model, where the high-lying cyclopropane orbitals are written in terms of localized CC σ -orbitals (diagram 38), have been discussed elsewhere¹⁸³.



5. Special cases

a. Deviations from planarity. The moderate bending and twisting of a single double bond has only a very small effect on its π -ionization energy because of an internal

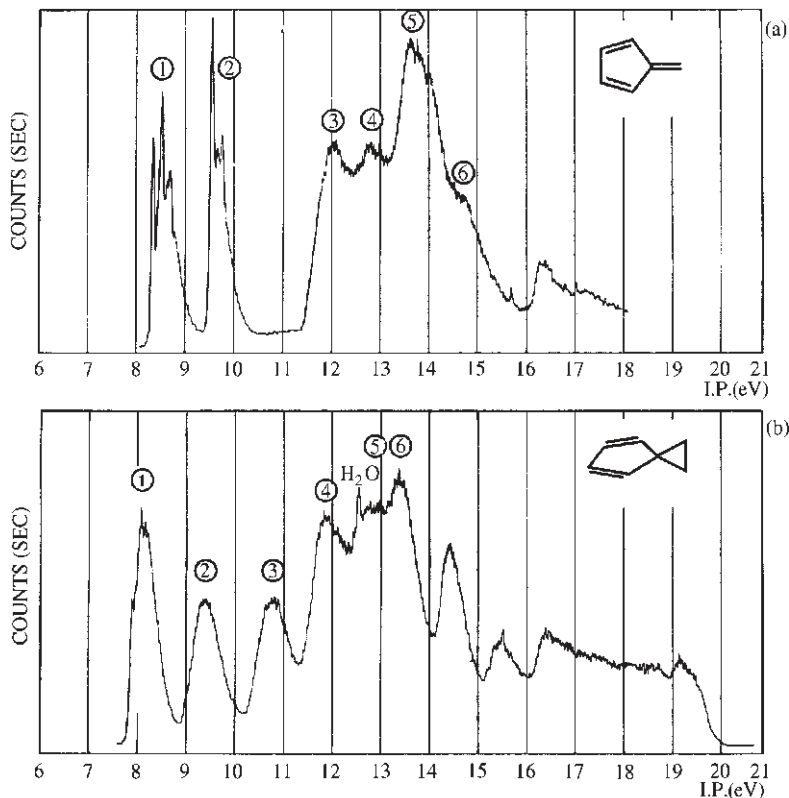


FIGURE 11. Comparison of the PE spectra of (a) fulvene **175** and (b) homofulvene (spiro[2.4]hepta-4,6-diene) **74**

compensation of different electronic effects¹⁸⁴. (An example is provided by the analysis of the PE spectrum of tricyclo[4.2.2.2^{2,5}]dodeca-1,5-diene **129**⁹⁶.) In contrast, the twisting about the single bond connecting two conjugated double bonds, e.g. in butadiene **2**, has a large effect on both π -ionization energies I_1^v and I_2^v leading in particular to a significant reduction of the gap $\Delta I = I_2^v - I_1^v$. As shown by Maier and Turner¹⁸⁵ this effect can be accounted for within an independent electron model by assuming that the cross term between the two conjugated π -orbitals π_1 and π_2 or between their linked atomic orbitals ϕ_2 and ϕ_3 depends on the twisting angle τ according to the equations

$$\langle \pi_1 | \mathbf{H} | \pi_2 \rangle = B_{1,2} = B \cos \tau \quad (39)$$

or

$$\langle \phi_2 | \mathbf{H} | \phi_3 \rangle = \beta_{2,3} = \beta \cos \tau \quad (40)$$

where $\tau = 0^\circ$ for the *s-trans* conformation. As a result the observed ionization energy gap depends on τ

$$\Delta I_\tau = I_2^v - I_1^v = \Delta I_{\tau=0} \cos \tau \quad (41)$$

This relationship has been used with success to derive the twisting angles τ between two conjugated double bonds¹⁸⁵, and a particularly nice example is provided by the PE spectroscopic determination of the dihedral angle $\tau = 58^\circ$ which perfluorobutadiene assumes in the gas phase^{19,186}. Figure 12 presents the PE spectra of the three isomers (2*Z*,4*Z*)-, (2*Z*,4*E*)- and (2*E*,4*E*)-3,4-dimethylhexa-2,4-diene (**26**, **27** and **28**)³⁷, from which it is seen that the gap ΔI_τ decreases with increasing steric interference between the two methyl groups, whereas the mean π -ionization energy $\bar{I}^\nu = (I_1^\nu + I_2^\nu)/2$ remains constant.

Molecule	26 (2 <i>Z</i> ,4 <i>Z</i>)	27 (2 <i>Z</i> ,4 <i>E</i>)	28 (2 <i>E</i> ,4 <i>E</i>)	
ΔI_τ (eV)	1.65	0.60	0.30	(42)
\bar{I}^ν (eV)	8.93	8.90	8.90	
τ	0°	69°	80°	

Assuming that the π -system of the (2*Z*,4*Z*) isomer **26** is flat, $\tau = 0^\circ$, equation 41 yields the twist angles τ indicated in the last line of display 42 for the other two isomers. A further example of strong steric prohibition of coplanarity is provided by 2,3-di-*t*-butylbuta-1,3-diene **35**³⁷, whose PE spectrum yields a gap $\Delta I_\tau = 0.3$ eV, corresponding to a twist angle $\tau = 80^\circ$.

Application of an extension of the above treatment to cyclooctatetraene **239** and other cyclic polyenes⁵⁰ yields a satisfactory determination of the twist angles τ between conjugated pairs of their double bonds, in excellent agreement with those derived by other methods.

b. Cumulenes. Although the formulae of the cumulenes allene **1**, butatriene **158** and pentatetraene **232** look deceptively simple, their PE spectra are among the most difficult to interpret. Allene, first investigated by Baker and Turner¹⁸⁷, and pentatetraene exhibit D_{2d} symmetry, with the result that their highest occupied molecular orbitals are degenerate. Removing an electron from this orbital pair leads to a degenerate doublet state of the corresponding radical cation, which therefore undergoes a Jahn–Teller distortion. This distortion can lead to a radical cation of C_{2v} or D_2 symmetry, depending on whether the distortion proceeds along the stretching B_2 or the twisting B_1 mode of vibration of the parent hydrocarbon, as has been shown by Haselbach¹⁸⁸. The resultant Franck–Condon envelopes are thus rather complicated and difficult to analyse. This complication can be partially avoided by breaking the D_{2d} symmetry, i.e. by correlating the π -band positions in the PE spectrum of allene with those in the spectra of methyl-substituted allenes **3**, **6**, **7**, **15** and **18**¹⁷, or of tetrafluoroallene¹¹⁵.

Butatriene **158**, belonging to the symmetry group D_{2h} , is planar, and therefore lacks degenerate orbitals. Notwithstanding this simplification its PE spectrum is far from simple. In particular, the first π -band at 9.15 eV is accompanied at higher energy by a second ‘mystery band’ at 9.63 eV, as shown in Figure 13¹¹⁴. This feature cannot be accounted for by an independent electron model, and not even by SCF models. It has been shown by von Niessen, Cederbaum and their coworkers¹⁸⁹ that it arises as a consequence of vibronic mixing of the ${}^2B_{2g}$ and ${}^2B_{3u}$ states of the butatriene radical cation. Supporting evidence for this interpretation is provided by an analysis of the PE spectra of tetrafluorobutatriene, tetramethylbutatriene **168** and tetra-*t*-butylbutatriene **172**¹¹⁵. It follows that the PE spectra of molecules containing cumulated double bonds cannot be interpreted with reference to the usual, naive, independent electron-orbital picture.

c. π -Systems exhibiting second-order bond fixation. A special case is given by cyclic π -systems for which two or more Kekulé structures can be written, but which tend to

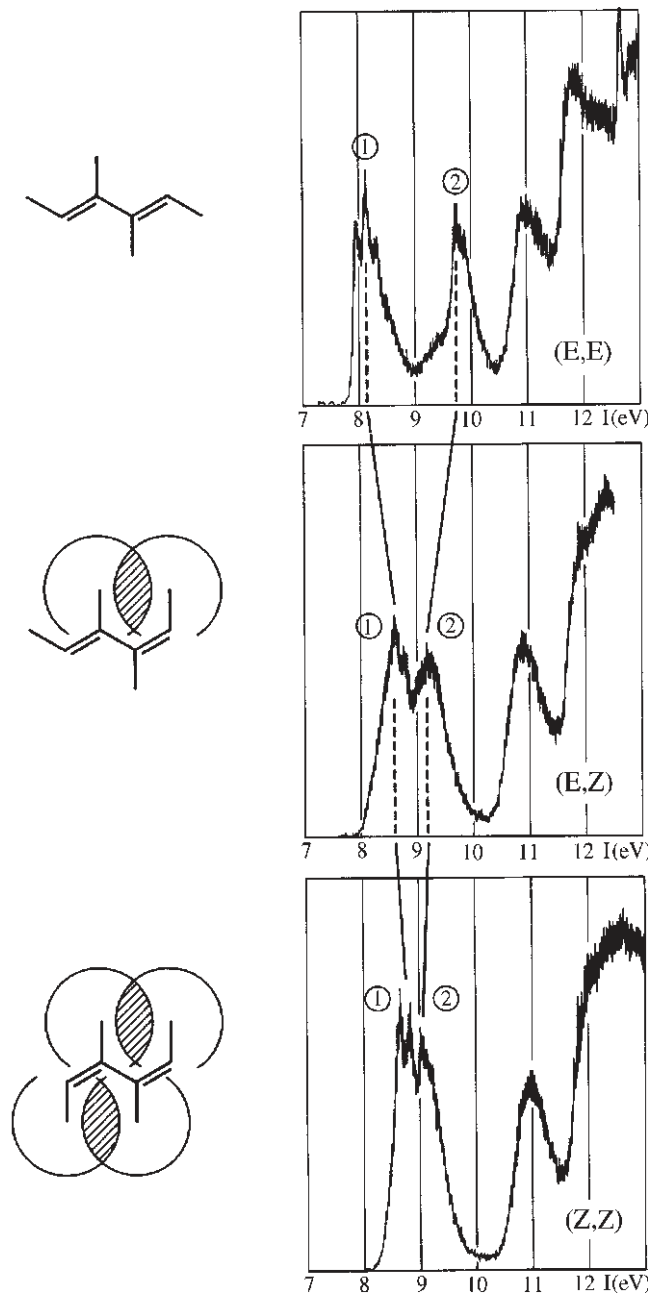


FIGURE 12. Correlation of the PE spectra of (2Z,4Z)-, (2Z,4E) and (2E,4E)-3,4-dimethylhexa-2,4-diene (26, 27 and 28, respectively)

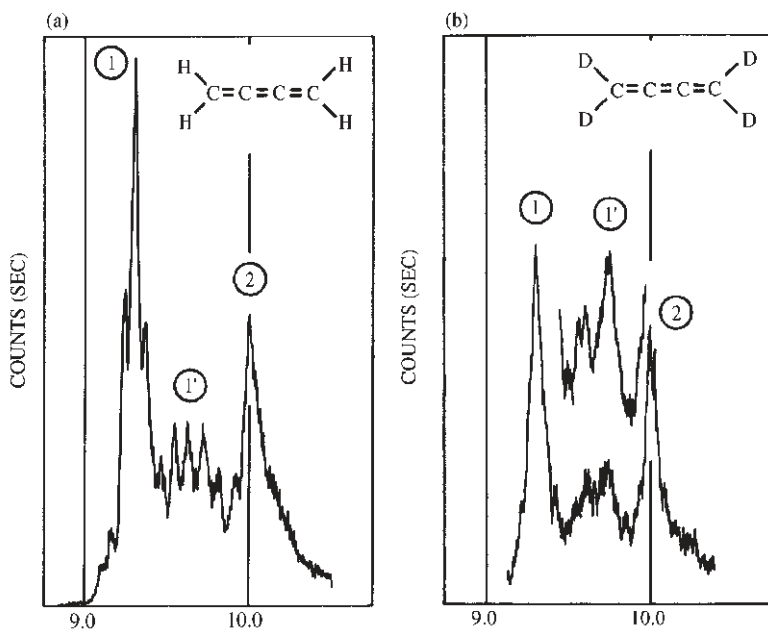


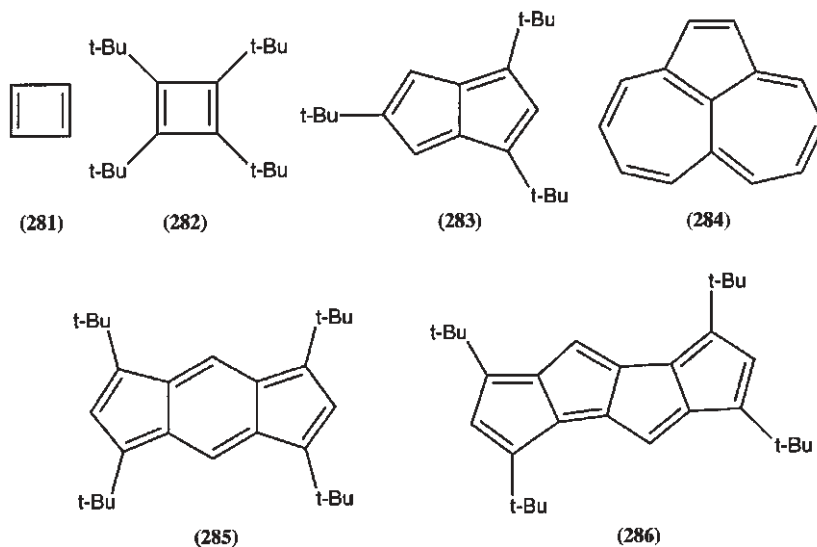
FIGURE 13. Franck-Condon envelopes of the low-energy part of the PE spectra of (a) butatriene **158** and (b) tetradeuteriobutatriene **159**. The central feature labeled 1' is the 'mystery band' mentioned in the text

localize their double bonds to assume a structure corresponding to only one or other of these Kekulé structures. It has been shown by Longuet-Higgins and Salem¹⁴ that this is a second-order effect which occurs in annulenes above a critical size. The tendency of a molecule towards second-order bond localization can be linked to the bond-bond polarizabilities $\pi_{\mu\nu,\rho\sigma}$ of its π -system^{190,191}. Typical examples are hydrocarbons containing cyclobutadiene, pentalene or heptalene moieties. Because bond-bond polarizabilities $\pi_{\mu\nu,\rho\sigma}$ of the neutral ground-state molecule M change when an electron is removed from an orbital φ_j , the tendency of the radical cation $M^{+\bullet}$ to localize its double bonds varies, depending on the electronic state ${}^2\tilde{\Psi}_j$ of $M^{+\bullet}$ ¹⁹⁰. This effect complicates the analysis of the PE spectra of such molecules.

The PE spectra of cyclobutadiene **281**¹⁹², tetra-*t*-butylcyclobutadiene **282**¹⁹³, 1,3,5-tri-*t*-butylpentalene **283**¹⁹⁴ and aceheptylene **284**¹⁹⁵, all of which are subject to second-order bond localization, have been described in the literature. Further examples are 1,3,5,7-tetra-*t*-butyl-*s*-indacene **285** (which exhibits a first double band 1,2 at $I_{1,2}^y = 6.75$ eV, followed by two bands at $I_3^y = 8.50$ eV and $I_4^y = 9.30$ eV) and the tetracyclic hydrocarbon 1,3,6,8-tetra-*t*-butylpentaleno[2,1-*a*]pentalene **286** (the first two bands of which are observed at 6.40 eV and 7.65 eV)¹⁹⁶.

6. Some cautionary remarks

The simple HMO model² has proved useful in many cases—and is in fact still used—for a first rationalization of the PE spectra of planar—almost planar—polyenes.



Notwithstanding its advantages, its limitations must be taken into account, even if it is applied only qualitatively and certainly if a semiquantitative discussion is intended. In this connection the following points are worth mentioning.

(1) The Hückel treatment and its simpler version presented in Section II.D.2 make the implicit assumption that the manifold of π -orbitals lies above and is well separated from the σ -orbital manifold. Whereas the first bands in the PE spectrum of a planar polyene with N conjugated double bonds are indeed due to ejection of an electron from π -orbitals, this is not necessarily true for all of its first N bands. The reason is that σ -orbitals are delocalized over the whole of the σ -frame of the molecule M —sometimes even more so than the π -orbitals—with the result that the top σ -orbitals move to higher energies with increasing size of the molecule. To give an example: the first band in the PE spectrum of ethane is found at $I_1^m = 11.5$ eV but that of the saturated tetracyclic hydrocarbon perhydropyrene is at $I_1^m = 9.0$ eV¹⁹⁷. This shift towards lower ionization energies occurs also if the σ -frame consists of sp^2 – sp^2 single bonds¹⁹⁷. As a consequence, the third band observed in the PE spectrum of (3*E*)-hexa -1,3,5-triene **161** at 11.9 eV (Figure 6 and Table 2) is due to the superposition of the third π -band and of the first σ -band, and the fourth band at 11.7 eV in the PE spectrum of (3*E*, 5*E*)-octa -1,3,5,7-tetraene **234** (Figure 6 and Table 2) is a σ -band preceding the fourth π -band at 12.2 eV. The implications will be discussed in a later section.

(2) Because independent electron treatments do not take electron–electron interactions into account explicitly, the ground configuration $^1\Phi_0$ or the configurations $^2\tilde{\Phi}_j$ obtained by removing a single electron from one of the orbitals φ_j will not mix with excited configurations. This excludes configuration interaction known to be an important factor. For instance, some of the standard Hückel molecular orbitals φ_j derived for molecules such as heptafulvene **287** or sesquifulvalene **288** are completely localized on only part of the molecule, e.g. on either the five- or the seven-membered ring of **288**. Removing an electron from such an orbital leads to a radical cation in which the positive charge is concentrated on one of the rings only. Obviously, the radical cation will avoid this unfavourable distribution by spreading the charge over the remainder of the system, thereby lowering its energy. It follows that the observed π -band positions in the PE spectra of **287** and

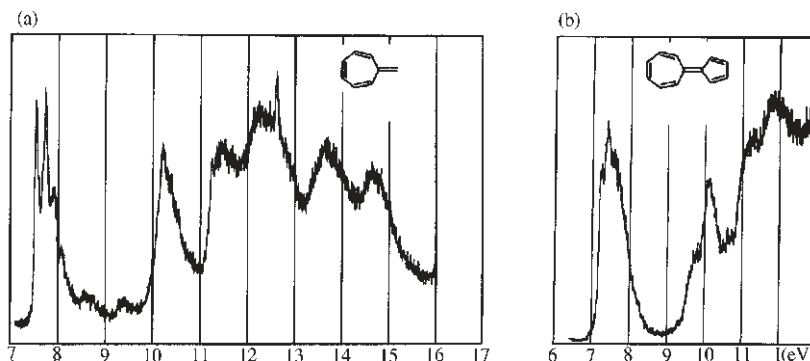
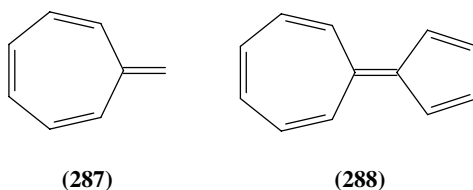


FIGURE 14. Photoelectron spectra of (a) heptafulvene **287** and (b) sesquifulvalene **288**

288 shown in Figure 14 173—and of similar molecules—will not fit the results of independent electron-model calculations. Spanguet-Larsen has shown¹⁹⁸ that the reasons for this failure are in fact more complicated than stated above.



(3) The assumption of constant interaction terms B between conjugated π_μ basis orbitals or of β between bonded $2p_z(\phi_\mu)$ orbitals assumes that all bonds in the polyene, both double and single, have the same length R_0 both in the neutral molecule M and in the radical cation M^+ , independent of its different configurations ${}^2\tilde{\Phi}_j$. However, this is not the case. In a first, crude approximation the interatomic distances $R_{\mu\nu}$ of the neutral molecule are linear functions of the bond orders $p_{\mu\nu}$ and those of the radical cation, $R_{\mu\nu}^+$, of the bond orders $p_{\mu\nu}^+ = p_{\mu\nu} - c_{\mu j}c_{\nu j}$, j being the quantum number of the vacated orbital φ_j . It has been shown¹⁹⁹ that this effect can be taken care of by a perturbation treatment (thereby improving the agreement) of the computed $I_{j,\text{calc}}^v$ values with the observed I_j^m ionization energies.

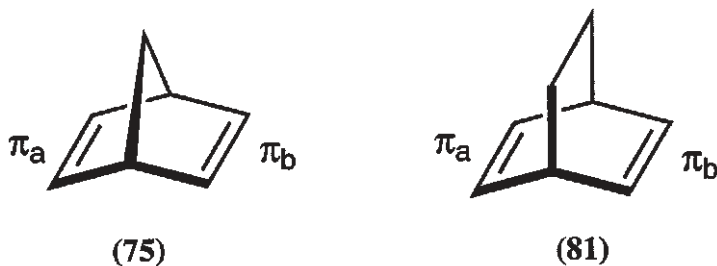
The take-home lesson is that independent electron treatments, e.g. the HMO model, should be used with caution, especially if semiquantitative predictions are intended. *Warning*: Concerning limitations and possible side-effects consult your PE spectroscopist or your neighbour theoretician.

E. Interaction Between Non-conjugated π -Orbitals

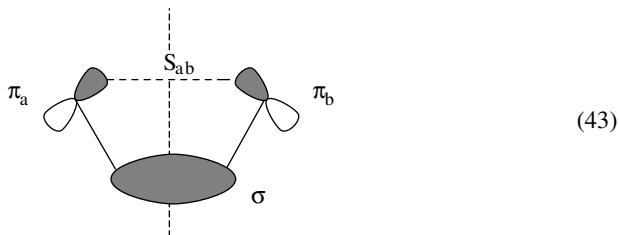
1. A naive, independent electron model

The disproof of the naive expectation that the PE spectrum of a (non-planar) hydrocarbon containing z non-conjugated double bonds would show z π -bands, where each one corresponds to the removal of an electron from only one of the z localized two-centre π -orbitals, was one of the earliest successes of PE spectroscopy. In particular, if in a

diene **M** the two double bonds, and thus the two π -orbitals π_a and π_b , are symmetry equivalent, one does not observe a single peak due to the superposition of two bands of the same ionization energy $I_a^v = I_b^v$ but two well-separated bands, as shown for example in the PE spectra of 1,1-divinylcyclopropane **46** (Figure 2), or norbornadiene **75** or of bicyclo[2.2.2]octadiene **81** (Figure 15). This means that there exists a large interaction between π_a and π_b .



Although *ab initio* or semiempirical SCF calculations account rather well for this observation, it has proved extremely enlightening, especially from a qualitative point of view, to discuss the interactions between non-conjugated π -orbitals in terms of the concepts of ‘through-space’ and ‘through-bond’ interactions introduced by Roald Hoffmann^{200–203}. With reference to the schematic diagram 43 of a non-planar diene, these interactions are defined as follows:



(1) ‘Through-space interaction’. Although the two π -orbitals π_a and π_b are not in conjugation, there exists a small but finite cross term B between them which, to a first approximation, will be proportional to their overlap integral $S_{ab} = \langle \pi_a | \pi_b \rangle$.

(2) ‘Through-bond interaction’. Because of the molecule’s lack of planarity, each of the two π -orbitals π_a and π_b will interact with those of the σ -frame’s σ -orbitals which exhibit the appropriate symmetry behaviour.

To illustrate the principles involved we shall use the independent electron model presented in Section II.D.2. For simplicity, we assume that we are dealing with a diene in which the basis π -orbitals π_a and π_b are symmetry equivalent, as is the case for the dienes **75** and **81**, both of which belong to the point group C_{2v} . (The same assumption underlies the schematic diagram 43). Disregarding the 1s orbitals of the carbon atoms, such a diene C_nH_m has $2(n-1) + m/2$ σ -orbitals. Of these we shall consider only a single one (σ), symmetric with respect to the operations which transform the linear combination $\pi_a + \pi_b$ into itself. (The extension to more σ -orbitals is trivial.) Under these conditions we are dealing with a mini-model—depicted in diagram 43—that can be represented by a graph \mathcal{G} with only three nodes representing π_a , π_b and σ , and three labelled edges, B representing the ‘through-space’ and Γ the ‘through-bond’ cross terms. Note that in

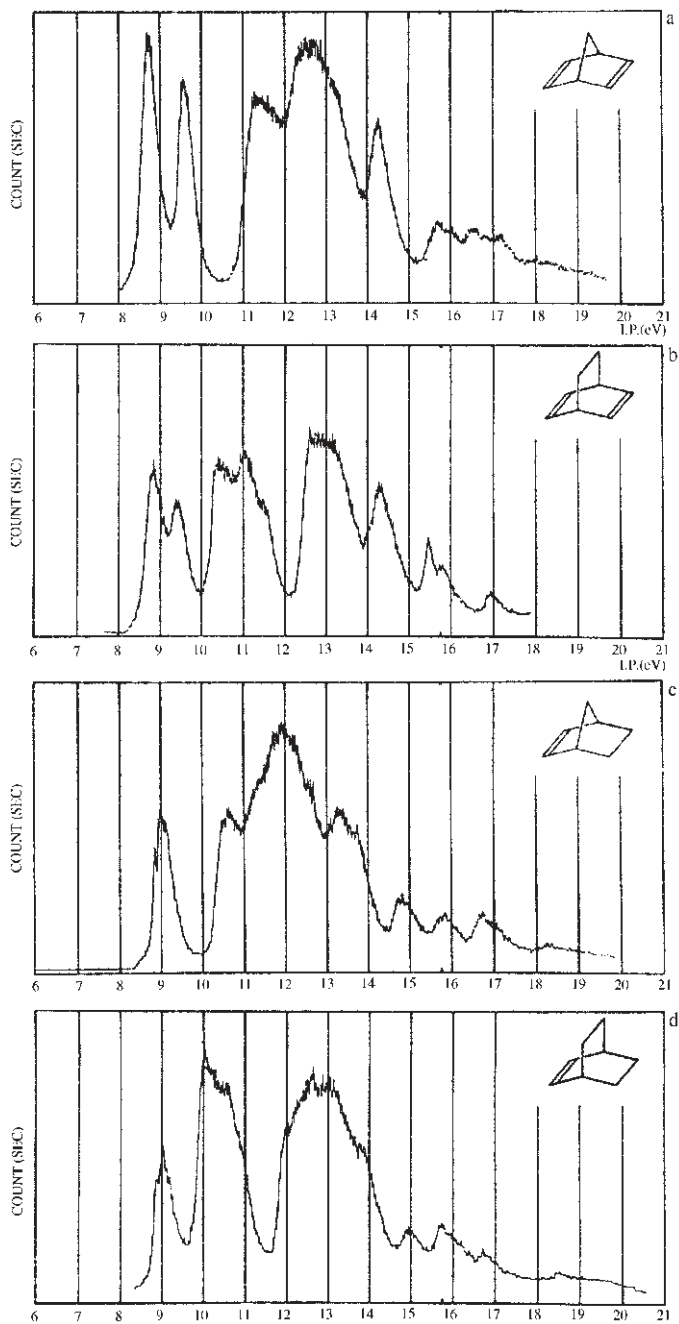
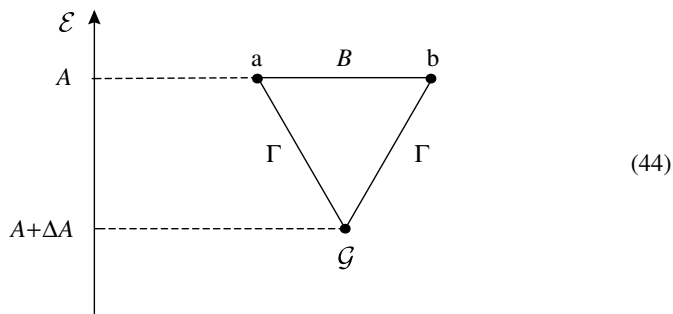


FIGURE 15. Photoelectron spectra of (a) norbornadiene **75** and (b) bicyclo[2.2.2]octadiene **81**, compared to those of (c) norbornene and (d) bicyclo[2.2.2]octene

presentation 44 the graph \mathcal{G} has been drawn in such a way that the projections of the nodes onto an energy ordinate labeled \mathcal{E} corresponds qualitatively to the relative energies of the basis orbitals.



The parameters are defined in equations 45–48. The parameters A , B and Γ are negative quantities if the orientation of the basis orbitals is defined as shown in diagram 43, and the same is true for ΔA if we assume that the energy of the σ -orbital lies below that of the two π -orbitals as indicated in presentation 44. The orbital energies \mathcal{E}_j are obtained by solving the secular determinant given by equation 49, which yields the solutions given in equations 50.

$$\langle \pi_a | \mathbf{H} | \pi_a \rangle = \langle \pi_b | \mathbf{H} | \pi_b \rangle = A \quad (45)$$

$$\langle \pi_a | \mathbf{H} | \pi_b \rangle = B \quad (46)$$

$$\langle \sigma | \mathbf{H} | \sigma \rangle = A + \Delta A, \text{ with } \Delta A < 0 \quad (47)$$

$$\langle \pi_a | \mathbf{H} | \sigma \rangle = \langle \pi_b | \mathbf{H} | \sigma \rangle = \Gamma \quad (48)$$

$$\begin{vmatrix} A - \mathcal{E} & B & \Gamma \\ B & A - \mathcal{E} & \Gamma \\ \Gamma & \Gamma & A + \Delta A - \mathcal{E} \end{vmatrix} = 0 \quad (49)$$

$$\begin{aligned} \mathcal{E}_{1,3} &= A + (\Delta A + B)/2 \pm \sqrt{[(B - \Delta A)/2]^2 + 2\Gamma^2} \\ \mathcal{E}_2 &= A - B \end{aligned} \quad (50)$$

Of the corresponding linear combinations φ_1 and φ_3 are symmetric, and φ_2 antisymmetric, as shown in Figure 16. To give an example, one obtains for the values $\Delta A = -2$ eV and $\Gamma = -1$ eV the dependence of \mathcal{E}_1 , \mathcal{E}_2 and \mathcal{E}_3 on the through-space parameter B shown in display 51.

B	$\mathcal{E}_1 - A$ (eV)	$\mathcal{E}_2 - A$ (eV)	$\mathcal{E}_3 - A$ (eV)
0.0	-2.732	0.000	0.732
-0.2	-2.776	0.200	0.576
-0.4	-2.825	0.400	0.425
-0.6	-2.878	0.600	0.278
-0.8	-2.936	0.800	0.136
-1.0	-3.000	1.000	0.000

(51)

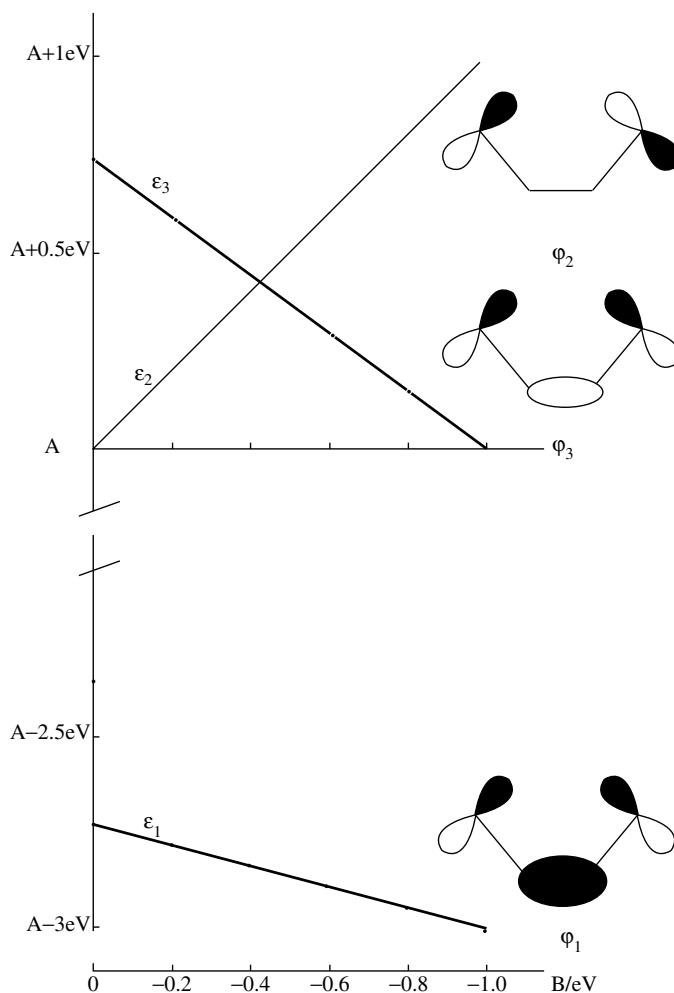


FIGURE 16. Dependence of the eigenvalues \mathcal{E}_1 , \mathcal{E}_2 and \mathcal{E}_3 (see equations 50 and display 51) on the through-space interaction parameter B for fixed $\Gamma = -1$ eV and $\Delta A = -2$ eV. The orbital diagrams are based on the sign convention for the basis orbitals shown in schematic diagram 43

It can be seen from display 51 and Figure 16 that pure through-bond interaction ($B = 0$) places the symmetric orbital φ_3 on top of the antisymmetric orbital φ_2 . This is known as the 'reversed' order. With increasing through-space interaction ($|B| > 0$), the energy gap $\mathcal{E}_3 - \mathcal{E}_2$ between φ_3 and φ_2 first decreases, then becomes zero, leading finally to a 'normal' order of φ_3 below φ_2 . The cross-over occurs when the parameters obey the condition

$$\Gamma = -\sqrt{B(B + \Delta A)} \quad (52)$$

i.e., for the example given above, if $B = -(\sqrt{2} - 1)$ eV = 0.41 eV.

2. A more detailed analysis of through-space and through-bond interactions

The heuristic success of the concepts of through-space and through-bond interactions introduced by Hoffmann²⁰⁰ made it desirable to link it to many electron procedures, at least on the level of semiempirical or *ab initio* SCF calculations. Such a treatment, which had been proposed some time ago²⁰⁴, has been reviewed in detail elsewhere¹⁷³. For this reason we shall only sketch the essential steps involved, using norbornadiene **75** as an example.

Step 1. Norbornadiene C_7H_8 of symmetry C_{2v} contains 8 CH single, 8 CC single and 2 π -bonds, occupied by 36 electrons. (We disregard the inner carbon 1s-orbitals). Accordingly, a SCF treatment yields 18 bonding canonical molecular orbitals (CMOs) φ_j ($j = 1, 2, \dots, 18$) of which 7 belong to the irreducible representation A_1 , 2 to A_2 , 4 to B_1 and 5 to B_2 . We collect these 18 CMOs in a column vector

$$\Phi = (\varphi_1, \varphi_2, \dots, \varphi_j, \dots, \varphi_{18})^T \quad (53)$$

Step 2. The set of CMOs φ_j is now transformed into an equivalent set of 18 localized, orthogonal molecular orbitals (LMOs) λ_j using, e.g., Ruedenberg's localization criterion²⁰⁵. This is achieved by multiplying Φ with an appropriate unitary transformation matrix \mathbb{L} :

$$\mathbb{L}\Phi = \lambda = (\lambda_1, \lambda_2, \dots, \lambda_j, \dots, \lambda_{18})^T \quad (54)$$

This transformation leaves invariant all observable molecular properties of ground-state norbornadiene that can be derived from our SCF model. Note that the two localized orbitals describing a double bond are two 'banana' LMOs $\lambda_{b,up}$ and $\lambda_{b,down}$, as shown on the left of Figure 17. Their normalized, out-of-phase linear combination

$$\pi = (\lambda_{b,up} - \lambda_{b,down})/\sqrt{2} \quad (55)$$

represents the double-bond π -orbital as shown on the right of Figure 17, and their in-phase combination $\sigma = (\lambda_{b,up} + \lambda_{b,down})/\sqrt{2}$ the double-bond σ -orbital.

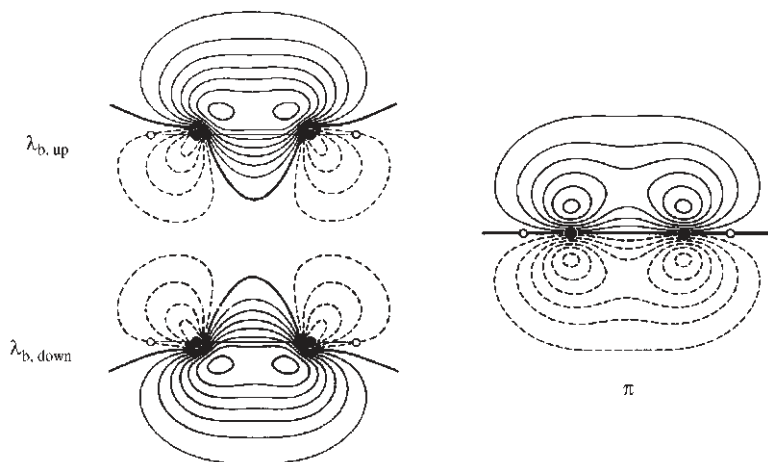


FIGURE 17. On the left is shown the pair of localized banana bond orbitals $\lambda_{b,up}$ and $\lambda_{b,down}$ obtained according to step 2 of Section II.E.2. Their out-of-phase linear combination $\pi = (\lambda_{b,up} - \lambda_{b,down})/\sqrt{2}$ defined in equation 5 yields the π basis orbital shown on the right

Step 3. We first remove the two π -orbitals π_a and π_b (located in positions 2,3 and 5,6 of the norbornadiene skeleton) from the set of LMOs, and form their linear combinations

$$\pi_+ = (\pi_a + \pi_b)/\sqrt{2} \quad \text{and} \quad \pi_- = (\pi_a - \pi_b)/\sqrt{2} \quad (56)$$

The combination π_+ belongs to the irreducible representation A_1 and π_- to B_2 . The remaining 16 σ -orbitals of norbornadiene are now transformed into 16 orthogonal linear combinations of which 6 belong to A_1 , 4 to B_2 , 2 to A_2 and 4 to B_1 . Only the former two sets, belonging to A_1 and B_2 , shown qualitatively in Figure 18, can interact with the target π -orbitals π_+ and π_- depicted on the right, thus serving as relay orbitals for through-bond interaction.

Step 4. This last step consists in calculating first the energies $\mathcal{E}(\pi_+)$ and $\mathcal{E}(\pi_-)$ corresponding to the linear combinations in equation 56. The differences relative to the energy $\mathcal{E}(\pi)$ of a single π -orbital defined according to equation 55 are those due to through-space interaction between π_a and π_b . Finally, the cross terms between π_+ and the set of relay orbitals of the same symmetry behaviour A_1 (top row of Figure 18), and of π_- with the B_2 relay orbitals (bottom row of Figure 18), are calculated. In analogy to our naive treatment discussed in Section II.E.1, this yields the energy shifts due to through-bond interaction.

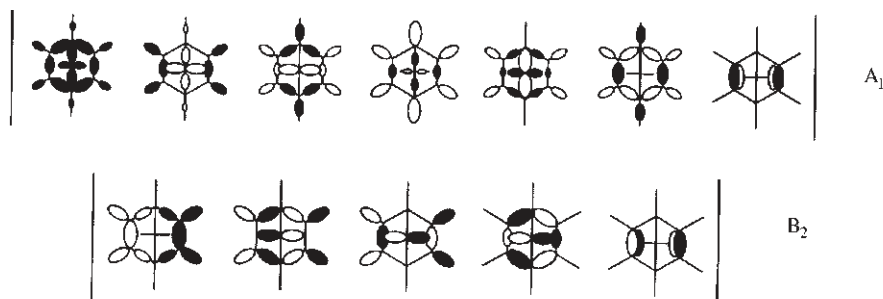
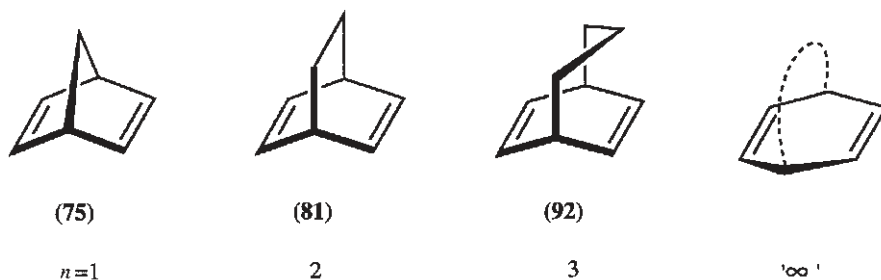


FIGURE 18. The symmetry-adapted, orthogonal linear combinations of the localized σ -orbitals of norbornadiene **75** belonging to the irreducible representations A_1 and B_2 of the point group C_{2v} . The A_1 and B_2 combinations are the relay orbitals for through-bond interaction between π_a and π_b which define, according to equation 56, the orbitals π_+ and π_- .

3. Some special cases of interaction between non-conjugated π -orbitals

The consequences of interactions between non-conjugated π -orbitals and their interpretation in terms of through-bond and through-space interactions have been reviewed extensively, by Hoffmann²⁰¹, Gleiter²⁰² and more recently by Gleiter and Schäfer²⁰⁶. Although some of the PE spectroscopic consequences of these types of interaction have been summarized before^{10,207}, the interested reader is referred to the detailed and authoritative review by Mirjana Eckert-Maksic²⁰⁸ who reports the relevant data and their quantum-chemical interpretation. For this reason we shall only refer briefly to a few typical examples.

a. The interplay of through-bond and through-space interactions in norbornadiene homologues. Bridging the positions 3 and 6 of cyclohexa-1,4-diene **45** by a polymethylene chain, $-(\text{CH}_2)_n-$, yields the bicyclic dienes norbornadiene **75** ($n = 1$), bicyclo[2.2.2]octadiene **81**, bicyclo[3.2.2]nona-6,8-diene **92** etc.



With increasing length n of the polymethylene bridge, the dihedral angle ω between the two C-CH=CH-C moieties increases from $\omega = 110^\circ$ in norbornadiene **75** ($n = 1$), to $\omega = 170^\circ$ to 180° in a hypothetical bicyclo[$n.2.2$]diene with $n \rightarrow \infty$, i.e. to the ω value observed in cyclohexa-1,4-diene **45**. Figure 19 shows the observed π -ionization energies of the bridged dienes as a function of ω (or of n), which correspond to the ejection of an electron from one or other of the two top orbitals φ_2 or φ_3 which are of the type depicted in Figure 16.

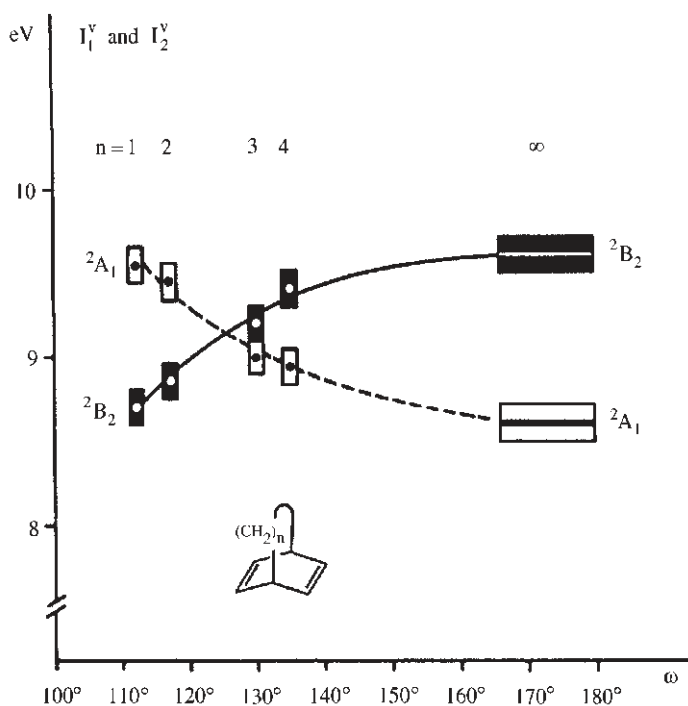


FIGURE 19. Correlation diagram of the π -ionization energies I_1^y and I_2^y of cyclohexa-1,4-diene, bridged in positions 3,6 by a polymethylene chain $-(\text{CH}_2)_n-$, as a function of the dihedral angle ω . The radical cation states ${}^2\tilde{A}_1$ and ${}^2\tilde{B}_2$ are those obtained by electron ejection from the π -orbitals a_1 and b_2 , respectively

With increasing ω the overlap integral $S_{ab} = \langle \pi_a | \pi_b \rangle$ between the two π -orbitals π_a and π_b decreases, and thus their cross term B decreases (see presentation 44 and equation 46). With reference to Figure 16 one sees that for small values of ω , i.e. for large values of B , the through-space interaction dominates, leading to the ‘natural’ order of the antisymmetric linear combination $\varphi_2(B_2)$ above the symmetric combination $\varphi_3(A_1)$. (The symmetry labels refer to an assumed symmetry C_{2v} of the dienes.) According to the Koopmans theorem (equation 11), this means that I_1^V , corresponding to 2B_2 is smaller than I_2^V , corresponding to 2A_1 , as shown in Figure 19. As ω increases and B decreases, through-bond interaction, characterized by the cross term Γ (see presentation 44 and equation 48), overcompensates the through-space interaction, yielding the ‘reversed’ order of $\varphi_3(A_1)$ above $\varphi_2(B_2)$. As can be seen from Figure 19, a cross-over occurs for $\omega \approx 125^\circ$, i.e. at a point where B and Γ satisfy the condition given by equation 52. At this point the orbital energies (equation 50) of $\varphi_2(B_2)$ and $\varphi_3(A_1)$ are

$$\mathcal{E}_2 = \mathcal{E}_3 = A + \Delta A/2 + \frac{1}{2}\sqrt{(\Delta A)^2 + 4\Gamma^2} \quad (57)$$

These orbital energies are equal to the orbital energy \mathcal{E}_π of a single π -orbital, say π_a , interacting with the σ -orbitals of the monoene which corresponds to the diene in question. \mathcal{E}_π is the result of solving the 2×2 determinant obtained by striking out the first row and first column of the determinant given by equation 49, i.e. by deleting the node b from the graph in presentation 44. It follows that the ionization energy $I_{\text{crossing}} = 9.1 \text{ eV} = -\mathcal{E}_\pi$ defined by the cross-over in Figure 19 should correspond to the π -ionization energy of bicyclo[2.2.2]octene or bicyclo[3.2.2]non-6-ene, i.e. the monoenes that correspond to the dienes **81** and **92** which bracket the cross-over. That this is indeed the case can be seen from Figure 15.

b. Brief comment on symmetry assignments using a correlation technique. The use of a simple independent electron model—coached in terms of through-space and through-bond interactions—can yield safe assignments if applied to a homologue set of molecules, as was shown above for the two top π -orbitals of bicyclic dienes, a result fully supported by more sophisticated calculations. The question is, whether such an assignment can be obtained if only a single diene is available instead of a homologue series. Using norbornadiene **75** as an example, the relative sequence of its π -orbitals $\varphi_2(B_2)$ and $\varphi_3(A_1)$ can be assessed through a simple correlation technique²⁰⁹ by letting them interact with a third localized π -orbital of known symmetry behaviour. In the instance of **75** which contains the symmetry equivalent orbitals π_a and π_b as shown at top of Figure 20, we include a third π -orbital π_c by adding an exocyclic double bond in position 7 of **75** to yield, e.g., 7-methylidenenorbornadiene **196**¹³¹ or 7-isopropylidenenorbornadiene **206**^{26,77}. The symmetry behaviour of π_c is known to be B_2 under C_{2v} , i.e. antisymmetric with respect to rotation about the twofold axis or with reflection through the x, z plane. This means that π_c can only interact with the antisymmetric π -orbital $b_2 \equiv \varphi_2(B_2)$ containing the linear combination $(\pi_a - \pi_b)/\sqrt{2}$, and not with the symmetric π -orbital $a_1 \equiv \varphi_3(A_1)$ containing $(\pi_a + \pi_b)/\sqrt{2}$. Disregarding small inductive shifts we expect therefore that \mathcal{E}_3 will remain the same going from **75** to **196** or **206**, whereas \mathcal{E}_2 should experience a significant change. As can be seen from Figure 20, the observed shifts of the π -bands are only compatible with the above deduction if the orbital energy \mathcal{E}_2 of the π -orbital $b_2 \equiv \varphi_2(B_2)$ lies above \mathcal{E}_3 of $a_1 \equiv \varphi_3(A_1)$. This ‘natural’ order is in perfect agreement with what we had derived from the correlation diagram of Figure 19 presented in the previous section.

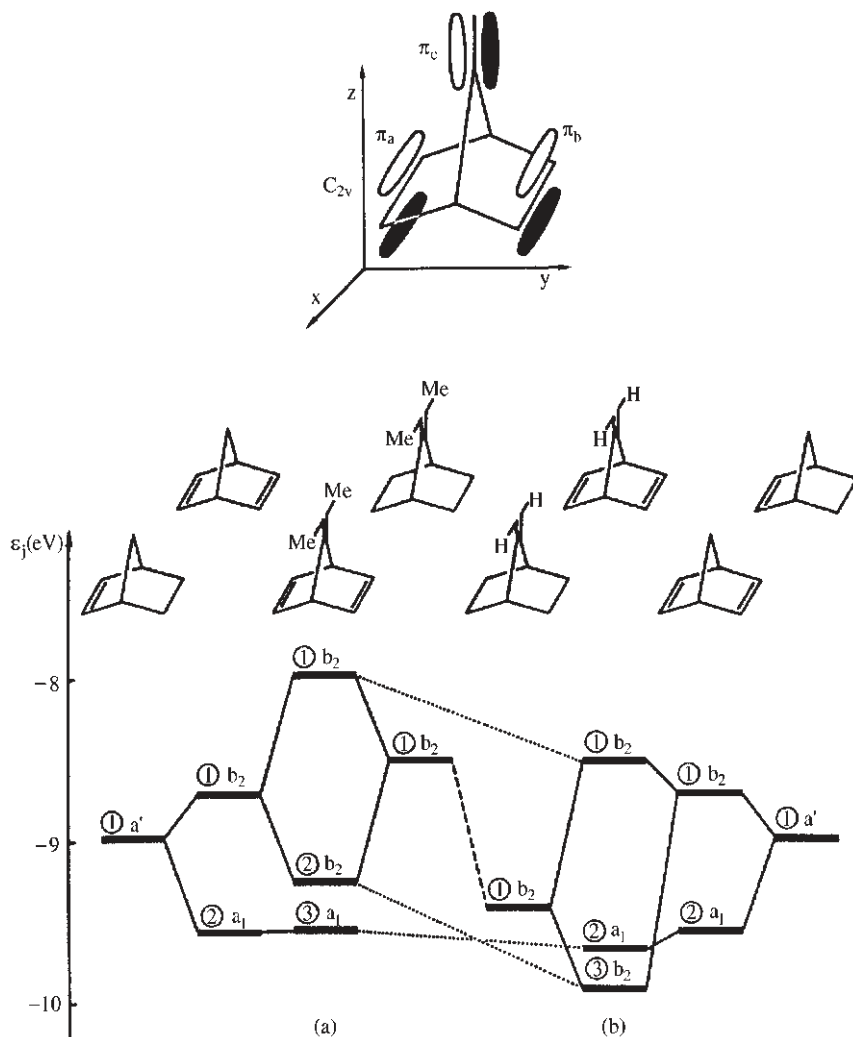
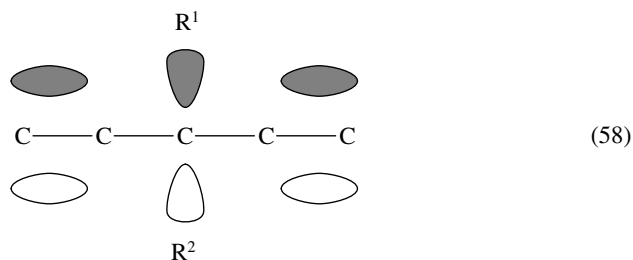
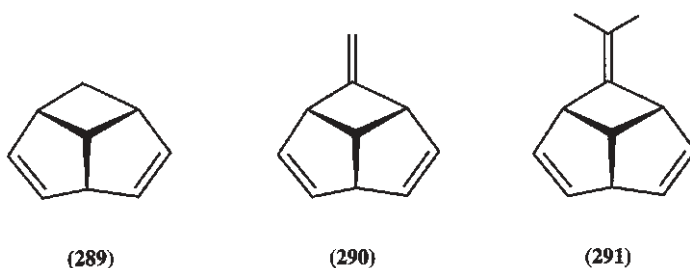


FIGURE 20. Top: Definition of the phase relationship of the three localized basis π -orbitals of a norbornadiene molecule with an exocyclic double bond in position 7. Bottom: Correlation diagram of the 'experimental' orbital energies $\mathcal{E}_j = -I_j^v$ of norbornadiene **75**, 7-methylidenenorbornadiene **196** and 7-isopropylidenenorbornadiene **206**, with those of the corresponding monoenes

c. Homoconjugation. A special case of interaction, known as 'homoconjugation', occurs between the π -orbitals of two double bonds separated by a methylene group, $-\text{CH}_2-$, or a $-\text{CR}^1\text{R}^2-$ group. As before, this situation can be discussed in terms of through-space and through-bond interactions, the special feature being that the 'relay orbital' for the latter type of interaction is now the out-of-phase combination of the two localized CH σ -orbitals of the methylene group, or of the two CC σ -orbitals linking the alkyl groups R^1 and R^2 to the central C atom, as shown in diagram 58.



A typical example of cyclic homoconjugation is provided by (*Z, Z, Z*)-cyclonona-1,4,7-triene **189**, which is the prototype of a ‘homoaromatic’ molecule, a term introduced by Winstein²¹⁰. Its spectrum^{26,49} is shown in Figure 21, together with a diagram illustrating the relative contributions of through-space and through-bond interaction. The double band at 8.8 and 9.0 eV in the PE spectrum of **189** corresponds to the ejection of an electron from the degenerate frontier orbital labelled *e* in Figure 21, yielding the corresponding radical cation in its ²*E* ground state. Because of this degeneracy the cation undergoes a Jahn–Teller distortion, which is the cause for the observed double-humped shape of the Franck–Condon envelope. The second feature at 9.8 eV is due to electron ejection from the totally symmetric orbital labelled *a*. The observed splitting of *ca* 1 eV has, unfortunately, been sometimes quoted as an indication of the ‘homoaromaticity’ of **189**. However, the interactions manifest in the PE spectrum have no noticeable effect on the ground-state properties of the molecule. A similar observation concerns triquinacene **213**, the PE spectrum of which^{136,211} shows again sizeable interactions between the three homoconjugated double-bond π -orbitals, but whose ground-state properties, as shown by Dewar and Holder²¹², present no significant effects which could be attributed to ‘homoaromaticity’. Finally, the PE spectroscopic investigation of nortriquinacene **289**, methylidenenortriquinacene **290** and isopropylidenenortriquinacene **291** by Houk and his coworkers²¹³ strongly supports the conclusion that the PE spectroscopic observation of homoconjugative interactions in molecules of this type should not be interpreted as evidence of ‘homoaromaticity’.



d. Spiroconjugation. We conclude this short list of examples with [4.4]spironatetraene **247**⁶³ — a hydrocarbon of D_{2d} symmetry — which is the paradigm of a molecule exhibiting ‘spiroconjugation’. Although the interaction between the four localized double-bond π -orbitals π_a , π_b , π_c and π_d across the spiro-centre 5 (see top of Figure 22) can be again discussed in terms of through-bond and through-space interaction, the feature of interest is the important role played by the high symmetry of the system. Indeed, the four π -orbitals π_a , π_b , π_c and π_d yield the symmetry-adapted, normalized linear combinations 59. These

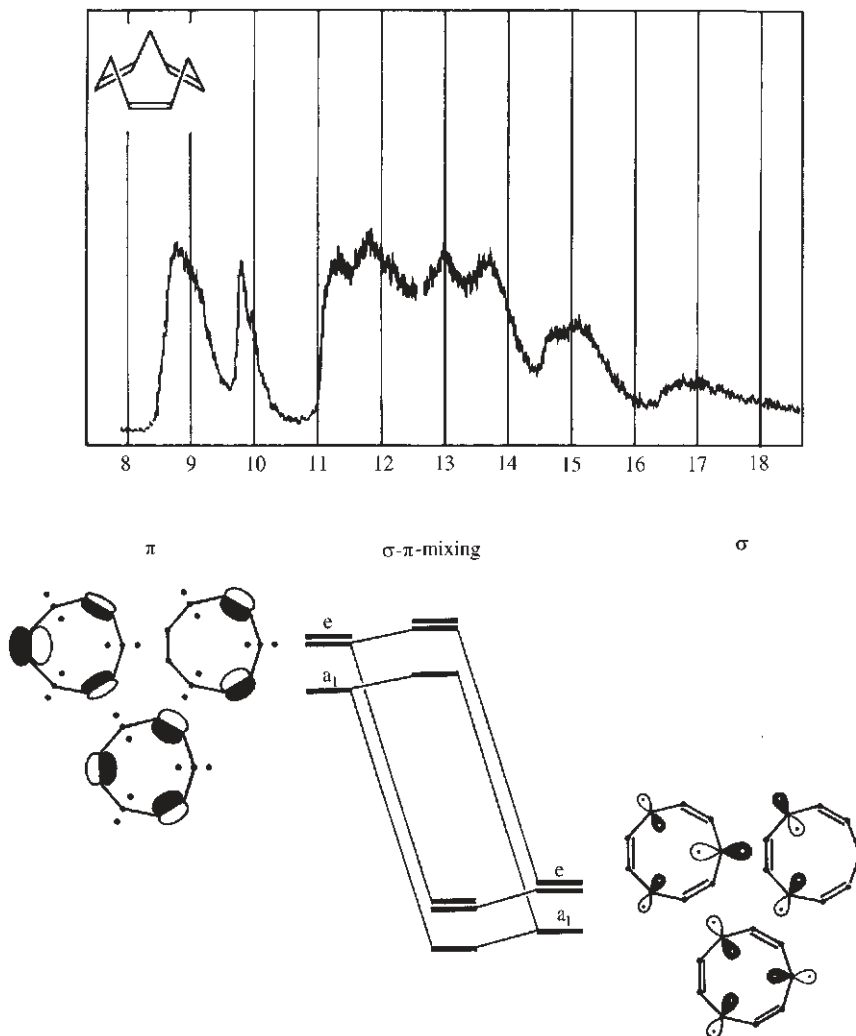


FIGURE 21. Top: Photoelectron spectrum of (Z,Z,Z)-cyclonona-1,4,7-triene **189**. Bottom: Diagram showing the homoconjugative σ/π -interaction between the symmetry-adapted linear combinations of the π - and of the methylene σ -orbitals

$$\begin{aligned}
 1a_2(\pi) &= (\pi_a - \pi_b - \pi_c + \pi_d)/2 \\
 1b_1(\pi) &= (\pi_a - \pi_b + \pi_c - \pi_d)/2 \\
 7e(\pi) &\begin{cases} = (\pi_a + \pi_b + \pi_c + \pi_d)/2 \\ = (\pi_a + \pi_b - \pi_c - \pi_d)/2 \end{cases} \quad (59)
 \end{aligned}$$

combinations, depicted in Figure 22, which determine the symmetry behaviour of the molecular orbitals to which they contribute. The resulting orbital energy diagram, where

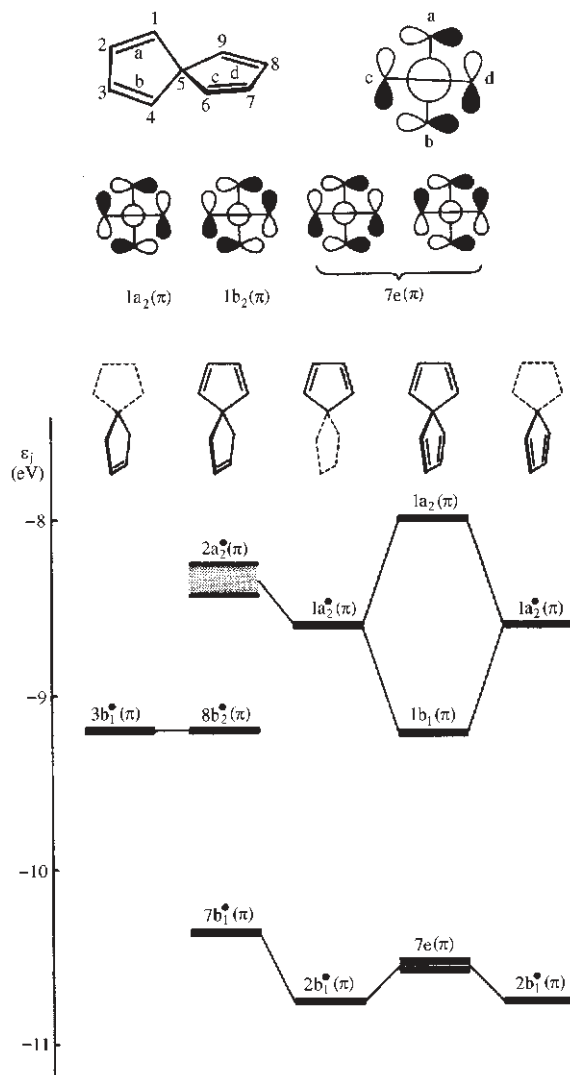


FIGURE 22. Top: Labels of the four localized basis π -orbitals of [4.4]spirononatetraene **247** and Newman projection defining their relative phases. Middle: Newman projections of the four linear combinations $1a_2(\pi)$, $1b_1(\pi)$ and $7e(\pi)$, defined in equation 59. Bottom: Correlation diagram showing the splitting due to spiroconjugation between the butadiene moieties in **247**

the \mathcal{E}_j -values are the ‘observed’ ones assuming the validity of the Koopmans theorem ‘in reverse’, i.e. $-I_j^v = \mathcal{E}_j$, is shown at the bottom of Figure 22.

Contrary to what is suggested by an independent electron treatment, the energy gap $\Delta I^v = I_2^v - I_1^v$ between the ionization energies corresponding to the first two bands in the PE spectrum of a molecule is not equal to the difference ΔE between the first two

electronic transitions of the neutral molecule. As has been pointed out by Haselbach and Schmelzer²¹⁴, the two quantities are related by the equation.

$$\Delta E = \Delta I^V - (J_{2,-1} - J_{1,-1}) - 2(K_{1,-1} - K_{2,-1}) \quad (60)$$

where $J_{i,j}$ and $K_{i,j}$ are the coulomb and exchange integrals, respectively, between the molecular orbitals φ_i and φ_j involved in the ionization process and in the electronic transitions. The remarkable feature of the above example is that the high symmetry conditions prevailing in **247** lead to the result that the difference between the (finite) coulomb integrals $J_{i,j}$ in equation 60 becomes vanishingly small and that the individual exchange integrals $K_{i,j}$ are practically zero. As a result the molecule **247** is one of the rare examples where the naive expectation $\Delta E = \Delta I^V$ suggested by an independent electron treatment turns out to be true⁶³.

III. EXCITED STATES OF POLYENE RADICAL CATIONS BY OTHER METHODS

A. Introduction

For many years, investigations on the electronic structure of organic radical cations in general, and of polyenes in particular, were dominated by PE spectroscopy which represented by far the most copious source of data on this subject. Consequently, attention was focussed mainly on those excited states of radical ions which can be formed by direct photoionization. However, promotion of electrons into *virtual* MOs of radical cations is also possible, but as the corresponding excited states cannot be attained by a one-photon process from the neutral molecule they do not manifest themselves in PE spectra. On the other hand, they can be reached by electronic excitation of the radical cations, provided that the corresponding transitions are allowed by electric-dipole selection rules. As will be shown in Section III.C, the description of such states requires an extension of the simple models used in Section II, but before going into this, we would like to discuss them in a qualitative way and give a brief account of experimental techniques used to study them.

Optical absorption spectroscopy of organic radical cations was pioneered by Hoijtink and coworkers²¹⁵ and others²¹⁶ before the advent of PE spectroscopy, but it was limited for a long time to aromatic amines, polycyclic aromatic hydrocarbons and similar compounds whose radical cations could be generated under stable conditions by chemical oxidation²¹⁷. It was observed that many colourless neutral compounds give rise to intensely coloured radical cations which indicates that excited states of these reactive species lie generally at much lower energy than those of the neutral parent molecules (the most famous example is perhaps Wurster's blue, the radical cation of the colourless tetramethyl-*p*-phenylenediamine).

This agrees with the observation that the energy differences between the first and one of the following bands in the PE spectra often lie in the visible energy range. As pointed out above, the optical spectra of radical ions should show additional bands which can be assigned to excitations into virtual MOs. In many radical cations with planar π -systems, the most prominent band in the electronic absorption (EA) spectrum is essentially due to a HOMO \rightarrow LUMO excitation (we will examine below to what extent this is also true for polyene radical cations). Interestingly, even this excitation occurs at much lower energy than in the corresponding neutrals. In a simple MO picture, this may be viewed as being due to the rise of the HOMO on removal of an electron.

The latter feature leads to the expectation that, in cases where the HOMO \rightarrow LUMO excitation in the neutral occurs in the visible, the corresponding state of the radical cation should turn out to be the lowest one. There are indeed several cases where this was

found to be true, most prominently in the cross-conjugated polyene radical cation of *o*-quinodimethane and in some of its derivatives. As the first excited state is usually the photochemically active one, it is important to know its character.

An interesting aspect of this alternative way of looking at the electronic structure of radical cations concerns the dependence of the excited state energies on *changes in structure*: Whereas the maxima of PE bands correspond to ionic state energies at the *neutral* equilibrium geometry, those of optical bands measure the energies of excited states at the *cation* equilibrium geometries. The occurrence of shifts between the two cases is most easily visualized by juxtaposing PE and EA spectra on the same energy scale, matching the energy origin of the latter with I_1^+ (or, if this cannot be discerned, with the onset) of the first PE band, assuming that this represents the energy of the relaxed radical cation.

As every chemical species undergoes *some* change of geometry upon ionization, one would expect that this always entails shifts in the excited state energies. However, in many cases where such comparisons were made (for example in aromatic hydrocarbons) these shifts were found to be insignificant, presumably because the changes in bond lengths upon ionization are too small, due to the stiffness of the σ -frame. However, the same appears to be true in polyene radical cations where significant bond-length changes take place upon ionization. In this case, as will be discussed below, the absence of shifts is due to a cancellation of effects. A group of compounds where a comparison of the PE spectrum of M and the EA spectrum of $M^{+\bullet}$ is particularly interesting are non-conjugated π -systems interacting through-space and/or through-bond, such as those discussed in Section II.E.

Finally, before turning to a brief review of methodological and theoretical aspects, we mention that one of the distinguishing features of planar conjugated polyene radical cations (cf Section II.D) is that their EA spectra reveal a breakdown of the single-configuration picture for ionic excited states which had been used so successfully in interpreting their PE spectra (cf. Section II).

B. Experimental Methods

1. Gas-phase experiments

a. Photodissociation spectroscopy. The first studies of the electronic structure of radical cations which cannot be formed under stable conditions in solution used a technique which takes advantage of the fact that *dissociation* is the predominant deactivation process of electronically excited radical cations in the gas phase. Thus it is possible to monitor the disappearance of a radical cation in an ion beam or an ICR trap (or the appearance of certain fragment ions) as a function of the exciting wavelength. As the quantum yield of fragmentation often shows little dependence on the excitation energy above threshold, the so-called *photodissociation* (PD) *spectra* obtained in this way are usually very similar to the corresponding optical absorption spectra.

This technique, whose analytical application was pioneered by Dunbar and colleagues²¹⁸, was mainly used to distinguish isomeric radical cations in the gas phase. It was also used for the investigation of many polyenes, and the efficiency of its high-resolution variant (using a dye laser as excitation source) was demonstrated on the example of hexatriene radical cation (Figure 23). From a spectroscopic point of view, its principal advantage is the possibility to obtain full UV/VIS spectra of radical cations in the absence of solvent. As an example, we show the PD spectrum of hexatriene radical cation²¹⁹ and an expanded high-resolution scan of the first band²²⁰.

b. Ion emission spectroscopy. Fluorescence of radical ions is much less common than that of neutral molecules. This is mainly due to the fact that the first excited states of

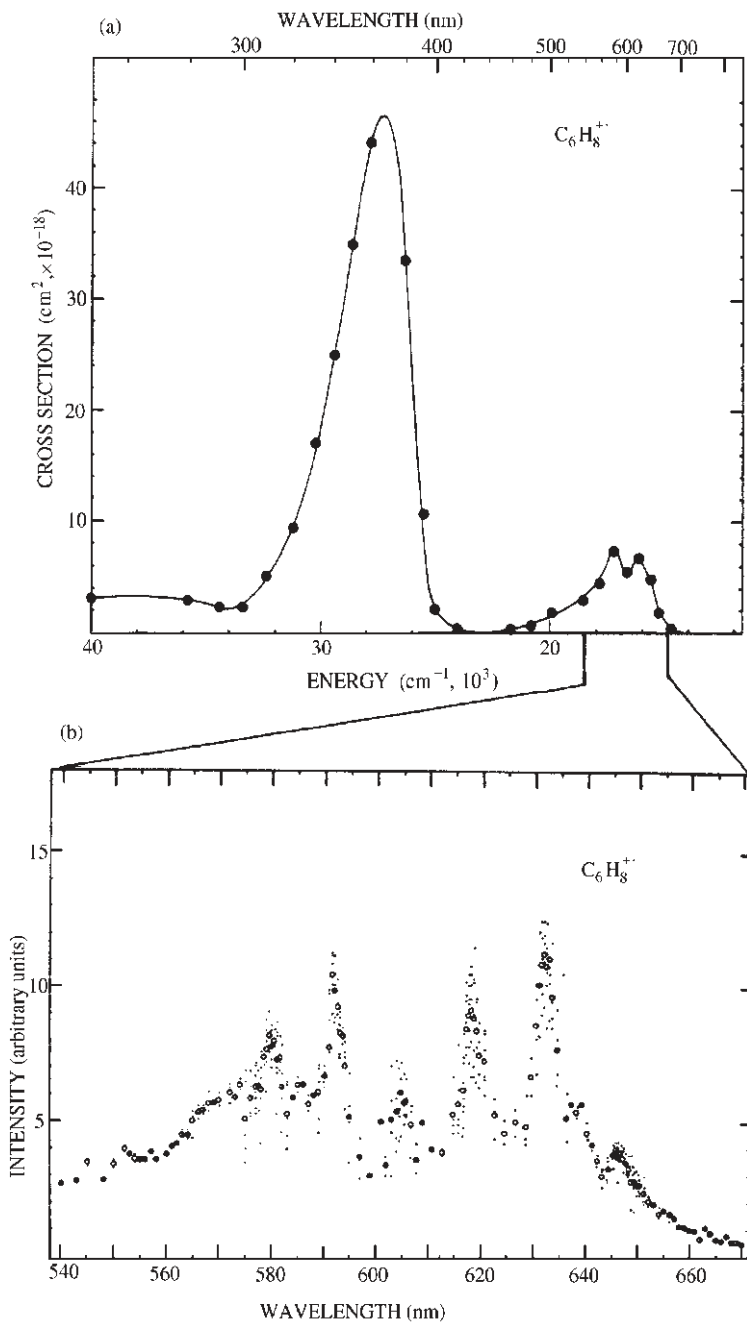


FIGURE 23. Gas-phase photodissociation (PD) spectra of the radical cation of hexatriene (a) at low resolution, (b) expanded scan of the first absorption band at high resolution^{219,220}

radical ions are usually at much lower energy, often in the NIR region, so that radiationless internal conversion to the ground state frequently wins out by virtue of the energy-gap law. Most emissive radical cations are either small (oligo)acetylenes and their derivatives, or fluorinated benzene derivatives. Notable exceptions are the radical cations of hexatriene and octatetraene, and therefore a brief discussion of the techniques used to study emission spectra of radical cations seems warranted in the present context²²¹.

Emission spectra of radical cations are obtained by vacuum UV ionization and subsequent laser excitation in noble-gas matrices (see below), or by electron-impact ionization of a beam of neutral parent molecules at energies above the first ionic excited state. After internal conversion to the first excited state, emission may compete more or less successfully with radiationless deactivation. If the experiment is carried out on a supersonic molecular beam one obtains highly resolved emission spectra which, in the case of small molecules, may contain sufficient information to allow a determination of the molecular structure.

In order to record *excitation spectra*, the radical ions must first be thermalized to the electronic ground state, which happens automatically if they are created in condensed phase (e.g. in noble-gas matrices, see below). In the gas-phase experiments where ionization is effected by collision with excited argon atoms (Penning ionization), the unexcited argon atoms serve as a heat bath which may even be cooled to 77 K if desired. After thermalization, excitation spectra may be obtained by laser-induced fluorescence.

Figure 24 shows as an example the gas-phase emission and excitation spectra of the radical cation of dimethyldiacetylene from the work of Maier and coworkers²²² and Miller and Bondybey²²³ who have pioneered these methods. For direct comparison, the bottom part of Figure 24 represents the same spectra taken in neon matrices²²³ (see below).

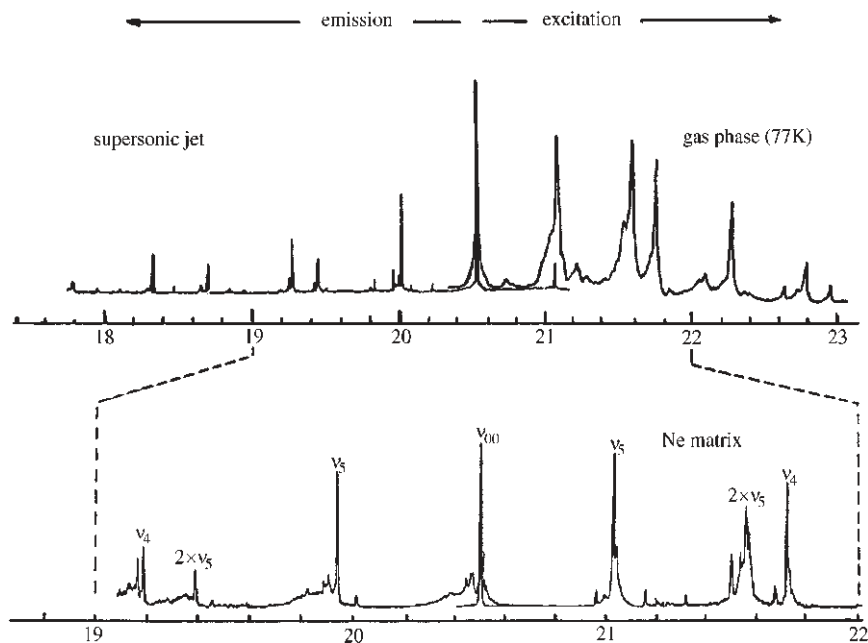


FIGURE 24. Emission and excitation spectra of $\text{H}_3\text{C}-\text{C}\equiv\text{C}-\text{C}\equiv\text{C}-\text{CH}_3^+$ in the gas phase^{222,223} (top) and in a neon matrix²²³ (bottom)

2. Condensed-phase experiments

a. Solution studies. Optical and ESR spectra of radical cations were first obtained on samples subjected to chemical ionization in solution²¹⁵. However, these methods were never applied to dienes and polyenes because their radical cations are too reactive to be observed under such conditions.

Radical cations can also be produced in solution by *photoinduced electron transfer* (PET) in polar solvents. Although this method is widely used to study the processes involved in the formation and decay of ion pairs²²⁴, free radical cations appear only as transients in such experiments.

Finally, radical cations can be generated in solution by different types of *pulse radiolysis*²²⁵. Like PET, this is inherently a method for transient spectroscopic observations, but it has proved to be invaluable in investigations of dimer cations, e.g. of polyenes, which form spontaneously upon diffusion of radical cations in the presence of an excess of the neutral parent compound, but a discussion of the electronic structure of such species is beyond the scope of this review. Pulse radiolysis is of interest in the present context because it allows the observation of large carotenoid radical cations which are difficult to create in solid-state or gas-phase experiments

b. Frozen glasses. Systematic investigations of optical spectra of polyene radical cations in condensed phase had to await the advent of methods allowing their production under conditions which prevent decay through charge recombination or other bimolecular processes. Such methods were pioneered in the 1960s by Hamill and Shida²²⁶ who found that radical ions are formed quite cleanly upon exposure of frozen solutions to ⁶⁰Co γ -irradiation (1.17 and 1.33 MeV).

Which species are formed in such experiments depends on the solvent, i.e. its capacity to trap either the holes or the electrons which are created in the primary radiolytic step (see Figure 25). Thus, holes are scavenged efficiently by methyltetrahydrofuran, presumably through proton transfer, whereas electrons are trapped by alkyl chlorides which dissociate into alkyl radicals and chloride anions (to the extent that this is possible in rigid matrices). Subsequently, the holes (electrons) travel through the solvent by resonant charge transfer until they encounter a solute of lower ionization energy (higher electron affinity), thus creating radical cations (radical anions) at a distant site from the carrier of the opposite charge. It is important to realize that ionization of the solute occurs actually *by charge transfer from the solvent* and not through interaction with the highly energetic γ -rays to which hydrocarbons are essentially transparent.

For the investigation of radical cations, Shida replaced the initially used solvent CCl₄ by a mixture of *n*-butyl chloride and isopentane which forms a transparent glass upon freezing. Later, Grimison and Simpson^{227a} found that a mixture of two freons, CFC₃ and CF₂BrCF₂Br, which had originally been proposed for low-temperature studies by Sandorfy^{227b} because of its glass-forming quality, represented an even better medium, due to the absence of C–H vibrational overtones in the NIR region. This proved to be very important, especially in studies of dimer cations which show characteristic absorptions in this range. In 1979 it was found—somewhat surprisingly—that it was also possible to record reasonably well resolved ESR spectra of radical cations in certain freons²²⁸. This led to many important investigations of radical cations which cannot be generated under stable conditions by chemical oxidation²²⁹.

The first systematic studies of *polyene radical cations* were carried out by Shida and coworkers²³⁰ using the above methods. In this connection an important feature of these species was discovered, namely that they exist in the form of multiple rotamers which do not interconvert easily due to the partial double-bond character which all polyene C–C bonds attain upon ionization (see below).

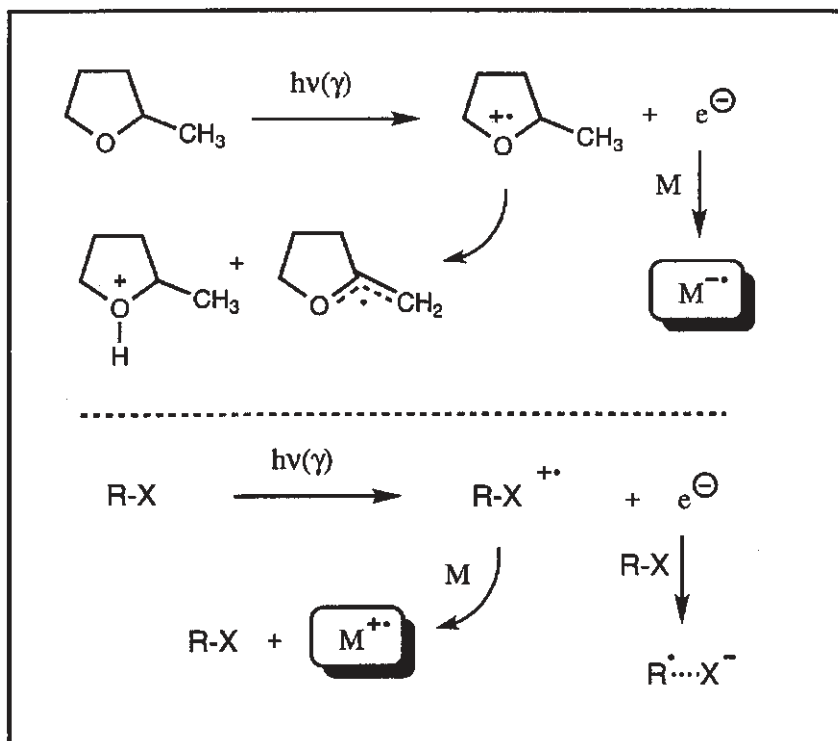


FIGURE 25. Mechanism of formation of radical anions $M^{\bullet-}$ and cations $M^{\bullet+}$ in frozen glasses of methyltetrahydrofuran (top) and alkyl chlorides (bottom), respectively

c. Matrix isolation experiments. The methods mentioned above suffer from several disadvantages: (a) solutes tend to form aggregates upon cooling the solution, (b) the halogenated solvents may undergo chemical interactions with some of the more reactive radical cations and (c) these solvents are not transparent below 300 nm and in the IR region, especially after γ -irradiation. Therefore, attempts were made in several laboratories to find suitable conditions for the creation of radical ions in solid *noble gases*, applying techniques of *matrix isolation* elaborated in the 1950s by Pimentel and others²³¹.

First successes were reported by Andrews and coworkers, who tried various methods to produce radical ions in the gas phase for subsequent trapping at 10 K. A particularly fruitful strategy involved excitation of the argon used for matrix isolation in a microwave discharge²³². Although it was never determined unambiguously how ionization of the substrate occurred under these conditions (Penning ionization or photolysis through light emitted by the excited argon atoms), the method proved quite generally applicable and was used in many studies of radical cations, in particular those of polyenes. The main disadvantage of the method is that it does not permit the recording of difference spectra which would yield the spectra of the radical cations unperturbed by those of the parent neutral.

At the same time, studies of *emission spectra* of matrix isolated radical cations were undertaken by Miller and Bondybej at Bell Laboratories²³³ and by Maier and coworkers

in Basel²³⁴. In these studies, the radical cations were created by FUV photolysis of the neutral molecules isolated in neon matrices, without adding an electron scavenger (see below). The yield of radical cations is quite low and side products are unavoidably formed under these conditions, but through choice of suitable excitation wavelengths and by virtue of the zero-background nature of the experiment, very clean and extremely well resolved spectra of many emissive radical cations were reported (see e.g. Figure 24).

In the early 1980s, one of the authors of this chapter began to study argon matrix isolation of radical cations²³⁵ by applying the radiolytic techniques elaborated by Hamill and Shida. A central factor was the addition of an *electron scavenger* to the matrix which was expected to increase the yield of radical cations and the selectivity of the method. For practical reasons, X-rays replaced γ -rays as a radiolytic source and argon was chosen as a matrix material because of its substantial cross section for interaction with keV photons (which presumably effect resonant core ionization of Ar). Due to the temporal separation of the process of matrix isolation of the neutral molecules and their ionization, it was possible to obtain difference spectra which show exclusively the bands of the radical cations.

This method proved quite generally applicable, in particular for the study of the electronic structure of several polyene radical cations and, more recently, for investigations of

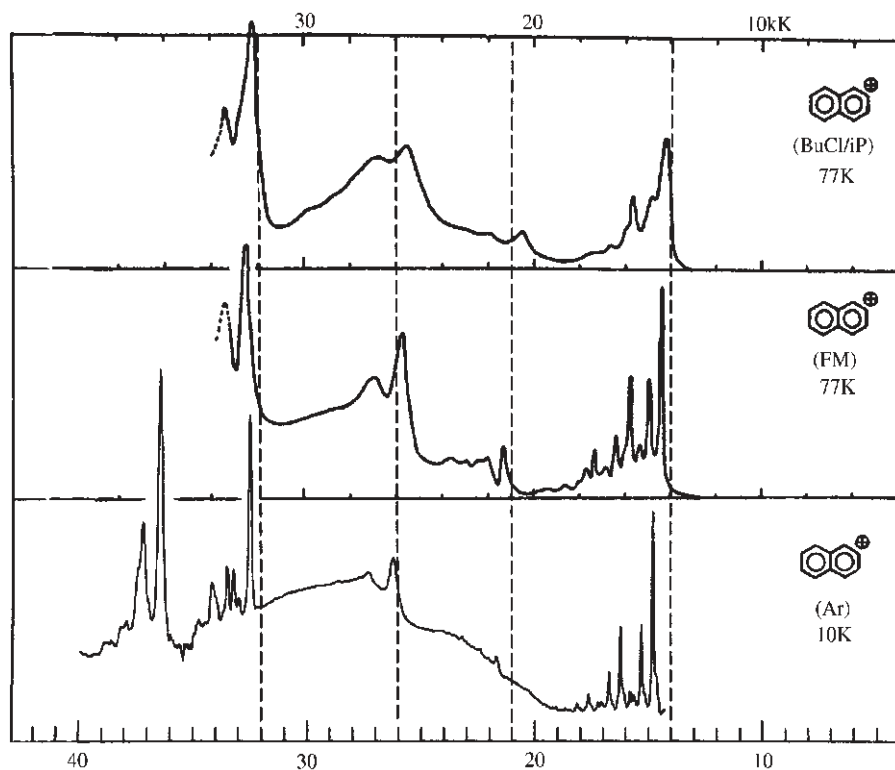


FIGURE 26. EA spectra of the radical cation of naphthalene in different media. Note the increase in resolution and optical range in argon matrices

their vibrational structure by IR spectroscopy. The main disadvantage is that the charge transfer from ionized argon is exothermic by several eV and that the excess energy imparted to the radical cations is only slowly dissipated by the argon lattice. Therefore, primary cations on occasion undergo partial rearrangement, sometimes to the extent that they are no longer observable. Unfortunately, attempts to circumvent this problem by addition of 'hole moderators' (matrix components of lower ionization energy than argon) or 'energy dissipators' (species capable of taking up excess vibrational energy) have so far met with limited success.

As an example of the application of the solid-state methods described above, we show the spectra of the naphthalene radical cation in different media²³⁶ (Figure 26). Note the increase in spectroscopic resolution and the extension of the range of observation into the UV when using argon matrices.

Table 3 lists all polyenes whose radical cations have been investigated by one or other of the above-described techniques and some of the structures listed are shown below the table. Note that some nonconjugated dienes do not retain their structure upon ionization [e.g. semibullvalene **104** (equation 61) or the cyclopentadiene dimers **126** and **294** (equation 62)] but break a bond to form a bisallylic radical cation, a rather common tendency of radical cations that have this possibility.

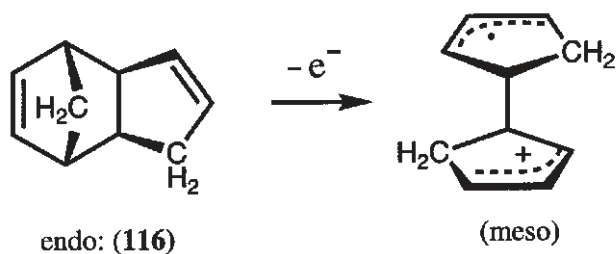
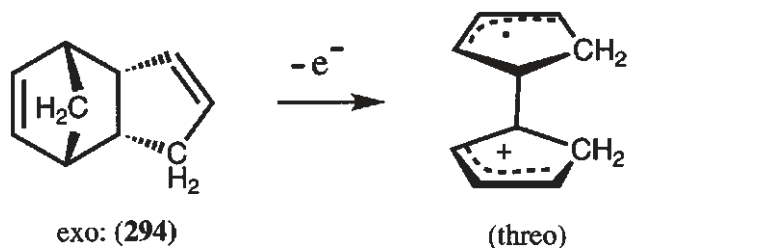
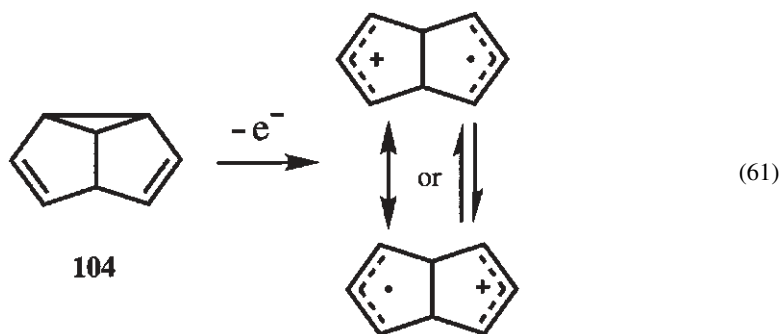


TABLE 3. Electronic spectra of dienes and polyenes C_nH_m
 $m = 2(n - d - r + 1)$ where d = number of double bonds and r = number of rings

r	n	m	No.	Name	References (Method) ^a	
Dienes: $d = 2$						
0	3	4	1	Allene	237 (PD)	
			2	1,3-Butadiene	238 (PD) 239, 240 (AS)	
	5	8	3	(3E)-1,3-Pentadiene (1-Methylbutadiene)	240 (AS), 243 (PD)	
			5	2-Methylbutadiene (Isoprene)	240 (AS)	
	6	10	10	Hexa-2,4-diene	24 (PD)	
			11	2,3-Dimethylbuta-1,3-diene	240 (AS)	
			16	(3E)-Hexa-1,3-diene	233, 238, 244 (PD)	
			292	(2E,4E)-Hepta-2,4-diene	245 (PD)	
	7	12	24	(3E)-Octa-1,3-diene	245 (PD)	
	8	14	25	2,5-Dimethylhexa-2,4-diene	238 (PD), 240 (AS)	
	12	22	293	1,4-Di- <i>t</i> -butylbuta-1,3-diene	246 (AS)	
	1	5	6	37	Cyclopentadiene	240 (AS), 247 (AS, AM)
				44	Cyclohexa-1,3-diene	245, 248 (PD) 249 (AS)
		7	10	45	Cyclohexa-1,4-diene	250, 251 (AM)
49				Cyclohepta-1,3-diene	240, 249 (AS)	
57				Cycloocta-1,3-diene	249 (AS), 252 (PD) 253 (AM)	
2	6	5	71	Dewar benzene (Bicyclo[2.2.0]hexa-2,5-diene)	238, 245 (PD), 250 (AM)	
			75	Norborendiene (Bicyclo[2.2.1]hepta-2,5-diene)	254 (AS)	
			79	Bicyclo[4.2.0]octa-2,4-diene	252 (PD) 255 (AM)	
3	8	8	81	Bicyclo[2.2.2]octadiene	256 (AS)	
			104	Semibullvalene	257 (AS)	
3	10	12	116	<i>endo</i> -Dicyclopentadiene	258 (AS)	
			294	<i>exo</i> -Dicyclopentadiene	259, 260 (AS)	
			139	<i>endo</i> , <i>endo</i> -1,4,4a,5,8,8a-Hexahydro-1,4:5,8-dimethanonaphthalene	261, 262 (AS), 263, 264 (AM)	
4	12	14	139	<i>endo</i> , <i>endo</i> -1,4,4a,5,8,8a-Hexahydro-1,4:5,8-dimethanonaphthalene	261, 262 (AS)	
10	20	20	156	Pagodiene	265, 266 (AS, AM)	
12	20	16	296	Dodecahedradiene	266 (AM)	
Trienes: $d = 3$						
0	6	8	161	(3E)-Hexa-1,3,5-triene	240 (AS), 241, 250 (AM)	
			162	(3Z)-Hexa-1,3,5-triene	267 (PD), 268 (EG)	
			297	1,6-Di- <i>t</i> -butylhexa-1,3,5-triene	269 (EM)	
			270	[3]Radialene	249 (AS), 268 (EG)	
1	6	6	298	5-Methylidenecyclohexa-1,3-diene	270 (AM)	
			173	[3]Radialene	246 (AS)	
			298	5-Methylidenecyclohexa-1,3-diene	271 (AS)	
1	7	8	174	3,4-Dimethylidenecyclobutene	272 (PD), 254, 273 (AM)	
			179	Cyclohepta-1,3,5-triene	274 (PD)	
					240 (AS), 252 (PD), 253, 255 (AM)	

TABLE 3. (continued)

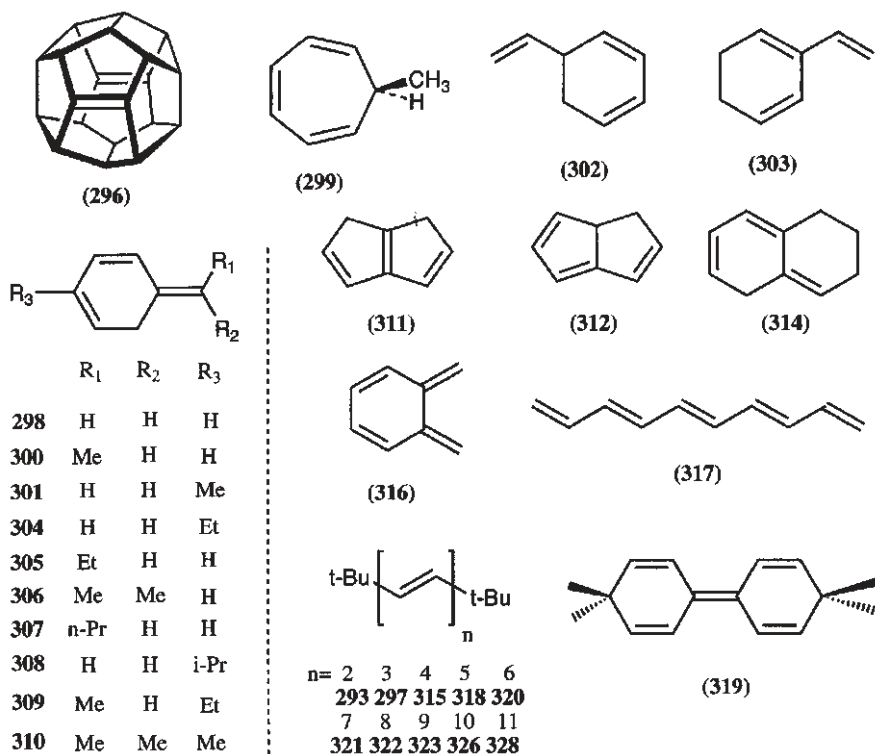
<i>r</i>	<i>n</i>	<i>m</i>	No.	Name	References (Method) ^a
Trienes: $d = 3$					
	8	10	184	Cycloocta-1,3,5-triene	240, 257 (AS), 263, 264, 275 (AM)
			299	7-Methylcyclohepta-1,3,5-triene	276 (AM)
			300	(<i>E/Z</i>)-5-Ethylidenecyclohexa-1,3-diene	276, 277 (AM)
			301	2-Methyl-5-methylidenecyclohexa-1,3-diene	276 (AM)
			302	5-Vinylcyclohexa-1,3-diene	258 (AS)
			303	2-Vinylcyclohexa-1,3-diene	279 (AS)
	9	12	304	2-Ethyl-5-methylidenecyclohexa-1,3-diene	277 (AM)
			305	5- <i>n</i> -Propylidenecyclohexa-1,3-diene	277 (AM)
			306	5-Isopropylidenecyclohexa-1,3-diene	277 (AM)
	10	14	307	5- <i>n</i> -Butylidenecyclohexa-1,3-diene	277 (AM)
			308	2-Isopropyl-5-methylidenecyclohexa-1,3-diene	277 (AM)
			309	2-Ethyl-5-ethylidenecyclohexa-1,3-diene	277 (AM)
			310	2-Methyl-5-isopropylidenecyclohexa-1,3-diene	277 (AM)
2	8	8	197	Barrelene	273 (AS)
			198	1,2-Dihydropentalene	278 (AS,AM)
			199	1,4-Dihydropentalene	278 (AS,AM)
			200	1,5-Dihydropentalene	278 (AS,AM)
			311	1,6-Dihydropentalene	278 (AS,AM)
			312	1,6 α -Dihydropentalene	278 (AS,AM)
	10	10	313	Bicyclo[6.2.0]deca-2,4,6-triene	285 (AM)
	10	12	314	1,2,3,5-Tetrahydronaphthalene	277 (AM)
Tetraenes: $d = 4$					
0	8	10	234	Octa-1,3,5,7-tetraene (different rotamers)	240, 258 (AS), 241, 263, 264, 275, 279 (AM), 280 (EG)
	16	26	315	1,8-Di- <i>t</i> -butylocta-1,3,5,7-tetraene	246 (AS)
1	8	8	239	Cyclooctatetraene	281 (PD), 240, 260, 282 (AS)
			316	<i>o</i> -Quinodimethane	283 (AM)
	11	12	250	2,2-Dimethyl(2 <i>H</i>)indene	284 (AS)
Polyenes: $d \geq 5$					
$d = 5$					
1	10	12	317	Deca-1,3,5,7,9-pentaene	261 (AS), 285 (AM)
	18	28	318	1,10-Di- <i>t</i> -butyldeca-1,3,5,7,9-pentaene	246 (AS)
2	16	20	319	Bis(3,3-dimethylcyclohexa-1,4-dienylidene)	286 (AS)
$d = 6$					
0	20	30	320	1,12-Di- <i>t</i> -butyldodeca-1,3,5,7,9,11-hexaene	246 (AS)
$d = 7$					
0	22	32	321	1,14-Di- <i>t</i> -butyltetradecaheptaene	246 (AS)
$d = 8$					
0	24	34	322	1,16-Di- <i>t</i> -butylhexadecaoctaene	246 (AS)
$d = 9$					
0	26	36	323	1,18-Di- <i>t</i> -butyloctadecanonaene	246 (AS)
	40	64	324	Phytoene (<i>cis</i> and <i>trans</i>)	287 (PR)
2	35	50	325	Septapreno- β -carotene	287 (PR)

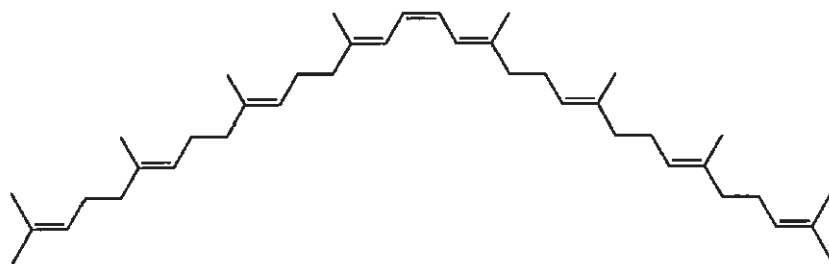
(continued overleaf)

TABLE 3. (continued)

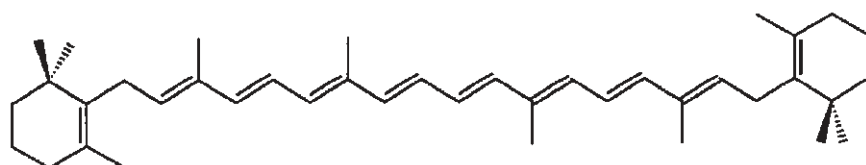
<i>r</i>	<i>n</i>	<i>m</i>	No.	Name	References (Method) ^a
<i>d</i> = 10					
0	28	38	326	1,20-Di- <i>t</i> -butyleicosadecaene	246 (AS)
2	40	58	327	7,7'-Dihydro- β -carotene	287 (PR)
<i>d</i> = 11					
0	30	40	328	1,22-Di- <i>t</i> -butyldocosauodecaene	246 (AS)
2	40	56	279	β -Carotene	287 (PR)
			280	(15 <i>Z</i>) - β -Carotene	287 (PR)
<i>d</i> = 13					
0	40	56	329	Lycopene (all- <i>trans</i>)	287 (PR)
<i>d</i> = 15					
2	50	68	330	Decapreno- β -carotene	287 (PR)
<i>d</i> = 19					
2	60	70	331	Dodecapreno- β -carotene	287 (PR)

^aPD, photodissociation; AS, absorption in frozen solvent; AM, absorption in Ar matrix; EG, gas-phase emission; EM, emission in neon matrix; PR, pulse radiolysis.

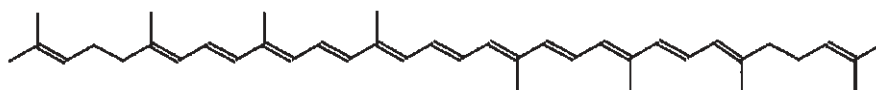




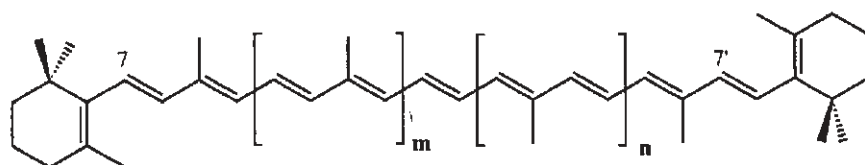
(324)



(327)



(329)



m	n		
1	0	Septapreno- β -carotene	325
1	1	β -carotene	279
2	2	decapreno- β -carotene	330
3	3	dodecapreno- β -carotene	331

C. Theoretical Methods

1. Koopmans and non-Koopmans states

In Section II.C (equations 7–10 and Figure 3) it was explained how electronic states of $M^{+\bullet}$ that give rise to PE bands can be related directly to orbital energies \mathcal{E}_j from Hückel or Hartree–Fock type calculations. In the present context it becomes necessary to extend this picture by taking into account excited configurations which arise through promotion of electrons into *virtual orbitals*. Excited states of $M^{+\bullet}$ described by such configurations cannot be related to orbital energies \mathcal{E}_j by the Koopmans theorem, and therefore it has become customary to call such states *non-Koopmans* states (as opposed to Koopmans states which are seen in PE spectra).

Figure 27 shows how different types of excited configurations can be formed from the ground configuration ${}^2\tilde{\Phi}_0$ of a radical cation $M^{+\bullet}$: electron promotion from doubly occupied MOs ϕ_{n-j} to the singly occupied HOMO ϕ_n give rise to Koopmans configurations ${}^2\tilde{\Phi}_1$ and ${}^2\tilde{\Phi}_2$, which are also called A-type configurations. Excitation from the HOMO into virtual MOs ϕ_{n+j} yields B-type configurations whereas promotion of electrons from doubly occupied into virtual MOs gives C-type configurations. The latter always come in pairs which correspond to promotion of α or β electrons (termed C_α and C_β , respectively). Due to differences in electron repulsion between α and β electrons, the corresponding excited states ${}^2\tilde{\Psi}_j$ ($M^{+\bullet}$) lie at different energies[†] and are also associated with different transition moments, a phenomenon which is unique to open-shell systems such as radical ions.

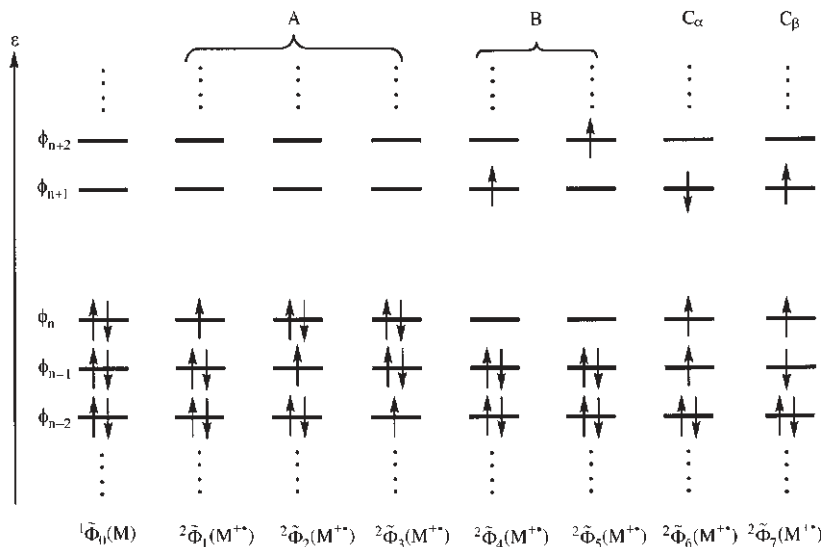


FIGURE 27. Different types of configurations of radical cations (the numbering does not imply an energetic ordering). A-type are Koopmans, B- and C-type are non-Koopmans configurations

[†] In actual fact, the three configurations corresponding to spin arrangements $\alpha/\alpha/\beta$, $\alpha/\beta/\alpha$ and $\beta/\alpha/\alpha$ (or the corresponding ones with two β and one α electron) are not eigenfunctions of the S^2 operator. Upon proper combination, they give rise to three spectroscopic states, two doublets and one of the components of a quartet.

2. Limitations and extension of single-determinant models

Although in many cases, particularly in PE spectroscopy, *single* configurations or Slater determinants ${}^2\tilde{\Phi}_j(M^{+\bullet})$ were shown to yield heuristically useful descriptions of the corresponding spectroscopic states ${}^2\tilde{\Psi}_j(M^{+\bullet})$, this is not generally true because the independent particle approximation (which implies that a many-electron wavefunction ${}^2\tilde{\Psi}_j$ can be approximated by a single product of one-electron wavefunctions, i.e. MOs ϕ , as represented by a Slater determinant ${}^2\tilde{\Phi}_j$) may break down in some cases. As this becomes particularly evident in polyene radical cations, it seems appropriate to briefly elaborate on methods which allow one to overcome the limitations of single-determinant models.

This can be achieved, for example, by introducing an additional degree of flexibility into the wavefunction through *mixing of different configurations* ${}^2\tilde{\Phi}_j(M^{+\bullet})$. It can be shown that by doing so one allows for a degree of correlation between the motions of different electrons which is suppressed in single-determinant MO models[†]. In the present context we will, however, not be concerned with the application of this so-called *Configuration Interaction* (CI) method for attempting a full recovery of electron correlation, but rather with its application to very simple cases (such as excited states of polyene radical cations) where only a few configurations must be considered in order to gain a qualitatively correct description of excited states[‡].

In analogy to using a linear combination of atomic orbitals to form MOs, a variational procedure is used to construct many-electron wavefunctions $\tilde{\Psi}_k$ from a set of N Slater determinants $\tilde{\Phi}_j$, i.e. one sets up a $N \times N$ matrix of elements $H_{ij} = \langle \tilde{\Phi}_i | \mathbf{H} | \tilde{\Phi}_j \rangle$ which, upon diagonalization, yields state energies E_k and associated vectors of coefficients a_{ki} used to define $\tilde{\Psi}_k$ as a linear combination of $N\tilde{\Phi}_i$ s:

$$\tilde{\Psi}_k = \sum_i^N a_{ki} \tilde{\Phi}_i \quad (63)$$

This is usually sufficient for a *qualitatively* correct description of electronically excited states of $M^{+\bullet}$, even though electron correlation is not well accounted for if N is small.

Unfortunately, the dynamic correlation energy[¶] is not constant for a given molecule but may vary considerably between different electronic states. Thus, any procedure geared towards *quantitative* accuracy in predicting excited-state energies must in some way account for these variations. The most economical way to achieve this is to introduce a number of parameters into the model. By scaling those to a set of experimental data

[†] In single-determinant models each electron is considered to be moving in the *average* field of the other electrons and the nuclei. Consequently, the different electrons cannot maximize their average distance at any moment by correlating their movements, which is what they do in reality. Allowing for electron correlation invariably leads to a lowering of the total energy of a molecule, by the so-called 'correlation energy'.

[‡] Note that only configurations of the same symmetry can interact. In radical ions (and, generally, open-shell systems) the symmetry of a configuration is obtained as the direct product of the irreducible representations of all singly occupied MOs. If there is only one of these, as is the case in all A- and B-type configurations of radical ions, this corresponds to the irreducible representation of that MO.

[¶] It has become customary in quantum chemistry to subdivide electron correlation effects into two classes according to the methods used to account for them. The first are termed 'non-dynamic' and they can be recovered by the above type of small CI. On the other hand, all deficiencies which remain once these 'non-dynamic' effects are taken care of are attributed to 'dynamic' correlation.

one hopes to ‘absorb’ all deficiencies of the model, including correlation effects. In these so-called ‘semiempirical’ methods, different kinds of experimental data usually require different parameters, in analogy to the simple HMO model where the values for β used to predict thermochemical or spectroscopic properties vary by almost a factor of two²⁸⁸.

In *ab initio* methods (which, by definition, should not contain empirical parameters), the dynamic correlation energy must be recovered by a true extension of the (single configuration or small CI) model. This can be done by using a very large basis of configurations, but there are more economical methods based on many-body perturbation theory which allow one to circumvent the expensive (and often impracticable) large variational CI calculation. Due to their importance in calculations of polyene radical ion excited states, these will be briefly described in Section 4.

3. Semiempirical CI methods

As conjugated polyenes are often (essentially) planar molecules, their electronic structure can be described quite satisfactorily in terms of their π -electrons alone. Thus, models involving CI between singly excited π -configurations were developed already in the early days of computational quantum chemistry. The Hückel MOs used originally²⁸⁹ were soon replaced by those obtained from semiempirical π -SCF procedures as in the popular PPP method²⁹⁰, which was adapted and tested for open-shell systems by Zahradník and Čársky in the late 1960s²⁹¹. Such models are usually adequate for a qualitatively correct interpretation of the spectra of the radical ions of planar π -systems, including those of polyenes, and continue to be used successfully for this purpose.

Analogous to the PPP method for planar π -systems, semiempirical *all-valence* methods can be and were extended to include CI, thus giving rise to a family of procedures based on the CNDO²⁹², INDO²⁹³ and NDDO²⁹⁴ variants of the zero-differential overlap (ZDO) approximation, many of which were applied also to the discussion of CI effects in radical cations. Due to the parametric incorporation of dynamic correlation effects, such procedures often yield rather accurate predictions of excited-state energies and they continue to be the methods of choice for treating very large chromophores which are not amenable to *ab initio* calculations.

Because of the inherent limitations of such semiempirical procedures, they can only be relied upon for yielding predictions for a limited set of data, the range of which includes the set of experimental data used for their parametrization. As such data are less abundant for open-shell species, such as radical ions, it is not surprising that there are examples of dramatic failures of semiempirical methods in predicting their electronic spectra, some of which will be discussed later. *Ab initio* methods are not burdened by these limitations but, as mentioned above, they require additional computations to account for dynamic electron correlation.

4. Many-body perturbation methods

Due to the size of the variational problem, a large CI is usually not a practicable method for recovering dynamic correlation. Instead, one usually resorts to some form of treatment based on many-body perturbation theory where an explicit calculation of all off-diagonal CI matrix elements (and the diagonalization of the matrix) are avoided. For a detailed description of such methods, which is beyond the scope of this review, the reader is referred to appropriate textbooks²⁹⁵. For the present purpose, it suffices to mention two important aspects.

Firstly, such methods, for example the popular Møller–Plesset (MP) or the more recent coupled cluster (CC) or quadratic CI (QCI) procedures, are implemented in several standard quantum-chemistry packages such as Gaussian, Gamess or Cadpac. Their application

is therefore quite straightforward, at least as long as single-determinant wavefunctions offer a qualitatively correct description of the system.

However, if this is not the case, the perturbations are large and perturbation theory is no longer appropriate. In other words, perturbation methods based on single-determinant wavefunctions cannot be used to recover non-dynamic correlation effects in cases where more than one configuration is needed to obtain a reasonable approximation to the true many-electron wavefunction. This represents a serious impediment to the calculation of well-correlated wavefunctions for excited states which is only possible by means of cumbersome and computationally expensive multi-reference CI methods.

Luckily, this impasse was removed through the recent introduction of the CASPT2 model, which combines a powerful procedure for treating cases of strong non-dynamic correlation (CASSCF)[†] with a very economical one for treating dynamic correlation²⁹⁶. As will be shown below, the CASPT2 method works very well for polyene radical cations.

D. Linear Conjugated Polyenes

Electronic spectra of linear conjugated polyene radical cations are of interest for several reasons. Firstly, such species occur as intermediates in different processes of biological relevance, e.g. the protection of the photosynthetic reaction centre²⁹⁷, the charge transfer processes in membranes²⁹⁸ or in model studies for photoinduced charge separation²⁹⁹. Secondly, they may be involved in the formation of solitons upon doping or photoexcitation of polyacetylene³⁰⁰, and finally, they are of theoretical interest because their interpretation requires models which account for non-dynamic correlation.

1. The minimal CI model

To illustrate the latter point, consider the butadiene radical cation (BD⁺). On the basis of Hückel theory (or any single-determinant Hartree–Fock model) one would expect this cation to show two closely spaced absorption bands of very similar intensity, due to $\pi_1 \rightarrow \pi_2$ and $\pi_2 \rightarrow \pi_3$ excitation (denoted by subscripts a and v in Figure 28), which are associated with transition moments μ_a and μ_v of similar magnitude and orientation. Using the approximation $\beta_{\text{HMO}} \approx -3 \text{ eV}^{288}$ the expected spacing amounts to about 0.7 eV.

Actually, two bands of quite different intensity separated by nearly 2 eV are observed! Whereas the positions of the two bands could possibly be accommodated by appropriate parametrization, this is not possible for the band intensities which reveals the limitations inherent in the single-configuration approximation.

Fortunately, a qualitatively correct modelling of the BD⁺ spectrum requires only a single further step, i.e. taking into account the interaction between the first two excited configurations ${}^2\tilde{\Phi}_a$ and ${}^2\tilde{\Phi}_v$ which are of the same 2A_u symmetry. Solving this simple 2×2 problem leads to two states

$${}^2\tilde{\Psi}_+ = {}^2\tilde{\Phi}_v + \Delta \cdot {}^2\tilde{\Phi}_a \quad \text{and} \quad {}^2\tilde{\Psi}_- = {}^2\tilde{\Phi}_a - \Delta \cdot {}^2\tilde{\Phi}_v \quad (64)$$

where Δ measures the degree of mixing between ${}^2\tilde{\Phi}_a$ and ${}^2\tilde{\Phi}_v$. The actual value of Δ depends on the Hamiltonian \mathbf{H} used to compute the integral $H_{av} = \langle {}^2\tilde{\Phi}_a | \mathbf{H} | {}^2\tilde{\Phi}_v \rangle$ but falls

[†] This procedure corresponds to a full CI (i.e. including all possible excitations) within a restricted set of occupied and virtual MOs (called the ‘active space’, hence the CAS acronym). In addition, the AO coefficients in the one-electron MOs are simultaneously optimized, such that these eventually represent an optimal basis set for the given CI.

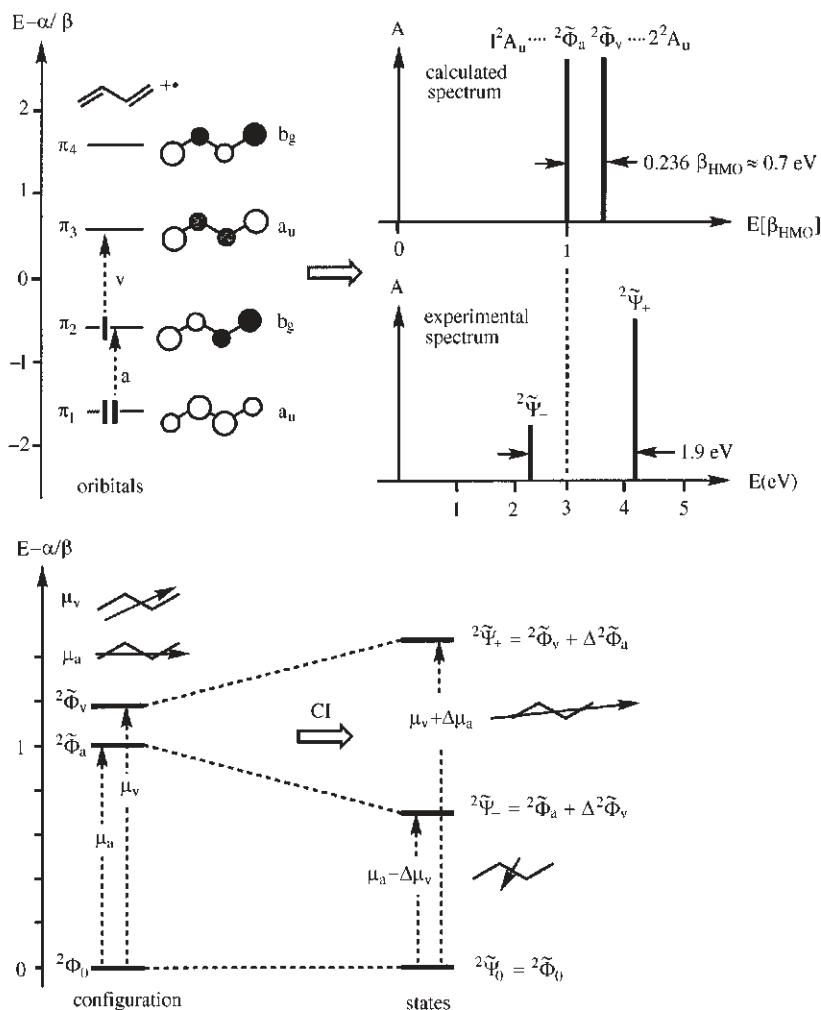


FIGURE 28. Top: π -MOs and configurations of the radical cation of butadiene (subscripts a and v correspond to excitations leading to ${}^2\tilde{\Phi}_a$ and ${}^2\tilde{\Phi}_v$, respectively). The resulting calculated spectrum is compared to the experimental one on the right. Bottom: The effect of a simple CI between ${}^2\tilde{\Phi}_a$ and ${}^2\tilde{\Phi}_v$ on excitation energies and on the transition moments μ_a and μ_v

generally in the range of 0.15 to 0.35. With regard to transition moments, the above 2×2 CI leads to a reduction due to partial cancellation of μ_a and μ_v in the first transition ${}^2\tilde{\Psi}_0 \rightarrow {}^2\tilde{\Psi}_-$ whereas the two reinforce each other in the higher-energy ${}^2\tilde{\Psi}_0 \rightarrow {}^2\tilde{\Psi}_+$ excitation[†], thus explaining the observed disparity in band intensities. Concurrently, the

[†] Due to the nature of the off-diagonal elements in a 2×2 CI matrix, the *negative* combination of determinants gets to lie below the positive combination, in contrast to the situation which prevails for interacting MOs.

energy separation between the two states increases, which naturally accounts for the larger spacing between the two bands.

The same treatment can be applied to longer polyenes, except that higher-lying π -excited configurations ${}^2\tilde{\Phi}_i$ will come into play. However, by virtue of the alternating a_u/b_g symmetries of polyene π -MOs, those immediately above ${}^2\tilde{\Phi}_a$ and ${}^2\tilde{\Phi}_v$ are usually of the same symmetry as ${}^2\tilde{\Phi}_0$ and therefore electronic excitation into the corresponding states ${}^2\tilde{\Psi}_i$ is dipole-forbidden within C_{2h} symmetry. Consequently, these configurations can be ignored when discussing EA spectra of polyene radical cations. The next π -excited states of the same symmetry as ${}^2\tilde{\Psi}_+$ and ${}^2\tilde{\Psi}_-$ as well as the σ -excited states are usually higher in energy than the first excited states of the neutral polyenes. They are associated with small transition moments and thus very difficult to detect in the presence of an excess of the neutral polyene, as is usual in EA experiments.

The EA spectra of linear conjugated polyene radical cations which have been observed so far conform well with the picture that emerges from the 2×2 CI model, i.e. they all show a weak low-energy and an often very intense high-energy band. In accord with qualitative expectations, both bands move to lower energies as the number of conjugated double bonds increases whereas their splitting decreases. This is due to the fact that the first two excited configurations move closer in energy as the chains grow longer and that the off-diagonal matrix element H_{av} which determines their splitting becomes smaller. This is shown schematically in Figure 29 where the energies of the first two excited states of the radical cations $t\text{-Bu}-(\text{CH}=\text{CH})_n\text{-Bu-}t^{+\bullet}$ ²⁴⁶ are plotted against $1/n$ (in addition, the energies corresponding to the second, intense EA band of some carotenoid radical cations observed in pulse radiolysis experiments²⁸⁷ have been included in Figure 29).

The literature records numerous, more or less successful, attempts to predict the energies of the first two excited states in linear conjugated polyene radical cations by semiempirical or *ab initio* methods. Some of these endeavours were reviewed elsewhere²⁴¹ whereas a more recent publication²⁴² gives an account of the difficulties met in predicting the energy of the second state accurately by *ab initio* CI procedures. However, it was recently shown that the CASSCF/CASPT2 model mentioned in Section III.C is capable of reproducing both excited-state energies of polyene cations $\text{H}-(\text{CH}=\text{CH})_n\text{-H}^{+\bullet}$ ($n = 2$ to 4) within 0.25 eV ³⁰¹. Thus, a model has finally become available which appears to provide reliable predictions of the energies of such excited states.

2. Long polyenes: Towards the polaron

Figure 29 raises the question of how the energies of these two excited states evolve as one goes to longer polyene chains, in analogy to those found in polyacetylenes which become conductive upon oxidative doping (= ionization) or photoexcitation.

The regression curves in Figure 29 tend to approach linearity for $n > 4$, which seems to suggest that a linear extrapolation to infinity ($1/n \rightarrow 0$) is appropriate. However, this is certainly not true because the charge and spin are not distributed evenly over the entire polyene cation chain. Consequently, longer polyene radical cations undergo a characteristic distortion leading to a localization of charge and spin around the centre of the chains. In solid state physics this distorted conjugated system, associated with a spin of $1/2$ and a single charge, is called a *polaron*, in analogy to the structure of odd-alternant radicals or cations where the single electron or the charge also accumulate about the centre (a *soliton* in solid state physics language). These charge-carrying polarons and solitons can move rather easily along chains of conjugated systems under the influence of an external electric field, an effect which is thought to be one of the reasons for the high conductivity of doped conjugated polymers such as polyacetylene.

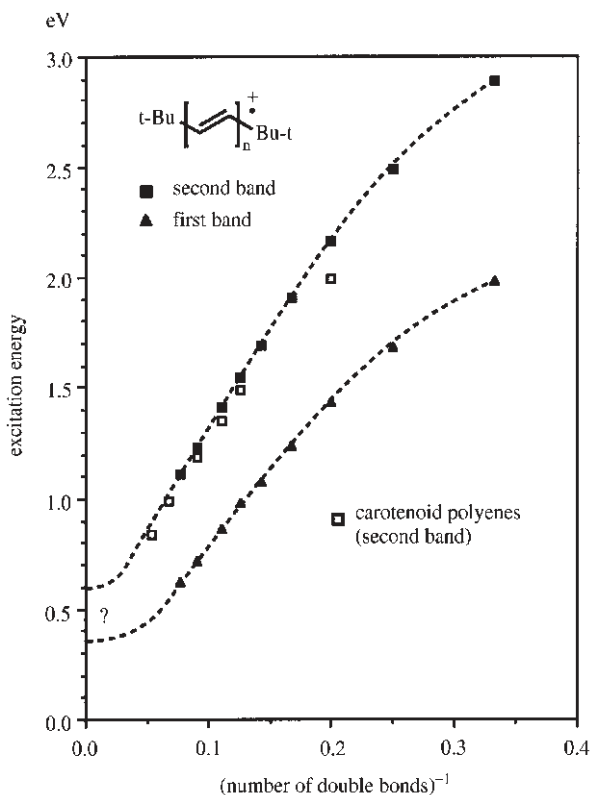


FIGURE 29. Energies of first (triangles) and second transition (squares) of radical cations $t\text{-Bu}-(\text{CH}=\text{CH})_n\text{-Bu-t}$ (filled symbols) and some carotenoid polyenes (open symbols) as a function of $1/n$

Because the extension of the polaron in polyene radical cations is finite (10–20 double bonds depending on the type of calculation), its electronic structure is independent of the number of double bonds attached to either side of it, so that the two lines in Figure 29 *must* bend at some point to meet the abscissa horizontally, as indicated by the dashed curves. Apparently, the point of inflection has not been reached for $n = 15$, but it is of interest that the curve for the first excited state could well extrapolate to 0.35 eV, which happens to be where the absorption of a polaron in polyacetylene has been observed³⁰⁰. If this is true, a second, more intense absorption band should occur between 0.5 and 0.7 eV, but the corresponding experiments have not yet been carried out.

3. Geometry dependence of excited-state energies

The realization of the polaronic nature of polyene radical cations leads naturally to the question, to what extent the pronounced relaxation of polyenes upon ionization affects their excited-state energies. Such changes can be assessed by comparing the ionization energy differences $I_1^Y - I_1^Y$ obtained from PE spectra with the positions of the band maxima in the radical cation's EA spectra which measure the same quantities at the radical cation

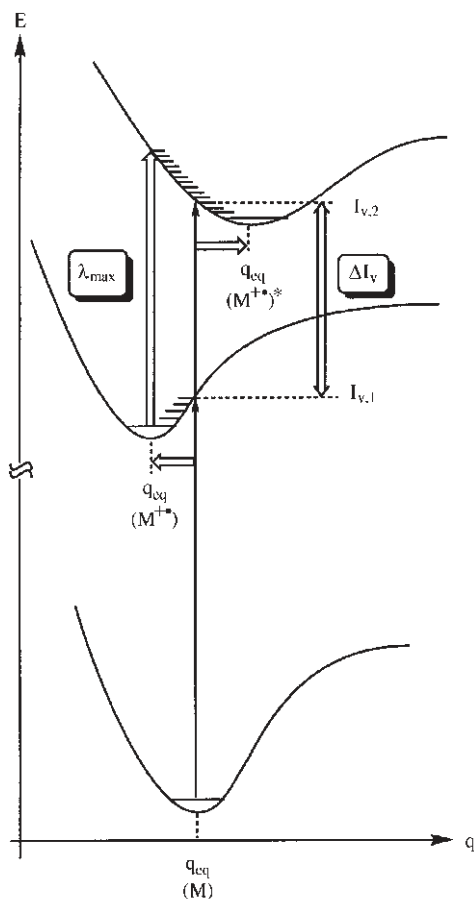


FIGURE 30. Potential energy curves for a neutral molecule M , and its radical cation $M^{+•}$ in the ground and first excited state (q_{eq} are the equilibrium distances with respect to an arbitrary coordinate q along which the three geometries differ). Note the shift in the $M^{+•}/(M^{+•})^*$ energy difference ΔE on going from q_{eq} of M ($\Delta E = \Delta I_v$ from the PE spectrum of M) to q_{eq} of $M^{+•}$ (ΔE corresponds to λ_{max} from the EA spectrum of $M^{+•}$)

equilibrium geometries, as illustrated schematically in Figure 30. A juxtaposition of PE and EA spectra for the first three members of the polyene radical cations shows that these changes are very small for the first π -excited state and perhaps somewhat larger for the second, which cannot be observed unambiguously in the PE spectra. This is surprising in view of the pronounced bond length changes which accompany the ionization of these polyenes and the corresponding ground-state relaxation energies which amount to several tenths of an eV. Indeed, the energies of the excited configurations ${}^2\tilde{\Phi}_a$ and ${}^2\tilde{\Phi}_v$ are very much affected by these changes, in accord with expectations from the nodal properties of the MOs involved. However, it was recently shown³⁰¹ that these effects are strongly attenuated in the corresponding excited states ${}^2\tilde{\Psi}_+$ and ${}^2\tilde{\Psi}_-$, i.e. that they are almost entirely washed out by dynamic correlation effects, at least for the first excited state. This

is, however, not generally true, as in the case of dihydropentalenes, where pronounced mismatches were observed between PE- and EA-band positions²⁷⁸.

4. Conformational isomerism in linear conjugated polyene radical cations

In neutral polyenes a clear distinction can be made between essential single bonds (which can be twisted fairly easily) and double bonds (which offer much more resistance to rotation). It has become customary to distinguish stable *isomers* (classified *E/Z* with regard to the configuration around the double bonds) and easily interconvertible *conformers* (classified as *s-cis*, *s-trans* or *gauche* with regard to the substituents on the essential single bonds) in polyenes.

Due to the fact that polyene HOMOs are invariably bonding along the double bonds and antibonding along the single bonds, removal of an electron from the HOMO entails a weakening of the former and a strengthening of the latter, i.e. a trend towards equalization of bond lengths³⁰¹, force constants^{302,303} and rotational barriers³⁰³ upon ionization. Eventually, a distinction between double and single bonds is no longer meaningful in polyene radical ions because all rotational isomers (rotamers) are stable in the sense that they do not readily interconvert.

In their first study on triene radical cations, Shida and coworkers found that irradiation of ionized hexatriene in frozen glasses yields a multitude of species with similar EA spectra, which could be selectively interconverted by narrow-band photolysis²⁴⁹. They assigned the observed band systems to four different rotamers of the hexatriene radical cation. Allan and Maier found that (3*E*)- and (3*Z*)-hexatriene gave distinct gas-phase emission spectra in agreement with the earlier PE findings²⁰. However, the two isomers could not be distinguished by photodissociation spectroscopy²⁶⁷.

In subsequent argon matrix isolation studies, similar bands were found when hexatriene or cyclohexadiene are ionized^{250,270}, and eventually, five of the six possible rotamers of hexatriene radical cation were identified by selective, wavelength-specific interconversions²⁷⁰. Similar results were later obtained for octatetraene^{264,275,279,285}, where six of the twenty possible rotamers are formed on ionization in argon (Figure 31) which could be interconverted and identified by selective photolysis^{275,279}. Interestingly, in the case of the butadiene radical cation the *s-cis* rotamer could not be detected, even if the diene radical cation was formed from the cyclobutene radical cation³⁰⁴. In contrast, in a recent resonance Raman study, some weak bands were detected and assigned to the *s-cis*-butadiene radical cation which might have escaped detection in the earlier ESR and EA experiments³⁰³.

One distinctive feature of polyene radical cations (especially of the long ones) is their great photosensitivity. For example, exposure of a sample of matrix isolated all-*trans* octatetraene radical cation to diffuse daylight leads, within about an hour, to a new photostationary equilibrium containing at least six rotamers. It is by virtue of this sensitivity, which is in part due to the very large absorptivities of the second EA bands, that a highly selective rotamer interconversion can be achieved, using a very narrow bandwidth^{270,279}.

In a recent comprehensive study at the CASSCF level of *ab initio* theory, Cave and Johnson have carried out calculations for all six rotamers of the hexatriene radical cation. In agreement with experiment they found that the first excited state is hardly affected by the additional interactions which prevail in partially *cis*-configured rotamers, whereas the energy of the second excited states decreases as the number of those *cis*-interactions increases. On this basis, they were able to confirm some of the original assignments of the observed spectra³⁰⁵ but proposed revisions for some of the others.

It was generally found that the all-*trans* rotamers always yield the shortest-wavelength second EA bands whereas *cis*-interactions result in bathochromic shifts, perhaps due to

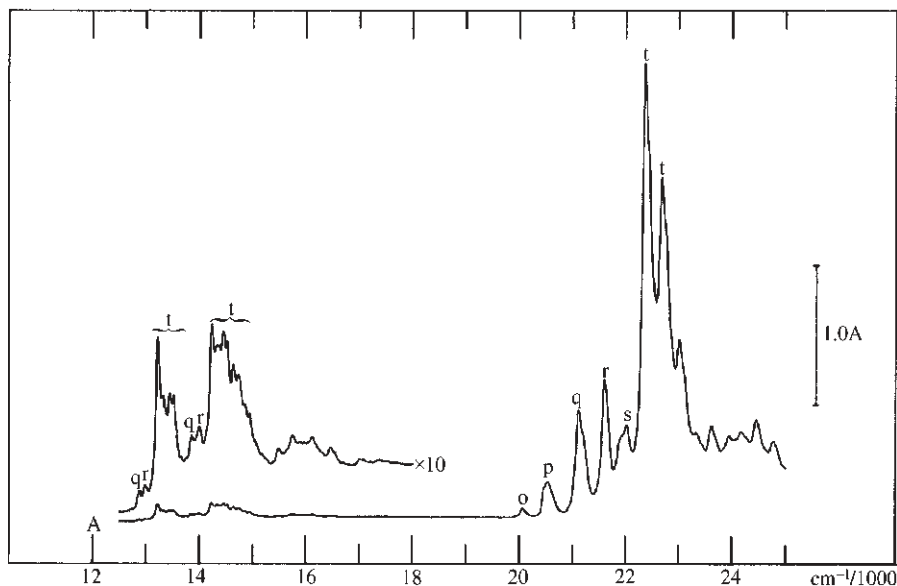


FIGURE 31. Spectrum obtained after ionization of all-*trans* octatetraene in argon. Note the occurrence of different rotamers (labelled o to t). The fine structure in the first absorption band of the t rotamer is due to site splittings²⁷⁹

slight deviations from planarity. Although this is difficult to prove in the absence of definitive assignments, these shifts appear to be roughly additive in the number of *cis*-configured bonds. With increasing red shift, the strong second absorption loses much of its intensity. When one goes to longer polyenes, the spread in the λ_{max} values of this band becomes smaller, perhaps due to a restriction in the number of *cis*-configured rotamers in rigid media²⁴⁶.

5. Alkylated and cyclic conjugated dienes and trienes

In the early days of PD spectroscopy, many alkylated polyenes were investigated because it was found that this method allows one to distinguish between isomers²³⁸. However, no systematic attempts were made to explain the band shifts due to the alkyl groups, as had been done for the corresponding PE spectra. Generally, the first excited state is affected only weakly by alkyl substituents, whereas the second excited state undergoes a more substantial shift which decreases as the polyene chain grows longer.

Several cyclic conjugated polyenes have been investigated^{238,240,245,247,250,252,257,285}, in part as independent sources of *cis*-configured conjugated open-chain polyenes. Although they retain the general feature of a weak low-energy and an intense high-energy band, the former sometimes appears only as a shoulder in diene spectra. Most of them readily undergo photochemical ring-opening to open-chain conjugated polyenes whereas the reverse reaction, i.e. cyclization, has never been observed in radical cations.

It is possible in principle to deduce from the position of the first absorption band the twisting angle between the double bonds in cyclic conjugated polyenes, e.g. on the basis of a simple LCBO model⁵⁰. This has been attempted for cycloocta-1,3,5-triene **184**²⁵⁷ and cyclooctatetraene **239**²⁶⁰. For the former it was deduced that the π -system becomes

essentially planar upon ionization whereas the tetraene radical cation retains a significant puckering. This is in contrast to the radical anion, which is planar³⁰⁶. From the point of view of its electronic structure, the cyclooctatetraene radical cation is an interesting case because excitation occurs to the second, degenerate excited state where a very pronounced Jahn–Teller distortion prevents the relaxation into the first excited state and causes the interesting photochemistry of this compound which takes place in violation of Kasha's rule^{260,278}.

6. Cross-conjugated polyenes

In spite of the continued interest in cross-conjugated polyenes ('dendralenes'), of which more than 100 are known³⁰⁷, surprisingly few of these have been investigated by PE or radical ion spectroscopy[†].

A special case are the radical cations of *o*- and *p*-quinodimethane which have low-lying non-Koopmans excited states. Due to mixing between A- and B-type configurations (cf Figure 27) these states sometimes show up as additional weak bands (so-called satellite bands) in the PE spectra^{148,150,283} and thus represent rare examples of cases where the number of PE bands exceeds the number of occupied MOs in the range of π -ionizations. In the case of *o*-quinodimethane and derivatives, the positions of these states were confirmed by the EA spectra of the corresponding radical cations^{283,284} whereas the same was not done for *p*-quinodimethanes.

Otherwise, not much can be said about this class of compounds, except that they share with their linear conjugated homologues the feature, that their excited-state energies appears to be hardly affected by the substantial bond length changes which accompany ionization²⁷⁸.

E. Interaction Between Non-conjugated π -Orbitals

We mentioned in Section III.A that one of the unique features of radical ion optical spectroscopy is that it allows one to measure excited-state energies of a molecule at two different geometries, namely that of the neutral species (I_i^V in PE spectra) and that of the relaxed radical cation (λ_{\max} of the EA bands). In many cases this feature is of little relevance because either the geometry changes upon ionization are too small to lead to noticeable effects (e.g. in aromatic hydrocarbons), or because such effects are obscured, due to the invisibility of the states in one or other of the two experiments (i.e. strong σ -ionizations in the PE spectrum) or because of the near-cancellation of opposing effects (as in the case of linear conjugated polyene radical cations).

However, one class of molecules not affected by the above limiting factors, and where much can be learned from a comparison of PE and EA spectra, are those which contain non-conjugated π -systems interacting through-space and/or through-bond. The radical cation of a simple model system consisting of a pair of ethylene moieties with facing π -MOs, π_a and π_b , will show a characteristic so-called 'charge resonance' absorption which corresponds to promotion of an electron from the bonding combination of π MOs $\pi_+ = N_+(\pi_a + \pi_b)$ to the antibonding combination $\pi_- = N_-(\pi_a - \pi_b)$. The energy E_{CR} of this transition is a measure of their energy splitting which, in a first approximation, is proportional to the overlap $S_{ab} = \langle \pi_a / \pi_b \rangle$ as discussed in Section II.E.1.

At the distance R between π_a and π_b which prevails in the neutral molecule (Figure 32), E_{CR} corresponds to $\Delta I_V = I_V(\pi_+) - I_V(\pi_-)$ which is used as a measure of the

[†] If we disregard the special class of pentafulvenes, these are the molecules **173, 174, 180, 194, 200, 237–241, 246, 250, 268, 277, 303, 314** and **318** in Tables 2 and 3.

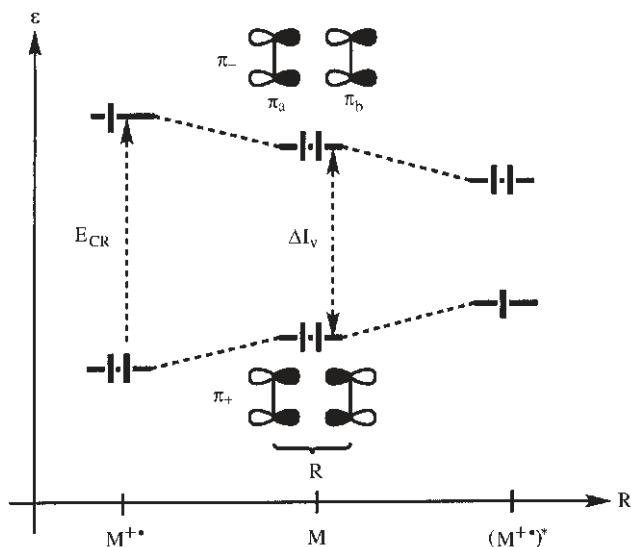


FIGURE 32. Schematic representation of the geometry changes of a hypothetical model of two facing π -systems with HOMOs π_a and π_b . The neutral molecule is represented in the centre. Upon ionization (removal of an electron from the HOMO π_-), the antibonding interactions which prevail in π_- are reduced, and the distance R decreases. As a consequence, the π_+/π_- overlap and E_{CR} increase. Conversely, upon electron ejection from π_+ (or on $\pi_+ \rightarrow \pi_-$ excitation), the bonding interaction in π_+ is diminished, which has the opposite effect on R and E_{CR} as described above

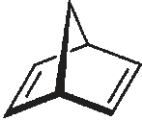

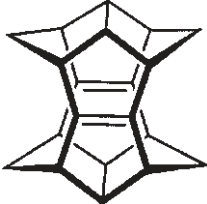

through-space interaction between π_a and π_b . At the geometry of the radical cation, E_{CR} is often significantly higher because the removal of an electron from π_- , decreases the antibonding interaction between π_a and π_b , thus allowing the two π -systems to come closer. This increases S_{ab} and leads to an overall stabilization of the system. The extent of this geometry change, and hence the change in E_{CR} , is limited by repulsive interactions between the interacting π -systems and by the stiffness of the σ -frame which connects them.

Such CR bands, which have been observed for many radical cations, usually manifest themselves by intense, broad bands in the visible or NIR part of the spectrum. The reason for the broadness is that, upon excitation of an electron from π_+ to π_- , the antibonding interaction is greatly enhanced. Consequently, the equilibrium distance of the π -systems in the excited state is significantly larger than in the ground state of the radical cation (or that of the neutral molecule) which results in a Franck–Condon envelope for the EA band which may be even broader than that for the corresponding PE band.

The above features can be illustrated by the molecules in Table 4, where the difference between the first and second ionization energy is compared to E_{CR} from the ion's optical spectra. The molecules are arranged in order of decreasing flexibility to show how this influences the difference between E_{CR} and ΔI_V .

In norbornadiene **75**, with its rather flexible σ -frame, the change in E_{CR} on going from the neutral molecule to the radical cation is more than 1 eV. In the more rigid dimethanonaphthalene derivative **139** it decreases to 0.84 eV, whereas in the already rather stiff pagodiene **295**, the change is only 0.54 eV. Finally, in the very strained dodecahedradiene **296**, E_{CR} , is nearly the same at the neutral molecule's and at the radical cation's geometry. As it happens, the geometry change upon electronic excitation in **296**⁺ coincides almost

TABLE 4. Change in E_{CR} and ΔI_V between neutral and cation geometry for a series of selected non-conjugated diene radical cations

No.	Compound	R (pm) ^a	ΔI_V (eV) ^b	E_{CR} (eV) ^c	Δ (eV) ^d
75		225	0.85 ⁴⁵	1.94	1.09
139		280 ³⁰⁸	1.26 ¹⁰⁵	2.10 ²⁶⁵	0.84
156		280 ³⁰⁹	1.91 ³¹⁰	2.43 ²⁶⁵	0.52
296		350 ³¹⁰	0.68 ³¹⁰	0.75 ²⁶⁶	0.07

^aDistance between the double bonds.

^b $I_{V,2} - I_{V,1}$ from PE spectra.

^cFrom EA spectra of radical cations.

^dIncrease in E_{CR} on going from the neutral to the radical cation's equilibrium geometry.

perfectly with an excited-state normal mode involving mainly a change in the distance between the double bonds. Therefore, the first EA band shows a single, well-resolved vibrational progression, a feature which is atypical for a charge resonance band.

The above considerations neglect the possible influence of through-bond interaction. That this must be very important becomes evident if one compares the dimethanonaphthalene derivative **139** with the pagodiene **156**: both have similar distances between perfectly facing double bonds, and yet E_{CR} is much larger in the latter due to an interaction via four single bonds which reinforces the through-space splitting. It is fair to assume that the magnitude of the through-bond interaction via the real σ -MOs does not change significantly with the geometry changes upon ionization, and that the change of E_{CR} is dictated mainly by the through-space term. Unfortunately, an attempt to assess the relative influence of the two effects by a study of the *syn*- and *anti*-dimers of cyclobutadiene (compounds **102** and **103**) failed because of the rapid rearrangement of the corresponding radical cations under the conditions of the EA experiment.

As shown in Section II.E, such through-bond interactions can be explained on the basis of a simple three-centre model involving the two interacting π -MOs and the intervening σ -MO. Of course, such models can also be applied to the changes in E_{CR} upon ionization, but all that can be learned from them in this context is that $B = \langle \pi_a | \mathbf{H} | \pi_b \rangle$ increases. If

one wants to relate this change to changes in geometry, one must resort to some quantum-chemical calculation. As it happens, through-space interactions which occur typically over distances of the order of van der Waals radii of the atoms involved, are difficult to assess by semiempirical methods because these often do not account properly for the fall-off in electron density at such distances.

This situation is exemplified in Figure 33, where the π_+/π_- splitting for a pair of ethylene molecules with facing π -MOs is plotted as a function of their distance R for two popular semiempirical methods and an *ab initio* SCF method (for the latter, the splittings obtained with the 3-21G and 6-31G* basis set are indistinguishable). Whereas the *ab initio* model (if applied to the molecules in Table 4) gives roughly correct results, the INDO/S method largely *overestimates* the effect of through-space interaction at all distances, although it shows the correct limiting behaviour. Conversely, AM1 strongly *underestimates* this effect, even at large distances. Consequently, the charge resonance absorptions of the first three cations in Table 4 are predicted to occur in the UV by INDO/S and in the IR by AM1 whereas they actually all occur in the visible range (500–630 nm), as predicted correctly by the *ab initio* models. Thus, caution should be exercised when

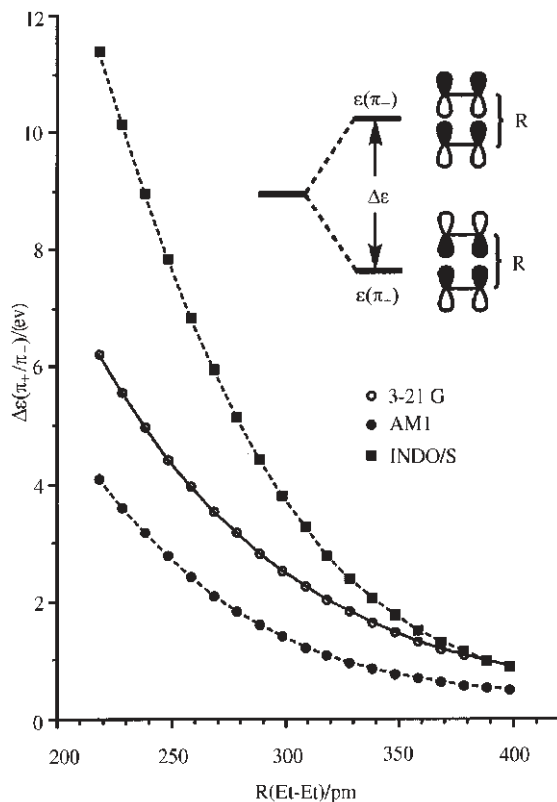


FIGURE 33. Energy difference ΔE between MOs π_+ and π_- of two ethylene molecules as a function of their distance R as calculated by an *ab initio* method (using the 3-21G basis set), by AM1 and by INDO/S. Note the strong underestimation of the through-space interaction by AM1 at all distances and the overestimation by INDO/S which diminishes, however, for large R

applying semiempirical methods for a quantitative prediction of E_{CR} values of π -systems interacting through space.

IV. ACKNOWLEDGEMENTS

We are extremely grateful to Dr. Engelbert Zass, Federal Institute of Technology, Zürich for his active and much appreciated help by providing a comprehensive computer search of the literature. Prof. Rolf Gleiter, University of Heidelberg, is thanked for his valuable help and advice and Prof. Jakob Wirz, University of Basel, for providing ancillary information. Finally, we wish to express our deep appreciation to Prof. Zvi Rappoport for his help in turning our manuscript into a readable contribution, and especially for his infinite patience with a pair of not overly diligent authors.

V. REFERENCES

1. L. Salem, *The Molecular Orbital Theory of Conjugated Systems*, W. A. Benjamin, New York, 1966; B. M. Gimarc, *Molecular Structure and Bonding: The Qualitative Molecular Orbital Approach*, Academic Press, New York, 1979; T. A. Albright, J. K. Burdett and M. H. Whangbo, *Orbital Interactions in Chemistry*, Wiley, New York, 1985.
2. A. Streitwieser, *Molecular Orbital Theory for Organic Chemists*, Wiley, New York, 1961; E. Heilbronner and H. Bock, *The HMO Model and Its Applications*, Wiley, London, 1968.
3. P. W. Atkins, *Physical Chemistry*, 5th ed., Oxford University Press, Oxford, 1994.
4. R. B. Woodward and R. Hoffmann, *Angew. Chem.*, **81**, 797 (1969); *Angew. Chem., Int. Ed. Engl.*, **8**, 781 (1969).
5. R. B. Woodward and R. Hoffmann, *The Conservation of Orbital Symmetry*, Academic Press, New York, 1970; N. T. Anh, *Die Woodward-Hoffmann-Regeln und ihre Anwendung*, Verlag Chemie, Weinheim, 1972.
6. M. I. Al-Joboury and D. W. Turner, *J. Chem. Phys.*, **37**, 3007 (1962); F. I. Vilesov, B. L. Kurbatov and A. N. Terenin, *Dokl. Akad. Nauk SSSR*, **139**, 1329 (1961).
7. D. W. Turner, C. Baker, A. D. Baker and C. R. Brundle, *Molecular Photoelectron Spectroscopy*, Wiley Interscience, London, 1970.
8. H. Siegbahn and L. Karlsson, *Photoelectron Spectroscopy*, in *Handbuch der Physik*, Vol. 31, *Corpuscles and Radiation in Matter: Part 1* (Ed. W. Mehlhorn), Springer-Verlag, Berlin, 1984.
9. J. H. D. Eland, *Photoelectron Spectroscopy*, Butterworths, London, 1984.
10. E. Heilbronner and J. P. Maier, *Some Aspects of Organic Photoelectron Spectroscopy*, in *Electron Spectroscopy: Theory, Techniques and Applications*, Vol. 1 (Eds. C. R. Brundle and A. D. Baker), Academic Press, London, 1976, p. 205.
11. E. Heilbronner, *The Photoelectron Spectra of Saturated Hydrocarbons*, in *The Chemistry of Alkanes and Cycloalkanes* (Eds. S. Patai and Z. Rappoport), Wiley, Chichester, 1992.
12. M. Eckert-Maksic, R. Gleiter, N. S. Zefirov, S. L. Kozhushkov and T. S. Kuznetsova, *Chem. Ber.*, **124**, 371 (1991).
13. R. D. Levin and S. G. Lias, *Ionization Potential and Appearance Potential Measurements*, U.S. Department of Commerce, National Bureau of Standards, Washington DC, 1982.
14. H. C. Longuet-Higgins and L. Salem, *Proc. R. Soc. London, Ser. A*, **251**, 172 (1959); **257**, 445 (1960); G. Binsch, E. Heilbronner and J. N. Murrell, *Mol. Phys.*, **11**, 305 (1966).
15. K. Kimura, S. Katsumata, Y. Achiba, T. Yamazaki and S. Iwata, *Handbook of He I Photoelectron Spectra of Fundamental Organic Molecules*, Japan Scientific Press, Tokyo, 1981.
16. G. Bieri, F. Burger, E. Heilbronner and J. P. Maier, *Helv. Chim. Acta*, **60**, 2213 (1977).
17. F. Brogli, J. K. Crandall, E. Heilbronner, E. Kloster-Jensen and S. A. Sojka, *J. Electron Spectrosc.*, **2**, 455 (1973).
18. J. H. D. Eland, *J. Mass Spectrom. Ion Phys.*, **2**, 471 (1969).
19. C. R. Brundle and M. B. Robin, *J. Am. Chem. Soc.*, **92**, 5550 (1970).
20. M. Beez, G. Bieri, H. Bock and E. Heilbronner, *Helv. Chim. Acta*, **56**, 1028 (1973).
21. P. Masclet, G. Mouvrier and J. F. Bocquet, *J. Chim. Phys. Phys.-Chim. Biol.*, **78**, 99 (1981).
22. R. Bombach, J. Dannacher and J. -P. Stadelmann, *J. Am. Chem. Soc.*, **105**, 1824 (1983).
23. T. Bally, S. Nitsche, K. Roth and E. Haselbach, *J. Am. Chem. Soc.*, **106**, 3927 (1984).
24. A. M. Woodward, W. A. Chupka and St. D. Colson, *J. Phys. Chem.*, **88**, 4567 (1984).

25. R. C. Dunbar and S. H. Young, *J. Am. Chem. Soc.*, **110**, 2726 (1988).
26. C. Fridh, L. Åsbrink and E. Lindholm, *Chem. Phys. Lett.*, **15**, 282 (1972).
27. G. Bieri and L. Åsbrink, *J. Electron Spectrosc.*, **20**, 149 (1980).
28. S. D. Worley, T. R. Webb, D. H. Gibson and T. S. Ong, *J. Organomet. Chem.*, **168**, C16 (1979).
29. J. C. Bünzli, A. J. Burak and D. C. Frost, *Tetrahedron*, **29**, 3735 (1973).
30. D. F. Eaton and T. G. Traylor, *J. Am. Chem. Soc.*, **96**, 7109 (1974).
31. N. H. Werstiuk and G. Timmins, *Can. J. Chem.*, **66**, 2954 (1988).
32. N. H. Werstiuk, G. Timmins, J. Ma and T. Wildman, *Can. J. Chem.*, **70**, 1971 (1992).
33. E. Heilbronner, T. Hoshi, J. L. von Rosenberg and K. Hafner, *Nouv. J. Chim.*, **1**, 105 (1977).
34. H. Bock, S. Mohmand, T. Hirabayashi, G. Maier and H. Reisenauer, *Chem. Ber.*, **116**, 273 (1983).
35. A. Schweig, U. Weidner, J. G. Berber and W. Grahn, *Tetrahedron Lett.*, 557 (1973).
36. N. H. Werstiuk, K. B. Clark and W. J. Leigh, *Can. J. Chem.*, **68**, 2078 (1990).
37. E. Honegger, Z. -Z. Yang, E. Heilbronner, W. v. E. Doering and J. Schmidhauser, *Helv. Chim. Acta*, **67**, 640 (1984).
38. S. W. Staley and T. D. Norden, *J. Am. Chem. Soc.*, **111**, 445 (1989).
39. P. Bischof and E. Heilbronner, *Helv. Chim. Acta*, **53**, 1677 (1970).
40. V. V. Plemenkov, V. V. Zverev, V. M. Vakar, L. V. Ermolaeva and A. V. Ignatchenko, *J. Gen. Chem. USSR*, **59**, 874 (1989); *Zh. Obshch. Khim.*, **59**, 992 (1989).
41. I. A. Boyarskaya, S. G. Semenov and I. N. Domnin, *J. Org. Chem. USSR*, **28**, 191 (1992); *Zh. Org. Khim.*, **28**, 237 (1992).
42. P. Hemmersbach, M. Klessinger and P. Bruckmann, *J. Am. Chem. Soc.*, **100**, 6344 (1978).
43. S. Cradock, E. A. V. Ebsworth, H. Morello and D. W. H. Rankin, *J. Chem. Soc., Dalton Trans.*, 390 (1975); S. Cradock, R. H. Findlay and M. H. Palemer, *J. Chem. Soc., Dalton Trans.*, 1650 (1974).
44. P. Bruckmann and M. Klessinger, *Chem. Ber.*, **107**, 1108 (1974).
45. P. Bischof, J. A. Hashmall, E. Heilbronner and V. Hornung, *Helv. Chim. Acta*, **52**, 1745 (1969).
46. L. Åsbrink, C. Fridh and E. Lindholm, *J. Am. Chem. Soc.*, **94**, 5501 (1972).
47. F. Brogli, E. Heilbronner and E. Vogel, *J. Electron Spectrosc.*, **9**, 227 (1976).
48. P. Asmus and M. Klessinger, *Tetrahedron*, **30**, 2477 (1974).
49. B. Bischof, R. Gleiter and E. Heilbronner, *Helv. Chim. Acta*, **53**, 1425 (1970).
50. C. Batich, P. Bischof and E. Heilbronner, *J. Electron Spectrosc.*, **1**, 333 (1972).
51. P. Bischof, R. Gleiter, K. Gubernator, R. Haider, H. Musso, W. Schwarz, W. Trautmann and H. Hopf, *Chem. Ber.*, **114**, 994 (1981).
52. V. V. Plemenkov, O. Y. Butenko, S. I. Kozhushkov and T. S. Kuznetsova, *J. Gen. Chem. USSR*, **62**, 332 (1992); *Zh. Obshch. Khim.*, **B62**, 411 (1992).
53. N. H. Werstiuk, J. Ma, J. B. Macaulay and A. G. Fallis, *Can. J. Chem.*, **70**, 2798 (1992).
54. P. Asmus, M. Klessinger, L. -U. Meyer and A. de Meijere, *Tetrahedron Lett.*, 381 (1975).
55. R. Boese, D. Bläser, R. Gleiter, K. -H. Pfeifer, W. E. Billups and M. M. Haley, *J. Am. Chem. Soc.*, **115**, 743 (1993).
56. R. Gleiter, G. Krennrich, P. Bischof, T. Tsuji and S. Nishida, *Helv. Chim. Acta*, **69**, 962 (1986).
57. G. Bieri, E. Heilbronner, M. J. Goldstein, R. S. Leight and M. S. Lipton, *Tetrahedron Lett.*, 581 (1975).
58. G. Bieri, E. Heilbronner, Z. Kobayashi, A. Schmelzer, M. J. Goldstein, R. S. Leight and M. S. Lipton, *Helv. Chim. Acta*, **59**, 2657 (1976).
59. M. H. Palmer, *J. Mol. Struct.*, **161**, 333 (1987).
60. P. Blickle, H. Hopf, M. Bloch and T. B. Jones, *Chem. Ber.*, **112**, 3691 (1979).
61. T. Bally, D. Hasselmann and K. Loosen, *Helv. Chim. Acta*, **68**, 345 (1985).
62. R. Gleiter, E. Heilbronner and A. de Meijere, *Helv. Chim. Acta*, **54**, 1029 (1971).
63. C. Batich, E. Heilbronner, E. Rommel, M. F. Semmelhack and J. S. Foss, *J. Am. Chem. Soc.*, **96**, 7662 (1974).
64. K. Ohno, T. Ishida, Y. Naitoh and Y. Izumi, *J. Am. Chem. Soc.*, **107**, 8082 (1985).
65. J. Spanget-Larsen, C. de Korschwagen, M. Eckert-Maksic and R. Gleiter, *Helv. Chim. Acta*, **65**, 968 (1982).
66. P. Bischof, R. Gleiter, A. de Meijere and L. -U. Meyer, *Helv. Chim. Acta*, **57**, 1519 (1974).
67. R. Gleiter, P. Bischof, K. Gubernator, M. Christl, L. Schwager and P. Vogel, *J. Org. Chem.*, **50**, 5064 (1985).
68. R. Gleiter, P. Bischof and M. Christl, *J. Org. Chem.*, **51**, 2895 (1986).

69. R. Gleiter, K. Gubernator and W. Grimme, *J. Org. Chem.*, **46**, 1247 (1981).
70. T. Bally, K. Roth and R. Straub, *Helv. Chim. Acta*, **72**, 73 (1989).
71. R. Gleiter, P. Bischof, W. E. Volz and L. A. Paquette, *J. Am. Chem. Soc.*, **99**, 8 (1977).
72. A. De Meijere, *Chem. Ber.*, **107**, 1684 (1974).
73. V. V. Vornonkov, V. N. Baidin, V. A. Machtin, E. M. Pliss and I. V. Utkin, *J. Org. Chem. USSR*, **21**, 270 (1985); *Zh. Org. Khim.*, **21**, 302 (1985).
74. F. Turecek, J. Pancir, D. Stahl and T. Gäumann, *Org. Mass Spectrom.*, **20**, 360 (1985).
75. M. J. Goldstein, E. Heilbronner, V. Hornung and S. Natowsky, *Helv. Chim. Acta*, **56**, 294 (1973).
76. W. Schmidt, A. Schweig, A. G. Anastassiou and H. Yamamoto, *J. Chem. Soc., Chem. Commun.*, 218 (1974).
77. E. Heilbronner and H. -D. Martin, *Helv. Chim. Acta*, **55**, 1490 (1972).
78. T. Kobayashi, S. Miki, Z. -I. Yoshida, Y. Asako and C. Kajimoto, *J. Am. Chem. Soc.*, **110**, 5622 (1988).
79. F. Marschner, H. Juds and H. Goetz, *Tetrahedron Lett.*, 3983 (1973); G. N. Taylor, *Z. Phys. Chem. (Munich)*, **101**, 237 (1976).
80. R. Gleiter, G. Jähne, G. Müller, M. Nixdorf and H. Irngartinger, *Helv. Chim. Acta*, **69**, 71 (1986).
81. R. Gleiter, E. Heilbronner, M. Heckman and H. -D. Martin, *Chem. Ber.*, **106**, 28 (1973).
82. H. -D. Martin, S. Kagabu and R. Schwesinger, *Chem. Ber.*, **107**, 3130 (1974).
83. R. Askani, R. Gleiter, E. Heilbronner, V. Hornung and H. Musso, *Tetrahedron Lett.*, 4461 (1971).
84. L. N. Domelsmith, K. N. Houk, C. A. Degenhardt and L. A. Paquette, *J. Am. Chem. Soc.*, **100**, 100 (1978).
85. F. Brogli, E. Heilbronner and J. Ipaktschi, *Helv. Chim. Acta*, **55**, 2447 (1972).
86. R. Gleiter, M. C. Böhm, A. de Meijere and T. Preuss, *J. Org. Chem.*, **48**, 796 (1983).
87. F. Brogli, W. Eberbach, E. Haselbach, E. Heilbronner, V. Hornung and D. M. Lemal, *Helv. Chim. Acta*, **56**, 1933 (1973).
88. Y. Harada, K. Ohno, K. Seki and H. Inokuchi, *Chem. Lett.*, 1081 (1974).
89. W. Grimme, L. Schumacher, R. Gleiter and K. Gubernator, *Angew. Chem.*, **93**, 98 (1981).
90. A. D. Baker, D. Betteridge, N. R. Kemp and R. E. Kirby, *Anal. Chem.*, **42**, 1064 (1970).
91. P. Bischof, R. Gleiter, E. Heilbronner, V. Hornung and G. Schröder, *Helv. Chim. Acta*, **53**, 1645 (1970).
92. R. Gleiter, A. Toyota, P. Bischof, G. Krennrich, J. Dressel, P. D. Pansegrau and L. A. Paquette, *J. Am. Chem. Soc.*, **110**, 5490 (1988).
93. R. Gleiter, B. Kissler and C. Ganter, *Angew. Chem.*, **99**, 1292 (1987); *Angew. Chem., Int. Ed. Engl.*, **26**, 1252 (1987).
94. L. A. Paquette, C. W. Doecke and G. Klein, *J. Am. Chem. Soc.*, **101**, 7599 (1979).
95. R. Gleiter, E. Heilbronner, L. A. Paquette, G. L. Thompson and R. E. Wingard, *Tetrahedron*, **29**, 565 (1973).
96. E. Honegger, K. B. Wiberg and E. Heilbronner, *J. Electron Spectrosc.*, **31**, 369 (1983).
97. R. Gleiter, E. Litterst and J. Drouin, *Chem. Ber.*, **121**, 923 (1988).
98. L. A. Paquette, S. Liang, G. DeLucca, L. Waykole, H. Jendrella, R. D. Rogers, D. Kratz and R. Gleiter, *J. Org. Chem.*, **55**, 1598 (1990).
99. R. Gleiter, J. Spanget-Larsen, H. Hopf and C. Mlynek, *Chem. Ber.*, **117**, 1987 (1984).
100. J. Spanget-Larsen, R. Gleiter, G. Klein, C. Doecke and L. A. Paquette, *Chem. Ber.*, **113**, 2120 (1980).
101. W. Schmidt and G. Wilkins, *Tetrahedron*, **28**, 5649 (1972).
102. G. Sedelmeier, H. Prinzbach and H. -D. Martin, *Chimia*, **33**, 329 (1979).
103. L. A. Paquette, P. Charumilind, M. C. Boehm, R. Gleiter, L. S. Bass and J. Clardy, *J. Am. Chem. Soc.*, **105**, 3136 (1983).
104. M. N. Paddon-Row, H. K. Patney, R. S. Brown and K. N. Houk, *J. Am. Chem. Soc.*, **103**, 5575 (1981).
105. H. -D. Martin and R. Schwesinger, *Chem. Ber.*, **107**, 3143 (1974).
106. H. Künzer, E. Litterst, R. Gleiter and L. A. Paquette, *J. Org. Chem.*, **52**, 4740 (1987).
107. H. -D. Martin and P. Pfoehler, *Angew. Chem.*, **90**, 901 (1978).
108. R. Gleiter, C. Sigwart, W. -D. Fessner, H. Müller-Böttcher and H. Prinzbach, *Chem. Ber.*, **126**, 2299 (1993).
109. M. N. Paddon-Row, L. M. Engelhardt, B. W. Skelton, A. H. White, F. S. Jørgensen and H. K. Patney, *J. Chem. Soc., Perkin Trans 2.*, 1835 (1987); F. S. Jørgensen, M. N. Paddon-Row and H. K. Patney, *J. Chem. Soc., Chem. Commun.*, 573 (1983).

110. B. Albert, D. Elsässer, H. -D. Martin, B. Mayer, T. Chow, A. P. Marchand, C. -T. Ren and M. N. Paddon-Row, *Chem. Ber.*, **124**, 2871 (1991).
111. R. Gleiter and M. Karcher, *Angew. Chem.*, **100**, 851 (1988).
112. B. Kovac, E. Heilbronner, H. Prinzbach and K. Weidmann, *Helv. Chim. Acta*, **62**, 2841 (1979).
113. D. Elsaesser, K. Hassenrueck, H. -D. Martin, B. Mayer, G. Lutz and H. Prinzbach, *Chem. Ber.*, **124**, 2853 (1991).
114. F. Brogli, E. Heilbronner, E. Kloster-Jensen, A. Schmelzer, A. S. Manocha, J. A. Pople and L. Radom, *Chem. Phys.*, **B4**, 107 (1974).
115. H. Basch, G. Bieri, E. Heilbronner and T. B. Jones, *Helv. Chim. Acta*, **61**, 46 (1978).
116. P. Bischof, R. Gleiter, H. Hopf and F. T. Lenich, *J. Am. Chem. Soc.*, **97**, 5467 (1975).
117. W. v. E. Doering and E. Schmidhauser, *J. Am. Chem. Soc.*, **106**, 5025 (1984).
118. E. E. Astrup, H. Bock, K. Witterl and P. Heimbach, *Acta Chem. Scand., Ser. A*, **29**, 827 (1975).
119. D. H. Parker, S. J. Sheng and M. A. El-Sayed, *J. Chem. Phys.*, **65**, 5534 (1976).
120. R. Gleiter, R. Haider, P. Bischof and H. -J. Lindner, *Chem. Ber.*, **116**, 3736 (1983).
121. E. Haselbach, T. Bally, R. Gschwinn, U. Klemm and Z. Lanyiova, *Chimia*, **33**, 405 (1979).
122. T. Bally, E. Haselbach, Z. Lanyiova and P. Baertschi, *Helv. Chim. Acta*, **61**, 2488 (1978).
123. T. Bally and E. Haselbach, *Helv. Chim. Acta*, **61**, 754 (1978).
124. E. Heilbronner, R. Gleiter, H. Hopf, V. Hornung and A. de Meijere, *Helv. Chim. Acta*, **54**, 783 (1971).
125. F. Brogli, P. A. Clark, E. Heilbronner and M. Neuenschwander, *Angew. Chem.*, **85**, 414 (1973); *Angew. Chem., Int. Ed. Engl.*, **12**, 422 (1973).
126. C. Fridh, L. Åsbrink and E. Lindholm, *Chem. Phys. Lett.*, **15**, 408 (1972).
127. K. Gubernator, J. Spanget-Larsen, R. Gleiter and H. Hopf, *J. Org. Chem.*, **48**, 2097 (1983).
128. L. A. Paquette, C. C. Liao, R. C. Burson, R. E. Wingard, C. N. Shih, J. Fayos and J. Clardy, *J. Am. Chem. Soc.*, **99**, 6935 (1977).
129. T. Bally and E. Haselbach, *Helv. Chim. Acta*, **58**, 321 (1975).
130. C. Müller, A. Schweig, W. Thiel, W. Grahn, R. C. Bergman and K. P. C. Vollhardt, *J. Am. Chem. Soc.*, **101**, 5579 (1979).
131. R. W. Hoffmann, R. Schüttler, W. Schäfer and A. Schweig, *Angew. Chem.*, **84**, 533 (1972).
132. E. Haselbach, E. Heilbronner and G. Schröder, *Helv. Chim. Acta*, **54**, 153 (1971).
133. T. Bally, L. Truttmann, J. T. Wang and F. Williams, *J. Am. Chem. Soc.*, **117**, 7923 (1995).
134. E. Haselbach and M. Rossi, *Helv. Chim. Acta*, **59**, 2635 (1976).
135. P. Bischof, J. A. Hashmall, E. Heilbronner and V. Hornung, *Tetrahedron Lett.*, 1033 (1970).
136. J. -C. Bünzli, D. C. Frost and L. Weiler, *Tetrahedron Lett.*, 1159 (1973).
137. H. -D. Martin, B. Mayer, R. W. Hoffmann, A. Riemann and P. Rademacher, *Chem. Ber.*, **118**, 2514 (1985).
138. T. L. Scott, I. Erden, W. R. Brunsvold, T. Schultz, K. N. Houk and M. N. Paddon-row, *J. Am. Chem. Soc.*, **104**, 3659 (1982).
139. J. Ipaktschi, J. Herber, H. -O. Kalinowski and R. Boese, *Chem. Ber.*, **123**, 305 (1990).
140. A. de Meijere, K. Michelsen, R. Gleiter and J. Spanget-Larsen, *Isr. J. Chem.*, **29**, 153 (1989).
141. J. E. McMurry, G. J. Haley, J. R. Matz, J. C. Clardy, G. Van Duyne, R. Gleiter, W. Schäfer and D. H. White, *J. Am. Chem. Soc.*, **108**, 2932 (1986).
142. J. E. McMurry, J. Gregory, J. R. Matz, J. C. Clardy and G. Van Duyne, *J. Am. Chem. Soc.*, **106**, 5018 (1984).
143. R. Gleiter, and O. Borzyk, *Angew. Chem.*, **107**, 1094 (1995); *Angew. Chem., Int. Ed. Engl.*, **34**, 1001 (1995).
144. G. Bieri, J. D. Dill, E. Heilbronner, J. P. Maier and J. P. Ripoll, *Helv. Chim. Acta*, **60**, 629 (1977).
145. M. Allan, L. Neuhaus and E. Haselbach, *Helv. Chim. Acta*, **67**, 1776 (1984).
146. C. Müller, A. Schweig, W. Thiel, W. Grahn, R. C. Bergman and K. P. C. Vollhardt, *J. Am. Chem. Soc.*, **101**, 5579 (1979).
147. T. Bally, U. Buser and E. Haselbach, *Helv. Chim. Acta*, **61**, 38 (1978).
148. T. Koenig, R. Wielesek, W. Snell and T. Balle, *J. Am. Chem. Soc.*, **97**, 3225 (1975).
149. E. W. Fu and R. C. Dunbar, *J. Am. Chem. Soc.*, **100**, 2283 (1978).
150. T. Koenig and S. Southworth, *J. Am. Chem. Soc.*, **99**, 2807 (1977).
151. M. C. Boehm and R. Gleiter, *Chem. Ber.*, **111**, 3516 (1978).
152. R. Gleiter, R. Haider, K. Gubernator and P. Bischof, *Chem. Ber.*, **116**, 2983 (1983).
153. R. Gleiter, H. Irgartinger and R. Merger, *J. Org. Chem.*, **58**, 456 (1993).

154. H. Bock and G. Rohn, *Helv. Chim. Acta*, **74**, 1221 (1991).
155. C. Batich, E. Heilbronner and M. F. Semmelhack, *Helv. Chim. Acta*, **56**, 2110 (1973).
156. M. T. Reetz, R. W. Hoffmann, W. Schäfer and A. Schweig, *Angew. Chem.*, **85**, 45 (1973).
157. E. Heilbronner, IUPAC Vol. 7, XXIII rd Int. Cong. Pure Appl. Chem., Butterworth's, London, 1971.
158. M. Mohraz, C. Batich, E. Heilbronner, P. Vogel and P. -A. Carrupt, *Recl. Trav. Chim. Pays-Bas*, **748**, 361 (1979).
159. W. T. Borden, S. D. Young, D. C. Frost, N. P. C. Westwood and W. L. Jorgensen, *J. Org. Chem.*, **44**, 737 (1979).
160. R. Gleiter, H. Zimmermann, W. -D. Fessner and H. Prinzbach, *Chem. Ber.*, **118**, 3856 (1985).
161. G. Gross, R. Schulz, A. Schweig and C. Wenstrup, *Angew. Chem.*, **93**, 1078 (1981).
162. T. Koenig, R. Winter and K. Rudolf, *J. Am. Chem. Soc.*, **109**, 2515 (1987).
163. M. Mohraz, J. -q. Wang, E. Heilbronner, P. Vogel and O. Pilet, *Helv. Chim. Acta*, **63**, 568 (1980).
164. E. Hasler, A. Hörmann, G. Persy, H. Platsch and J. Wirz, *J. Am. Chem. Soc.*, **115**, 5400 (1993).
165. R. Gleiter, W. Dobler, E. Vogel, S. Boehm and J. Lex, *J. Am. Chem. Soc.*, **109**, 5156 (1987).
166. N. Wada and T. Sagawa, *J. Phys. Soc. Jpn.*, **43**, 2107 (1977).
167. H. M. Brown, P. C. Kingzett and O. H. Griffith, *Photochem. Photobiol.*, **27**, 445 (1978).
168. M. Wautelet, L. D. Lande and A. H. Madjid, *Chem. Phys. Lett.*, **51**, 530 (1977).
169. J. A. Pople and D. L. Beveridge, *Approximate Molecular Orbital Theory*, McGraw-Hill, New York, 1970.
170. J. N. Murrell and A. J. Harget, *Semi-empirical Self-consistent Molecular Orbital Theory of Molecules*, Wiley-Interscience, London, 1972; G. H. Wagnière, *Introduction to Elementary Molecular Orbital Theory and to Semiempirical Methods*, Springer-Verlag, Berlin, 1976; J. Sadlej, *Semi-empirical Methods of Quantum Chemistry*, Wiley, New York, 1985.
171. T. Koopmans, *Physica*, **1**, 104 (1934).
172. R. Hoffmann, *J. Chem. Phys.*, **39**, 1397 (1963).
173. E. Honegger and E. Heilbronner, *The Equivalent Orbital Model and the Interpretation of PE Spectra*, in *Theoretical Models of Chemical Bonding, Part 3* (Ed. Z. B. Maksic), Springer-Verlag, Berlin, 1991, p. 99.
174. E. Hückel, *Z. Physik*, **70**, 204 (1931); *Grundzüge der Theorie ungesättigter und aromatischer Verbindungen*, Verlag Chemie, Berlin, 1938.
175. A. Graovac, I. Gutman and N. Trinajstić, *Topological Approach to the Chemistry of Conjugated Molecules*, Springer-Verlag, Berlin, 1972.
176. P. Masclet, D. Grosjean and G. Mouvier, *J. Electron Spectrosc.*, **2**, 225 (1973); D. A. Krause, J. W. Taylor and R. F. Fenske, *J. Am. Chem. Soc.*, **100**, 718 (1978).
177. R. W. Taft Jr., *J. Am. Chem. Soc.*, **74**, 3120 (1952); **75**, 4231 (1953).
178. R. S. Mulliken, C. A. Rieke and W. G. Brown, *J. Am. Chem. Soc.*, **63**, 41 (1941); M. J. S. Dewar, *Hyperconjugation*, Ronald, New York, 1962; cf. also References 1 and 2.
179. R. Hoffmann and R. A. Olofson, *J. Am. Chem. Soc.*, **88**, 943 (1966); R. Hoffmann, C. Levin and R. A. Moss, *J. Am. Chem. Soc.*, **95**, 629 (1973).
180. A. D. Walsh, *Nature*, **159**, 167, 712 (1947); *Trans. Faraday Soc.*, **45**, 179 (1947); T. M. Sugden, *Nature*, **160**, 367 (1947).
181. T. Förster, *Z. Phys. Chem. B*, **43**, 58 (1939).
182. C. A. Coulson and W. E. Moffitt, *J. Chem. Phys.*, **15**, 151 (1949); *Philos. Mag.*, **40**, 1 (1949).
183. E. Honegger, E. Heilbronner, A. Schmelzer and J. -q. Wang, *Isr. J. Chem.*, **22**, 3 (1982); E. Honegger, E. Heilbronner and A. Schmelzer, *Nouv. J. Chim.*, **6**, 519 (1982).
184. E. Honegger, A. Schmelzer and E. Heilbronner, *J. Electron Spectrosc.*, **28**, 79 (1982).
185. J. P. Maier and D. W. Turner, *Discuss. Faraday Soc.*, **54**, 149 (1972); J. Daintith, J. P. Maier, D. A. Sweigart and D. W. Turner, in *Electron Spectroscopy* (Ed. D. Shirley), North-Holland, Amsterdam, 1972.
186. C. R. Brundle, M. B. Robin, N. A. Kuebler and H. Basch, *J. Am. Chem. Soc.*, **94**, 1451 (1972).
187. C. Baker and D. W. Turner, *Chem. Commun.*, 480 (1969).
188. E. Haselbach, *Chem. Phys. Lett.*, **7**, 428 (1970).
189. W. von Niessen, G. H. F. Diercksen, L. S. Cederbaum and W. Domcke, *Chem. Phys.*, **18**, 469 (1976); L. S. Cederbaum, W. Domcke, H. Köppel and W. von Niessen, *Chem. Phys.*, **26**, 169 (1977).
190. G. Binsch and E. Heilbronner, *Tetrahedron*, **24**, 1215 (1968).
191. G. Binsch, I. Tamis and R. D. Hill, *J. Am. Chem. Soc.*, **91**, 2446 (1969); G. Binsch and I. Tamis, *J. Am. Chem. Soc.*, **91**, 2450 (1969).

192. D. W. Kohn and P. Chen, *J. Am. Chem. Soc.*, **115**, 2844 (1993).
193. E. Heilbronner, T. B. Jones, A. Krebs, G. Maier, K.-D. Malsch, J. Pocklington and A. Schmelzer, *J. Am. Chem. Soc.*, **102**, 564 (1980).
194. P. Bischof, R. Gleiter, K. Hafner, K. H. Knauer, J. Spanget-Larsen and H. U. Süss, *Chem. Ber.*, **111**, 932 (1978).
195. P. Bischof, R. Gleiter, K. Hafner, M. Kobayashi and J. Spanget-Larsen, *Ber. Bunsenges. Phys. Chem.*, **80**, 532 (1976).
196. Unpublished results.
197. E. Heilbronner, E. Honegger, W. Zambach, P. Schmitt and H. Günther, *Helv. Chim. Acta*, **67**, 1681 (1984).
198. J. Spangnet-Larsen, *Croat. Chem. Acta*, **57**, 991 (1984).
199. F. Brogli and E. Heilbronner, *Theor. Chim. Acta*, **26**, 289 (1972).
200. R. Hoffmann, A. Imamura and W. J. Hehre, *J. Am. Chem. Soc.*, **90**, 1499 (1968).
201. R. Hoffmann, *Acc. Chem. Res.*, **4**, 1 (1971).
202. R. Gleiter, *Angew. Chem.*, **86**, 770 (1974).
203. R. Hoffmann, E. Heilbronner and R. Gleiter, *J. Am. Chem. Soc.*, **92**, 706 (1970).
204. E. Heilbronner and A. Schmelzer, *Helv. Chim. Acta*, **58**, 936 (1975).
205. C. Edmiston and K. Ruedenberg, *Rev. Mod. Phys.*, **35**, 457 (1963); *J. Chem. Phys.*, **43**, 597 (1965); W. England, L. S. Salmon and K. Ruedenberg, *Fortschr. Chem. Forsch.*, **23**, 31 (1971).
206. R. Gleiter and W. Schäfer, *Acc. Chem. Res.*, **23**, 369 (1990).
207. E. Heilbronner, *Some Aspects of UPS*, in *The World of Quantum Chemistry* (Eds. R. Daudel and B. Pullman), D. Reidel, Dordrecht, 1974.
208. M. Eckert-Maksic, *Through-space and Through-bond Interaction as Mirrored in Photoelectron Spectra*, in *Theoretical Models of Chemical Bonding*, Vol. 3 (Ed. Z. B. Maksic), Springer-Verlag, Berlin, 1991, p. 153.
209. E. Heilbronner, *Isr. J. Chem.*, **10**, 143 (1972).
210. S. Winstein, *J. Am. Chem. Soc.*, **81**, 6524 (1959); *Quart. Rev.*, **23**, 141 (1969).
211. P. Bischof, D. Bosse, R. Gleiter, M. J. Kukla, A. de Meijere and L. A. Paquette, *Chem. Ber.*, **108**, 1218 (1975); G. G. Christoph, J. L. Muthardt, L. A. Paquette, M. C. Bohm and R. Gleiter, *J. Am. Chem. Soc.*, **100**, 7782 (1978).
212. M. J. S. Dewar and A. J. Holder, *J. Am. Chem. Soc.*, **111**, 5384 (1989).
213. L. N. Domelsmith, K. N. Houk, C. R. Degenhardt and L. A. Paquette, *J. Am. Chem. Soc.*, **100**, 100 (1978).
214. E. Haselbach and A. Schmelzer, *Helv. Chim. Acta*, **54**, 1575 (1971).
215. P. Balk, G. J. Hoijtink and J. W. H. Schreurs, *Recl. Trav. Chim. Pays-Bas*, **76**, 813 (1957); K. H. J. Buschow, J. Dieleman and G. J. Hoijtink *J. Chem. Phys.*, **42**, 1993 (1965) and earlier papers in the series.
216. D. E. Paul, D. Lipkin and S. I. Weissman, *J. Am. Chem. Soc.*, **78**, 119 (1956).
217. The early history of organic radical ion spectroscopy and chemistry was reviewed excellently by A. J. S. Bard, A. Ledwith and H. J. Shine, *Adv. Phys. Org. Chem.*, **13**, 155 (1976).
218. See, e.g., R. Dunbar, in *Gas Phase Ion Chemistry*, Vol. 3 (Ed. M. T. Bowers), Academic Press, New York, 1984.
219. R. C. Dunbar and H. H. -I. Teng, *J. Am. Chem. Soc.*, **100**, 2279 (1978).
220. R. C. Dunbar, *J. Am. Chem. Soc.*, **98**, 4671 (1976).
221. For more detailed descriptions and examples see, e.g., J. Maier, *Acc. Chem. Res.*, **15**, 18 (1982); *J. Electron Spectrosc. Relat. Phenom.*, **40**, 203 (1986).
222. D. Klapstein, S. Leutwyler and J. P. Maier, *Chem. Phys. Lett.*, **84**, 534 (1981).
223. T. A. Miller and V. Bondybey, *J. Chim. Phys.*, **77**, 695 (1980).
224. M. A. Fox and M. Chanon (Eds.), *Photoinduced Electron Transfer*, Elsevier, Amsterdam, 1989.
225. See, for example, K. Asmus, *Acc. Chem. Res.*, **12**, 436 (1979).
226. W. H. Hamill, in *Radical Ions* (Eds. E. T. Kaiser and L. Kevan), Wiley Interscience, New York, 1968; T. Shida and W. H. Hamill, *J. Chem. Phys.*, **44**, 2369, 2375, 4372 (1968).
227. (a) A. Grimison and G. A. Simpson, *J. Phys. Chem.*, **72**, 1776 (1968).
(b) C. Sandorfy, *Can. J. Spectrosc.*, **10**, 85 (1965).
228. T. Shida and T. Kato, *Chem. Phys. Lett.*, **68**, 106 (1979); T. Shida, Y. Egawa, H. Kubodera and T. Kato, *J. Chem. Phys.*, **73**, 5963 (1980).
229. See, for example, the special volume of *Faraday Discuss. Chem. Soc.*, **78** (1984), in particular pp. 1–81, where all major groups which were and are active in this field made contributions.

230. T. Shida, T. Kato and Y. Nosoka, *J. Phys. Chem.*, **81**, 1095 (1977).
231. See, for example, G. C. Pimentel, *Pure Appl. Chem.*, **4**, 61 (1962) or one of the excellent monographs on the subject, such as: S. Cradock and A. J. Hitchcliff, *Matrix Isolation*, Cambridge Univ. Press, Cambridge, 1975.
232. L. A. Wight, B. S. Ault and L. Andrews, *J. Chem. Phys.*, **60**, 81 (1974).
233. T. A. Miller and V. Bondybey, *Annu. Rev. Phys. Chem.*, **33**, 157 (1982).
234. D. Klapstein, J. P. Maier and L. Misev, in *Molecular Ions: Spectroscopy, Chemistry and Structure* (Eds. T. A. Miller and V. Bondybey), North-Holland, Amsterdam, 1983.
235. T. Bally, in *Radical Ionic Systems* (Eds. A. Lund and M. Shiotani), Kluwer, Amsterdam, 1991, p.3
236. T. Bally, S. Nitsche and K. Roth, unpublished results.
237. R. C. Dunbar and E. W. Fu, *J. Am. Chem. Soc.*, **95**, 2716 (1973).
238. R. C. Dunbar, *Anal. Chem.*, **48**, 723 (1976).
239. E. Haselbach, T. Bally, R. Gschwind, U. Klemm and Z. Lanyiova, *Chimia*, **33**, 405 (1979).
240. T. Shida, *Electronic Absorption Spectra of Radical Ions* (Physical Sciences Data, Vol. 34), Elsevier, Amsterdam, 1988.
241. T. Bally, S. Nitsche, K. Roth and E. Haselbach, *J. Am. Chem. Soc.*, **106**, 3927 (1984).
242. T. Bally, W. Tang and M. Jungen, *Chem. Phys. Lett.*, **190**, 453 (1992).
243. R. E. Krailler and D. H. Russell, *Anal. Chem.*, **57**, 1211 (1985).
244. R. C. Benz, P. C. Claspy and R. C. Dunbar, *J. Am. Chem. Soc.*, **103**, 1799 (1981).
245. R. C. Dunbar, G. R. Fitzgerald and J. D. Hays, *Int. J. Mass Spectrom. Ion Phys.*, **66**, 313 (1983).
246. T. Bally, K. Roth, W. Tang, R. R. Schrock, K. Knoll and L. Y. Park, *J. Am. Chem. Soc.*, **114**, 2440 (1992).
247. L. Truttmann, K. R. Asmis and T. Bally, *J. Phys. Chem.*, **99**, 17844 (1995).
248. P. N. T. Van Velzen and W. J. Van der Hart, *Org. Mass Spectrom.*, **19**, 190 (1984).
249. T. Shida, T. Kato and Y. Nosoka, *J. Phys. Chem.*, **81**, 1095 (1977).
250. B. J. Kelsall and L. Andrews, *J. Phys. Chem.*, **88**, 2723 (1984).
251. T. Bally, S. Nitsche, K. Roth and E. Haselbach, *J. Phys. Chem.*, **89**, 2528 (1985).
252. R. C. Dunbar and E. W. Fu, *J. Am. Chem. Soc.*, **95**, 2716 (1973).
253. L. Andrews and B. W. Keelan, *J. Am. Chem. Soc.*, **102**, 5732 (1980).
254. T. Bally and S. Matzinger, to be published.
255. B. J. Kelsall and L. Andrews, *J. Am. Chem. Soc.*, **105**, 1413 (1983).
256. E. Haselbach, T. Bally, Z. Lanyiova and P. Baertschi, *Helv. Chim. Acta*, **62**, 583 (1979).
257. T. Bally, K. Roth and R. Straub, *Helv. Chim. Acta*, **72**, 73 (1989).
258. Y. Fujisaka, M. Makino, J. Takahashi, T. Shida, K. Roth, R. Straub and T. Bally, *J. Phys. Chem.*, **96**, 2205 (1992).
259. T. Bally, L. Truttmann, S. Dai, J. T. Wang and F. Williams, *Chem. Phys. Lett.*, **212**, 141 (1993).
260. T. Bally, L. Truttmann, S. Dai and F. Williams, *J. Am. Chem. Soc.*, **117**, 7916 (1995).
261. T. Shida, T. Momose and N. Ono, *J. Phys. Chem.*, **89**, 815 (1985).
262. T. Momose, T. Shida and T. Kobayashi, *Tetrahedron*, **42**, 6337 (1986).
263. I. R. Dunkin, L. Andrews, J. T. Lurito and B. J. Kelsall, *J. Phys. Chem.*, **89**, 1701 (1985).
264. L. Andrews and J. T. Lurito, *Tetrahedron*, **42**, 6343 (1986).
265. T. Bally and K. Roth, unpublished results; K. Roth, PhD thesis (No. 958), University of Fribourg, 1989.
266. T. Bally, Z. Zhu and H. Prinzbach, to be published.
267. R. C. Dunbar and H. H-I. Teng, *J. Am. Chem. Soc.*, **100**, 2279 (1978).
268. M. Allan, J. Dannacher and J. P. Maier, *J. Chem. Phys.*, **73**, 3114 (1980).
269. V. E. Bondybey, J. H. English and T. A. Miller, *J. Mol. Spectrosc.*, **80**, 200 (1980).
270. T. Bally, S. Nitsche, K. Roth and E. Haselbach, *J. Phys. Chem.*, **89**, 2528 (1985).
271. T. Bally and E. Haselbach, *Helv. Chim. Acta*, **61**, 2488 (1978).
272. R. C. Dunbar and R. Klein, *J. Am. Chem. Soc.*, **99**, 3744 (1977).
273. T. Bally, D. Hasselmann and K. Loosen, *Helv. Chim. Acta*, **68**, 345 (1985).
274. W. J. Van der Hart, L. J. De Koning, N. M. M. Nibbering and M. L. Gross, *Int. J. Mass Spectrom. Ion Phys.*, **72**, 99 (1986).
275. T. Bally, E. Haselbach, S. Nitsche and K. Roth, *Tetrahedron*, **42**, 6325 (1986).
276. B. J. Kelsall, L. Andrews and G. J. McGarvey, *J. Phys. Chem.*, **87**, 1788 (1983).
277. B. J. Kelsall and L. Andrews, *J. Phys. Chem.*, **88**, 5893 (1984).
278. T. Bally, L. Truttmann, J. T. Wang and F. Williams, *J. Am. Chem. Soc.*, **117**, 7923 (1995).

279. T. Bally, S. Nitsche and K. Roth, *J. Chem. Phys.*, **84**, 2577 (1986).
280. T. B. Jones and J. P. Maier, *Int. J. Mass Spectrom. Ion Phys.*, **31**, 287 (1979).
281. E. W. Fu and R. C. Dunbar, *J. Am. Chem. Soc.*, **100**, 2283 (1978).
282. T. Shida and S. Iwata, *J. Am. Chem. Soc.*, **95**, 3473 (1973).
283. K. Kesper, N. Münzel, W. Pietzuch, H. Specht and A. Schweig, *J. Mol. Struct. (Theochem)*, **200**, 375 (1989).
284. P. Forster, R. Gschwind, E. Haselbach, U. Klemm and J. Wirz, *Nouv. J. Chim.*, **4**, 365 (1980).
285. L. Andrews, I. R. Dunkin, B. J. Kelsall and J. T. Lurito, *J. Phys. Chem.*, **89**, 821 (1985).
286. T. Bally, L. Neuhaus, S. Nitsche, E. Haselbach, J. Janssen and W. Lüttke, *Helv. Chim. Acta*, **66**, 1288 (1983).
287. R. V. Bensasson, E. J. Land and T. G. Truscott (Eds.), *Flash Photolysis and Pulse Radiolysis*, Chap. 3, Pergamon Press, Oxford, 1983; See also: E. A. Dawe and E. J. Land, *J. Chem. Soc., Faraday Trans. 1*, **71**, 2162 (1975); J. Lafferty, A. Roach, R. S. Sinclair, T. G. Truscott and E. J. Land, *J. Chem. Soc., Faraday Trans. 1*, **73**, 416 (1977).
288. E. Heilbronner and H. Bock, *Das HMO-Modell und seine Anwendung*, Verlag Chemie, Weinheim, 1968.
289. R. Pariser and R. G. Parr, *J. Chem. Phys.*, **21**, 466, 767 (1953). For an application of this method to radical ions, see: G. J. Hoijtink and D. J. Zandstra, *Mol. Phys.*, **3**, 371 (1960).
290. See R. Zahradník, *Fortschr. Chem. Forsch.*, **10**, 1 (1968).
291. R. Zahradník and P. Čársky, *J. Phys. Chem.*, **74**, 1235, 1240, 1249 (1970).
292. CNDO/S-CI: J. Del Bene and H. H. Jaffé, *J. Chem. Phys.*, **48**, 1807, 4050; **49**, 1221 (1968); **50**, 1126 (1969). Application to radical ions: P. Čársky and R. Zahradník, *Theor. Chim. Acta*, **20**, 343 (1971); **27**, 121 (1972); H. M. Chang and H. H. Jaffé, *Chem. Phys. Lett.*, **23**, 146 (1973). See also the more recent modified procedures of Scholz [G. Kluge and M. Scholz, *Monatsh. Chem.*, **111**, 15 (1980)] and Bigelow [R. Bigelow, *Int. J. Quantum Chem.*, **29**, 35 (1986) and earlier papers by the same author].
293. INDO/S-CI: J. Ridley and M. Zerner, *Theor. Chim. Acta*, **33**, 111 (1973); **42**, 223 (1976).
294. LNDO/S: G. Lauer, K. -W. Schulte and A. Schweig, *J. Am. Chem. Soc.*, **100**, 4925 (1978); H. L. Hase, G. Lauer, K. -W. Schulte and A. Schweig, *Theor. Chim. Acta*, **48**, 47 (1978).
295. See, for example, B. O. Roos, *Lecture Notes in Chemistry*, **58**, 177 (1992).
296. K. Andersson, P. -Å. Malmqvist, B. O. Roos, A. J. Sadlej and K. Wolinski, *J. Phys. Chem.*, **94**, 5483 (1990); K. Andersson, P. -Å. Malmqvist and B. O. Roos, *J. Chem. Phys.*, **96**, 1218 (1992).
297. See, for example, J. O. L. Rivàs, A. Telfer and J. Barber, *Biochim. Biophys. Acta*, **142**, 155 (1992) and references cited therein.
298. Y. Koyama, *J. Photochem. Photobiol.*, **B9**, 265 (1991) and references cited therein; H. A. Frank, C. A. Violette, J. K. Trautman, A. P. Shreve, T. G. Owens and A. C. Albrecht, *Pure Appl. Chem.*, **63**, 109 (1991).
299. D. Gust, T. A. Moore and A. L. Moore, *Acc. Chem. Res.*, **26**, 198 (1993).
300. L. Rothberg, T. M. Jedju, P. D. Townsend, S. Etamad and G. L. Baker, *Mol. Cryst. Liq. Cryst.*, **194**, 1 (1991).
301. M. P. Fülischer, S. Matzinger and T. Bally, *Chem. Phys. Lett.*, **236**, 167 (1995).
302. W. Tang, X. -L. Zhang and T. Bally, *J. Phys. Chem.*, **97**, 4373 (1993).
303. T. Keszthelyi, R. Wilbrandt and T. Bally, *J. Phys. Chem.*, in press.
304. J. N. Aebischer, T. Bally, K. Roth, E. Haselbach, F. Gerson and X. -Z. Qin, *J. Am. Chem. Soc.*, **111**, 7909 (1989).
305. R. J. Cave and J. L. Johnson, *J. Phys. Chem.*, **96**, 5332 (1992).
306. C. Samet, J. L. Rose, S. B. Piepho, J. Laurito, L. Andrews and P. N. Schatz, *J. Am. Chem. Soc.*, **116**, 11109 (1994) and references cited therein.
307. H. Hopff, *Angew. Chem., Int. Ed. Engl.*, **23**, 984 (1984).
308. O. Ermer, C. D. Bädecker and H. Preuss, *Angew. Chem.*, **96**, 576 (1984).
309. B. A. R. C. Murthy, P. R. Spurr, R. Pinos, C. Grund, W. -D. Fessner, D. Hunkler, H. Fritz, W. R. Roth and H. Prinzbach, *Chimia*, **41**, 32 (1987).
310. H. -D. Martin, B. Mayer, K. Weber, F. Wahl and H. Prinzbach, *Justus Liebigs Ann. Chem.*, 2019 (1995).